Thermodynamic Study to Form More Stable and Soluble Drug-Polymer Mixtures Using Soluplus® and Its Component Homopolymers

A Dissertation

Presented to the Graduate Faculty of the University of the Sciences in Philadelphia in Partial Fulfillment of the Requirements for the Degree of

DOCTOR OF PHILOSOPHY

By

Mohammad Abdulaziz Altamimi

March 25, 2015

Abstract

Solid dispersions of crystalline drugs in polymer matrices are promising as an approach to improve bioavailability. However, the high energy of amorphous drug in a solid dispersion leads to crystallization. In this work, the Flory-Huggins Theory predicts the solubility of crystalline drugs in the triblock graft copolymer Soluplus® and its homopolymers components, namely polyvinyl caprolactam (PCL), polyvinyl acetate (PVAc), and polyethylene glycol (PEG). Evaluation of the physicochemical and in vitro characteristics of solid dispersions of each drug with Soluplus® and its component homopolymers was conducted.

Nifedipine (NIF) and sulfamethoxazole (SMX) of 99.3 and 99.5% purity, respectively, were selected as BCS II crystalline model drugs. The melting point depression of each drug measured at various polymer levels using differential scanning calorimetry (DSC) allowed calculation of χ, the interaction parameter. χ provides a measure of drug-polymer interaction strength and allows the estimation of the free energy of mixing of the drug with the polymer and, ultimately, its solubility in that polymer. Solubility is calculated by solving solubility equations and by construction of a phase diagram. A low molecular weight PEG was used as a solvent to experimentally measure model drug solubility. Solid dispersions were prepared by lyophilization and by spray drying. Drug crystallinity in the dispersions was evaluated by DSC. Dissolution studies were conducted in simulated gastric and intestinal fluids without enzymes at 37 °C.

The Flory-Huggins Theory indicates that Soluplus® interacts effectively with each drug. The predicted solubility in Soluplus® compared favorably across the two methods and

with literature values. PVAc demonstrated weak interactions with each drug and it is unlikely to participate in drug solubilization. PCL was not a suitable candidate for the selected method due to its elevated T_g. Soluplus® and PEG 6000, however, interacted well with each drug, would solubilize them, and would enhance the dissolution rate in an aqueous medium; the dissolution rate for NIF improved to a greater extent than for SMX. Faster dissolution rates for PEG 6000 in comparison to Soluplus® dispersions were due to the more hydrophilic nature of PEG. DSC analysis revealed no crystalline material in the dispersions.

UNIVERSITY OF THE SCIENCES IN PHILADELPHIA

This is to Certify that the Dissertation Prepared by

Mohammad Abdulaziz Altamimi

Titled

Thermodynamic Study to Form More Stable and Soluble Drug-Polymer Mixtures Using Soluplus® and Its Component Homopolymers

Complies with the Policies of the Graduate Faculty of the University of the Sciences in Philadelphia and is Approved by the Research Advisory Committee as Fulfilling the Dissertation Requirements for the degree of

DOCTOR OF PHILOSPHY

March 25, 2015

Steven H. Neau, Ph. D.
Chairman, Research Advisory Committee

Rodney J. Wigent, Ph. D.
Member, Research Advisory Committe

Pardeep K. Gupta, Ph. D.
Member, Research Advisory Committe

Patrick J. Marsac, Ph. D.
Member, Research Advisory Committe

Alexander Sidorenko, Ph. D.
Reviewer

Dedicated to my parents Abdulaziz and Hessah Altamimi, my wife, Anhal, and my children Jomana and Lateen

Acknowledgments

"And He is Allah; there is no deity except Him. To Him is [due all] praise in the first [life] and the Hereafter. And His is the [final] decision, and to Him you will be returned". (Al-Qasas, 28:70)

Writing this thesis was a unique bequest from Allah and I counted as the greatest blessing of my life, so far.

I would like to express my immeasurable gratitude to my father and mother Abdulaziz & Hessah Altamimi. They are always emphasizing the values of knowledge and self-improvements. Thank you for your unconditional love, it always keeps me moving forward.

My sincere appreciation goes to my mentor Dr. Steven Neau. His theoretical training, practical training, scientific guidance, and great patience, have helped me become a reliable scientist. Thank you for investing the time and effort into my professional growth.

I am very thankful and grateful to my graduate committee members Dr. Rodney wigent, Dr. Paradeep Gupta, and Dr. Patrick Marsac and Dr. Alexander Sidorenko. Thank you for your scientific guidance, suggestions, and critiques that vastly contributed to my research.

I would like to acknowledge my supportive wife Anhal Altamimi. Your presence has made this scientific journey happier than I could imagine. You are truly the person I rely on and you always stand beside me. It is true that you are part of every success I acquire.

Thanks and deep appreciations, also, go to my siblings Aisha, Malak, Azhaar, Saud, Amal, Atheer, and Saad. We have been thorough a lot since the deterioration of my dad's health. Without you this thesis would not finish on time. Saud, you have proved yourself a true reliable man and you are the person I should, mostly, be proud of.

My life as a graduate student would not be as productive and fulfilling as it was without the company of different people to whom I carry tremendous gratitude. First and foremost, I would like to thank Mohammed Alamri and Mohammad alhashim for the support, motivation, and assistance one way or another. Chahinaz Kouba, thank you for your instructive demonstration of the DSC and HPLC. In addition, the thanks go to James Schwing, Anuja Rane, Matthew Bhar, Brian Rogers, Colin Pinto, Nikhil Loka, Nader Namazi, Kush Patel, Curie Javiya, Manasi Chawathe, and Abdulkareem Alanzi.

I would like to extend my special thanks to, my cousin and brother in law, Ibrahim Altamimi. His great assistance had helped in every way and I ask Allah to grant him every wishes.

Table of Contents

A. Preliminary sections

a. Title Page I

b. Abstract II

c. Certification Page IV

d. Dedication V

e. Acknowledgments VI

f. Table of Contents VII

g. List of Abbreviations XIII

h. List of Figures and Tables XVI

1. Chapter One: General Introduction 1

1.1. Solid state of the pharmaceutical ingredients 1

1.1.1. Glass forming ability 3

1.1.2. Glass transition temperature of amorphous solids 3

1.2. Factors that contribute to the crystallization tendency of amorphous solids 4

1.2.1. Molecular mobility 4

1.2.2. Configurational entropy 7

1.2.3. The influence of moisture on amorphous solids 10

1.3. Additives that influence the solubility of pharmaceutical solids 10

1.3.1 Drug dispersion as a potential strategy to improve solubility 11

1.3.2 Polymers influence on dispersed pharmaceutical solids 12

1.4. The thermodynamic of mixing for binary mixtures 15

1.4.1. Thermodynamics of the Regular Solution Theory 15

1.4.2. Flory-Huggins Theory for polymer solutions 17

1.4.3. Melting point depression theory 19

1.4.4. Solubility of crystalline drugs in amorphous polymers 20

1.5. Methods currently used to form solid dispersions 21

1.5.1. Lyophilization (freeze drying) 21

1.5.1.1. Freezing 22

1.5.1.2. Primary drying 22

1.5.1.3. Secondary drying 22

1.5.2. Spray drying 23

1.5.3. Melt extrusion 23

1.6. Research design 25

1.7. References 26

2. Chapter Two: Use of the Flory-Huggins Theory to predict the solubility of nifedipine and sulfamethoxazole in the triblock graft copolymer Soluplus® 32

2.1. Abstract 32

2.2. Keywords 33

2.3. Introduction 34

2.4. Materials 39

2.5. Methods 40

2.5.1. True density measurements 40

2.5.2. Differential scanning calorimetry 40

2.5.3. Thermogravimetric analysis 41

2.5.4. Melting point depression 41

2.5.5. Gibbs free energy of the drug-polymer mixture 42

2.5.6. Solubility prediction 43

2.5.7. Phase diagram construction 44

2.6. Results and discussion 47

2.6.1. Melting point depression 47

2.6.2. Gibbs free energy of mixing 56

2.6.3. Solubility prediction 60

2.6.4. Phase diagram 64

2.7. Conclusions 75

2.8. References 76

3. Chapter Three: A study to identify the contribution of Soluplus® component homopolymers to the solubilization of nifedipine and sulfamethoxazole using the melting point depression method 80

3.1. Abstract 80

3.2. Keywords 81

3.3. Introduction 82

3.4. Materials 85

3.5. Methods 86

3.5.1 Differential scanning calorimetry 86

3.5.2. Thermal gravimetrical analysis 87

3.5.3. Solubility of SMX and NIF in PEG 400 87

3.5.4. Melting point depression 88

3.5.5. Solubility prediction 89

3.6. Results and discussion 91

3.6.1. Melting point depression 91

3.6.2. Gibbs free energy 109

3.6.3. Predicted solubility 112

3.7. Conclusions 120

3.8. References 121

4. Chapter Four: Investigation of the in vitro characteristics of drug-Soluplus® and drug PEG 6000 dispersions when prepared using spray drying or lyophilization 125

4.1. Abstract 125

4.2. Keywords 126

4.3. Introduction 127

4.4. Materials 129

4.5. Methods 131

4.5.1 Preparation of a solid dispersion 131

4.5.1.a. Spray drying 131

4.5.1.b. Lyophilization 131

4.5.2. Differential scanning calorimetry 132

4.5.3. Scanning electron microscopy 132

4.5.4. Fourier transform infrared spectroscopy 132

4.5.5. Drug dissolution studies 133
4.5.5.1. Dissolution tests 133
4.5.5.2. Data analysis of release data 133
4.5.5.2.a. Mathematical models of release kinetics 133
4.5.5.2.b. Analysis of the drug release data 135
4.5.5.2.c. Comparison of release profiles 136
4.5.6. Drug stability studies 136
4.5.6.1. Storage conditions for stability studies 136
4.6. Results and discussion 137
4.6.1. Differential scanning calorimetry 137
4.6.1.a. Spray dried solid dispersion 138
4.6.1.b. Lyophilized solid dispersions 143
4.6.2. Drug stability studies 147
4.6.3. Scanning electron microscopy 152
4.6.4. Fourier transform infrared spectroscopy 156
4.6.5. Drug dissolution studies 164
4.6.6. Mathematical models for the release profiles 174
4.6.7. Comparison of release profiles 179
4.7. Conclusions 180
4.8. References 181
5. Appendix A: Chapter One supplemental information 187

6. Appendix B: Chapter Two supplemental information 195

7. Appendix C: Chapter Three supplemental information 204

8. Appendix D: Chapter Four supplemental information 222

List of Abbreviations

DSC	Differential Scanning Calorimetry
SMX	Sulfamehtoxazole
NIF	Nifedipine
Soluplus®	Polymer consists of Polyvinyl caprolactam, polyvinyl acetate, and polyethylene glycol
PEG6000	Polyethylene glycol
PCL	Polyvinyl caprolactam
PVA	Polyvinyl acetate
T_m	Melting temperature
$T_{m\ mix}$	Melting temperature of the mixture
$T_{m\ pure}$	Melting temperature of the pure substance
T_{onset}	The onset of melting endotherm
T_{end}	The end of melting endotherm
T_g	Glass transition temperature
ϕ_{drug}	Volume fraction of the drug
$\phi_{polymer}$	Volume fraction of the polymer
ΔC_p	Specific heat capacity
ΔH_f	Enthalpy of fusion
m	Ratio of the molar volume of the polymer to the molar volume of the drug
χ	Flory-Huggins interaction parameter

ΔG_m	Gibbs free energy of mixing
γ_{drug}	The activity coefficient of the drug
X_{drug}	Temperature difference in a sample
ΔT	Mole fraction solubility of the drug
β	Heating rate
ρ_{th}	Thermal resistance
Ø	Heat flow rate
m	Sample mass
MW	Molecular weight
SIF	Simulated intestinal fluid
SGF	Simulated gastric fluid
X_1	Drug mole fraction solubility
M_0	The amount of drug release at the beginning
M_t	The amount of drug release at time t
M_∞	The amount of drug release at infinite time
k_0	Zero order rate constant
k_1	First order rate constant
k_H	Higuchi rate constant
k_{HC}	Hixson-Crowell rate constant
k_{RP}	Ritger-Peppas rate constant
f_2	Similarity factor

R_i	Percentage drug released for the reference product
T_i	Percentage drug released from the comparison product at different time points
R	Universal gas constant
T_k	Kauzman temperature
MDSC	Modulated differential scanning calorimetry
$\Delta C_{p\ conf}$	Configurational heat capacity at T_g
M	Molarity
W_1	Weight fraction of the amorphous drug
W_2	Weight fraction of the amorphous polymer
ρ_1	Density of the amorphous drug
ρ_2	Density of the amorphous polymer
T_c	Collapse temperature
T_{eu}	Eutectic temperature
MPD	Melting point depression

List of Figures and Tables

1.	**Chapter One**	1
Figure 1.1.	Schematic presenting the change of volume, enthalpy, and free energy with temperature	2
Figure 1.2.	Typical DSC thermogram	5
Figure 1.3.	Depiction of the heat capacity change for crystalline and amorphous material as the temperature goes through the T_g	10
Figure 1.4.a.	Soluplus® (BASF, Tarrytown, NY) is a graft copolymer with polyvinyl caprolactam (i), polyvinyl acetate (m), and polyethylene glycol (n) in the ratio 57:30:13, respectively	14
Figure 1.4.b.	The structure that amphiphilic copolymers are likely to take when forming micelles	14
2.	**Chapter Two**	32
Figure 2.1.	Chemical structure of a. Soluplus®, b. nifedipine, and c. sulfamethoxazole	38
Figure 2.2.	Phase diagram with glass transition temperatures and melting point depression curve	45
Table 2.1.	Material properties	46
Figure 2.3.	DSC thermograms for a. nifedipine , b. sulfamethoxazole, and c. Soluplus®	47
Figure 2.4.	Results from thermogravimetric analysis reveal the degradation temperature for Soluplus®, sulfamethoxazole, and nifedipine.	48
Figure 2.5.	DSC results for T_{onset} (a) and T_{end} (b) of the melting endotherm for sulfamethoxazole mixtures with 0, 5, 10, 16.7, 20, and 25 % w/w Soluplus®, presented as a function of the volume fraction of Soluplus®	49
Figure 2.6.	DSC results for T_{onset} (a) and T_{end} (b) of the melting endotherm for nifedipine mixtures with 0, 5, 10, 16.7, 20, and 25 % w/w Soluplus®, presented as a function of the volume fraction of Soluplus®	50

Figure 2.7.	DSC results for SMX (a) and NIF (b) showing the enthalpy of fusion for each drug at different concentrations of Soluplus®, presented as a function of the volume fraction of Soluplus®. Numbers between the parentheses represent the standard error	51
Figure 2.8.	The interaction parameter, χ, calculated using the T_{onset} and T_{end} for SMX (a) and NIF (b). Numbers between the parentheses represent the standard error	54
Figure 2.9.	Temperature-normalized Gibbs free energy of mixing for SMX (a) and NIF (b) with Soluplus® at different χ values	57
Figure 2.10.	Temperature-normalized Gibbs free energy of mixing for SMX (a) and NIF (b) with Soluplus® at particular χ value and different MW of the polymer	58
Figure 2.11.	Determination of the mole fraction solubility for SMX (a) and NIF (b) in Soluplus at 298 K	60
Table 2.2.	Predicted solubility of sulfamethoxazole and nifedipine in Soluplus® expressed in % w/w units	62
Figure 2.12.a.	Phase diagram for SMX with Soluplus® where the curves predicted using Eq. 2.2 were extrapolated to intersect the $T_{g\,mix}$ curve	65
Figure 2.12.b.	Phase diagram for NIF with Soluplus® where the curves predicted using Eq. 2.2 were extrapolated to intersect the $T_{g\,mix}$ curve	66
Table 2.3.	Predicted solubility using the phase diagram method for sulfamethoxazole and nifedipine in Soluplus® expressed in % w/w units	70
Figure 2.13.	Phase diagram for NIF with VA64 where the MPD curve was extrapolated to the $T_{g\,mix}$ curve	71
3.	**Chapter Three**	80
Figure 3.1.	Chemical structures of a. Soluplus®, b. nifedipine, c. sulfamethoxazole, d. polyethylene glycol, e. polyvinyl acetate, and f. polyvinyl caprolactam	84
Table 3.1.	Properties of the materials in the study	90
Figure 3.2.	The DSC thermograms for (from top to bottom): nifedipine, sulfamethoxazole, Soluplus®, polyethylene glycol, and polyvinyl acetate	91
Figure 3.3.	The DSC thermogram for lyophilized polyvinyl caprolactam	93

Figure 3.4.	The TGA thermograms for nifedipine, sulfamethoxazole, Soluplus®, polyethylene glycol, polyvinyl acetate, and polyvinyl caprolactam	94
Figure 3.5.	DSC results for SMX (a) and NIF (b), showing the onset melting temperature for each drug at different concentrations of PEG 6000, presented as a function of the volume fraction of PEG 6000	95
Figure 3.6.	DSC results for SMX (a) and NIF (b), showing the onset melting temperature for each drug at different concentrations of PVAc, presented as a function of the volume fraction of PVAc	96
Figure 3.7.	DSC results for SMX (a) and NIF (b), showing the melting temperature for each drug at different concentrations of PCL, presented as a function of the weight percentage of PCL	97
Figure 3.8.	DSC results for SMX (a) and NIF (b), showing the enthalpy of melting for each drug at different concentrations of PEG 6000, presented as a function of the volume fraction of PEG 6000. Numbers between the parentheses represent the standard error	98
Figure 3.9.	DSC results for SMX (a) and NIF (b), showing the enthalpy of melting for each drug at different concentrations of PVAc, presented as a function of the volume fraction of PVAc. Numbers between the parentheses represent the standard error	99
Figure 3.10.	DSC results for SMX (a) and NIF (b), showing the enthalpy of melting for each drug at different concentrations of PCL, presented as a function of the volume fraction of PCL. Numbers between the parentheses represent the standard error	100
Figure 3.11.	Plots to obtain the interaction parameter, χ, for (a) SMX-PEG6000, (b) NIF-PEG6000 binary mixtures. Numbers between the parentheses represent the standard error	102
Figure 3.12.	Plots to obtain the interaction parameter, χ, for (a) SMX-PVAc, (b) NIF-PVAc binary mixtures. Numbers between the parentheses represent the standard error	103
Table 3.2.	The interaction parameter, χ, for each binary mixture	104
Figure 3.13.	T_g temperature-composition profiles for PCL with (a) SMX, and (b) NIF	107
Figure 3.14.	Predicted temperature normalized free energy of mixing for (a) SMX and (b) NIF using Eq. 3.2 vs. Φ of PEG 6000 using different values for the interaction parameter	110
Figure 3.15.	Predicted temperature normalized free energy of mixing for (a) SMX and (b) NIF using Eq. 3.2 vs. Φ of PVAc using different values for	111

	the interaction parameter	
Table 3.3.	The predicted solubility of each drug in Soluplus® and its component homopolymers and the experimental solubility in PEG 400	113
Figure 3.16.a	Phase diagram for SMX with PVAc where the curve predicted using Eq. 3.1 was extrapolated to intersect the $T_{g\,mix}$ curve	115
Figure 3.16.b	Phase diagram for NIF with PVAc where the curve predicted using Eq. 3.1 was extrapolated to intersect the $T_{g\,mix}$ curve	116
4.	**Chapter Four**	125
Figure 4.1.	Chemical structures of a. nifedipine, b. sulfamethoxazole, and c. polyethylene glycol, and d. Soluplus®	129
Table 4.1.	Materials properties	130
Figure 4.2.	DSC thermograms for (top to bottom) sulfamethoxazole, PEG 6000, Soluplus®, and nifedipine	137
Figure 4.3.a.	DSC thermograms of sulfamethoxazole:Soluplus® spray dried mixtures at a mass ratio of 1:1, 1:5, and 1:9	139
Figure 4.3.b.	DSC thermograms of sulfamethoxazole:PEG 6000 spray dried mixtures at mass ratios of 1:5 and 1:9	140
Figure 4.4.a.	DSC thermograms of nifedipine:Soluplus® spray dried mixtures at mass ratios of 1:1, 1:5, and 1:9	141
Figure 4.4.b.	DSC thermograms for nifedipine:PEG 6000 spray dried mixtures at mass ratios of 1:5, and 1:9	142
Figure 4.5.a.	DSC thermograms for sulfamethoxazole:Soluplus® lyophilized mixtures at mass ratios of 1:1, 1:5, and 1:9	143
Figure 4.5.b.	DSC thermograms for the sulfamethoxazole:PEG 6000 lyophilized mixtures at mass ratios of 1:1, 1:5, and 1:9	144
Figure 4.6.a.	DSC thermograms for the nifedipine:Soluplus® lyophilized mixtures at mass ratios of 1:1, 1:5, and 1:9	145
Figure 4.6.b.	DSC thermograms for nifedipine:PEG 6000 lyophilized mixtures at mass ratios of 1:1, 1:5, and 1:9	146
Figure 4.7.a.	DSC thermograms for SMX mixtures with Soluplus® and with PEG 6000 at a mass ratio of 1:9 stored for six months at 0% RH and 25 °C	148
Figure 4.7.b.	DSC thermograms for NIF mixtures with Soluplus® and with PEG 6000 at a mass ratio of 1:9 stored for six months at 0% RH and 25 °C	149

Figure 4.7.c.	DSC thermograms for SMX mixtures with Soluplus® and with PEG 6000 at a mass ratio of 1:9 stored for six months at 0% R.H. and 50 °C	150
Figure 4.7.d.	DSC thermograms for NIF mixtures with Soluplus® and with PEG 6000 at a mass ratio of 1:9 stored for six months at 0% RH and 50 °C	151
Figure 4.8.	Scanning electron microscopy images showing the morphology of the neat drugs and polymers, and their respective dispersed mixtures	154
Figure 4.9.a.	FTIR analysis for the used materials	156
Figure 4.9.b.	FTIR analysis for SMX-polymer mixtures (S denotes spray dried, and L denotes lyophilized)	157
Figure 4.9.c.	FTIR analysis for NIF-polymer mixtures (S denotes spray dried, and L denotes lyophilized)	158
Table 4.2.	The characteristic vibrational stretching wavenumbers for functional groups found in the materials and their corresponding values from the literature	163
Figure 4.10.a.	Sulfamethoxazole and spray dried SMX with Soluplus® or PEG 6000 in SIF (n=3). SMX alone in deionized water was added for comparison. Error bars represent standard deviation	165
Figure 4.10.b.	Sulfamethoxazole and spray dried SMX with Soluplus® or PEG 6000 in SGF (n=3). Error bars represent standard deviation	165
Figure 4.10.c.	Sulfamethoxazole and lyophilized SMX with Soluplus® or PEG 6000 in SIF (n=3). Error bars represent standard deviation	167
Figure 4.10.d.	Sulfamethoxazole and lyophilized SMX with Soluplus® or PEG 6000 in SGF (n=3). Error bars represent standard deviation	167
Figure 4.11.a.	Nifedipine and spray dried NIF with Soluplus® or PEG 6000 in SIF (n=3). NIF alone in deionized water was added for comparison. Error bars represent standard deviation	170
Figure 4.11.b.	Nifedipine and spray dried NIF with Soluplus® or PEG 6000 in SGF (n=3). Error bars represent standard deviation	170
Figure 4.11.c.	Nifedipine and lyophilized NIF with Soluplus® or PEG 6000 in SIF (n=3). Error bars represent standard deviation	172
Figure 4.11.d.	Nifedipine and lyophilized NIF with Soluplus® or PEG 6000 in SGF (n=3). Error bars represent standard deviation.	172
Table 4.3.	The kinetic models for dissolution of SMX or release of SMX from Soluplus® or PEG 6000 dispersions prepared using spray drying or lyophilization techniques. ± standard errors ($p < 0.05$)	176

Table 4.4.	The kinetic models for dissolution of SMX or release of SMX from Soluplus® or PEG 6000 dispersions prepared using spray drying or lyophilization techniques. ± standard errors ($p < 0.05$). * For ($p > 0.05$)	177
Table 4.5.	The release profile comparisons for SMX-polymer mixtures.	178
Table 4.6.	The release profile comparisons for NIF-polymer mixtures	178
5.	**Appendix A**	187
Figure 5.1	Heat capacity for SMX as a function of temperature. The area of discontinuity represents sulfamethoxazole melting temperature	187
Figure 5.2.	Heat capacity for NIF as a function of temperature. The area of discontinuity represents nifedipine melting temperature	188
Figure 5.3.	Experimental 37 ^{o}C equilibrium solubility of sulfamethoxazole in simulated gastric fluid, intestinal gastric fluid, and water	189
Figure 5.4.	Experimental 37 ^{o}C equilibrium solubility of nifedipine in simulated gastric fluid, intestinal gastric fluid, and water	190
Figure 5.5.	Experimental 37 ^{o}C concentration of sulfamethoxazole in simulated intestinal fluids in the presence of different Soluplus® concentrations	191
Figure 5.6.	Molar solubilization capacity of Soluplus® with sulfamethoxazole in simulated intestinal fluids	192
Figure 5.7.	Experimental 37 ^{o}C concentration of nifedipine in simulated intestinal fluids in the presence of different Soluplus® concentrations	193
Figure 5.8.	Molar solubilization capacity of Soluplus® with nifedipine in simulated intestinal fluids	194
6.	**Appendix B**	195
Figure 6.1.	DSC thermograms of the melting endotherm for nifedipine mixtures with 0, 5, 10, 16.7, 20, and 25 % w/w Soluplus®	195
Figure 6.2.	DSC thermograms of the melting endotherm for sulfamehtoxazole mixtures with 0, 5, 10, 16.7, 20, and 25 % w/w Soluplus®	196
Figure 6.3.	DSC thermogram representing the onset of melting at 20% w/w for SMX-Soluplus® mixture	197
Figure 6.4.	DSC thermogram representing the T_{end} of melting at 20% w/w for SMX-Soluplus® mixture	198

Table 6.1.	DSC onset of melting endotherm for SMX-Soluplus® mixtures	199
Table 6.2.	DSC onset of melting endotherm for NIF-Soluplus® mixtures	200
Figure 6.5.	The interaction parameter, χ, calculated using the T_{onset} for NIF with VA64. Number between the parenthesis represents the standard error	201
Figure 6.6.	The excess, non-ideal, Gibbs free energy of mixing for SMX in Soluplus®. This plot shows the impact of the enthalpy after subtracting the entropy from equation 2.4	202
Figure 6.7.	The excess, non-ideal, Gibbs free energy of mixing for NIF in Soluplus®. This plot shows the impact of the enthalpy after subtracting the entropy from equation 2.4	203
7.	**Appendix C**	204
Figure 7.1.	DSC thermograms of the melting endotherm for nifedipine mixtures with 0, 5, 10, 16.7, and 20 % w/w PEG 6000	204
Figure 7.2.	DSC thermograms of the melting endotherm for nifedipine mixtures with 0, 5, 10, 16.7, 20, and 25 % w/w PVAc	205
Figure 7.3.	DSC thermograms of the melting endotherm for nifedipine mixtures with 0, 5, 10, 16.7, 20, and 25 % w/w PCL	206
Figure 7.4.	DSC thermograms of the melting endotherm for sulfamethoxazole mixtures with 0, 5, 10, and 12.5 % w/w PEG 6000	207
Figure 7.5.	DSC thermograms of the melting endotherm for sulfathoxazole mixtures with 0, 5, 10, 16.7, 20, and 25 % w/w Soluplus®	208
Figure 7.6	DSC thermograms of the melting endotherm for sulfamethoxazole mixtures with 0, 5, 10, 16.7, 20, and 25 % w/w PCL	209
Figure 7.7.	The predicted temperature normalized Gibbs free energy of mixing for PEG 6000 and SMX, with inclusion of different M_W of PEG.	210
Figure 7.8.	The predicted temperature normalized Gibbs free energy of mixing for PEG 6000 and NIF, with inclusion of different M_W of PEG	211
Figure 7.9.	The excess, non-ideal, Gibbs free energy of mixing for SMX in PEG 6000. This plot shows the impact of the enthalpy after subtracting the entropy from equation 3.2	212
Figure 7.10.	The excess, non-ideal, Gibbs free energy of mixing for NIF in PEG 6000. This plot shows the impact of the enthalpy after subtracting the entropy from equation 3.2	213

Figure 7.11.	The excess, non-ideal, Gibbs free energy of mixing for SMX in PVAc. This plot shows the impact of the enthalpy after subtracting the entropy from equation 3.2	214
Figure 7.12.	The excess, non-ideal, Gibbs free energy of mixing for NIF in PVAc. This plot shows the impact of the enthalpy after subtracting the entropy from equation 3.2	215
Figure 7.13.	Determination of mole fraction solubility for SMX in PEG 6000 at 298 K	216
Figure 7.14.	Determination of mole fraction solubility for NIF in PEG 6000 at 298 K	217
Figure 7.15.	Determination of mole fraction solubility for SMX in PVAc at 298 K	218
Figure 7.16.	Determination of mole fraction solubility for NIF in PVAc at 298 K	219
Figure 7.17.	Standard curve representing the absorbance of different concentrations of SMX in PEG 400 at 260 nm	220
Figure 7.18.	Standard curve representing the absorbance of different concentrations of NIF in PEG 400 at 350 nm	221
8.	**Appendix D**	222
Figure 8.1.	DSC thermograms of sulfamethoxazole:PEG 6000 spray dried mixtures at mass ratios of 1:5 and 1:9	222
Figure 8.2.	DSC thermograms for SMX mixtures with Soluplus® and with PEG 6000 at a mass ratio of 1:9 stored for six months at 0% RH and 25 °C	223
Figure 8.3.	DSC thermograms for SMX mixtures with Soluplus® and with PEG 6000 at a mass ratio of 1:9 stored for six months at 0% R.H. and 50 °C	224
Figure 8.4.	DSC thermograms for NIF mixtures with Soluplus® and with PEG 6000 at a mass ratio of 1:9 stored for six months at 0% RH and 25 °C	225
Figure 8.5.	DSC thermograms of sulfamethoxazole:PEG 6000 spray dried mixtures at mass ratios of 1:5 and 1:9	226
Figure 8.6.	Standard curve representing the absorbance of different concentrations of SMX in SIF at 260 nm	227
Figure 8.7.	Standard curve representing the absorbance of different concentrations of SMX in SGF at 260 nm	228

Figure 8.8.	Standard curve representing the absorbance of different concentrations of SMX in water at 260 nm	229
Figure 8.9.	Standard curve representing the absorbance of different concentrations of NIF in SIF at 240 nm	230
Figure 8.10.	Standard curve representing the absorbance of different concentrations of NIF in SGF at 240 nm	231
Figure 8.11.	Standard curve representing the absorbance of different concentrations of NIF in water at 240 nm	232

1. General Introduction

1.1. Solid state of pharmaceutical ingredients

Advancements in drug discovery, such as combinatorial chemistry and high-throughput screening, often lead to potential drug candidates that lack an adequate aqueous solubility. Due to this growing challenge, development of new methods by which the pharmaceutical industry can improve solubility or the delivery of poorly soluble drugs is crucial. In addition, the drug solid state form determines its physicochemical properties, such as melting temperature, stability, dissolution rate, and solubility [1-8].

Solubility is a process that implies an equilibrium state between a solvent and a solute to form a solution. Also, it is defined as the maximum concentration the drug can achieve in a given solvent, i.e., a saturation limit [9]. The lattice energy within a solid drug dramatically affects its solubility. Higher lattice energies result in lower solubilities in any solvent. In particular, an amorphous compound can have a solubility that is a hundred or even a thousand times that of its crystalline counterpart [10] due to the absence of long range intra-molecular order in the amorphous material.

Crystalline drugs have a wel defined crystal lattice and ordered long range intra-molecular packing. On the contrary, amorphous drugs have no defined lattice and have at best weak short range order to their molecular arrangement [11]. Forming an amorphous material is practically easy when the following apply:

(i) Thermodynamics: The free energy barrier of the amorphous materials is large enough to prevent recrystallization.

(ii) Kinetics: The nucleation and the crystallization rate are slow, likely due to a mechanism that restricts the mobility of the molecules.

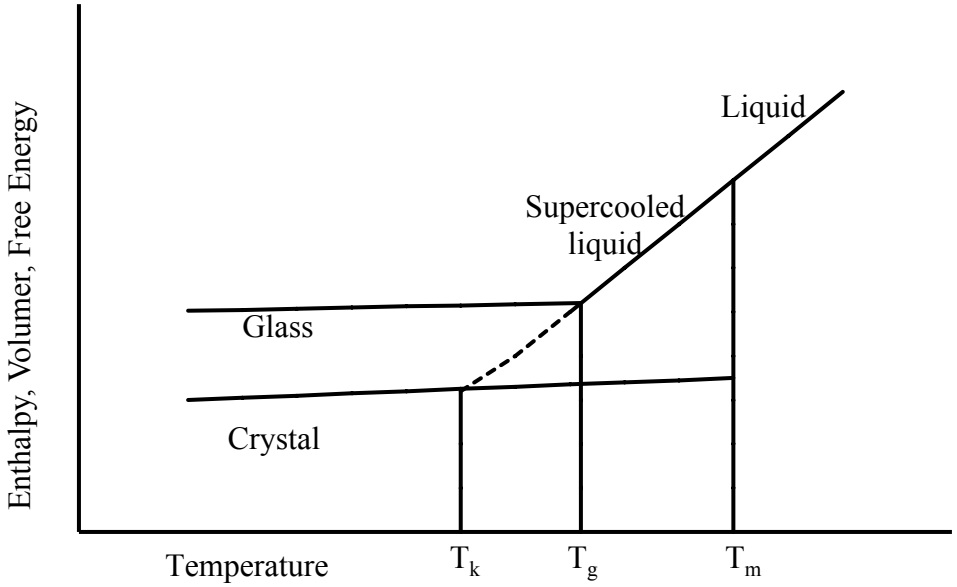

Figure 1.1. Schematic presenting the change of volume, enthalpy, or free energy with temperature [12].

Figure 1.1., shows that heating the crystal gradually increases the enthalpy, volume, or free energy until the melting point temperature is reached at T_m. A vast increase in the enthalpy is found at T_m as the liquid is formed. Rapidly cooling the liquid below the melting temperature renders a supercooled liquid. Maintaining the cooling rate will bring the supercooled liquid to the glass transition temperature, T_g. Below the glass transition temperature, a glassy state is found. Glassy materials have relatively higher enthalpy, volume, and free energy than do their crystalline counterparts. The Kauzman temperature, T_k, represents the temperature at which the supercooled liquid line intersects the crystal state line. This suggests that the existence of a stable glass is found at some temperature below the T_g [13].

1.1.1. Glass forming ability

Chemicals are generally classified based on their glass forming. In addition, glass-former compounds are divide into (a) stable glass and (b) nonstable-glass formers. Nonglass-formers are characterized by crystallization throughout the cooling of the molten compound and show no distinctive exothermic peak during thermal analysis. Glass formers, however, show a recrystallization peak above the T_g or present the T_g only during a heating step [14, 15]. It was found that the organic chemicals with a molecular weight (M_W) above 300 g/mole are practically easy to prepare in their amorphous form using standard thermal procedures. However, chemicals with a M_W less than 200 g/mole are practically difficult to form as a glass. For chemicals with a M_W in the range of 200-300 g/mole, it is difficult to predict their glass forming ability [14, 15].

1.1.2. Glass transition temperature of amorphous solids

Amorphous solids exhibit some solid and some liquid properties. Within a certain temperature range, amorphous solids go from the glassy state (solid-like) to the supercooled liquid state (liquid-like). In calorimetry the temperature range over which this transition takes place is called the glass transition temperature, T_g [16]. This temperature range varies based on the heating rate and some prefer to report T_g using the onset, the midpoint, or the end temperature for the transition [17, 18]. Determination of a specific glass transition temperature depends on the experimental techniques used to assess this temperature. The importance of the T_g arises from its ability to characterize pure amorphous solids and also solid dispersions that have amorphous content. When amorphous materials are found in a particular temperature, their properties vary

substantially based on the temperature difference from their glass temperatures [19]. In addition, T_g can be used as a potential indicator for instability of different formulations. In particular, it was found that nearly all drug candidates and their amorphous dispersions in a carrier polymer are more likely to experience instability due to chemical degradation when stored above the respective glass transition temperature [20].

Different thermal analysis techniques can be employed to measure the glass transition temperature. Differential scanning calorimetry (DSC) is, by far, the mostly widely used technique to assess the T_g of amorphous solids. It is important to note that the T_g value is dependent on existing thermal history of the selected substance and the employed heating rate during the analysis [19, 21, 22]. The report from DSC analysis is called a thermogram and a typical thermogram is presented in Figure 1.2.

1.2. Factors that contribute to the crystallization tendency of amorphous solids

1.2.1. Molecular mobility

Two steps are necessary for successful recrystallization of amorphous solids: nucleation followed by crystal growth. These steps require a specific arrangement of the molecules to form an aggregate. The term diffusion can be used to describe the migration of molecules towards each other to form a stable nucleus of molecules arranged in a pattern that leads to crystal formation (nucleation) [20]. When amorphous solids are in the glassy state, their respective thermodynamic potentials are relatively large. In particular, a glass has excess free volume relative to its crystalline counterpart, and this allows molecular mobility even below the T_g. Literature has shown that the possibility of recrystallization

is high even when the amorphous solids are kept 55 °C below their corresponding T_g [19].

The molecular mobility mainly depends on temperature. When the molten solid is cooled fast enough to the supercooled liquid state, two phenomena are observed: the liquid viscosity substantially increases and the free volume significantly decreases. It has been reported that viscosity can go from 10^{12} Pa s below the T_g to as low as 10^{-4} Pa s above the melting temperature, T_m [23, 24].

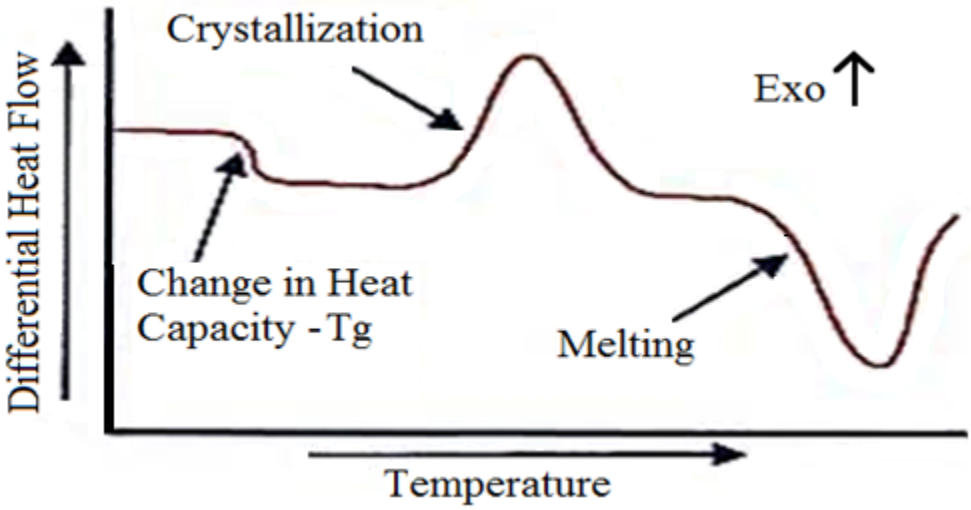

Figure 1.2. Typical DSC thermogram where T_g represents the temperature at which there is a change in heat capacity between the glassy and supercooled (rubbery) state. More often than not amorphous material will experience crystallization over which the molecules release excess energy, resulting in an exothermic peak. Crystals eventually melt due to infused heat resulting in an endothermic peak [25].

The influence of the molecular mobility on the recrystallization rate of amorphous solids can be quantitatively evaluated. Comparing the recrystallization rate to the structural relaxation time, τ, which is a parameter that indicates molecular mobility, is widely used approach. The most recognized model that relates temperature, T, and the structural relaxation time, τ, is the Adam-Gibbs-Vogel model. Equation 1.1., describes the molecular relaxation time of glassy solids as a function of temperature below the T_g.

$$\tau = \tau_0 \exp\left(\frac{DT_0}{T(1-\frac{T_0}{T_f})}\right) \tag{1.1}$$

where τ is the molecular relaxation time, τ_0 is the relaxation time at high temperatures, and T is the temperature. T_f is the fictive temperature which is defined as the temperature where the configuration entropy for the liquid is similar to that of the real glass at a specific temperature, D, and T_0 are constants related to the fragility of the material [26]. The relationship that best describes the dependence of molecular relaxation time on temperatures above the T_g is the Vogel-Tammann-Fulcher model (Eq. 1.2.):

$$\tau = \tau_0 \exp\left(\frac{DT_0}{T-T_0}\right) \tag{1.2}$$

The equation for viscosity is similar [27], Equation 1.3:

$$\eta = A \exp\left(\frac{DT}{T-T_o}\right) \tag{1.3}$$

The value of T_0 is believed to equal the Kauzman temperature, T_k, and A is considered a constant [24, 28].

1.2.2. Configurational entropy

Heat capacity at constant pressure, C_p, is one of the accessible thermodynamic parameters, and it has proved to be of importance in the characterization of amorphous solids. In particular, configurational heat capacity, $C_{p\,conf}$, is an indicator of the nonvibrational molecular mobility and overall molecular complexity. The difference between the crystalline heat capacity C_p^c and the amorphous heat capacity C_p^a at T_g equals the configurational heat capacity (see Figure 1.3). The correlation between the increase in $C_{p\,conf}$ and the materials fragility has been reported. The fragility is an indicator of the relaxation time that a compound needs to become a liquid [29, 30]. It is important to point out, however, that some exceptions for such a correlation has been reported in the literature [31]. When integrating the configurational heat capacity with temperature, other configurational thermodynamic parameters can be calculated (Eqs. 1.4-1.6):

$$H_c = \Delta H_m + \int_{T_m}^{T} C_{p\,conf}\, dT \tag{1.4}$$

$$S_c = \Delta S_m + \int_{T_m}^{T} \frac{C_{p\,conf}}{T} dT \tag{1.5}$$

$$G_c = H_c - TS_c \tag{1.6}$$

where ΔH_m and ΔS_m are the enthalpy and entropy of melting. The importance of such configurational quantities is detailed in Shamblin et al., [30]. The authors tested four chemicals, namely indomethacin, sorbitol, sucrose, and trehalose. The crystalline chemical was converted to a completely amorphous form by rapidly cooling the melts at 20 deg/min in the DSC, or by lyophilizing the aqueous solution. Modulated differential

scanning calorimetry (MDSC) was employed to measure the heat capacity of the crystalline and the amorphous forms. They found that the heat capacity of the crystalline form was lower than the amorphous counterpart. In addition, the difference in heat capacity was significant at the T_g. On the basis of the configurational heat capacity values, sorbitol (has the higher value) and indomethacin (has the lower value) were found to be most and least fragile of the four compounds, respectively.

Above the T_g, however, the configurational heat capacity is expected to be generally dependent on temperature Eq. 1.7:

$$C_{p\,conf}(T) = \frac{K}{T} \tag{1.7}$$

where K is a constant.

The Kauzman temperature, T_K, is the temperature at which the difference between the supercooled entropy and the crystal entropy is minimal [32]. Therefore, Eq. 1.7., allows the estimation of $C_{p\,conf}$ between the crystal and the supercooled liquid at the melting temperature. Using the configuration entropy and enthalpy yields predicted values for T_k, as shown in Equation 1.8, and Equation 1.9:

$$\frac{1}{T_{KS}} = \frac{1}{T_m}\left(1 + \frac{\Delta H_m}{K}\right) \tag{1.8}$$

$$\frac{1}{T_{KH}} = \frac{1}{T_m}\exp\left(\frac{\Delta H_m}{K}\right) \tag{1.9}$$

where T_{KS} is the Kauzman temperature calculated using the configurational entropy, and T_{KH} is the Kauzman temperature calculated based on the configurational enthalpy. The Kauzman temperature was found to be lower when the configurational enthalpy was used. However, they suggested that using the configurational entropy should be sufficient when molecular movement is restricted.

Neau et al., [33] have suggested that $C_{p\,conf}$ can be approximated by the heat capacity difference between the liquid and crystalline forms at the melting temperature. In their procedure, an exactly weighed empty pan and lid served as the reference. The sample and the reference are isothermally equilibrated followed by a heating rate of 1 deg/min for at least 10 min and then equilibrated isothermally for at least 2 min. The previous cycle was repeated to provide the heat capacity over at least a thirty degree range before and after the melting temperature. DSC can measure the heat provided to the sample cell as opposed to the reference cell, resulting in a Δq_s. The heat capacity at each temperature can be calculated using Equation 1.10:

$$\Delta q_s = \frac{m\bar{C}_p \Delta T}{M_W} \tag{1.10}$$

where m is the sample mass, M_W is sample molecular weight, and ΔT is temperature range of the run. $\bar{C}_p$ is the molar heat capacity at constant temperature. The temperature reported for each temperature range was the midpoint temperature of the respective range.

Experimental data for heat capacity difference at T_m for sulfamethoxazole SMX and nifedipine NIF can be found in the supplemental section A, Figures 1. and 2.

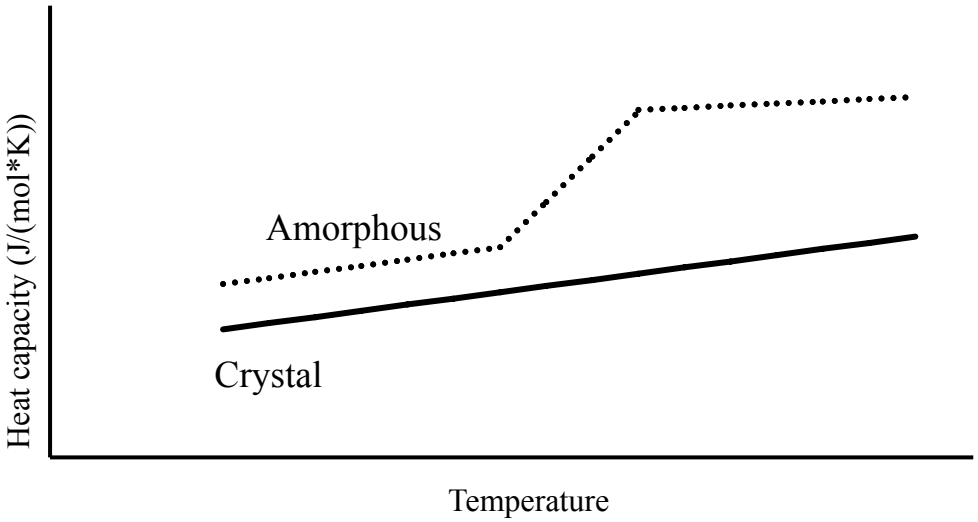

Figure 1.3. Depiction of the heat capacity change for crystalline and amorphous material as the temperature goes through the T_g.

1.2.3. The influence of moisture on amorphous solids

The presence of moisture changes the T_g value for amorphous materials. Water increases the molecular mobility and, therefore, depresses the glass transition temperature. Not only does water affect the T_g, but it is likely to be linked to chemical instability [34, 35].

Hancock et al., [36] were able to correlate water content in amorphous pharmaceuticals to physicochemical changes. The authors found that water acted as a profound plasticizer with a resultant rapid decrease in T_g as the water content increased. It is important to point out, however, nearly constant T_g was achieved at higher water content. They concluded that the plasticizing effect of water is similar to other small molecular weight molecules and no specific interaction was involved.

1.3. Additives that influence the solubility of pharmaceutical solids

The drug permeability and solubility profoundly influence its oral bioavailability. The Noyes-Whitney equation (Eq. 1.11) provides insight into how the dissolution rate can be improved [37, 38]:

$$\frac{dm}{dt} = \frac{AD(C_s - C)}{h} \tag{1.11}$$

where dm/dt is the dissolution rate, h is the boundary layer thickness of the dissolving material, A and D are the surface area and the diffusion coefficient, respectively, C_s is the drug solubility in the dissolution medium, and C is the drug current concentration.

Reducing the particle size dramatically improves the surface area of exposure to the dissolution medium and, therefore, is crucial to improving the dissolution rate. In addition, maintaining sink conditions will ensure the greatest difference between C_s and C to improve the dissolution rate.

Goldberg et al., have published a series of articles reporting a significant increase in the dissolution of eutectic mixtures that eventually led to overall improvement in the drug solubility. The eutectic mixture was believed to produce finer particles with better wettability in the dissolution medium [39-42].

1.3.1. Drug dispersion as a potential strategy to improve solubility

A dispersion is a product that includes at least two different components in the mixture and one of the components can be reasonably evenly distributed in the other. For a pharmaceutical solid dispersion, it is fair to expect that one component is a hydrophobic

crystalline drug and the other component is a hydrophilic carrier [43]. Different chemical compounds have been used to improve drug solubility; examples include citric acid, urea, dextrose, polyvinyl pyrrolidone (PVP), polyethylene glycol (PEG), and hydroxypropyl methylcellulose (HPMC) [44].

It is important to point out, however, that solid dispersions are broadly classified to eutectic mixtures and solid solutions. Eutectic mixture consists of two crystalline components that are completely miscible in the liquid form and crystallize simultaneously, at a specific mass ratio, at the same exact rate upon cooling. A solid solution, on the other hand, is a one phase system regardless of the number of components. The choice of hydrophilic carrier component, however, determines the dissolution rate of the dispersed drug [44].

The chemical used as the carrier has changed through the years. Initially, carriers were small molecular weight crystalline molecules, then large molecular weight amorphous molecules, and most recently surfactant and self-emulsifying polymer carriers [43]. For solid dispersions, a reduction in the crystalline particle size was believed to be the major contribution to the improved dissolution rate and overall solubility. Later, it was speculated that other factors, such as formation of amorphous drug, enhanced wettability for the drug, and carriers that served as co-solvents contributed to enhanced drug concentrations in solution [44].

1.3.2. Polymer influence on dispersed pharmaceutical solids

A polymer can be defined literally as many –mers (the chemical unit of a polymer), where the -mers are repeated monomer units. However, the monomers might be

chemically altered when they participate in the polymer chemical structure. Polymers consist of many of these small molecular weight monomers that are connected covalently to form a high molecular weight material. When the number of connected monomers is less than 10, the molecule is considered an oligomer. Polymers can be classified based on their structure as homopolymers or copolymers. Homopolymers consist of only one type of monomer and copolymers have two or more chemically different monomers [45]. Polymers can have different shapes, including linear polymers such as cellulose, closed rings such as cyclodextrins, branched polymers (or graft copolymers) such as xanthan gum, branching polymers such as the dendrimers, and cross-linked polymers, such as Carbopol, that form a network.

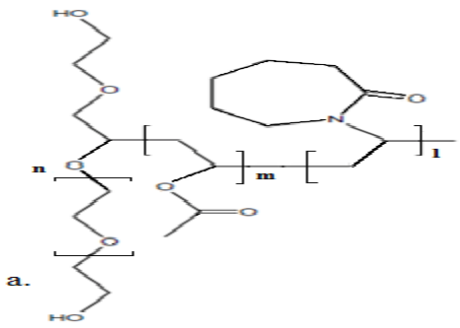

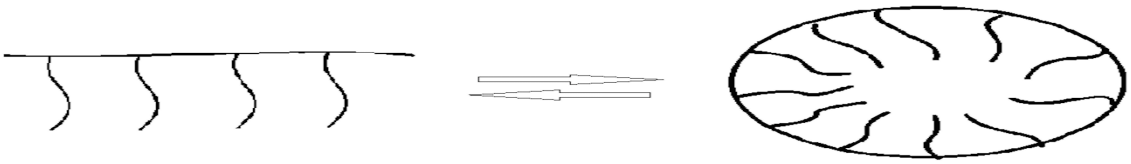

b.

Figure 1.4.a. Soluplus® (BASF, Tarrytown, NY) is a graft copolymer with polyvinyl caprolactam (l), polyvinyl acetate (m), and polyethylene glycol (n) in the ratio 57:30:13, respectively. In addition, 1, m, and n are 484, 412, and 349, respectively [46].

Figure 1.4.b. The structure that amphiphilic graft copolymers are likely to take when forming micelles [47].

Soluplus® is an example of a graft copolymer (see figure 1.4.a.). It consists of three different homopolymers, namely polyethylene glycol (PEG) as the backbone, with a polyvinyl acetate (PVAc) branch that leads to polyvinyl caprolactam (PCL). Soluplus® is considered an amphiphilic copolymer, where PEG qualifies as the hydrophilic component, whereas PVAc and PCL are the hydrophobic part [48, 49]. This synthetic amphiphilic graft copolymer possesses surfactant behavior. Indeed, Soluplus® forms micelles at 7.6 mg/l in aqueous media[46].

Formation of micelles can provide a poorly soluble drug a hydrophobic environment within an aqueous medium by which the total concentration of that drug, $Drug_{Total}$, in the aqueous medium is enhanced. The total concentration of a crystalline drug in the presence of a specific concentration of an amphiphilic polymer, $Polymer_{amphi}$, in an aqueous medium can be calculated by using Equation 1.12 [50-52]:

$$\mathrm{Drug_{Total}} = \mathrm{K_m}\left(\mathrm{Polymer_{amphi}} - \mathrm{Polymer_{CMC}}\right) + \mathrm{Drug_0} \qquad (1.12)$$

where the subscripts Total and CMC indicate the total concentration in the medium that included Soluplus® and its respective concentration when Soluplus® is at its CMC. K_m is the molar solubilization capacity, defined as the moles of drug that can be solubilized by one mole of this micelle-forming polymer. Detailed experiment to test the ability of Soluplus® to enhance SMX and NIF aqueous equilibrium solubility at 37 °C can be found in the supplemental section A, Figures 1.3., Figure 1.4., Figure 1.5., and Figure 1.6.

1.4. The thermodynamics of mixing for binary mixtures

The process of solubilizing small molecular weight solutes in a specific solvent is of great interest. The solubility can be summarized in three steps [53] (1) The initial step involves breaking the bonds between the solute molecules at a specific temperature. After each molecule escapes this region of pure solute, the vacancy it creates is filled in with solvent molecule(s). (2) The second step is to create a void in the solvent molecules to accept the escaped solute molecule. Once again, breaking bonds between solvent molecules must take place. (3) The escaped solute molecule fits into the open space within the solvent molecules and becomes a solute molecule in the solution. The bonds formed between solvent molecule(s) that filled the site where the solute molecule escaped and the solute molecules surrounding that site, and the bonds formed between the escaped solute molecule and the solvent molecules that allowed it to become a solute molecule in a solution in effect return some of the energy required to remove the solute molecule from its original environment and some of the energy required to create the void in the solvent molecules. This return of energy reduces the enthalpy requirement for making a solution from pure solute and pure solvent.

1.4.1. Thermodynamics of Regular Solution Theory

Exploiting a statistical model allows the estimation of the free energy of mixing in binary solutions. In the simplest case, it is assumed that each solvent molecule occupies a single site in the three-dimensional cubic lattice. Each solute molecules will likewise occupy a single lattice site [45]. The entropy of mixing is obtained by using Boltzmann equation, Equation 1.13:

$$S = k_B \ln \Omega \tag{1.13}$$

where S is the entropy of mixing in the binary solution, k_B is Boltzmann's constant, and Ω is the total possible adaptable configurations in the system.

The above assumption regarding a lattice site for each solvent or solute molecule suggests that the two types of molecules have the same molar volume. By using the method of approximations, the change in entropy with mixing per mole of lattice sites is found using Equation 1.14:

$$\Delta S_m = -R \{X_1 \ln X_1 + X_2 \ln X_2\} \tag{1.14}$$

where X_1 and X_2 are the mole fraction for each component in the solution, and R is the universal gas constant. It is important to note that entropy always favors mixing as the mole faction is going to be always less than one and the natural logarithm term renders negative values.

The lattice model theory allows derivation of the enthalpy of mixing, assuming no volume change occurs with mixing, by using Equations 1.15-1.21:

$$H_1 = \frac{1}{2} m_1 z w_{11} \tag{1.15}$$

$$H_2 = \frac{1}{2} m_2 z w_{22} \tag{1.16}$$

$$\Delta H_m = \frac{1}{2}\, m_1 \{z x_1 w_{11} + z x_2 w_{12}\} + \frac{1}{2}\, m_2 \{z x_1 w_{12} + z x_2 w_{22}\} \tag{1.17}$$

$$\Delta H_m = \frac{m_1 m_2}{m}\, z \Delta w \tag{1.18}$$

$$\Delta w = w_{12} - \frac{w_{11}}{2} - \frac{w_{22}}{2} \tag{1.19}$$

$$\chi = \frac{z\Delta w}{kT} \tag{1.20}$$

$$\frac{\Delta G_m}{RT} = \{m_1 \ln X_1 + m_2 \ln X_2 + m_1 X_2 \chi\} \tag{1.21}$$

where m_1, m_2 are the number of molecules of the two components, m is the total number of molecules in the system, w_{11} and w_{22} are the interaction energy between molecule one and molecule one and between molecule two and molecule two, respectively, w_{12} is the interaction energy between molecule one and molecule two, z is the number of neighboring molecules, Δw is the energy exchange between the cohesive and the adhesive forces of the binary components in the solution, χ is the interaction parameter, and ΔG is the Gibbs free energy of mixing.

It is recognizable that the first two terms in the right hand side of Equation 1.21, represent the entropy of mixing and it always favors mixing. The enthalpy part, however, represented by the term involving the interaction parameter, χ, determines the spontaneity of the mixing. When mixing renders an exothermic reaction (heat is being released) the binary solution will mix spontaneously. The mixing is thermodynamically hindered when an endothermic reaction is obtained (heat being absorbed). For more details refer to Hiemenz et al., [45].

1.4.2. Flory-Huggins Theory for polymer solutions

Flory and Huggins independently developed the Gibbs free energy of mixing, ΔG, for polymer solutions. This theory is an extension of Regular Solution Theory and is based

on the assumption that each monomer of one polymer occupies the same volume as one monomer of the solvent. This has been extended to describe mixing of a polymer with a small molecular weight solvent, with the assumption that the solvent molecule and the repeating unit in the polymer occupy the same volume. Therefore, each lattice site in the solution can hold one solvent molecule or one monomer from the polymer. The polymer would therefore occupy n such sites in the solution, depending on its degree of polymerization, n. Volume fraction is typically used instead of mole fraction in calculations due to the large molecular weight of a polymer and a lack of knowledge of its molecular weight distribution [54, 55].

The entropy of mixing in a polymer solution can be derived by assuming that the conformational changes in the polymer segments are the same whether the polymer is in bulk or in solution. In addition, each segment has a number of monomers that occupies that specific number of lattice sites. Equation 1.22 and Equation 1.23, are used to calculate the total entropy and enthalpy in polymer solutions.

$$\Delta S_m = -R\{n_1 \ln\Phi_1 + n_2 \ln\Phi_2\} \quad (1.22)$$

$$\Delta H_m = n_1 \Phi_2 \chi RT \quad (1.23)$$

Thus, Equation 1.24, gives The Gibbs free energy of mixing in polymer solution.

$$\frac{\Delta G_m}{RT} = \{n_1 \ln\Phi_1 + n_2 \ln\Phi_2 + n_1 \Phi_2 \chi\} \quad (1.24)$$

It can be seen that the mixing will be spontaneous when χ is negative. For dilute polymer solutions, however, the connectivity within each polymer coil limits the predicted complete uniformity within the solution. Such aspect renders clustering coils in certain areas of the solution. Therefore, it is correct to assume that the predicted accuracy for Flory-Huggins model significantly improved for concentrated polymer solutions.

1.4.3. Melting point depression theory

In 1975, Nishi et al., examined the compatibility between an amorphous polymer and a crystalline polymer [56]. By employing a reduced melting phenomenon at different mass ratios, they successfully extended Flory-Huggins Theory from crystalline polymers in small molecular weight solvents to crystalline polymers in amorphous polymers. Later, using a small molecular weight crystalline drug in an amorphous polymer was the natural extension that allows the estimation of the thermodynamics of mixing in solid dispersions [8, 57-60].

The following derivations are adapted from equations for mixing a crystalline polymer with an amorphous polymer. Thus, different thermodynamic parameters are obtained for the solid dispersion systems.

The chemical potential μ that must be the same, assuming that no effect from the mixture's interface, for the mixed and unmixed phases which is described in Equation 1.25:

$$\mu_{\text{Drug}}^{\text{Crystal}} - \mu_{\text{Drug}}^{\text{Liquid}} = \mu_{\text{Drug}}^{\text{Mixture}} - \mu_{\text{Drug}}^{\text{Liquid}} \tag{1.25}$$

The difference in the chemical potential can be approximated to be equal to the negative free energy of fusion for the crystalline drug.

$$\mu_{Drug}^{Crystal} - \mu_{Drug}^{Liquid} = -\left(\Delta H_{Drug} - T\Delta S_{Drug}\right) \approx -\Delta H_{Drug}\left(1 - \frac{T}{T_m}\right) \quad (1.26)$$

Assuming that the chemical potential is identical between the solid and liquid phase of the drug at the melting point, T_m, yields Equation 1.27:

$$\mu_{Drug}^{Crystal} - \mu_{Drug}^{Liquid}|_{T_m} = RT\left\{\ln\Phi_{Drug} + \left(1 - \frac{1}{m}\right)\Phi_{Polymer} + \chi\Phi_{Polymer}^2\right\} \quad (1.27)$$

Using equation 1.26 in equation 1.27, yields Equation 1.28, that permits the estimation of the interaction parameter between crystalline drugs and amorphous polymers.

$$\frac{1}{T_m^{mix}} - \frac{1}{T_m^{Pure}} = \frac{-R}{\Delta H_{fus}}\left\{\ln\Phi_{Drug} + \left(1 - \frac{1}{m}\right)\Phi_{Polymer} + \chi\Phi_{Polymer}^2\right\} \quad (1.28)$$

1.4.4. Solubility of crystalline drugs in amorphous polymers

Solubility means that the polymer acts like a solvent to dissolve the drug. Equation 1.29, relates the mole fraction solubility of crystalline drugs, X_{drug}, in low molecular weight solvent as a function of relevant thermodynamic parameters.

$$\ln\gamma_{drug}X_{drug} = -\frac{\Delta\bar{H}_f}{RT}\left(1 - \frac{T}{T_m^{pure}}\right) - \frac{\Delta C_p}{R}\left[\left(1 - \frac{T_m^{pure}}{T}\right) + \ln\left(\frac{T_m^{pure}}{T}\right)\right] \quad (1.29)$$

Here, γ_{drug} is the activity coefficient of the drug in the solvent system and X_{drug} is the mole fraction solubility of the drug in that solvent at a specific temperature. T is temperature and ΔC_p is the difference in configurational heat capacity between crystalline

and amorphous drug. The activity coefficient can be described for drug-polymer mixtures using Equation 1.30:

$$\ln\gamma_{drug}X_{drug} = \ln\Phi_{Drug} + \left(1 - \frac{1}{m}\right)\Phi_{Polymer} + \chi\Phi^2_{Polymer} \qquad (1.30)$$

the drug's activity, $\gamma_{drug}X_{drug}$, is affected by drug-polymer disparity in molecular weight and the interaction parameter. Therefore, the drug's activity will reflect the interaction between rubbery polymer, which behaves like a supercooled liquid, and the drug.

1.5. Methods currently used to form solid dispersions

Different methods by which to produce solid dispersions are detailed in the literature. Examples of these methods include fusion method, solvent method, melt extrusion, lyophilization, and spray drying [43]. The latter three methods, however, are the most attractive to the pharmaceutical industry at this time.

1.5.1. Lyophilization (freeze drying)

Lyophilization is an excellent technique that is widely used in the pharmaceutical industry to dry heat sensitive materials. In addition, this technique can be utilized to form spherical nanoparticles with improved stability [61]. Solutions of labile drugs, such as proteins, with certain excipients become solid forms wherein the active has acceptable stability [62]. Three essential steps are carefully taken to ensure the completion of the lyophilization cycle, namely (i) freezing, (ii) primary drying, and (iii) secondary drying.

1.5.1.1. Freezing

In this step, the solution or suspension is cooled below its freezing temperature. Ice crystals start to from during the cooling process. At a later time, water crystallization rate is hindered, rendering an amorphous, crystalline, or partially crystalline product [61].

1.5.1.2. Primary drying

The sublimation of ice crystal takes place in this step. In this process, the reduced pressure inside the chamber promotes the sublimation of the ice crystals. In addition, heat transfer between the shelf and the product drives sublimation. In addition, a slight increase in pressure was found to improve the drying rate. The pores are found in the product representing the regions previously occupied by ice crystals. This step is expected to be done when the product temperature equals the shelf temperature [62].

1.5.1.3. Secondary drying

This step deals with bound water molecules. This water neither formed crystals nor was it removed during primary drying. This molecules, described as tightly bound, is found in intimate contact with the material left behind as a solid and can amount to 10% of the product [62, 63]. Since this water is tightly bound, the energy necessary to remove it is correspondingly higher. This is accomplished by raising the temperature of the shelf in the lyophilizer with its maintained vacuum to a temperature typically higher than room temperature.

Critical product properties that should be considered for successful formulation include the collapse temperature, T_c, and glass transition temperature T_g. When the temperature is

found to be at least 2 degrees above the glass transition temperature the amorphous portion in the product collapses [64].

1.5.2. Spray drying

Many pharmaceutical formulations are prepared using spray drying. This method is excellent in rendering a dry homogenous product [65]. This process involves spraying a specific solution or suspension using predetermined feeding rate, inlet temperature, and chamber moisture content. During the spraying process the formed droplets are rapidly dried, rendering mostly spherical particles.

Spray drying was used to obtain a more compressible product for tableting [66]. Pharmaceutical products with improved aqueous solubility are obtained by rendering the active pharmaceutical ingredient, API, amorphous by methods such as spray drying, successfully dispersing the API in a hydrophilic carrier, or reducing the products particle size [65].

1.5.3. Melt extrusion

In 1961, Sekiguchi et al., introduced urea to sulfathiazole to form a eutectic mixture [67]. A reduction in the particle size was observed along with an improved dissolution rate. The enhanced characteristics of sulfathiazole were ascribed to the change in its physical state in the mixture. Hot melt extrusion (HME), in particular, is popular in the plastics industry [68], but only recently has the pharmaceutical industry adopted this method. This process is defined as introducing raw materials to continuously rotating screws under controlled temperature to produce a uniform ribbon [68]. Clearly, this method

renders a uniform mixture without the need for any solvents, which is a great advantage over other processing techniques. The cost for the solvent is eliminated, as is the cost for the energy and equipment to remove the solvent. In addition, manufacturing time is reduced by fewer processing steps and less equipment cleaning time.

In recent years, the pharmaceutical community was interested in overcoming the formidable hurdle of the low aqueous solubility of newly synthesized drug. By using HME to enhance the physicochemical properties of a crystalline drug by mixing it with a hydrophilic carrier polymer, HME became an indispensable processing tool for the pharmaceutical industry. It is important to note that both components must be stable at the processing temperature [68] and this prohibits its use with heat-labile drugs.

1.6. Research design

The specific aims for this research are:

(A) To predict the solubility of nifedipine and sulfamethoxazole in the triblock graft copolymer Soluplus® using a faster melting point depression technique and validating the results by using a phase diagram method

(B) To use the melting point depression method to identify the contribution of Soluplus® component homopolymers to the solubilization of nifedipine and sulfamethoxazole

(C) To investigate the in-vitro performance difference of solid dispersions of each of the two model drugs in Soluplus® or PEG 6000 prepared using spray drying and lyophilization

1.7. References

1. Huang L-F, Tong W-QT. Impact of solid state properties on developability assessment of drug candidates. Adv Drug Deliv Rev. 2004. 56(3): 321-34

2. Vasconcelos T, Sarmento B, Costa P. Solid dispersions as strategy to improve oral bioavailability of poor water soluble drugs. Drug Discov Today. 2007. 12(23): 1068-75

3. Serajuddin A. Solid dispersion of poorly water-soluble drugs: early promises, subsequent problems, and recent breakthroughs. J Pharm Sci. 1999. 88(10): 1058-66

4. Wegiel LA, Mauer LJ, Edgar KJ, Taylor LS. Crystallization of amorphous solid dispersions of resveratrol during preparation and storage-Impact of different polymers. J Pharm Sci. 2013. 102(1): 171-84

5. Murdande SB, Pikal MJ, Shanker RM, Bogner RH. Solubility advantage of amorphous pharmaceuticals, Part 3: Is maximum solubility advantage experimentally attainable and sustainable? J Pharm Sci. 2011. 100(10): 4349-56

6. Hughey JR, Keen JM, Brough C, Saeger S, McGinity JW. Thermal processing of a poorly water-soluble drug substance exhibiting a high melting point: The utility of KinetiSol® dispersing. Int J Pharm. 2011. 419(1-2): 222-30

7. Sun Y, Tao J, Zhang GGZ, Yu L. Solubilities of crystalline drugs in polymers: An improved analytical method and comparison of solubilities of indomethacin and nifedipine in PVP, PVP/VA, and PVAc. J Pharm Sci. 2010. 99(9): 4023-31

8. Lin D, Huang Y. A thermal analysis method to predict the complete phase diagram of drug–polymer solid dispersions. Int J Pharm. 2010. 399(1–2): 109-15

9. Grant DJ, Higuchi T. Solubility behavior of organic compounds. 1990.

10. Yalkowsky SH. Solubility and solubilization in aqueous media. 1999.

11. Yu L. Amorphous pharmaceutical solids: preparation, characterization and stabilization. Adv Drug Deliv Rev. 2001. 48(1): 27-42

12. Graeser KA, Patterson JE, Zeitler JA, Rades T. The role of configurational entropy in amorphous systems. Pharmaceutics. 2010. 2(2): 224-44

13. Angell C, MacFarlane D, Oguni M. The Kauzmann Paradox, Metastable Liquids, and Ideal Glasses: A Summary. Annals of the New York Academy of Sciences. 1986. 484(1): 241-7

14. Alhalaweh A, Alzghoul A, Kaialy W, Mahlin D, Bergström CA. Computational Predictions of Glass-Forming Ability and Crystallization Tendency of Drug Molecules. Mol pharm. 2014. 11(9): 3123-32

15. Mahlin D, Bergström CA. Early drug development predictions of glass-forming ability and physical stability of drugs. E J Pharm Sci. 2013. 49(2): 323-32

16. Narayanaswamy OS. A model of structural relaxation in glass. J Am Ceram Soc. 1971. 54(10): 491-8

17. Busch R, Kim Y, Johnson W. Thermodynamics and kinetics of the undercooled liquid and the glass transition of the Zr41. 2Ti13. 8Cu12. 5Ni10. 0Be22. 5 alloy. J Appl Phys. 1995. 77(8): 4039-43

18. Richard A. Interface and surface effects on the glass-transition temperature in thin polymer films. Faraday Discussions. 1994. 98: 219-30

19. Baird JA, Taylor LS. Evaluation of amorphous solid dispersion properties using thermal analysis techniques. Adv drug del R. 2012. 64(5): 396-421

20. Hancock BC, Shamblin SL, Zografi G. Molecular mobility of amorphous pharmaceutical solids below their glass transition temperatures. Pharmaceutical research. 1995. 12(6): 799-806

21. Surana R, Pyne A, Suryanarayanan R. Effect of aging on the physical properties of amorphous trehalose. Pharmaceutical research. 2004. 21(5): 867-74

22. Ford JL, Timmins P. Pharmaceutical thermal analysis: techniques and applications: Ellis Horwood Chichester; 1989.

23. Hancock BC, Dupuis Y, Thibert R. Determination of the viscosity of an amorphous drug using thermomechanical analysis (TMA). Pharm Res. 1999. 16(5): 672-5

24. Hancock BC, Zografi G. Characteristics and significance of the amorphous state in pharmaceutical systems. J Pharm Sci. 1997. 86(1): 1-12

25. Reddy MA, Thomas A, Srinivas K, Rao VJ, Bhanuprakash K, Sridhar B, Kumar A, Kamalasanan MN, Srivastava R. Synthesis and characterization of 9,10-bis(2-phenyl-1,3,4-oxadiazole) derivatives of anthracene: Efficient n-type emitter for organic light-emitting diodes. J Mat Chem. 2009. 19(34): 6172-84

26. Yoshioka S, Aso Y, Kojima S. Temperature-and glass transition temperature-dependence of bimolecular reaction rates in lyophilized formulations described by the Adam-Gibbs-Vogel equation. J Pharm Sci. 2004. 93(4): 1062-9

27. Angell CA. Thermodynamic aspects of the glass transition in liquids and plastic crystals. P Appl Chem. 1991. 63(10): 1387-92

28. Craig DQ, Royall PG, Kett VL, Hopton ML. The relevance of the amorphous state to pharmaceutical dosage forms: glassy drugs and freeze dried systems. Int J Pharm. 1999. 179(2): 179-207

29. Zhou D, Zhang GG, Law D, Grant DJ, Schmitt EA. Physical stability of amorphous pharmaceuticals: importance of configurational thermodynamic quantities and molecular mobility. J Pharm Sci. 2002. 91(8): 1863-72

30. Shamblin SL, Tang X, Chang L, Hancock BC, Pikal MJ. Characterization of the time scales of molecular motion in pharmaceutically important glasses. J Phys Chem. 1999. 103(20): 4113-21

31. Angell C, Alba-Simionesco C, Fan J, Green J. Hydrogen bonding and the fragility of supercooled liquids and biopolymers. Hydrogen Bond Networks: Springer; 1994. p. 3-22.

32. Stillinger FH, Debenedetti PG. Glass transition thermodynamics and kinetics. Annu Rev Condens Matter Phys. 2013. 4(1): 263-85

33. Neau SH, Bhandarkar SV, Hellmuth EW. Differential molar heat capacities to test ideal solubility estimations. Pharm Res. 1997. 14(5): 601-5

34. Yang B, Min Huang W, Li C, Hoe Chor J. Effects of moisture on the glass transition temperature of polyurethane shape memory polymer filled with nano-carbon powder. European Polymer Journal. 2005. 41(5): 1123-8

35. Bhandari B, Howes T. Implication of glass transition for the drying and stability of dried foods. Journal of Food Engineering. 1999. 40(1): 71-9

36. Hancock BC, Zografi G. The relationship between the glass transition temperature and the water content of amorphous pharmaceutical solids. Pharm Res. 1994. 11(4): 471-7

37. Costa P, Sousa Lobo JM. Modeling and comparison of dissolution profiles. European journal of pharmaceutical sciences. 2001. 13(2): 123-33

38. Noyes AA, Whitney WR. The rate of solution of solid substances in their own solutions. Journal of the American Chemical Society. 1897. 19(12): 930-4

39. Goldberg AH, Gibaldi M, Kanig JL, Mayersohn M. Increasing dissolution rates and gastrointestinal absorption of drugs via solid solutions and eutectic mixtures IV: Chloramphenicol—urea system. J Pharm Sci. 1966. 55(6): 581-3

40. Goldberg AH, Gibaldi M, Kanig JL. Increasing dissolution rates and gastrointestinal absorption of drugs via solid solutions and eutectic mixtures III: Experimental evaluation of griseofulvin—succinic acid solid solution. J Pharm Sci. 1966. 55(5): 487-92

41. Goldberg AH, Gibaldi M, Kanig JL. Increasing dissolution rates and gastrointestinal absorption of drugs via solid solutions and eutectic mixtures II: Experimental evaluation of a eutectic mixture: Urea-acetaminophen system. J Pharm Sci. 1966. 55(5): 482-7

42. Goldberg AH, Gibaldi M, Kanig JL. Increasing dissolution rates and gastrointestinal absorption of drugs via solid solutions and eutectic mixtures I. Theoretical considerations and discussion of the literature. J Pharm Sci. 1965. 54(8): 1145-8

43. Karolewicz B, Górniak A, Probst S, Owczarek A, Pluta J, Zurawska-Płaksej E. Solid dispersions in pharmaceutical technology. Part I. Classification and methods to obtain solid dispersions. Polimery w medycynie. 2012. 42(1): 17

44. Leuner C, Dressman J. Improving drug solubility for oral delivery using solid dispersions. European journal of pharmaceutics and biopharmaceutics. 2000. 50(1): 47-60

45. Hiemenz PC, Lodge TP. Polymer Chemistry, 2nd edition FL: CRC press, Taylor & Francis group; 2007.

46. BASF. <Soluplus Technical Information>. 2009.

47. Torchilin VP. Structure and design of polymeric surfactant-based drug delivery systems. Journal of Controlled Release. 2001. 73(2): 137-72

48. Yu H, Xia D, Zhu Q, Zhu C, Chen D, Gan Y. Supersaturated polymeric micelles for oral cyclosporine A delivery. European Journal of Pharmaceutics and Biopharmaceutics. 2013. 85(3): 1325-36

49. Linn M, Collnot E-M, Djuric D, Hempel K, Fabian E, Kolter K, Lehr C-M. Soluplus® as an effective absorption enhancer of poorly soluble drugs< i> in vitro</i> and< i> in vivo</i>. E Pharm Sci. 2012. 45(3): 336-43

50. Gokturk S, Caliskan E, Talman RY, Var U. A study on solubilization of poorly soluble drugs by cyclodextrins and micelles: complexation and binding characteristics of sulfamethoxazole and trimethoprim. Scientific World J. 2012. 2012: 718791

51. Yang G, Jain N, Yalkowsky SH. Combined effect of SLS and (SBE) 7M-β-CD on the solubilization of NSC-639829. Int J Pharm. 2004. 269(1): 141-8

52. Alvarez-Núñez F, Yalkowsky S. Relationship between Polysorbate 80 solubilization descriptors and octanol–water partition coefficients of drugs. Int J Pharm. 2000. 200(2): 217-22

53. Sinko PJ, Allen Jr LV, Popovich NG, Ansel HC. Martin's Physical Pharmacy and Pharmaceutical Sciences. Fifth, editor: Lippincott Williams and Wilkins; 2006.

54. Huggins ML. The viscosity of dilute solutions of long-chain molecules. IV. Dependence on concentration. J Amer Chem Soci. 1942. 64(11): 2716-8

55. Flory PJ. Thermodynamics of high polymer solutions. J Chem Phys. 1942. 10(1): 51-61

56. Nishil T WT. Melting point depression and kinetic effects of cooling on crystallization in poly(viny1idene fluoride)-poly (methyl methacrylate) mixtures. Macromolecules. 1975. 8: 909-15

57. Tian Y, Booth J, Meehan E, Jones DS, Li S, Andrews GP. Construction of drug–polymer thermodynamic phase diagrams using Flory–Huggins Interaction Theory: Identifying the relevance of temperature and drug weight fraction to phase separation within solid dispersions. Mol Pharm. 2012. 10(1): 236-48

58. Zhao Y, Inbar P, Chokshi HP, Malick AW, Choi DS. Prediction of the thermal phase diagram of amorphous solid dispersions by Flory-Huggins theory. J Pharm Sci. 2011. 100(8): 3196-207

59. Marsac PJ, Li T, Taylor LS. Estimation of drug-polymer miscibility and solubility in amorphous solid dispersions using experimentally determined interaction parameters. Pharm Res. 2009. 26(1): 139-51

60. Marsac PJ, Shamblin SL, Taylor LS. Theoretical and practical approaches for prediction of drug–polymer miscibility and solubility. Pharm Res. 2006. 23(10): 2417-26

61. Abdelwahed W, Degobert G, Stainmesse S, Fessi H. Freeze-drying of nanoparticles: formulation, process and storage considerations. Adv Drug Deliv Rev. 2006. 58(15): 1688-713

62. Wang W. Lyophilization and development of solid protein pharmaceuticals. Int J Pharm. 2000. 203(1): 1-60

63. Pikal M, Shah S, Roy M, Putman R. The secondary drying stage of freeze drying: drying kinetics as a function of temperature and chamber pressure. Int J Pharm. 1990. 60(3): 203-7

64. Tang XC, Pikal MJ. Design of freeze-drying processes for pharmaceuticals: practical advice. Pharm Res. 2004. 21(2): 191-200

65. Sollohub K, Cal K. Spray drying technique: II. Current applications in pharmaceutical technology. J Pharm Sci. 2010. 99(2): 587-97

66. Takeuchi H, Yasuji T, Hino T, Yamamoto H, Kawashima Y. Spray-dried composite particles of lactose and sodium alginate for direct tabletting and controlled releasing. Int J Pharm. 1998. 174(1): 91-100

67. Keiji Sekiguchi NO. Studies on Absorption of Eutectic Mixture. I. A Comparison of the Behavior of Eutectic Mixture of Sulfathiazole and that of Ordinary Sulfathiazole in Man. Chem Pharm Bull. 1961. 9(11): 866-72

68. Crowley MM, Zhang F, Repka MA, Thumma S, Upadhye SB, Kumar Battu S, McGinity JW, Martin C. Pharmaceutical applications of hot-melt extrusion: part I. Drug Dev In Pharm. 2007. 33(9): 909-26

2. Use of the Flory-Huggins Theory to predict the solubility of nifedipine and sulfamethoxazole in the triblock graft copolymer Soluplus®

2.1. Abstract

Purpose: Solid dispersions of crystalline drugs in polymer matrices are promising as an approach to improve bioavailability. However, the high energy of an amorphous drug in a solid dispersion leads to crystallization. In this work, the Flory-Huggins Theory predicts the solubility of crystalline drugs in the triblock graft copolymer Soluplus® to provide a solid solution of molecularly dispersed drug with negligible opportunities for crystallization.

Methods: The melting point depression of each of two BCS II drugs, sulfamethoxazole (SMX) and nifedipine (NIF), was measured at various polymer levels using differential scanning calorimetry to allow calculation of the interaction parameter, χ. χ provides a measure of drug-polymer interaction strength and allows the estimation of the free energy of mixing the drug with the polymer and, hence, its solubility in that polymer. Drug solubility in the polymer is calculated by solving solubility equations and by construction of a phase diagram.

Results: A negative interaction parameter for SMX and NIF with Soluplus® indicated a relatively strong drug-polymer interaction. The free energy of mixing and the solubility of each drug in Soluplus® were then estimated. The calculated solubility of each drug is in agreement across the two methods.

Conclusion: The Flory-Huggins Theory indicates that Soluplus® interacts effectively with each of the drugs. The predicted solubility of the drugs in Soluplus® compared favorably across the two methods and with literature values. This approach proves to be faster and more efficient than others reported in the literature.

2.2. Keywords

Flory-Huggins Theory, solid solution, phase diagram, nifedipine, sulfamethoxazole, Soluplus®, miscibility, solubility.

2.3. Introduction

Converting the physical state of a drug, in whole or in part, from crystalline to the amorphous state will enhance its dissolution rate and solubility in aqueous media. Since most new drugs are crystalline, the major limitation to the use of the high energy and entropy amorphous form is the tendency for amorphous material to return to its stable crystal form [1-5]. Mixing a hydrophilic polymer with a miscible drug to generate a solid solution will eliminate the crystallization tendency of the amorphous form and, thus, improve drug stability. A solid solution is defined as the molecular level mixing of drug with the carrier polymer, such that drug molecules cannot form the nucleus that leads to crystallization. A solid solution is, thus, different from a solid dispersion that, by definition, would include not only solid solutions but also solids where amorphous drug is dispersed in the carrier. Typical methods to prepare solid solutions include dissolution of their mixture in a common solvent that would be removed later [6] or mixing the two using a method such as hot melt extrusion [7].

To reach this desired one-phase system using a mixture of two different substances, miscibility should be thermodynamically driven. During hot melt extrusion, such mixing takes place at a temperature above the glass transition temperature of the polymer. To prevent drug nucleation when the mixture is brought to room temperature, drug saturation of the polymer matrix at ambient conditions cannot be exceeded [8]. Therefore, knowing the solubility of a drug in a carrier polymer, i.e., the maximum loading of drug that still allows molecular level mixing, at room temperature is critical to the physical stability of the dispersion and the chemical stability of the drug [4, 9, 10].

A negative Gibbs free energy of mixing (ΔG_m) indicates miscibility, as described in Eq. 2.1:

$$\Delta G_{mix} = \Delta H_{mix} - T\Delta S_{mix} \quad (2.1)$$

The positive entropy of mixing always favors miscibility and solubility because it appears as a negative term, -TΔS, but the positive enthalpy contribution must not exceed this negative entropy term or solubility is not a spontaneous process [11]. Drug-polymer miscibility suggests that a single phase can be achieved; with an amorphous polymer, this phase would also be amorphous. This single phase is reflected by a single glass transition temperature (T_g) instead of one T_g for the drug and another for the polymer [12].

As an extension of Regular Solution Theory, the Flory-Huggins Theory was developed to describe polymers in solution [13, 14]. This theory is based on the assumption that each repeating unit of the polymer occupies the same volume as the solvent molecule. Thus, each lattice site in the solution can hold one solvent molecule and each polymer repeating unit would occupy one such lattice site. The polymer would, therefore, occupy n such sites in the solution depending on its degree of polymerization, n. Volume fraction is typically used instead of mole fraction in calculations due to the large molecular weight of a polymer and the practical difficulty to obtain the precise molecular weight distribution [15]. The Flory-Huggins Theory was then extended to describe crystalline polymer-amorphous polymer interactions and the depression of the melting point of a crystalline polymer was proposed to reflect the interaction between the crystalline and amorphous polymers. The Flory-Huggins Theory allowed estimation of the thermodynamic parameters associated with this mixing [16].

Recently, the application of the Flory-Huggins Theory was extended to describe the thermodynamics associated with the solubility of a crystalline drug in an amorphous polymer. The drug is considered a small molecular weight solute and the amorphous polymer is considered a solvent. Marsac et al., [10, 17] generated melting point depression data for crystalline drug in the presence of amorphous polymer to measure the interaction parameter, χ, and to predict the solubility of the drug in the polymer. It has been noted that the drug must be totally crystalline; otherwise, the chemical potential will be lowered. Furthermore, the thermodynamic measurements were made at the drug melting point and the two substances might interact differently at room temperature [18].

The interaction parameter, χ, has been considered a constant [10, 17]. Also, the interaction parameter was found to be a function of temperature and the composition of polymer blends [8, 19]. However, it is typically assumed that the interaction parameter is a function of temperature only and that the respective concentrations in the mixture do not affect it [4]. An empirical formula has been proposed to predict χ at ambient temperature using a linear relationship, but linearity is difficult to obtain without omitting the data points at lower polymer content [4]. The predicted χ at ambient temperature is then used in the Gibbs free energy equation to calculate the saturation limit of the polymer matrix [8].

Although copolymers have been utilized [3, 10, 16-18, 20], to our knowledge, this is the first use of a triblock graft copolymer in a melting point depression or phase diagram study of drug solubility. In this study, a differential scanning calorimeter (DSC) was used to obtain the melting point at different concentrations of the polymer Soluplus®, in the drug and the variation in the melting point was used to predict the drug solubility [10]. A

phase diagram was also constructed that proved useful to estimate the solubility near the glass transition temperature where the time for the drug-polymer mixture to reach equilibrium is expected to be longer due to the rigidity of the glassy polymer. Preparation methods that allow time for equilibrium might yield solubility estimates that exceed drug saturation in the polymer and would result in regions of amorphous drug that can recrystallize at a later time. Shorter experimental time-scale procedures will avoid supersaturation and the chemical instability that longer time-scale methods might yield. After drug solubility in the polymer was estimated by these two different methods, a comparison between these methods and relevant discussion are provided.

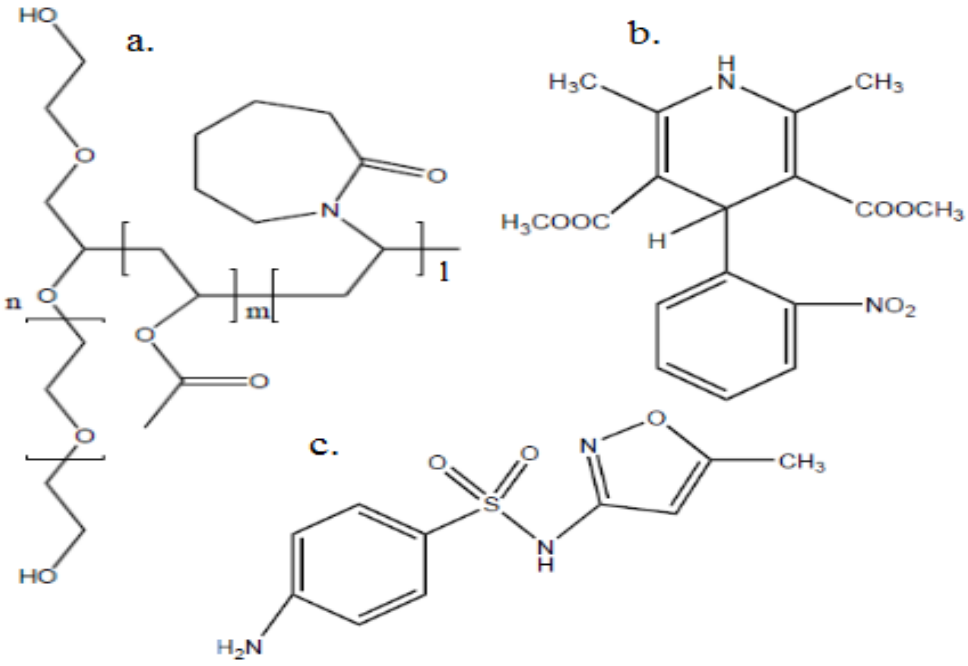

Figure 2.1. Chemical structure of a. Soluplus®, b. nifedipine, and c. sulfamethoxazole.

2.4. Materials

Soluplus® (Fig. 2.1.a.), provided by BASF (Tarrytown, NY), exhibits easy extrudability in hot melt extrusion, and greater enhancement of drug dissolution rates than observed with other polymers [21]. Furthermore, Soluplus® is not orally bioavailable and its oral toxicity (DL_{50}) is greater than 5 g/kg [22]. Poly(vinylpyrrolidone)-poly(vinylacetate) copolymer, marketed as Kollidon VA64® and provided by BASF, has a M_w of 40,000-70,000 g/mol, density of 0.97 g/cm^3, and glass transition temperature of 101 ^oC . Crystalline nifedipine (NIF), purchased from C.F.M. Co. Farmaceutica Milanese S.P.A. (Milano, Italia), exhibits low water solubility and high photosensitivity [23, 24]. NIF is dimethyl 1,4-dihydro-2,6-dimethyl-2-nitrophenyl)-3,5-pyridinedicarboxylate (Fig. 2.1.b.). It is a calcium channel antagonist used in coronary heart disease. Crystalline sulfamethoxazole (SMX) was purchased from Flavine International Inc. (Closter, NJ). SMX is 4-amino-N-(5-methylisoxazol-3-yl) benzenesulfonamide (Fig. 1.c.) which is used as an antibiotic to inhibit bacterial para-aminobenzoic acid participation in folic acid synthesis that contributes to DNA synthesis [25]. Each of the sulfonamide drugs is limited in aqueous solubility and, therefore, in dissolution rate [25, 26]. Other properties of these materials are presented in Table 2.1.

Materials for this project were sieved to collect particles less than 500 μm in diameter due to the effects of drug particle size on its melting and polymer particle size on drug diffusion within the polymer matrix. Materials were dried by storage in a desiccator over calcium sulfate for at least one week prior to mixing. NIF, in particular, was kept in an amber bottle to prevent photodegradation.

2.5. Methods

2.5.1. True density measurements

The true density of each material was measured using a helium pycnometer (model MPY- 1, micropycnometer, Quantachrome corp., NY, USA). The materials were kept in a desiccator for at least a week prior to the measurements. The concept is based on the volume displacements using a specific volume cell that contained a known mass of a given material. Helium was chosen, however, due to its ability to penetrate the finest pores in a given materials [27, 28].

First, the helium is purged into the materials to ensure the absence of any residual moisture. Second, an exactly measured mass is placed in the volume cell, which was placed in the cell holder. The pressure difference is measured between the reference and the volume cell, which, later, was converted to a true volume. Finally, the material's true density is obtained by dividing the mass over the true volume.

2.5.2. Differential scanning calorimetry

Physical mixtures were prepared using a geometric dilution method. For the thermal analysis, polymer effects were evaluated at 0, 5, 10, 16.7, 20, and 25% w/w polymer in the drug-polymer mixture. Each sample, weighing 5 mg, was hermetically sealed in an aluminum pan (Part No. 219-0062, Perkin-Elmer, USA). Three to six samples were prepared at each polymer concentration. The onset and offset melting temperatures (T_{onset} and T_{end}, respectively) of sulfamethoxazole and nifedipine in the presence of various levels of Soluplus® were measured with a TA 2910 DSC (TA Instruments, New Castle,

DE) at a scan rate of 1 deg/min. The DSC was calibrated for temperature and enthalpy with indium (100% pure, melting point 156.60 °C, heat of fusion 6.80 cal/g). The sample and reference cells were purged with nitrogen at 50 ml/min. The results were analyzed using Thermal Advantage 1.1 A software. A tangent to the linear portion of the leading edge of the melting endotherm was extrapolated to the baseline to define each onset of melting. A tangent to the linear portion of the curve that follows the peak of the melting endotherm was extrapolated to the baseline to define the offset of melting.

2.5.3. Thermogravimetric analysis

A TGA/SDTA851[e] Thermogravimetric Analyzer (Mettler Toledo, Columbus, OH) was used to measure the thermal stability of nifedipine, sulfamethoxazole, and Soluplus®. The results were analyzed using Mettler Toledo STAR[e] software. The materials were dried in a desiccator for at least one week prior to testing. A 5-15 mg sample was placed in a 70 µl aluminum oxide crucible in the sample chamber under a 20 ml/min nitrogen flow. Samples were heated at 10 deg/min from ambient temperature to 500 °C.

2.5.4. Melting point depression

The influence of the interaction parameter between crystalline drug and an amorphous polymer, χ, on the reduction in the melting point of the drug when it is involved in a mixture with that amorphous polymer is presented in Eq. 2.2 [4, 10, 17, 18, 29]:

$$\frac{1}{T_m^{Mix}} - \frac{1}{T_m^{Pure}} = -\frac{R}{\Delta\overline{H}_{fus}}\left[\ln\Phi_{drug} + \left(1 - \frac{1}{m}\right)\Phi_{polymer} + \chi\Phi^2_{polymer}\right] \qquad (2.2)$$

Eq. 2.2 uses the extent of the reduction in the melting point from that of the pure drug, T_m^{Pure}, to that of the drug in the drug-polymer mixture, T_m^{Mix}. ΔH_{fus} is the molar enthalpy of fusion of the pure drug and R is the universal gas constant. Φ_{drug} and $\Phi_{polymer}$ are the volume fraction of the drug and polymer, respectively. m is the ratio of the molar volume of the polymer to the molar volume of the drug [8].

Rearranging Eq. 2.2 to Eq. 2.3 and plotting the left side of Eq. 2.3 as a function of the square of the polymer volume fraction should present linearized data with a slope equal to χ:

$$-\frac{\Delta\overline{H}_{fus}}{R}\left(\frac{1}{T_m^{Mix}}-\frac{1}{T_m^{Pure}}\right)-\ln\Phi_{drug}-\left(1-\frac{1}{m}\right)\Phi_{polymer}=\chi\Phi_{polymer}^2 \qquad (2.3)$$

2.5.5 Gibbs free energy of the drug-polymer mixture

The entropic driving force for mixing of the drug-polymer mixture solubility is assumed to be the statistical mixing of the two components, as in Regular Solution Theory [15]. The free energy of mixing, normalized to temperature, is calculated using Eq. 2.4:

$$\frac{\Delta G_{mix}}{RT}=n_{drug}\ln\Phi_{drug}+n_{polymer}\ln\Phi_{polymer}+n_{drug}\Phi_{polymer}\chi \qquad (2.4)$$

here, n_{drug} is the number of moles of the drug, and $n_{polymer}$ is the number of moles of the polymer. The first two terms on the right-hand side of the equation represent the influence of the entropy of mixing and the last term represents the influence of the enthalpy of mixing.

2.5.6. Solubility prediction

It is important to the success of solid solution preparation to estimate well the solubility of the crystalline drug in the polymer. In this case, solubility means that the polymer acts like a solvent to dissolve the drug. Eq. 2.5 describes the mole fraction solubility of crystalline drugs in low molecular weight solvent, X_{drug}, as a function of relevant thermodynamic parameters:

$$\ln\gamma_{drug}X_{drug} = -\frac{\Delta\bar{H}_f}{RT}\left(1-\frac{T}{T_m^{Pure}}\right)-\frac{\Delta C_p}{R}\left[\left(1-\frac{T_m^{Pure}}{T}\right)+\ln\left(\frac{T_m^{Pure}}{T}\right)\right] \quad (2.5)$$

where γ_{drug} is the activity coefficient of the drug at the temperature and in the solvent system and X_{drug} is the mole fraction solubility of the drug in that solvent at that temperature. T is taken to be 298 K for calculations of solubility near room temperature. ΔC_p is the difference in heat capacity between crystalline and amorphous drug (assumed to equal the difference in constant pressure heat capacity of the liquid and solid forms of the drug at its melting point, $C_p^l - C_p^s$). Using the Flory-Huggins Theory, the activity coefficient can be described for drug-polymer mixtures using Eq. 2.6:

$$\ln\gamma_{drug}X_{drug} = \ln\Phi_{drug} + \left(1-\frac{1}{m}\right)\Phi_{polymer} + \chi\Phi_{polymer}^2 \quad (2.6)$$

From Eq. 2.6, the drug's activity is affected by drug-polymer molecular size disparity and the interaction parameter. Therefore, the drug's activity, $\gamma_{drug}X_{drug}$, will reflect the interaction between rubbery polymer, that behaves like a supercooled liquid, and the drug

[10, 17, 29]. The left-hand side of Equations 5 and 6 each represent drug solubility under the experimental conditions.

2.5.7. Phase diagram construction

A phase diagram is constructed using the data for the glass transition temperature of drug-polymer mixtures and the effect of the polymer content on the depression of the drug melting point (Fig. 2.2). The melting point depression (MPD) curve presents the miscibility demarcation and, thus, the miscibility conditions, found in region a, where binary mixtures above the demarcation curve should result in one-phase. Miscibility is, therefore, achieved at lower temperatures only when the polymer content increases. In the ideal condition, however, cooling the liquid mixture would result in crystallization of the pure drug at the MPD curve. On the other hand, experimentally, varying the cooling rate of the miscible mixture below the MPD curve results in a two-phase system, one drug-rich and the other polymer-rich. If cooling is continued, drug in the drug-rich phase could crystallize in region b. It is important to note that the separation will occur at later times not after cooling below MPD curve. Also, the high cooling rate, exemplifying the kinetic factor in this process, most likely will maintain one phase system below the T_g curve. The glassy state for each mixture, where diffusivity is dramatically diminished, is found at temperatures below the $T_{g\ mixture}$ line that defines regions c and d. In region c, the drug concentration exceeds its miscibility in the polymer and two glass transition temperatures could be observed. Experimentally, however, one single T_g is often observed over the total drug concentration range, indicative of a single-phase [8]. Furthermore, below the MPD curve, two glass transition temperatures are reported [4]. These observations clearly confirm the limitation of using the existence of a single T_g as the sole indicator for

miscibility [30]. A glassy solid solution is found in region d, where the drug content is miscible in the polymer, thereby, one glass phase is found and the mixing is thermodynamically driven [4, 31].

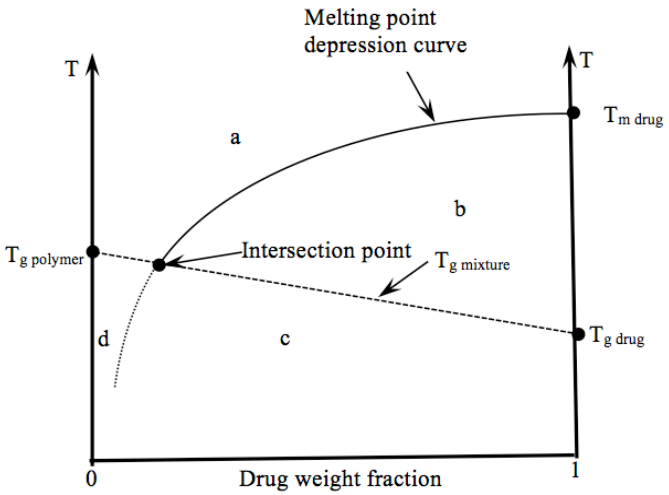

Figure 2.2. Phase diagram with glass transition temperatures and melting point depression curve [3, 8].

In Figure 2.2., the drug melting depression curve, represented by Eq. 2.2, is shown between the $T_{m\ drug}$ and the intersection point. The line between $T_{g\ polymer}$ and $T_{g\ drug}$ represents the glass transition temperature of the mixture. Therefore, constructing the phase diagram permits the prediction of the drug solubility near the glass transition temperature of the polymer. Furthermore, calculating the glass transition temperature of mixtures with higher drug concentrations might prove difficult since the amorphous polymer content would be low and the shift in heat capacity at the T_g would be correspondingly small. The $T_{g\ mixture}$ line in Fig. 2.2., is expected to be linear when essentially ideal mixing occurs. In other cases, positive or negative deviation from

linearity is found [12], such as predicted by the Fox equation[32] or the Gordon-Taylor equation [33].

Table 2.1. Material properties.

	MW (g/mol)	*Density (g/cm^3)	Molar volume (cm^3/mol)	ΔH_{fus} (kJ/mol)	T_m (K)	T_g (K)
Sulfamethoxazole	253	1.42	172.30	28.70	443	289**
Nifedipine	346	1.34	288.62	36.5	447	316
Soluplus®	118000	1.08	109000	-	-	347
Kollidon VA64	40000-70000	0.97	56701	-	-	374

*Density was measured using helium pycnometry.

** Ref. [34]

2.6. Results and discussion

2.6.1. Melting point depression

The heating rate of 1 deg/min was chosen because such a low rate should facilitate equilibrium between drug and polymer in each mixture [4, 10, 18], although scanning at higher and lower rates are found in the literature [4, 29]. The thermogram of each material is found in Fig. 2.3.

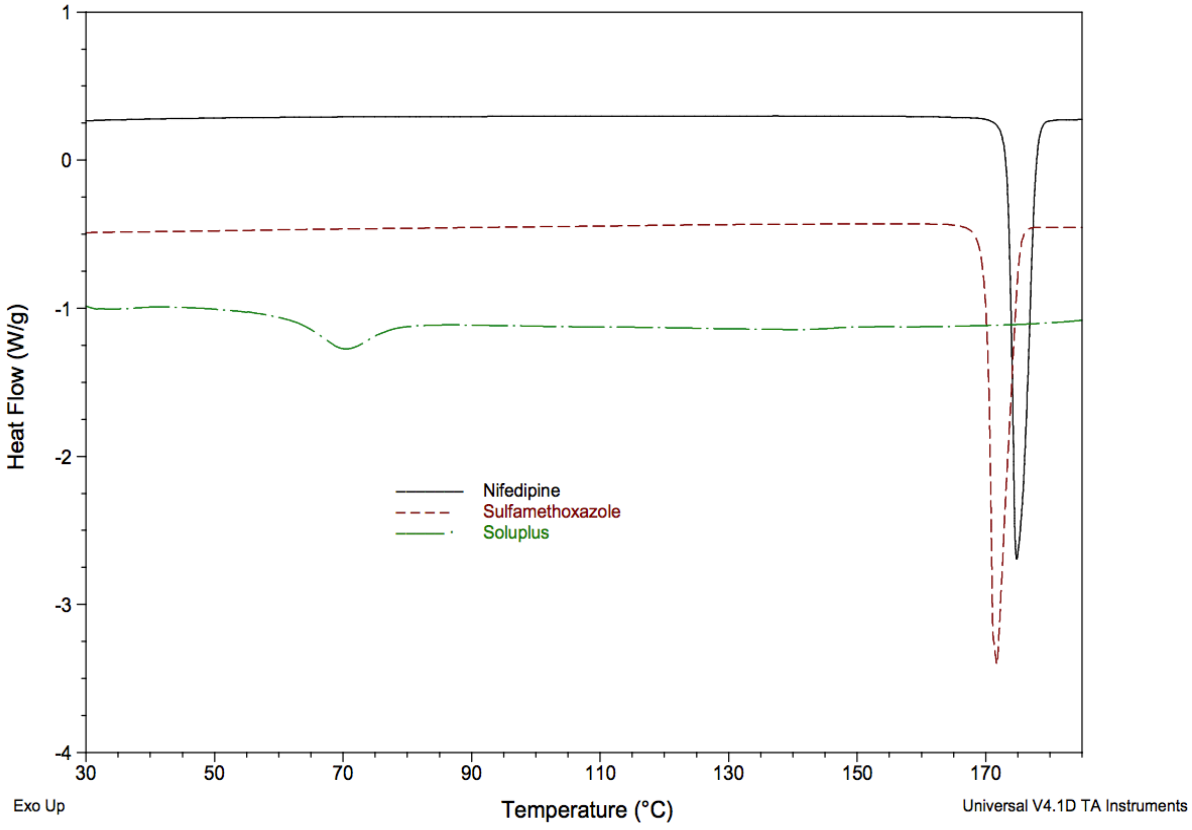

Figure 2.3. DSC thermograms for a. nifedipine , b. sulfamethoxazole, and c. Soluplus®.

Figure 2.3 shows that sulfamethoxazole has a melting point of 169.87 °C, nifedipine has a melting point of 173.05 °C, and Soluplus® has a T_g around 70 °C. An amorphous polymer is necessary to fulfill the requirements of the melting point depression approach [10, 17]. For each sample in the DSC study, the mixture was heated up to 185 °C. Thermogravimetric analysis, therefore, was conducted to ensure that no chemical degradation occurred during the DSC analysis. Figure 2.4., reveals the degradation temperature for sulfamethoxazole at 233 °C, nifedipine at 270 °C, and Soluplus® at 297 °C. Soluplus® loses 5% of its mass between 45 and 95 °C that represents the moisture content[35].

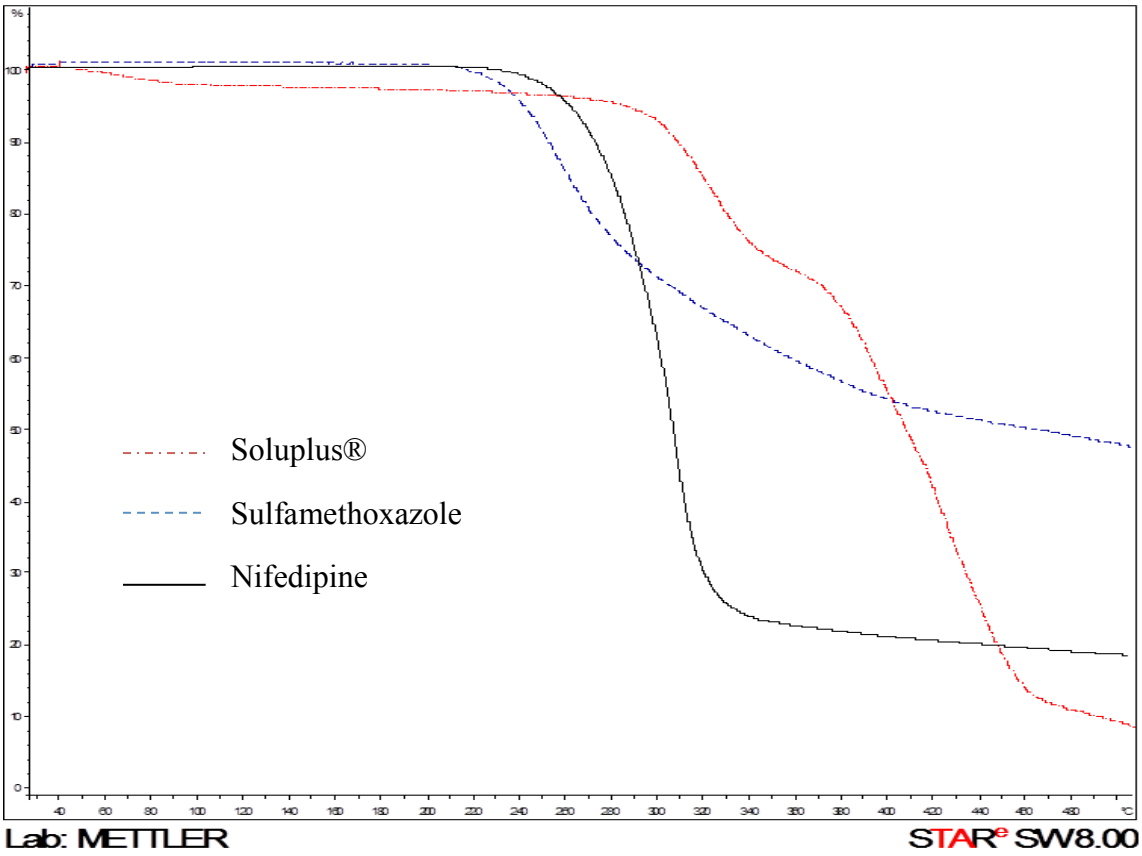

Figure 2.4. Results from thermogravimetric analysis reveal the degradation temperature for Soluplus®, sulfamethoxazole, and nifedipine.

The melting point of each mixture was taken and the T_{onset} and T_{end} of melting for SMX-Soluplus® mixtures are presented in Fig. 2.5.a. and 2.5.b., respectively.

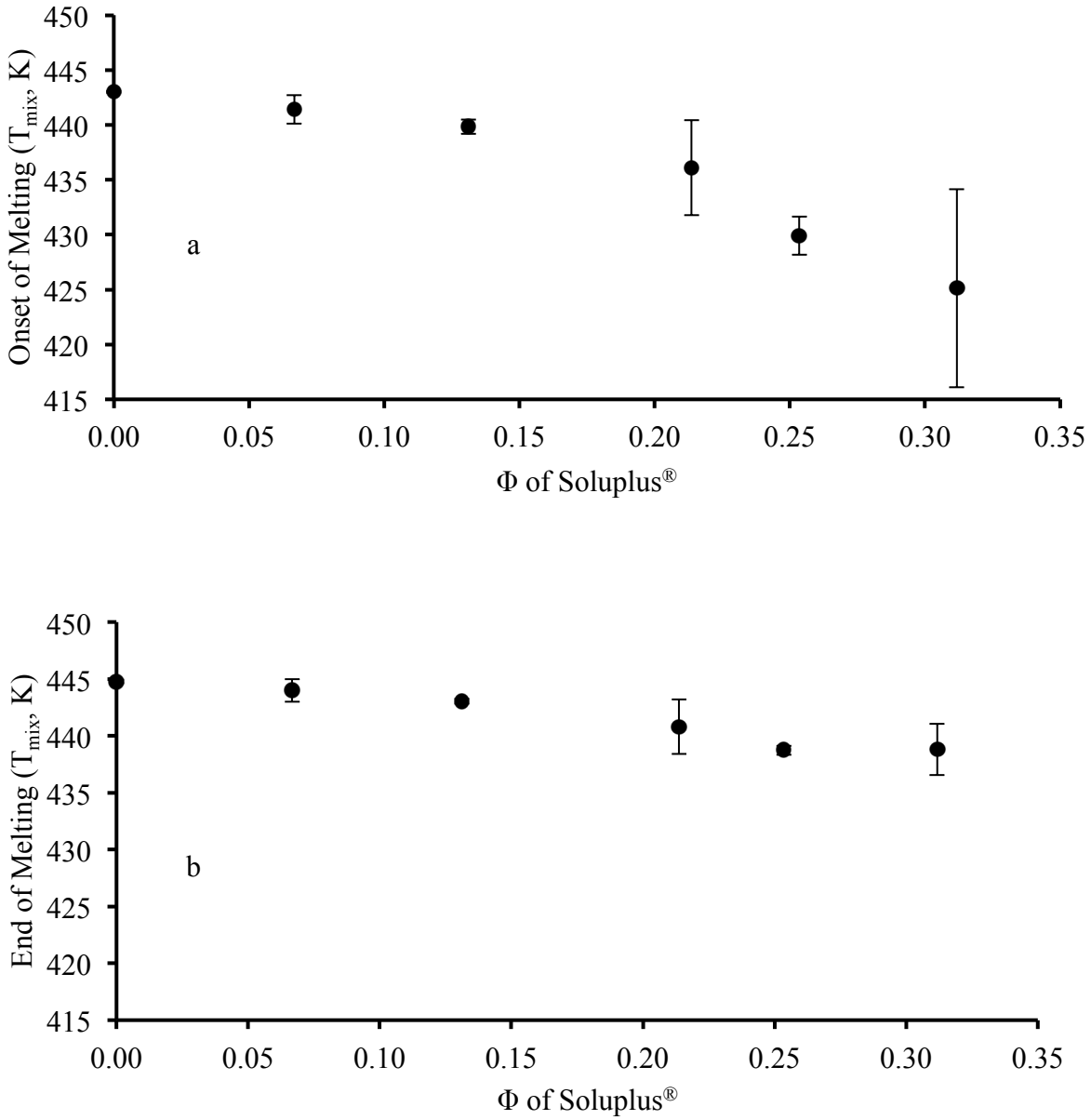

Figure 2.5. DSC results for T_{onset} (a) and T_{end} (b) of the melting endotherm for sulfamethoxazole mixtures with 0, 5, 10, 16.7, 20, and 25 % w/w Soluplus®, presented as a function of the volume fraction of Soluplus®.

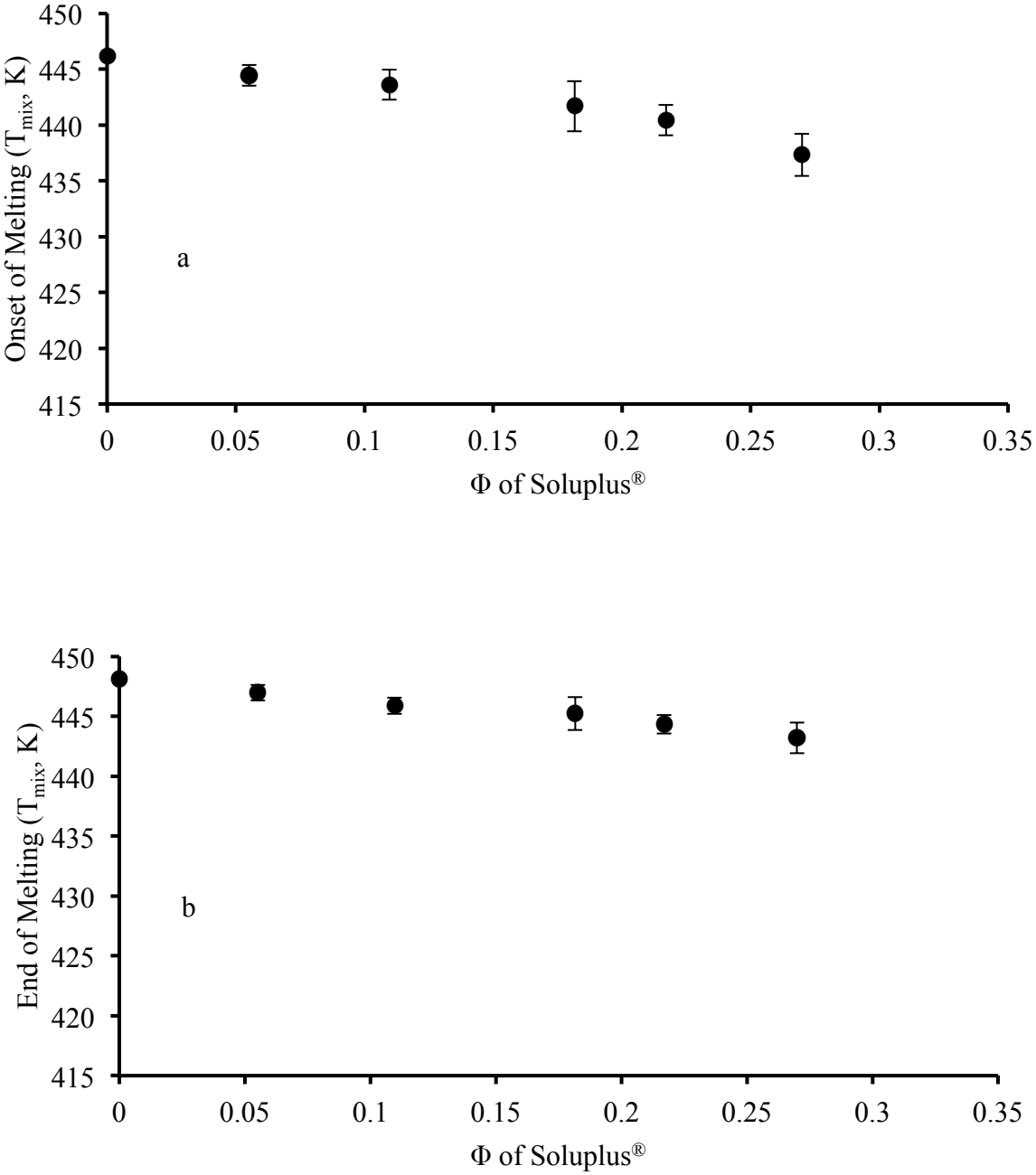

Figure 2.6. DSC results for T_{onset} (a) and T_{end} (b) of the melting endotherm for nifedipine mixtures with 0, 5, 10, 16.7, 20, and 25 % w/w Soluplus®, presented as a function of the volume fraction of Soluplus®.

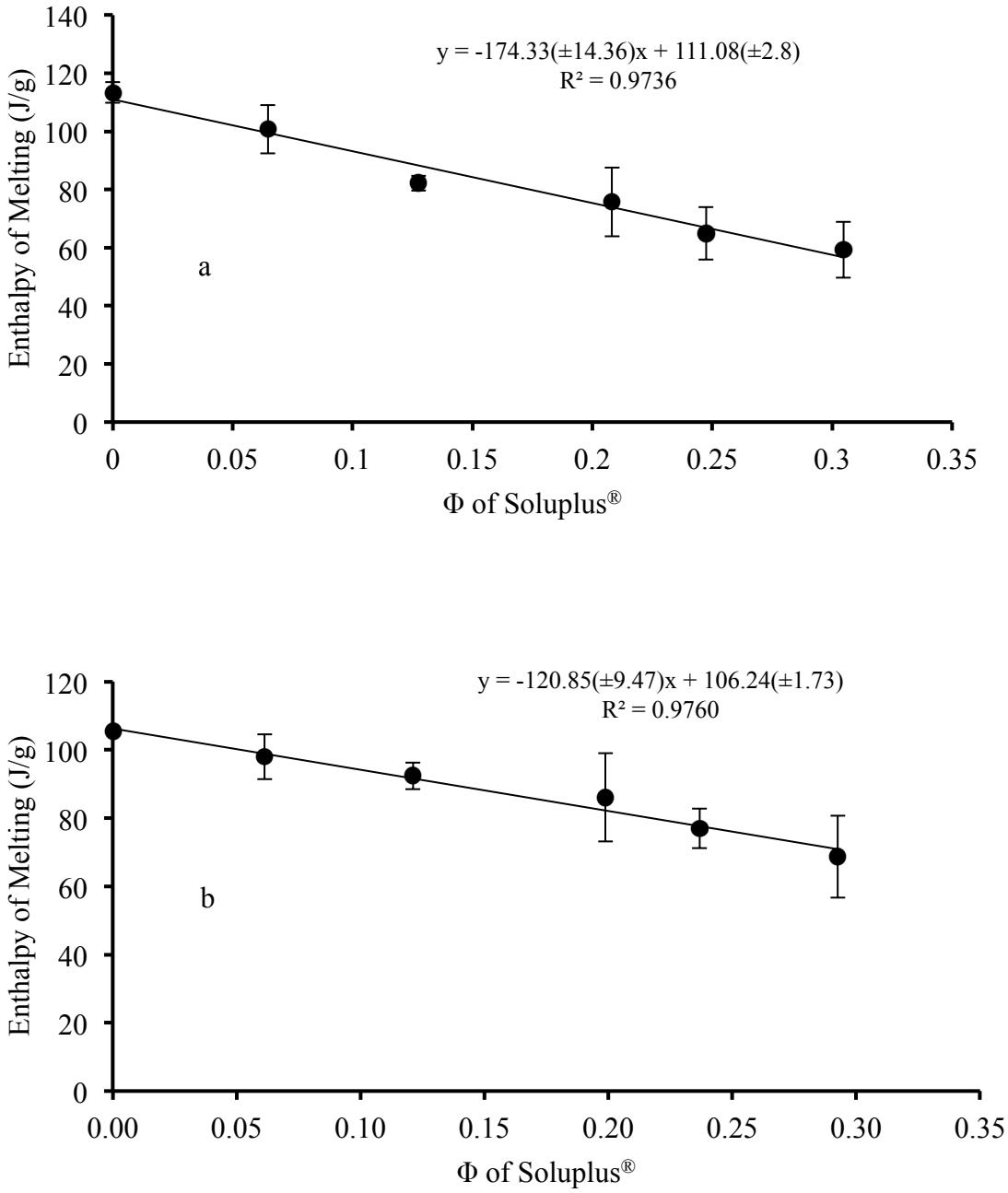

Figure 2.7. DSC results for SMX (a) and NIF (b) showing the enthalpy of fusion for each drug at different concentrations of Soluplus®, presented as a function of the volume fraction of Soluplus®. Numbers between the parentheses represent the standard error.

The T_{onset} and T_{end} of the melting endotherm for SMX-Soluplus® and NIF-Soluplus® mixtures are presented in Fig. 2.5.a. and 2.5.b., respectively. It can be seen in Figs. 2.5.a. and 2.5.b., that the onset of melting is more profoundly influenced by the increase in Soluplus® content in the mixture than is the end of melting. This is not surprising since the onset of melting depends on the polymer influence on the melting drug molecules that interface with the polymer and not on those in the interior of SMX particles that melt and diffuse later as the sample approaches the end temperature for the melt.

Extrapolation of the enthalpy associated with the melting endotherms to 0 J/g can provide an estimate of the solubility of each drug in Soluplus®. This extrapolation was easily accomplished since the linear relationship across the data (see Fig. 2.7.a. and 2.7.b.) was the best fit model equation for the data. The lack of a melting endotherm indicates that the drug is miscible with the polymer matrix and crystalline drug is no longer present. Since the drug particles used in the preparation of the samples for DSC analysis are crystalline, the presence of amorphous drug is not an issue in this extrapolation. For SMX the zero enthalpy of melting occurs at 50.9 % w/w and for NIF at 25.2 % w/w.

Polymer contact at the interface with the drug particles reduces the melting point of the crystalline drug molecules because the polymer behaves as an impurity in the solid mixture with the drug. The van't Hoff equation [36] predicts the effect of a certain mole fraction of polymer impurity, X_2, on the melting point of the primary component in a solid mixture, T_m^{Mix}:

$$T_m^{Mix} = T_m^{Pure} - \frac{X_2 R (T_m^{Pure})^2}{\Delta \bar{H}_f} \quad (2.7)$$

In this equation, the melting point of the mixture refers to the initial melting temperature, represented by T_{onset}, since there is no increase in temperature during the melting process. The equation reveals that the melting point of the mixture should decrease with increasing polymer content. Once melted, drug molecules diffuse into the polymer by an endothermic process but the sample temperature will not rise to match that of the reference in the differential scanning calorimeter until the entire drug has melted. The point where the sample temperature has increased to match the reference temperature would be represented by the time associated with T_{end}. Therefore, T_{end} is higher than predicted by the theoretical equations in the Flory Huggins Theory that deal with melting and not the subsequent diffusion process.

The use of T_{end} is gaining more interest due to the fact that melted drug diffusion is indeed included in the endotherm associated with melting [4, 8, 17, 20]. Thus, it is logical to use T_{end} as the temperature for hot melt extrusion (HME) of crystalline drug with an amorphous polymer to prepare solid dispersions since this will encourage melting of the drug present and its successful diffusion into the polymer in a short time period equal to or less than the mixing time in the extruder.

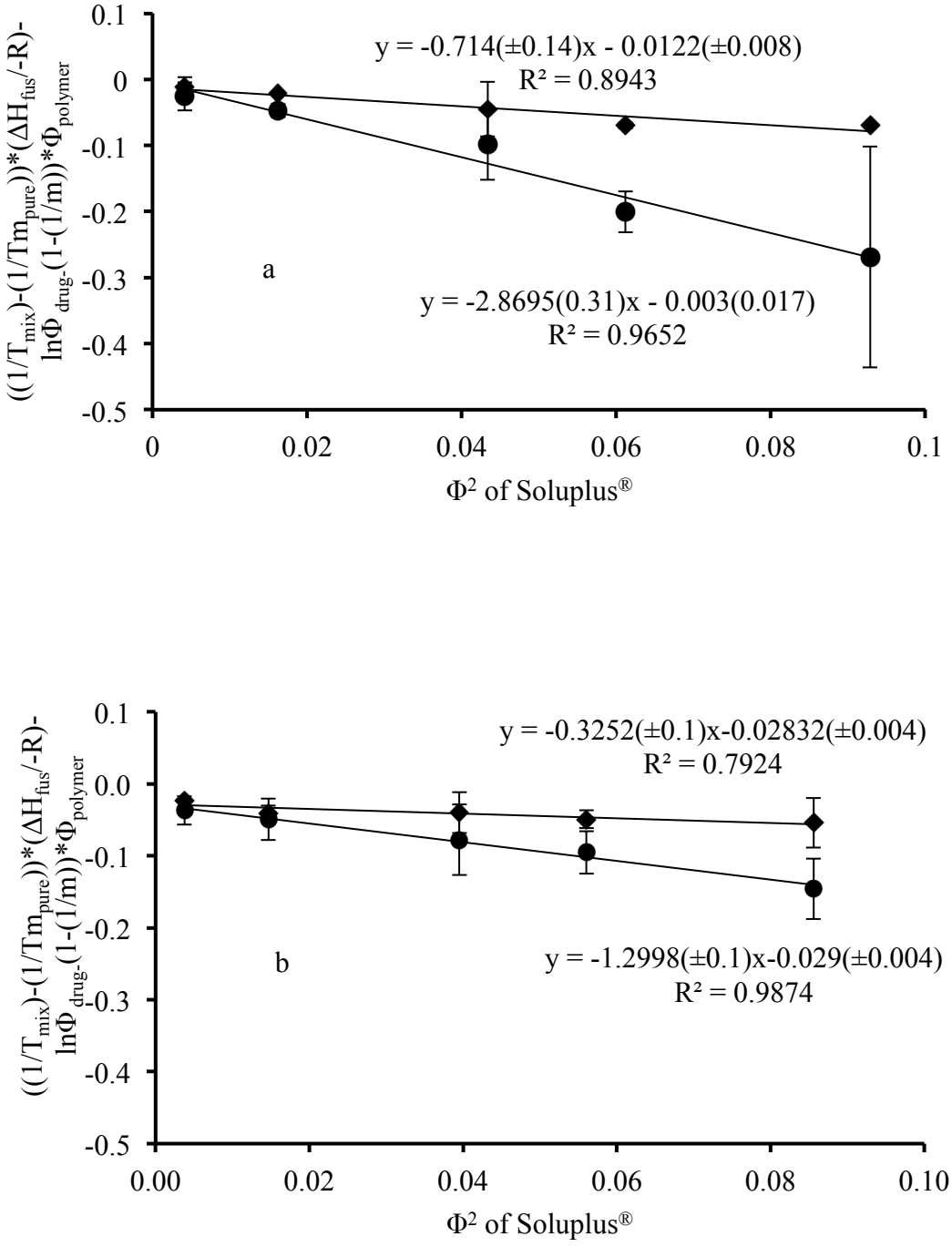

Figure 2.8. The interaction parameter, χ, calculated using the T_{onset} and T_{end} for SMX (a) and NIF (b). Numbers between the parentheses represent the standard error.

Plotting the data as presented in Eq. 2.3 using T_{onset} or T_{end} as the melting point of the mixture provided a linearization of the data for Soluplus® with the two model drugs (Figs. 2.8.a. and 2.8.b.). Higher polymer content lowers the melting point even further, but the linearity in this plot is eventually lost likely due to difference in thermal conductivity in the samples, or due to lower diffusivity of the melted drug into the more viscous polymer matrix at lower temperatures that would slow exposure of new solid surfaces to the influence of the rubbery polymer on the melting phenomenon. A negative interaction parameter indicates that the drug-polymer attraction is stronger than the drug-drug or polymer-polymer attraction. In addition, a negative interaction parameter of higher magnitude indicates a stronger interaction between the drug and the polymer.

The slopes of the respective plots provide an estimate of the interaction parameter for SMX and for NIF with Soluplus® that are reported in Table 2.2. Using either T_{onset} or T_{end} as the reduced melting point renders a negative χ value, indicating a favorable interaction between drug and polymer. A lower enthalpy of mixing is expected when the polymer more profoundly reduces the melting point of a crystalline drug [17]. The solubility of SMX in Soluplus® should therefore be higher than that of NIF at any temperature.

One should consider that the interaction parameter would have a different value at room temperature than at temperatures close to the melting point of the drug[37, 38]. At the melting point, the polymer is at a temperature above its glass transition temperature and is therefore in its rubbery state. The greater polymer flexibility allows formation of ample interfacial area with the drug particles. In addition, drug diffusion into the polymer matrix occurs more readily. At lower temperatures, the polymer matrix is more viscous and the diffusivity of drug molecules into the polymer will diminish. Even if one phase can be

achieved at a higher temperature, partial separation into two phases is known to occur when the mixture is reduced to a lower temperature. Such phenomena will be addressed in the phase diagram discussion.

2.6.2. Gibbs free energy of mixing

When the Gibbs free energy of mixing, as calculated using Eq. 2.4, is negative, it reveals the spontaneity of mixing between a drug and a polymer. The entropy portion always favors mixing. The enthalpy portion reflected by the interaction parameter term is expected to have a negative value that drives mixing. Temperature normalized Gibbs free energy for several values of interaction parameters, including each of those found in Table 2.2, are presented in Figs. 2.9.a. and 2.9.b. Clearly, with the negative interaction parameters calculated for SMX and NIF in Soluplus®, the Gibbs free energy of mixing predicts spontaneous mixing of drug with polymer across the whole range of possible Soluplus® content. The inclusion of $\chi = 2$ reveals how the temperature normalized free energy of mixing can exceed zero if the interaction parameter is a positive value, suggesting at least a region of immiscibility.

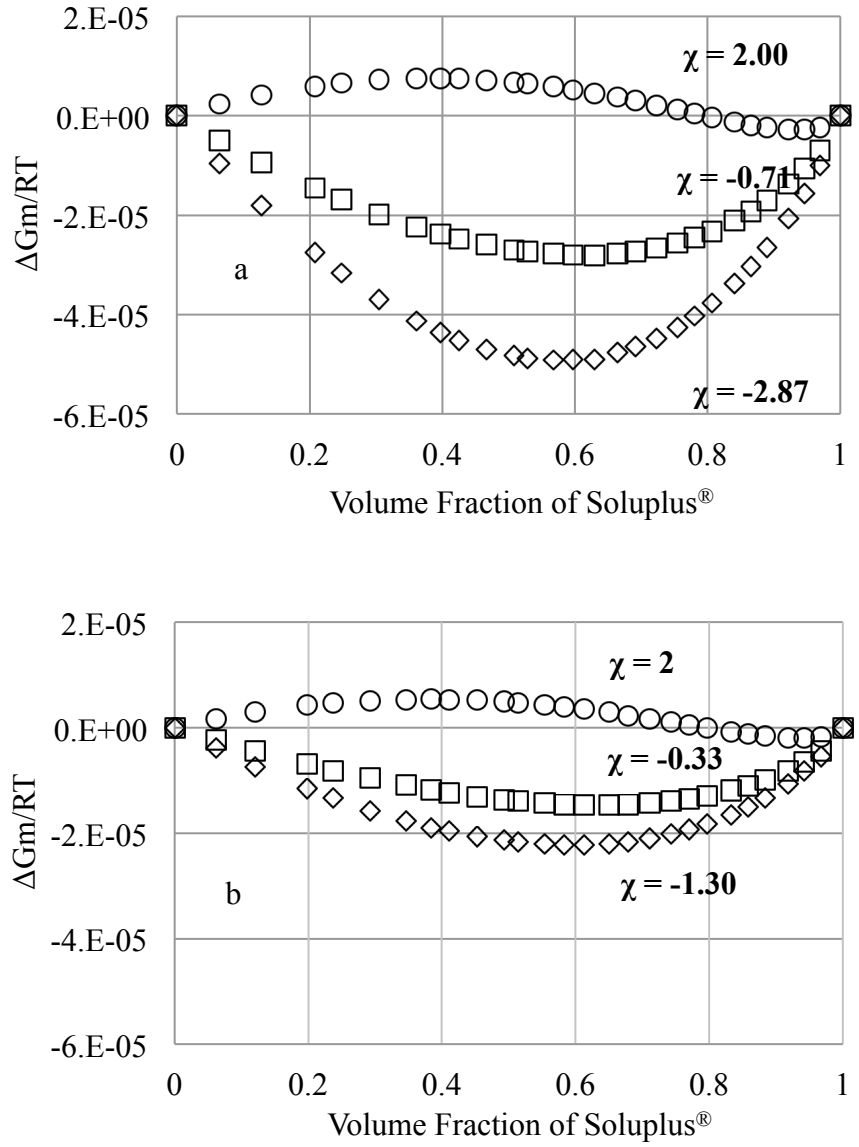

Figure 2.9. Temperature-normalized Gibbs free energy of mixing for SMX (a) and NIF (b) with Soluplus® at different χ values.

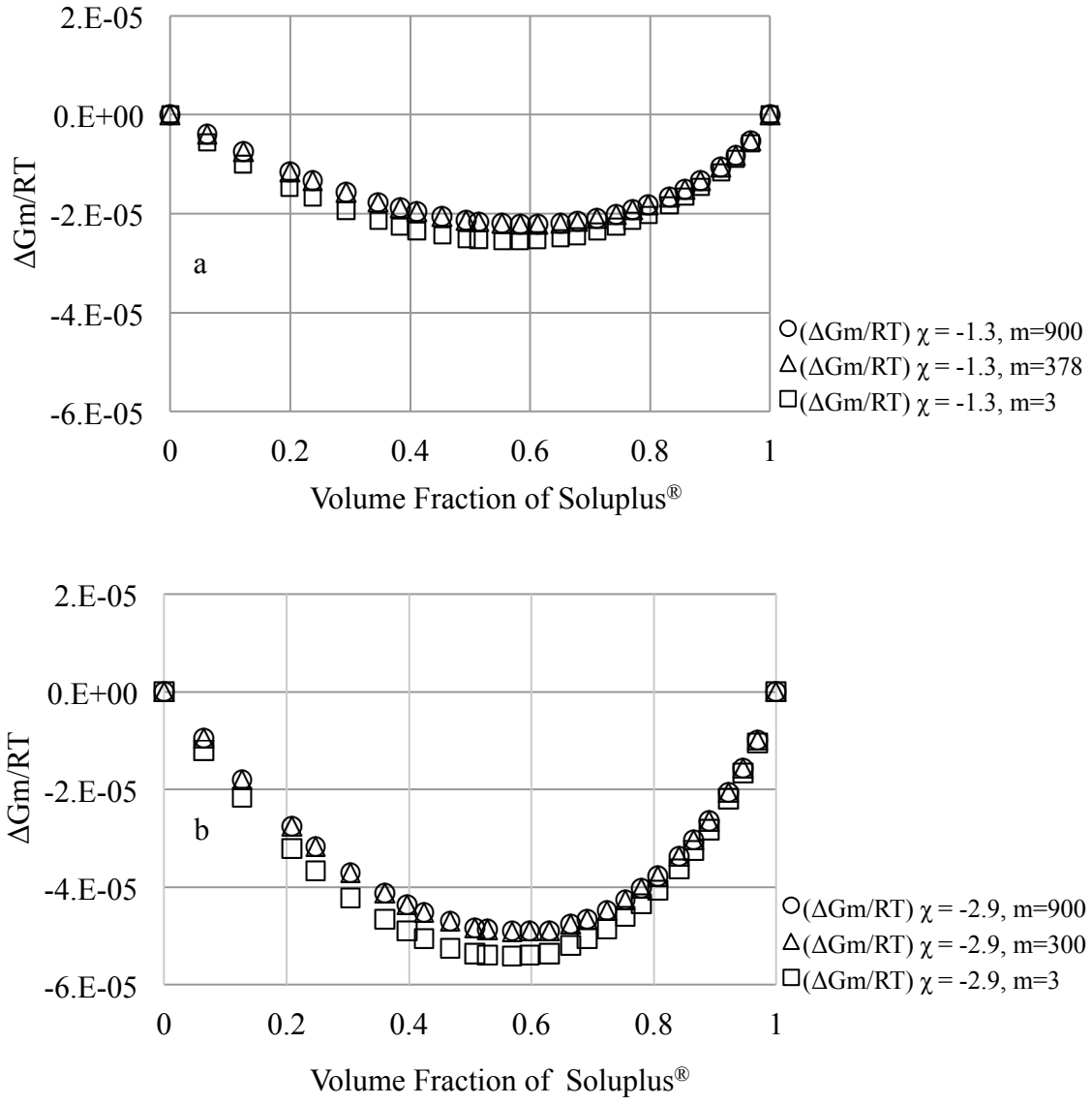

Figure 2.10. Temperature-normalized Gibbs free energy of mixing for SMX (a) and NIF (b) with Soluplus® at particular χ value and different MW of the polymer.

The interaction parameter term in Eq. 2.4, represents the enthalpy in the free energy calculation. The calculated interaction parameter was more negative when using T_{onset} data that reflected greater reductions in the melting endotherm. The free energy simulation curves indicate miscibility for the drug-polymer mixtures used in this study largely because the negative interaction parameters lead to less endothermic reactions.

The polymer molecular weight largely impacts the entropy contribution to the free energy of mixing, as reflected in the parameter m for the ratio of the molar volumes of the polymer and drug. However, the influence of the entropy terms is relatively small and the magnitude of the free energy is largely determined by the enthalpy contribution, see Figures 2.10.a. and 2.10.b. Therefore, if free energy disfavors mixing, one should consider a different polymer rather than choosing the same polymer with a different molecular weight.

2.6.3. Solubility prediction

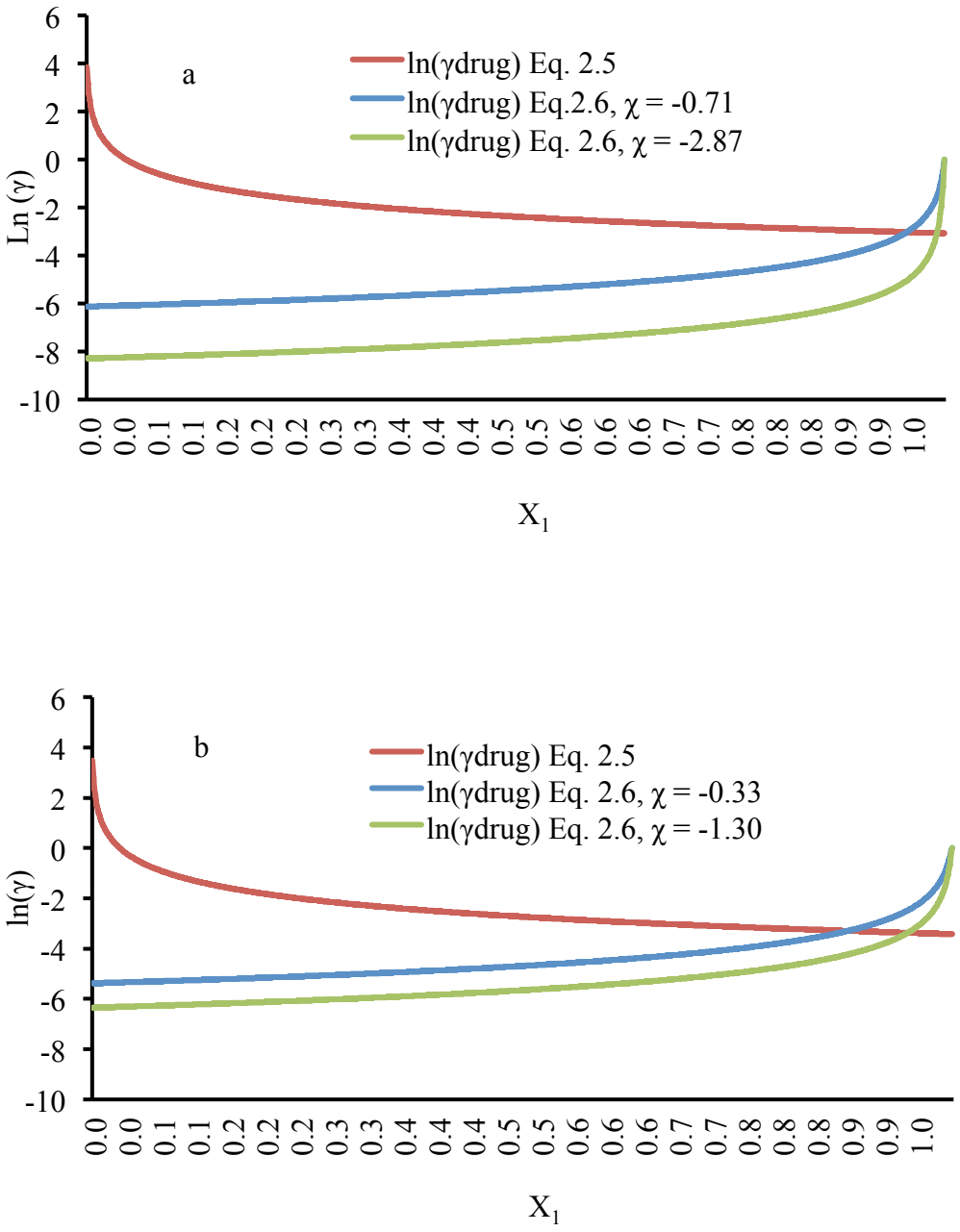

Figure 2.11. Determination of the mole fraction solubility for SMX (a) and NIF (b) in Soluplus at 298 K.

The drug solubility is defined as the level of crystalline drug that can dissolve in a rubbery, amorphous polymer that behaves like a viscous liquid to yield molecularly dispersed drug. Eq. 2.5 was developed to describe the solubility of a crystalline solute in a low molecular weight solvent. In this work, it is assumed that the polymer acts as the solvent. Using the Flory-Huggins Theory for a drug-polymer system, the activity coefficient is described in Eq. 2.6. It is clear that both entropy and enthalpy contributions to the solubility are represented in this equation.

Figs. 2.11.a. and 2.11.b., present curves for the activity coefficient based on the mole fraction solubility of each drug in Soluplus® at 298 K, based on Eq. 2.6 with one of the two values of the interaction parameter given in Table 2.2 and based on Eq. 2.5 volume fractions in equation 2.6 were calculated based on the mole fraction solubility from the x-axis, and the molar volumes of the drug and the polymer (see Table 2.1). The two curves for Eq. 2.6 show the sensitivity of the solubility of the drug to changes in χ. Solving Eqs. 2.5 and 2.6 simultaneously, as represented by the intersection of the Eq. 2.5 curve with one of the Eq. 2.6 curves (see Fig. 2.11.), allows prediction of the mole fraction solubility at the temperature used in Eq. 2.5. The predicted solubility expressed in % w/w units for each drug in Soluplus® is found in Table 2.2. Marsac et al., used these equations to predict the solubility of nifedipine and felodipine in methyl pyrrolidone, which showed good agreement between the predicted and observed values [10].

	Calculations based on T_{onset}		Calculations based on T_{end}	
Selected Drugs in Soluplus®	**Sulfamethoxazole**	**Nifedipine**	**Sulfamethoxazole**	**Nifedipine**
Interaction Parameter	-2.87 ± 0.31	-1.30 ± 0.1	-0.714 ± 0.14	-0.325 ± 0.10
Solubility (% w/w)	19.3 ± 3.4	5.18 ± 0.54	4.46 ± 0.54	1.99 ± 0.1

Table 2.2. Predicted solubility of sulfamethoxazole and nifedipine in Soluplus® expressed in % w/w units.

± Represents the standard error.

Using T_{onset} will give relatively lower endothermic mixing. Sulfamethoxazole is predicted to have about 20 % w/w solubility at room temperature based on the -2.87 interaction parameter. The predicted solubility was 4.0 times less for the same drug using T_{end}. For nifedipine, the use of T_{onset} rather than T_{end} resulted in improved solubility by a factor of 2.7.

This method is convenient and useful in the solubility prediction of drug-polymer mixtures. However, measuring the interaction parameter at temperatures where both substances behave as a liquid often induces miscibility of relatively larger concentrations than at lower temperatures. It is expected that solubility calculation at room temperature often gives higher drug concentration in the polymer than observed. Lin et al., used an empirical formula to describe the change in χ as a function of temperature. Using this formula will often give high positive value for χ at room temperature and will predict very low solubility using the above equations. On the contrary, a phase diagram plot can be used to find the room temperature solubility with some accuracy.

2.6.4. Phase diagram

Temperatures higher than the glass transition provide a kinetic state where the molecules are liberated from the confinement of the glassy state. However, the high viscosity near the glass transition temperature could slow the diffusion of the dissolved drug into the polymer beyond that of a realistic experimental timeframe.

A more efficient method for detecting the solubility at the glass transition temperature is discussed here. The drug-polymer mixture was prepared as described in the experimental section. The heating rate is chosen to be 1 °C/min and both T_{onset} and T_{end} are measured. The calculated interaction parameter is then introduced into Eq. 2.2 to estimate T_{mix} for mixtures[4] with different mass ratios, based on calculation of the respective volume fractions. The glass temperature was found for the neat polymers. Then, the drug was added at 10% increments and mixed before the DSC analysis. The heating rate was chosen to be 10 °C/min followed by cooling to zero degree at 60 °C/min. The mixture was then heated back to 185 °C using a heating rate of 10 °C/min for at least two cycles. The T_g onset was used in this experiment. The glass phase was experimentally obtained for mixtures with 90 and 100% SMX and NIF, respectively. Materials can be classified based on their crystallization tendency to (i) non-glass former, (ii) glass-former [39]. Sulfamethoxazole recrystallizes upon cooling, which is considered a class one, non-glass former. On the other hand, NIF is considered a class two, non-stable glass-former, where crystallization occurs during heating [39].

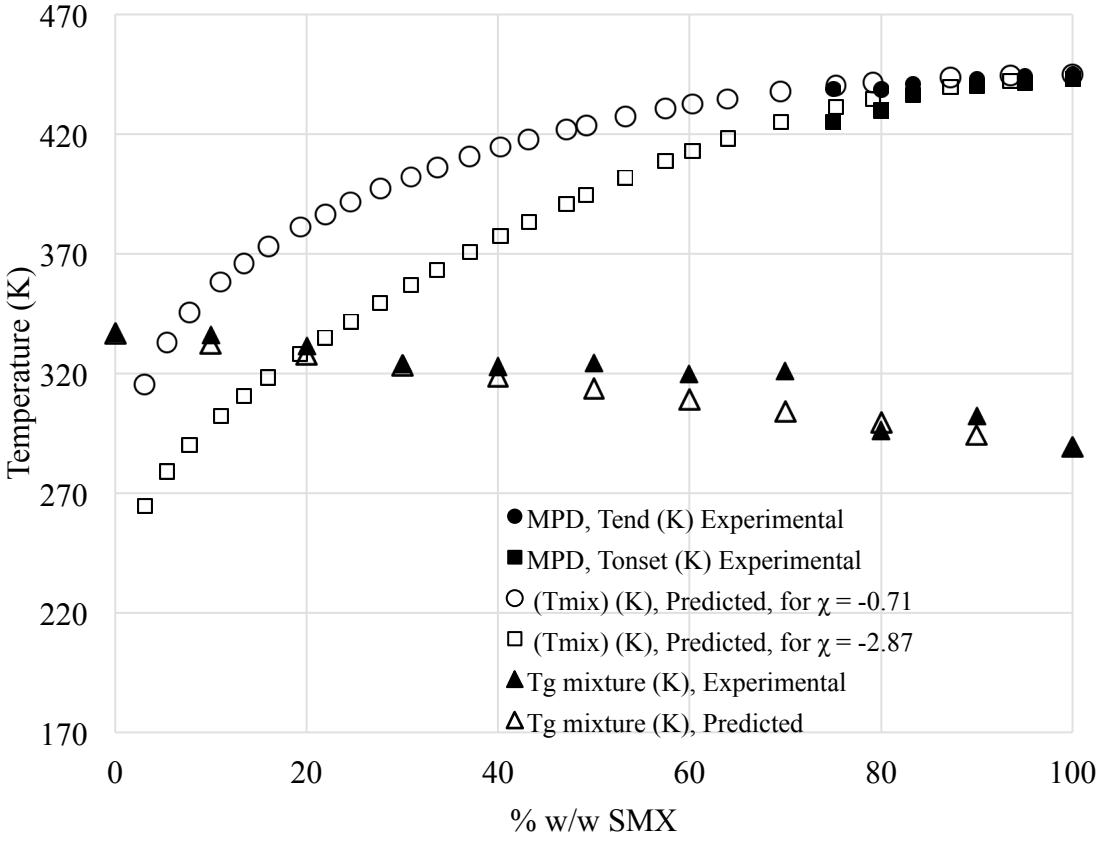

Figure 2.12.a. Phase diagram for SMX with Soluplus® where the curves predicted using Eq. 2.2 were extrapolated to intersect the $T_{g\ mix}$ curve.

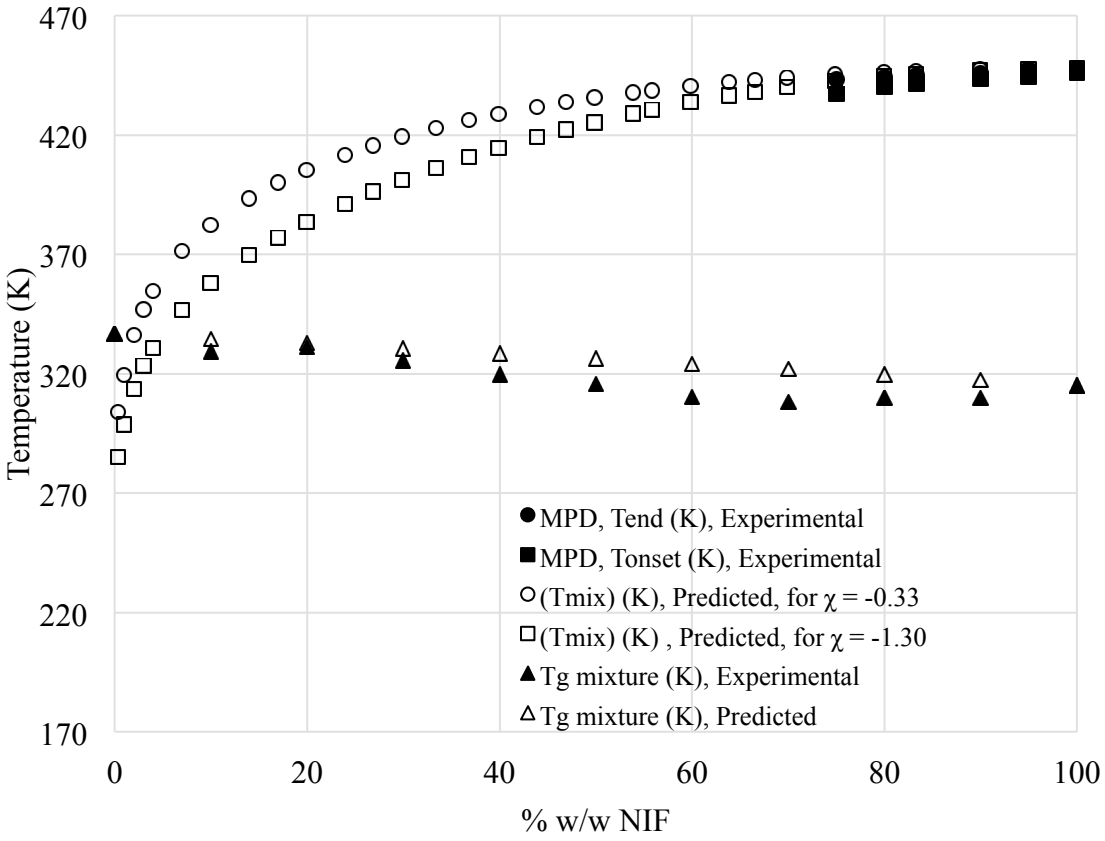

Figure 2.12.b. Phase diagram for NIF with Soluplus® where the curves predicted using Eq. 2.2 were extrapolated to intersect the $T_{g\,mix}$ curve.

The glass transition temperature for SMX was estimated to be 16 °C [34, 40]. To validate the phase diagram method, Kollidon VA 64 will be used with nifedipine to compare the results with those in the literature. The DSC thermograms provided an evident melting endotherm of the drug up to a 25% w/w polymer concentration. The experimental and the predicted melting points for SMX with varying Soluplus® content in the mixture are found in Fig. 2.12.a. The glass transition for the mixture was obtained for polymer with drug concentration up to 100%. A negative interaction parameter of greater magnitude contributed to the prediction of a higher drug solubility. Fig. 2.12.b., shows a similar pattern for NIF data.

The MPD curves in Fig. 2.12., represent the depression in the melting point of the drug as the polymer percentage by weight increases. Any mixture above the MPD curve is expected to be miscible. However, under the MPD curve the drug might exceed its solubility in the polymer and two phases are expected. Since the melted drug has diffused into the polymer at temperatures above its depressed melting point, drug crystallization involving the excess drug is likely to occur if drug is in excess of its solubility in the polymer and the cooling rate was slow enough to start nucleation. If the drug fraction is totally miscible in the polymer, the higher temperature will facilitate drug detection of sites on the polymer molecules where the bonding energy is high enough to produce a solid solution, i.e., molecularly dispersed drug in the polymer matrix. Molecularly dispersed drug should allow the rubbery mixture to transition to a glassy solid solution when the temperature decreases below the mixture T_g, without drug crystallization taking place. Therefore, the point where MPD curve intersects the Tg mixture line should represent the drug solubility in the polymer. In the glassy state, the movement of drug or

polymer molecules is restricted and phase separation is unlikely to happen. Because the drug is molecularly dispersed in the polymer matrix, a solid solution exists and no melting endotherm for the drug should be evident in the DSC thermogram for such a sample.

Numerous methods were devised to estimate the glass transition temperature for binary mixtures. Gordon and Taylor developed, based on the polymer free volume theory, the most popular empirical formula to predict the T_g for binary mixtures as a function of components composition Eq. 2.8 and 2.9 [12, 30, 33, 41].

$$T_{g\,mix} = \frac{W_1 * T_{g1} + K * W_2 * T_{g2}}{W_1 + K * W_2} \tag{2.8}$$

$$K = \frac{T_{g1} * \rho_1}{T_{g2} * \rho_2} \tag{2.9}$$

where W_1 and W_2 are the weight fraction of the drug and the polymer. T_{g1} and T_{g2} are the glass transition temperature of the amorphous drug and polymer. K is a constant related to the true density for the drug and the polymer, ρ_1 and ρ_2. The true densities are 1.42 and 1.34 (g/cm^3) for crystalline SMX and NIF, respectively. It is true to estimate the density of the amorphous counterpart of each drug candidates to be 95% of the drug crystalline density resulting in 1.35 and 1.27 (g/cm^3) for amorphous SMX and NIF, respectively [12]. The predicted glass transition temperature for any mixture matches the experimental data if two conditions are met; mixing occur at the molecular level (ideal mixing) and no changes in the volume during mixing.

Figure 2.12.a., shows a minimal deviation between the experimental and the predicted $T_{g\ mix}$ data. This small deviation might be ascribed to the experimental errors during the DSC analysis. Clearly, based on these data the miscibility between SMX and Soluplus® is not limited and no phase separation is expected.

The observed deviation of the experimental data form the theoretical data calculated from Eqs. 2.8 and 2.9 is attributed to the possibility of limited miscibility between NIF and Soluplus® or VA 64 see Figures 2.12.b. and 2.13. Other possibilities include; volume change during mixing and difference in the molecular interaction.

The solubility is calculated for each drug based on intersection in the phase diagram and is reported in Table 2.3. It is important to note that these results are relevant at temperatures higher than room temperature. However, the solubility is not expected to change by much since the movement of both the drug and the polymer molecules becomes limited below the T_g of the mix. The points of intersection were found to be 63 and 58 °C for SMX using T_{end} and T_{onset}, respectively; NIF solubility were detected at 63 and 61 °C using T_{end} and T_{onset}, respectively. These corresponded to 6.32 and 20.30 % w/w for SMX and 2.4 and 5.10 % w/w for NIF.

The predicted solubility for each drug in Soluplus® by the two methods is in good agreement. The first method was employed to predict the drug solubility in Soluplus® at room temperature, whereas the phase diagram method predicts the solubility at $T_{g\ mix}$. Such agreement shows that the predicted solubility at $T_{g\ mix}$ can be expected to be close to the solubility at room temperature.

	Calculations based on T_{onset}		Calculations based on T_{end}	
Selected Drugs in Soluplus®	**Sulfamethoxazole**	**Nifedipine**	**Sulfamethoxazole**	**Nifedipine**
Interaction Parameter	-2.87 ± 0.31	-1.30 ± 0.1	-0.714 ± 0.14	-0.325 ± 0.10
Solubility (% w/w)	20.3 ± 2.5	5.10 ± 0.68	6.32 ± 1.1	2.40 ± 0.37

Table 2.3. Predicted solubility using the phase diagram method for sulfamethoxazole and nifedipine in Soluplus® expressed in % w/w units.

± Represents the standard error.

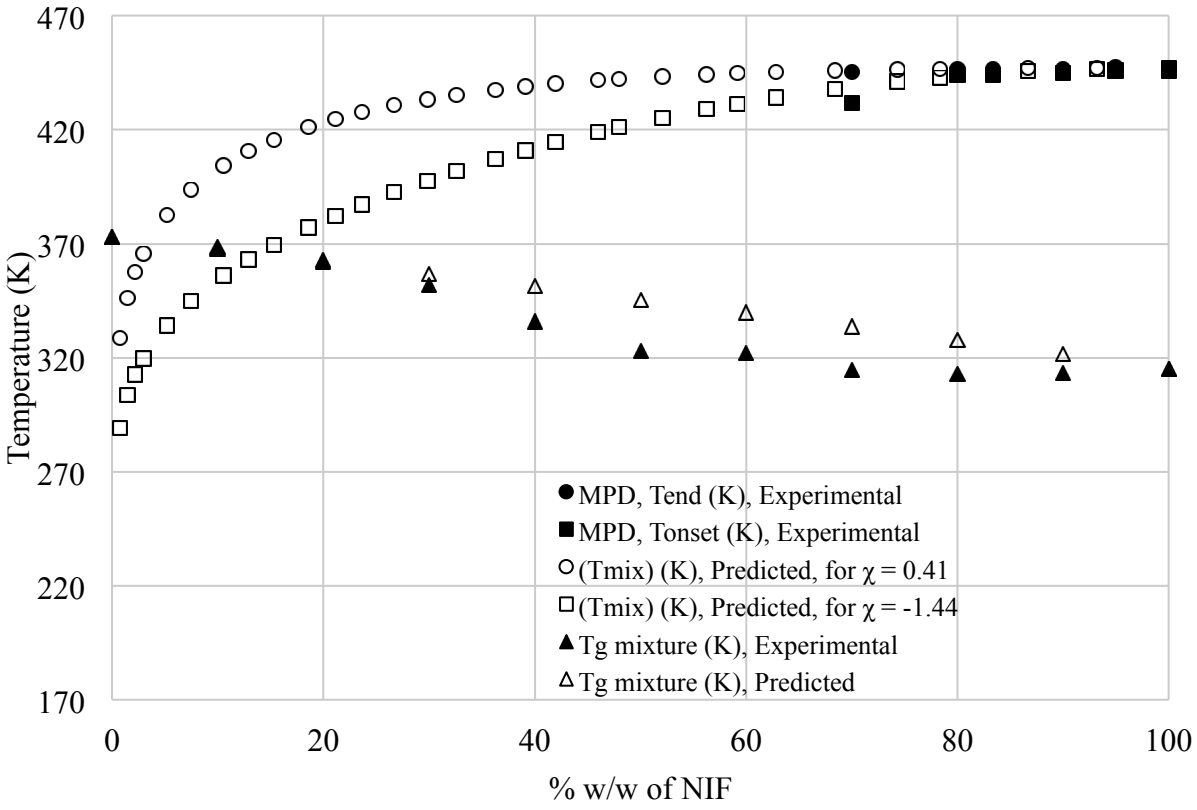

Figure 2.13. Phase diagram for NIF with VA64 where the MPD curve was extrapolated to the $T_{g\ mix}$ curve.

A phase diagram for Kollidon VA64 with NIF was constructed to validate the modified method presented here and to support the assertion of choosing T_{onset} for these calculations. Tao et al., predicted the solubility of NIF in Kollidon VA64 to be 12 % w/w using T_{end} in their calculations [20]. The drug-polymer mixture went through many cryomilling cycles to reduce the drug and polymer particle size and to distribute drug particles in the polymer prior to DSC analysis. When efficient physical mixing is pursued prior to DSC analysis, the diffusion of melted drug is facilitated by the tremendous interfacial area between drug and polymer that facilitates melted drug diffusion into the polymer, exposing new surfaces of crystalline drug to melt. The result is an endotherm of shorter duration in the thermogram than seen with hand milling or ball-milling, T_{end} is substantially lowered, and the choice between using T_{onset} or T_{end} in calculations becomes less of an issue. Fig. 2.13., shows the phase diagram for NIF with Kollidon VA64 that predicts the solubility at T_g to be 4.2 and 13.1 % w/w using T_{end} and T_{onset}, respectively. This confirms that T_{onset} serves well in the prediction of the solubility of crystalline drug in a copolymer even when efficient mixing techniques such as cryomilling have not taken place.

Clearly, the interaction parameter, χ, considered a constant in the previous calculations. However, chi expected to be a function of both temperature and composition. Others suggest that temperature mainly affects chi and an empirical formula was developed to define chi. Here, chi when treated as a function of temperature rendered a large positive value at room temperature that eventually translated to predicted solubility < 0.001 % w/w. In this experiment, chi behaves the best when considered a constant.

The heating rate and the type of physical mixing of the drug-polymer mixture can have profound effects on T_{onset}. With inadequate physical mixing of the components, the percentage of the drug particle surface area that is in contact with the polymer is low in comparison to what could be achieved with appropriate physical mixing yielding a non-linear relationship. The low enthalpy requirement at T_{onset} corresponding to this low interfacial area results in a negligible appearance of early melting in the melting endotherm. A heating rate of 10 deg/min or more reveals no depression in the melting point, likely because an opportunity for the polymer to affect the melting of the drug is compromised. At higher heating rates, the sample can absorb heat directly from the surrounding oven and this is not measured by the heat flow sensor [42]. The heat flow rate to the sample increases in parallel with the higher heating rate and thermal resistance contributes to "smearing of the measured signals" [42]. Low thermal conductivity in the sample mixture can lead to thermal lag, with sample in contact with the pan heating at a faster rate than the rate of heat conduction to polymer and drug particles in the interior of the sample, leading to a temperature differential in the sample, ΔT, and a subsequently higher measurable T_{onset}. The temperature differential is dependent on both the effective thermal resistance, ρ_{th}, and the heat flow rate, $\emptyset$ [42]:

$$\Delta T = \rho_{th}\, \emptyset \tag{2.10}$$

To reduce thermal lag, the thermal resistance and the heat flow rate across the resistance should both be minimized. The only way to accomplish this when increasing the heating rate is to reduce sample mass, m:

$$\emptyset = cm\beta \tag{2.11}$$

where c is the specific heat capacity, m is the sample mass, and β is the heating rate[42].

2.7. Conclusions

Melting point depression predicted by Flory-Huggins theory was utilized successfully with a triblock graft copolymer, Soluplus®, to predict the solubility of poorly soluble drugs in the polymer. A comparison of the interaction parameter calculated for SMX and NIF with Soluplus® using T_{onset} and T_{end} was made. Solubility in the polymer was predicted using the ideal solubility equation derived for crystalline solutes in low molecular weight solvents and using the equation for the solubility of small molecules in polymers based on the Flory-Huggins Theory. Where the two solubility curves intersect should provide a good approximation of the solubility of the drug in the polymer near room temperature. A phase diagram was also used to predict drug solubility at the glass transition temperature. The methods provided similar solubility results. This experimental approach proved to be a fast and efficient method to predict the solubility of crystalline drugs in an amorphous polymer.

2.8. References

1. Hughey JR, Keen JM, Brough C, Saeger S, McGinity JW. Thermal processing of a poorly water-soluble drug substance exhibiting a high melting point: The utility of KinetiSol® dispersing. Int J Pharm. 2011. 419(1-2): 222-30

2. Murdande SB, Pikal MJ, Shanker RM, Bogner RH. Solubility advantage of amorphous pharmaceuticals, Part 3: Is maximum solubility advantage experimentally attainable and sustainable? J Pharm Sci. 2011. 100(10): 4349-56

3. Sun Y, Tao J, Zhang GGZ, Yu L. Solubilities of crystalline drugs in polymers: An improved analytical method and comparison of solubilities of indomethacin and nifedipine in PVP, PVP/VA, and PVAc. J Pharm Sci. 2010. 99(9): 4023-31

4. Lin D, Huang Y. A thermal analysis method to predict the complete phase diagram of drug–polymer solid dispersions. Int J Pharm. 2010. 399(1–2): 109-15

5. Wegiel LA, Mauer LJ, Edgar KJ, Taylor LS. Crystallization of amorphous solid dispersions of resveratrol during preparation and storage-Impact of different polymers. J Pharm Sci. 2013. 102(1): 171-84

6. Pandya P, Gattani S, Jain P, Khirwal L, Surana S. Co-solvent evaporation method for enhancement of solubility and dissolution rate of poorly aqueous soluble drug simvastatin: in vitro-in vivo evaluation. AAPS PharmSciTech. 2008. 9(4): 1247-52

7. Song Y, Wang L, Yang P, Wenslow RM, Jr., Tan B, Zhang H, Deng Z. Physicochemical characterization of felodipine-kollidon VA64 amorphous solid dispersions prepared by hot-melt extrusion. J Pharm Sci. 2013. 102(6): 1915-23

8. Tian Y, Booth J, Meehan E, Jones DS, Li S, Andrews GP. Construction of drug–polymer thermodynamic phase diagrams using Flory–Huggins Interaction Theory: Identifying the relevance of temperature and drug weight fraction to phase separation within solid dispersions. Mol Pharm. 2012. 10(1): 236-48

9. Mahieu A, Willart J-F, Dudognon E, Danède F, Descamps M. A new protocol to determine the solubility of drugs into polymer matrixes. Mol Pharm. 2012. 10(2): 560-6

10. Marsac PJ, Shamblin SL, Taylor LS. Theoretical and practical approaches for prediction of drug–polymer miscibility and solubility. Pharm Res. 2006. 23(10): 2417-26

11. Morgen M, Bloom C, Beyerinck R, Bello A, Song W, Wilkinson K, Steenwyk R, Shamblin S. Polymeric nanoparticles for increased oral bioavailability and rapid

absorption using celecoxib as a model of a low-solubility, high-permeability drug. Pharm Res. 2012. 29(2): 427-40

12. Weuts I, Van Dycke F, Voorspoels J, De Cort S, Stokbroekx S, Leemans R, Brewster ME, Xu D, Segmuller B, Turner YT, Roberts CJ, Davies MC, Qi S, Craig DQ, Reading M. Physicochemical properties of the amorphous drug, cast films, and spray dried powders to predict formulation probability of success for solid dispersions: Etravirine. J Pharm Sci. 2011. 100(1): 260-74

13. Flory PJ. Thermodynamics of high polymer solutions. J Chem Phys. 1942. 10(1): 51-61

14. Huggins ML. The viscosity of dilute solutions of long-chain molecules. IV. Dependence on concentration. J Amer Chem Soci. 1942. 64(11): 2716-8

15. Hiemenz PC, Lodge TP. Polymer Chemistry, 2nd edition FL: CRC press, Taylor & Francis group; 2007.

16. Nishil T WT. Melting point depression and kinetic effects of cooling on crystallization in poly(viny1idene fluoride)-poly (methyl methacrylate) mixtures. Macromolecules. 1975. 8: 909-15

17. Marsac PJ, Li T, Taylor LS. Estimation of drug-polymer miscibility and solubility in amorphous solid dispersions using experimentally determined interaction parameters. Pharm Res. 2009. 26(1): 139-51

18. Zhao Y, Inbar P, Chokshi HP, Malick AW, Choi DS. Prediction of the thermal phase diagram of amorphous solid dispersions by Flory-Huggins theory. J Pharm Sci. 2011. 100(8): 3196-207

19. Qian C, Mumby SJ, Eichinger B. Phase diagrams of binary polymer solutions and blends. Macromolecules. 1991. 24(7): 1655-61

20. Tao J, Sun Y, Zhang GZ, Yu L. Solubility of small-molecule crystals in polymers: d-Mannitol in PVP, indomethacin in PVP/VA, and nifedipine in PVP/VA. Pharm Res. 2009. 26(4): 855-64

21. BASF. <Soluplus Technical Information>. 2009.

22. Ali S. L, N., Djuric, D., Kolter, K.,. Eye on excipients, http://www.pharma-ingredients.basf.com/Soluplus/Home.aspx ingredients.basf.com/Soluplus/Home.aspx accessed. May 5, 2013.:

23. Matsuda Y, Teraoka R, Sugimoto I. Comparative evaluation of photostability of solid-state nifedipine under ordinary and intensive light irradiation conditions. Int J Pharm. 1989. 54(3): 211-21

24. Bayomi MA, Abanumay KA, Al-Angary AA. Effect of inclusion complexation with cyclodextrins on photostability of nifedipine in solid state. Int J Pharm. 2002. 243(1–2): 107-17

25. Özdemir N, Erkin J. Enhancement of dissolution rate and bioavailability of sulfamethoxazole by complexation with β-cyclodextrin. Drug Dev Ind Pharm. 2012. 38(3): 331-40

26. Pereira AV, Cass QB. High-performance liquid chromatography method for the simultaneous determination of sulfamethoxazole and trimethoprim in bovine milk using an on-line clean-up column. J Chrom B. 2005. 826(1–2): 139-46

27. Liew CV, Chan LW, Ching AL, Heng PWS. Evaluation of sodium alginate as drug release modifier in matrix tablets. Int J Pharm. 2006. 309(1): 25-37

28. Viana M, Jouannin P, Pontier C, Chulia D. About pycnometric density measurements. Talanta. 2002. 57(3): 583-93

29. Yang M, Wang P, Gogos C. Prediction of acetaminophen's solubility in poly(ethylene oxide) at room temperature using the Flory–Huggins theory. Drug Dev Ind Pharm. 2012. 1-7

30. Forster AH, J. Tucker, I. Rades. T. The potential of small-scale fusion experiments and the gordon-taylor equation to predict the suitability of drug/polymer blends for melt extrusion. Drug Dev Ind Pharm. 2001. 27(6): 549-60

31. Cheng SZ. Phase Transitions in Polymers: The Role of Metastable States. Amsterdam: Elsevier; 2008.

32. Witold B RC, Ioannis M K, Aglaia V,. Prediction of glass transition temperatures: Binary blends and copolymers. M letters. 2008. 62(17-18): 3152-5

33. Gordon M, Taylor JS. Ideal copolymers and the second-order transitions of synthetic rubbers. i. non-crystalline copolymers. J Appl Chem. 1952. 2(9): 493-500

34. Baird JA, Van Eerdenbrugh B, Taylor LS. A classification system to assess the crystallization tendency of organic molecules from undercooled melts. J Pharm Sci. 2010. 99(9): 3787-806

35. Simerdeep SG AM, Tapan P, Abu T.M. Serajuddin. Investigation of thermal and viscoelastic properties of polymers relevant to hot melt extrusion, I: Polyvinylpyrrolidone and related polymers. J Excip F chem. 2014. 5(1): 32-45

36. Araújo AAS, Bezerra MdS, Storpirtis S, Matos JdR. Determination of the melting temperature, heat of fusion, and purity analysis of different samples of zidovudine (AZT) using DSC. B J Pharm Sci. 2010. 46: 37-43

37. Janssens S, Van den Mooter G. Review: physical chemistry of solid dispersions. J Pharm Pharmacol. 2009. 61(12): 1571-86

38. Qian F, Huang J, Hussain MA. Drug-polymer solubility and miscibility: stability consideration and practical challenges in amorphous solid dispersion development. J Pharm Sci. 2010. 99(7): 2941-7

39. Alhalaweh A, Alzghoul A, Kaialy W, Mahlin D, Bergström CA. Computational Predictions of Glass-Forming Ability and Crystallization Tendency of Drug Molecules. Mol pharm. 2014. 11(9): 3123-32

40. Mahlin D, Bergström CA. Early drug development predictions of glass-forming ability and physical stability of drugs. E J Pharm Sci. 2013. 49(2): 323-32

41. Baird JA, Taylor LS. Evaluation of amorphous solid dispersion properties using thermal analysis techniques. Adv drug del R. 2012. 64(5): 396-421

42. Schick C. Differential scanning calorimetry (DSC) of semicrystalline polymers. Anal Bioanal Chem. 2009. 395(6): 1589-611

3. A study to identify the contribution of Soluplus® component homopolymers to the solubilization of nifedipine and sulfamethoxazole using the melting point depression method

3.1. Abstract

Purpose: The Flory-Huggins Theory was employed successfully to predict the solubility in Soluplus®. In the present study, the strengths of Sulfamethoxazole (SMX) and nifedipine (NIF) interactions with Soluplus® nonionic homopolymer components, namely polyvinyl caprolactam (PCL), polyvinyl acetate (PVAc), and polyethylene glycol (PEG), were measured. A prediction of the strength of the interaction, free energy of mixing, and the solubility of each drug in each polymer was performed. Also, a comparison between the solubility of the drug candidates in Soluplus® and its individual homopolymers was conducted.

Methods: The depression of the melting point for each crystalline drug in the presence of Soluplus® component homopolymers was measured at various drug levels using differential scanning calorimetry. The predicted solubility of crystalline materials in each polymer was calculated. A low molecular weight polymer solvent was used to experimentally calculate the model drug solubility.

Results: PEG 6000 exhibited a negative interaction parameter with SMX and NIF, indicating a relatively strong drug-polymer interaction. For PVAc, a positive interaction parameter was found, indicating a relatively weak drug-polymer interaction. PCL, however, was not suitable for the applied method. The free energy of mixing and the solubility of each drug in the Soluplus® component homopolymers were estimated using

the interaction parameter. The predicted solubility of each drug in PEG 6000 was compared to the corresponding solubility in PEG 400, a lower molecular weight version of PEG 6000 that is liquid at room temperature.

Conclusion: The Flory-Huggins Theory allowed identification of the contribution of each polymer to the solubilization of NIF and SMX. PVAc demonstrated weak interactions with each drug and they are unlikely to participate in drug solubilization. Soluplus® and PEG 6000, however, interacted well with each drug and would substantially contribute to the drug solubilization.

3.2. Keywords

Flory-Huggins Theory, solid solution, sulfamethoxazole, nifedipine, Soluplus®, PEG 6000, PVAc, PCL, miscibility, solubility.

3.3. Introduction

Incorporating a small molecular weight drug in a polymeric carrier matrix has long proved to be effective in enhancing and altering many physical and chemical characteristics of different drugs. Examples include a considerable increase in the dissolution rate, higher equilibrium solubility [1-11], change in the melting temperature T_m, the glass transition temperature T_g [1, 12-15], and newly formed chemical bonds with the carrier matrix [7, 10, 16, 17].

Deeming a single-phase system that shows unique physicochemical characteristics requires any two components to be miscible. With the majority of newly synthesized molecules lacking the required aqueous solubility [8, 18], a deeper understanding of the interactions between miscible blends is essential. It has been suggested that acquiring a single T_g is considered a sufficient indicator to find miscible drug-polymer mixtures [19, 20]. However, such indicator does not elucidate the mixing thermodynamics in that system.

Flory-Huggins Lattice Theory is widely used due to its accessibility. Employing this theory is an important to measure the thermodynamic quantities of different blends by establishing the interaction parameter. The interaction parameter, χ, reveals the interaction strength in the mixed blends [21]. The melting point depression method, derived from Flory-Huggins Theory, permits the exploration of the thermodynamic driving forces of drug-polymer mixtures. It was first introduced for amorphous polymer/crystal polymer blends [22]. Later, it was successfully utilized for amorphous polymer crystal drug mixtures. [23-26].

The reduction in the melting temperature is due to a process similar to dissolution, in which, the polymer is considered a solvent for the crystalline drug. If the forces of attraction, such as dispersion forces and hydrogen bonding, between the drug and the polymer are larger than the cohesive forces in the pure polymer or pure drug, the crystal melting temperature will be reduced as the polymer content in the mixture increases. The dissolved drug, in whole or in part, is expected to distribute randomly within the polymer matrix. Clearly, the dissolved portion will have different physical and chemical characteristics than that of pure amorphous drug [27].

The experimental plan that was executed successfully to predict the solubility of SMX and NIF in Soluplus® is found elsewhere (see Chapter Two). A mixing technique, somewhat different from the conventional method found in the literature, was used in the melting point depression method to calculate the interaction parameter. A phase diagram method was constructed to validate the previous method. Both methods rendered similar results (see Chapter Two).

The melting point depression approach was utilized to access the mixing thermodynamics between different kinds of co-polymers [23-26]. However, an investigation of the contribution of each component homopolymer to the solubility process has never been studied. In this study, the solubility of SMX and NIF in each component homopolymer of Soluplus® was calculated based on the Flory-Huggins model. Prediction of the solubility in Soluplus®, based on the solubility of each drug in the different component homopolymers, is made. Furthermore, the theoretical solubility values in PEG 6000 were compared to the experimental values in low molecular weight PEG 400. The effect of the

interaction parameter, the molecular weight variations, and the suitability of this method to identify the influence of each homopolymer are discussed.

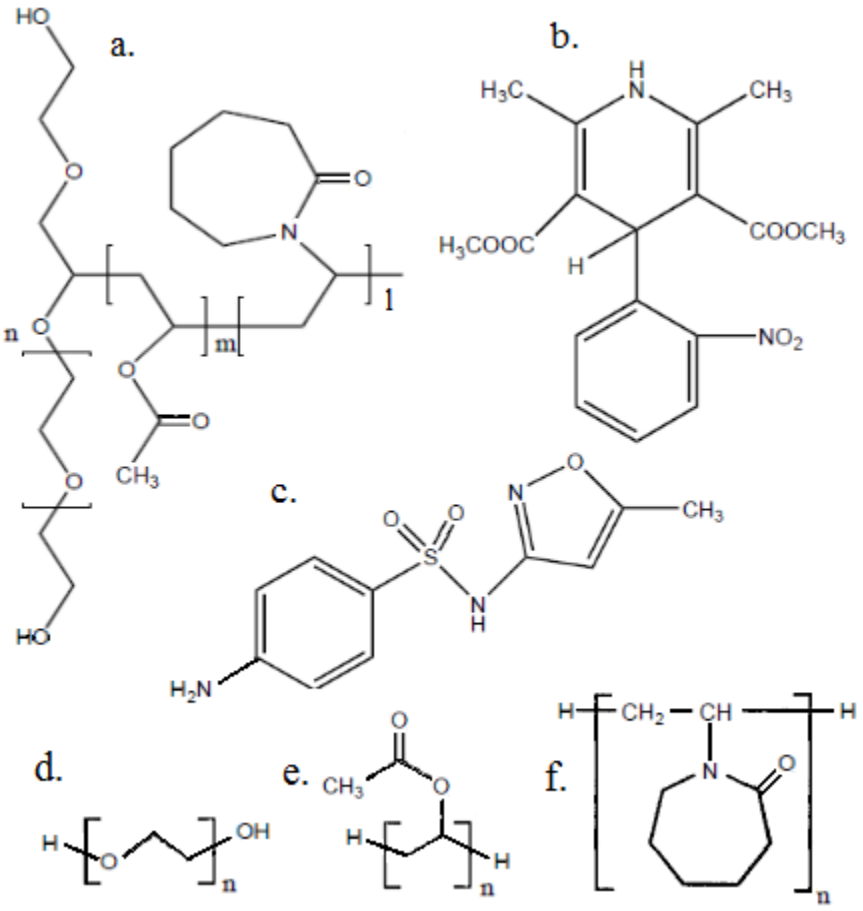

Figure 3.1. Chemical structures of a. Soluplus®, b. nifedipine, c. sulfamethoxazole, d. polyethylene glycol, e. polyvinyl acetate, and f. polyvinyl caprolactam.

3.4. Materials

Soluplus® (Fig. 3.1.a.), (M_w = 118000 g/mol, density = 1.08 g/cm^3) provided by BASF (Tarrytown, NY), is an amorphous polymer and has a T_g around 70 °C. Crystalline nifedipine (Fig. 3.1.b.), (M_w = 346.34 g/mol, density = 1.34 g/cm^3) was purchased from (C.F.M. Co. Farmaceutica Milanese S.P.A., Milano, Italia). Crystalline sulfamethoxazole (Fig. 3.1.c.), (M_w = 253.28 g/mol, density = 1.42 g/cm^3) was purchased from Flavine International Inc. (Closter, NJ). PEG 6000 (Fig. 3.1.d.), (M_w = 6000 g/mol, density = 1.08 g/cm^3) and PCL (Fig. 3.1.f.), (K40), density = 0.96 g/cm^3) were generous gifts from BASF (Tarrytown, NY). PVAc (Fig. 3.1.e.), (M_w = 500,000 g/mol, density = 1.19 g/cm^3) and PEG 400 (M_w = 400 g/mol, density = 1.13 g/cm^3) were purchased from Sigma-Aldrich Co. (St. Louis, MO, USA).

3.5. Methods

3.5.1 Differential scanning calorimetry

The method of sample preparation is described in Chapter Two. In essence, particle size of less than 500 μm in diameter were collected and kept in a desiccator for at least a week prior to mixing to ensure no moisture was involved. Photodegradation was prevented by keeping NIF in an amber bottle. For the thermal analysis, the influence of 0, 5, 10, 16.7, 20, and 25% w/w of polymer in the drug-polymer mixture was assessed. Each sample weighing exactly 5 mg was placed in an aluminum pan and an aluminum lid was crimped to form a hermetic seal. At least three samples were prepared at each polymer concentration. The onset melting temperature of sulfamethoxazole and nifedipine alone and in the presence of PVAc, PEG 6000, and PCL were measured with a TA 2910 DSC (TA Instruments, New Castle, DE) at a scan rate of 1 deg/min. The DSC was calibrated for temperature and enthalpy with indium (100% pure, melting point 156.60 °C, heat of fusion 6.80 cal/g). The sample and reference cells were purged with nitrogen at 50 ml/min.

The results were analyzed using Thermal Advantage 1.1 A software. A tangent to the linear portion of the leading edge of the melting endotherm was extrapolated to the baseline to define each onset of melting.

3.5.2. Thermal gravimetrical analysis

A TGA/SDTA851^{e} Thermogravimetric Analyzer (Mettler Toledo, Columbus, OH) was used to measure the thermal stability of nifedipine, sulfamethoxazole, Soluplus®, PEG 6000, PVAc, and PCL. The results were analyzed using Mettler Toledo STAR^{e} software. The materials were dried in a desiccator for at least one week prior to testing. A 5-15 mg sample was placed in a 70 µl aluminum oxide crucible in the sample chamber under a 20 ml/min nitrogen flow. Samples were heated at 10 deg/min from ambient temperature to 500 °C.

3.5.3. Solubility of SMX and NIF in PEG 400

SMX and NIF solubility in PEG 400 was measured using a SpectraMax Plus UV-Vis Spectrophotometer (Molecular Devices Inc., Sunnyvale, CA, USA). An excess of crystalline drug was added to a capped vial that contained PEG 400 maintained at 25 °C. The NIF vial was covered with aluminum foil to prevent photolysis. Each of the vials was continuously shaken for at least 48 h. The resulting suspensions were centrifuged using J2-21 centrifuge, (Beckman, city, CA) and filtered through a 0.20 µm SFCA syringe filter (Corning Inc., Corning, NY). Samples were diluted with methanol as needed and compared to the standard curve.

3.5.4. Melting point depression

The interaction parameter between crystalline drug and amorphous polymer, χ, is calculated using Eq. 3.1 [23, 25, 26, 28, 29]:

$$-\frac{\Delta\overline{H}_{fus}}{R}\left(\frac{1}{T_m^{Mix}}-\frac{1}{T_m^{Pure}}\right)-\ln\Phi_{drug}-\left(1-\frac{1}{m}\right)\Phi_{polymer}=\chi\Phi_{polymer}^2 \quad (3.1)$$

Eq. 3.1 uses the extent of the reduction in the melting point from that of the pure drug, T_m^{Pure}, to that of the drug in the drug-polymer mixture, T_m^{Mix}. ΔH_{fus} is the molar enthalpy of fusion of the pure drug and R is the universal gas constant. Φ_{drug} and $\Phi_{polymer}$ are the volume fraction of the drug and polymer, respectively, and m is the ratio of the molar volume of the polymer to the molar volume of the drug. Regular Solution Theory can be exploited to determine the molar Gibbs energy of mixing using Eq. 3.2 [30]. The first two terms on the right hand side of the equation represent the influence of the entropy of mixing and the last term represents the influence of the enthalpy of mixing.

$$\frac{\Delta G_{mix}}{RT}=n_{drug}\ln\Phi_{drug}+n_{polymer}\ln\Phi_{polymer}+n_{drug}\Phi_{polymer}\chi \quad (3.2)$$

Here n_{drug} is the number of moles of the drug, $n_{polymer}$ is the number of moles of the polymer, and the other parameters are described above.

3.5.5. Solubility prediction

The activity of crystalline drugs in low molecular weight solvent is described by Eq. 3.3 [23]:

$$\ln\gamma_{drug}X_{drug} = -\frac{\Delta\overline{H}_f}{RT}\left(1-\frac{T}{T_m^{Pure}}\right)-\frac{\Delta C_p}{R}\left[\left(1-\frac{T_m^{Pure}}{T}\right)+\ln\left(\frac{T_m^{Pure}}{T}\right)\right] \quad (3.3)$$

where γ_{drug} is the activity coefficient of the drug in the solvent and X_{drug} is the mole fraction solubility of the drug in the solvent, which is the polymer in this study. T is taken to be 298 K. ΔC_p is the difference in heat capacity between crystalline and amorphous drug. Using Flory-Huggins Theory, the activity coefficient can be described for drug-polymer mixtures using Eq. 3.4:

$$\ln\gamma_{drug}X_{drug} = \ln\Phi_{drug} + \left(1-\frac{1}{m}\right)\Phi_{polymer} + \chi\Phi^2_{polymer} \quad (3.4)$$

From Eq. 3.4, the drug's activity is affected by drug-polymer molecular size dispersity and the interaction parameter. Solving equation 3.3. and 3.4. simultaneously will render the mole fraction solubility, $X_{drug.}$

Table 3.1. Properties of the materials in the study.

	M_W (g/mol)	*Density (g/cm^3)	Molar volume (cm^3/mol)	ΔH_{fus} (KJ/mol)	T_M (K)	T_g (K)
Sulfamethoxazole	253	1.42	172.30	28.70	443	289**
Nifedipine	346	1.34	288.62	36.5	447	316
Soluplus®	118000	1.08	109000	-	-	343
Polycaprolactam	18000	0.96	18700	-	-	458
Polyethylene glycol	6000	1.08	5556	1072	333	251
Polyvinyl acetate	500000	1.19	420000	-	-	318

* Density was measured using helium pycnometry.

** Ref. [31]

3.6. Results and discussion

3.6.1. Melting point depression

The thermogram for each material is found in Figure 3.2.

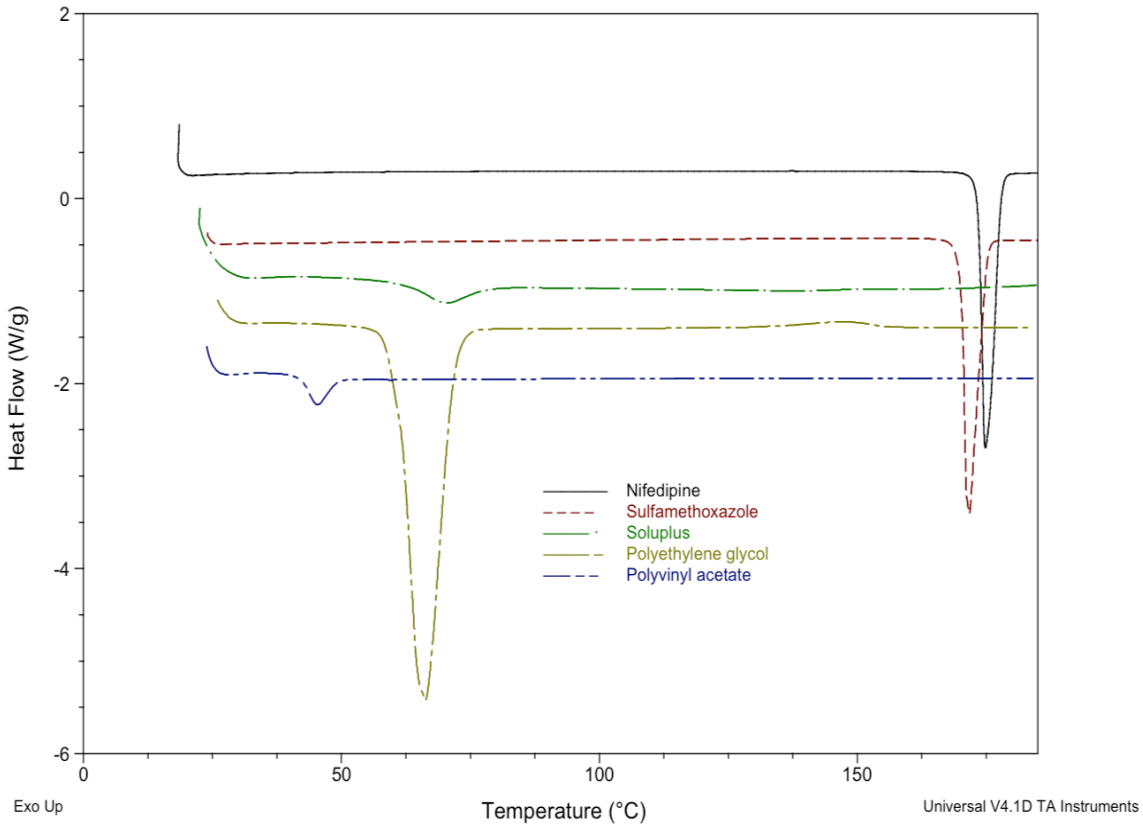

Figure 3.2. The DSC thermograms for (from top to bottom): nifedipine, sulfamethoxazole, Soluplus®, polyethylene glycol, and polyvinyl acetate.

As seen in the Figure 3.2., nifedipine has a melting point of 173.05 °C, sulfamethoxazole has a melting point of 169.87 °C, Soluplus® has a T_g around 70 °C, polyethylene glycol has a T_g around -22 °C (not shown in the figure above) and melting temperature of 60 °C, and polyvinyl acetate has a T_g around 42 °C. Note that Polyvinyl caprolactam comes in a liquid form (40% w/v, ethanol). Upon drying, the polymer shows a melting endotherm around 220 °C indicating some crystallinity (not shown in the figure).

One needs an amorphous polymer to fulfill the requirement of the melting point depression approach. Polyvinyl caprolactam went through a lyophilization process to successfully obtain the amorphous form. The T_g was found to be around 185 °C (see Figure 3.3). It is important to note that amorphous polymer acts as a solvent before the melting of the crystalline drug takes place. Also, it is recommended that the polymer glass transition temperature precedes the drug melting temperature by a considerable temperature difference, the reason being is that the reduced polymer viscosity facilitates the equilibrium between the drug and the polymer during the time of the DSC analysis [26]. Having the polymer T_g above the melting temperature of the crystalline drug negates the melting point depression MPD requirements for the polymer. Therefore, the thermodynamic parameters are not accessible through this current method. Polyethylene glycol 6000 is mostly crystalline, around 98% crystallinity [32]. It has been proved that converting PEG 6000 to be completely amorphous is practically difficult and its recrystallization rate is apparently fast [33].

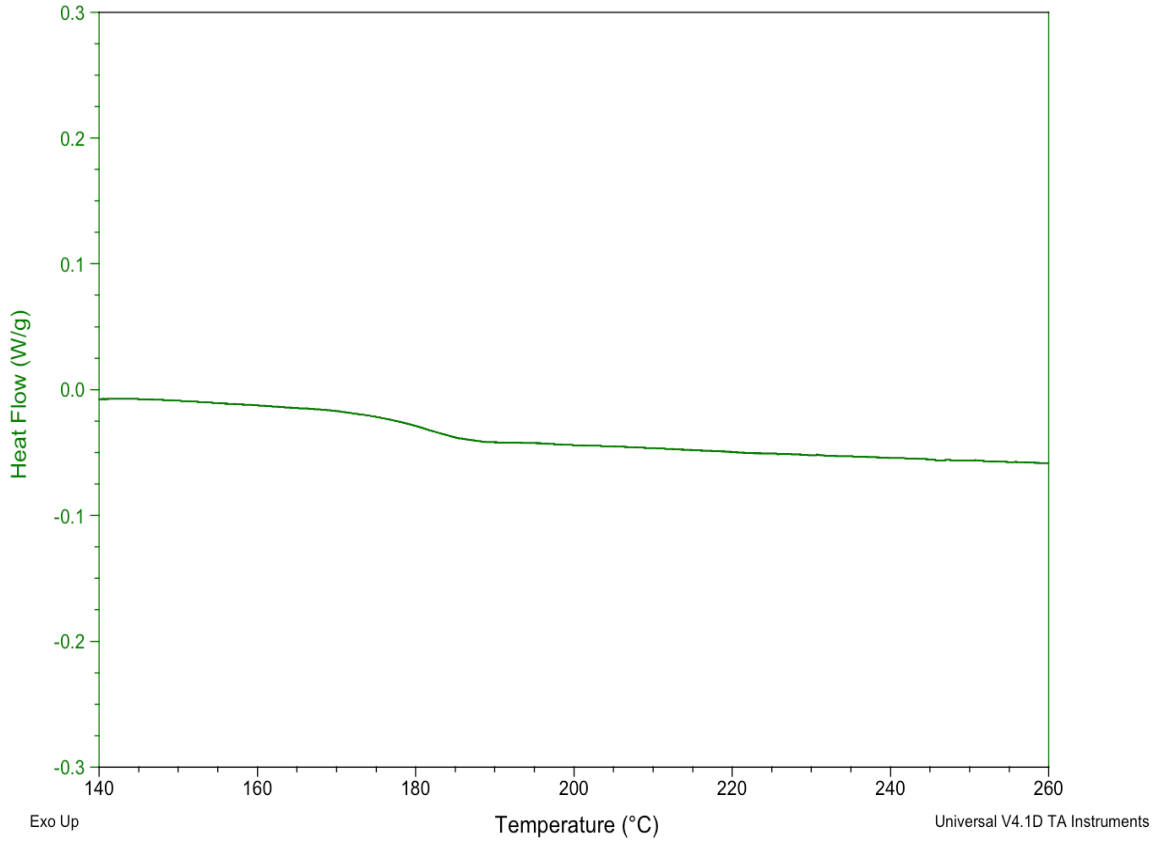

Figure 3.3. The DSC thermogram for lyophilized polyvinyl caprolactam.

Thermogravimetric analysis was conducted to avoid any possibility of chemical degradation during the DSC analysis. Figure 3.4., reveals the degradation temperature for sulfamethoxazole at 233, nifedipine at 270, Soluplus® at 297, polyethylene glycol at 290, polyvinyl acetate at 320, and polyvinyl caprolactam at 390 °C.

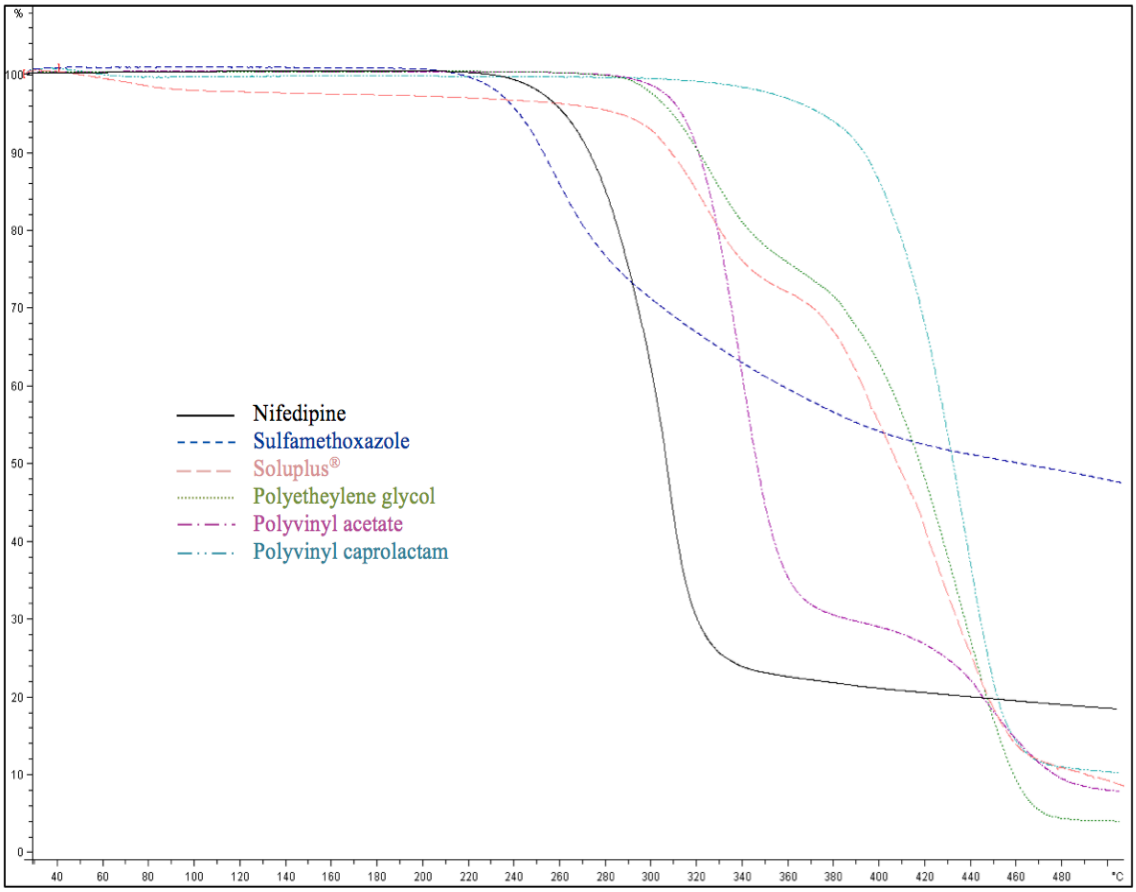

Figure 3.4. The TGA thermograms for nifedipine, sulfamethoxazole, Soluplus®, polyethylene glycol, polyvinyl acetate, and polyvinyl caprolactam.

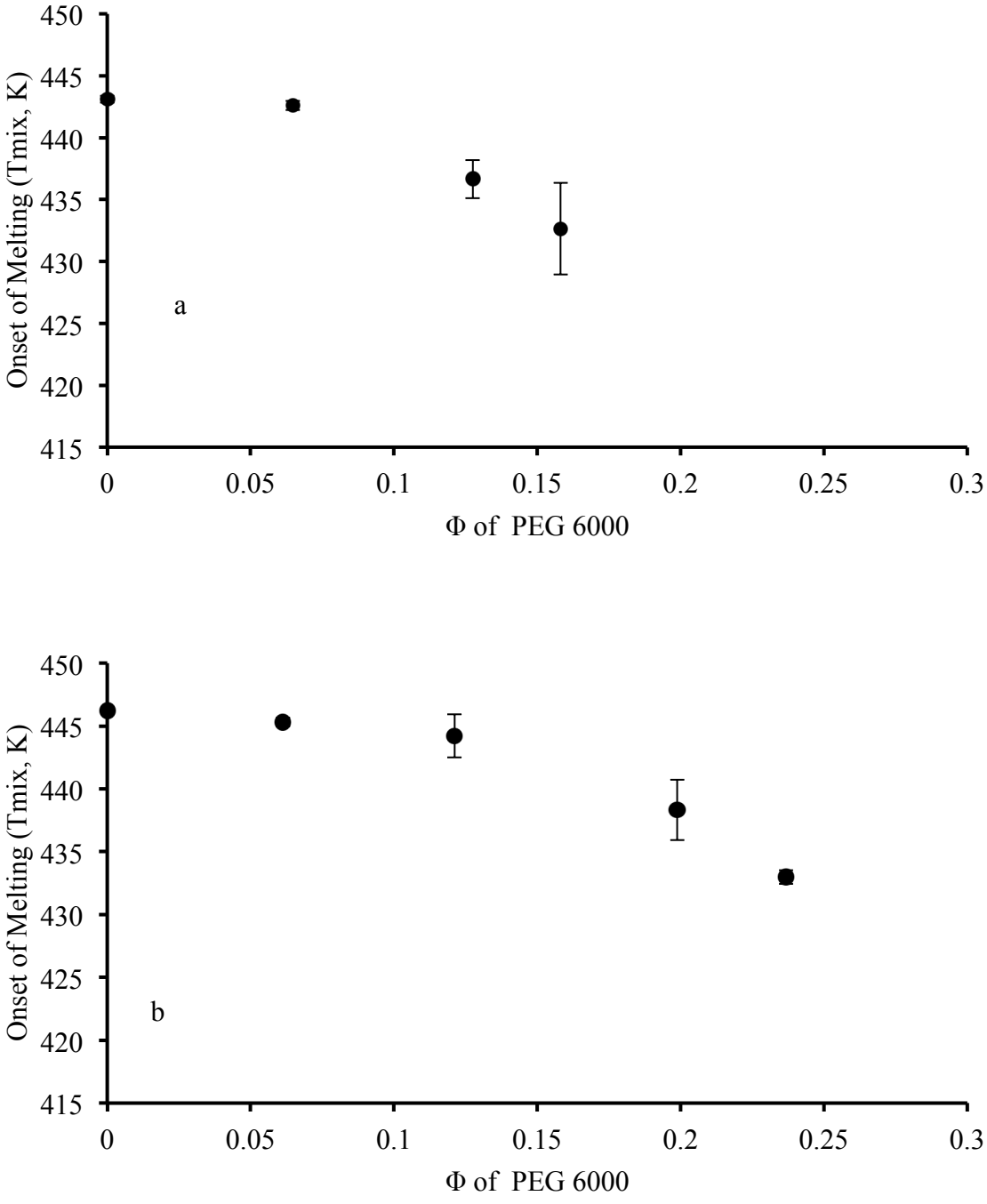

Figure 3.5. DSC results for SMX (a) and NIF (b), showing the onset melting temperature for each drug at different concentrations of PEG 6000, presented as a function of the volume fraction of PEG 6000.

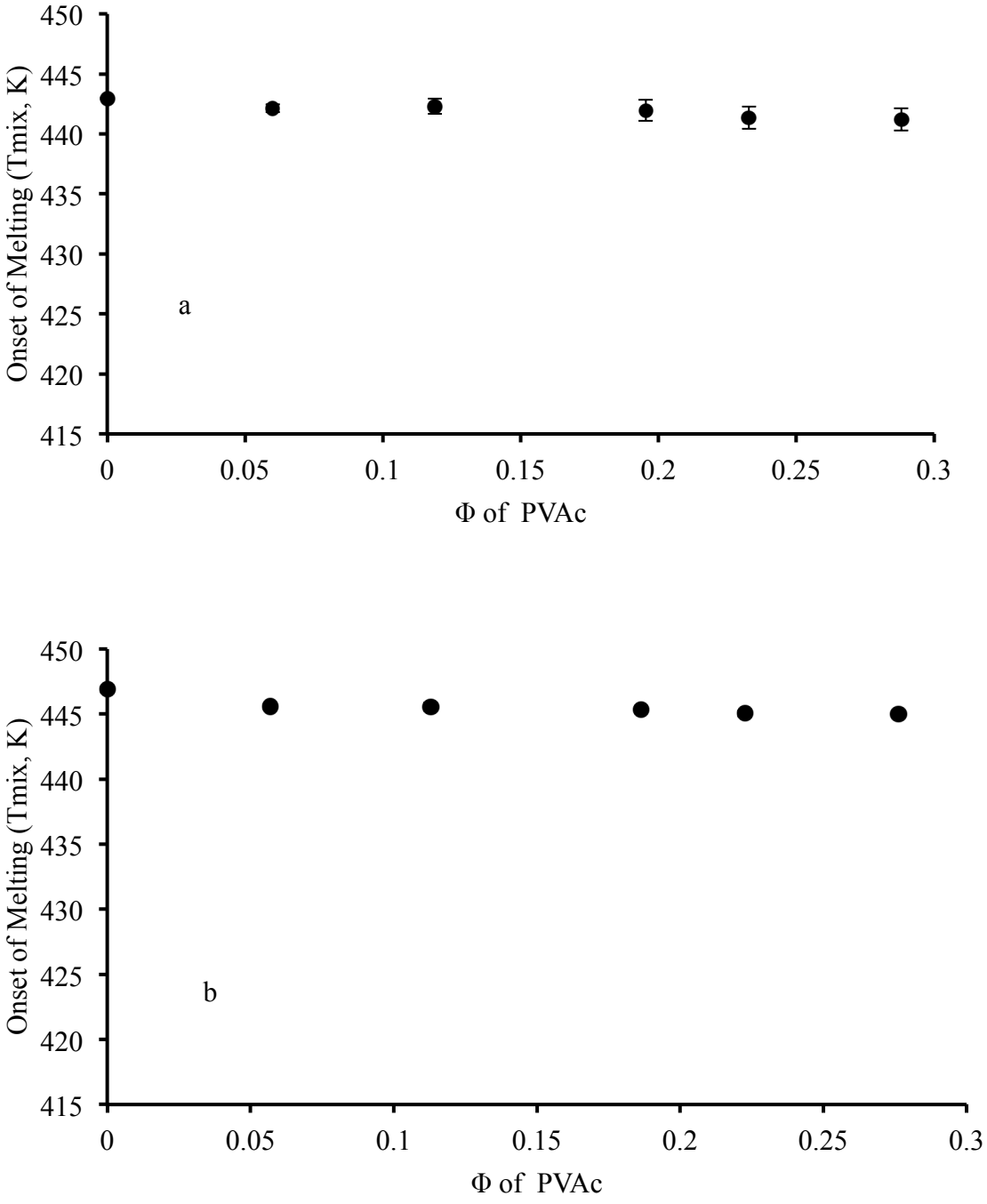

Figure 3.6. DSC results for SMX (a) and NIF (b), showing the onset melting temperature for each drug at different concentrations of PVAc, presented as a function of the volume fraction of PVAc.

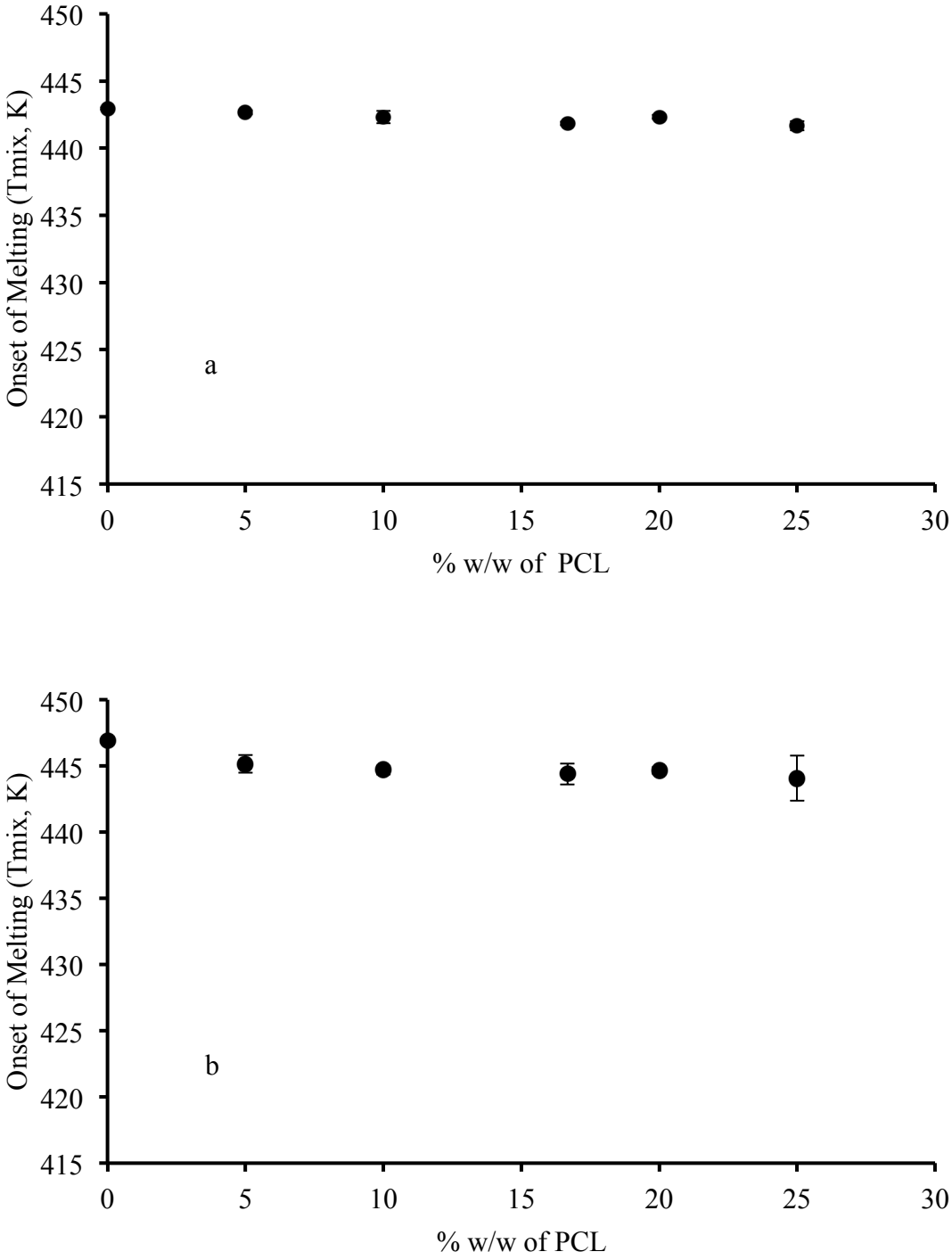

Figure 3.7. DSC results for SMX (a) and NIF (b), showing the melting temperature for each drug at different concentrations of PCL, presented as a function of the weight percentage of PCL.

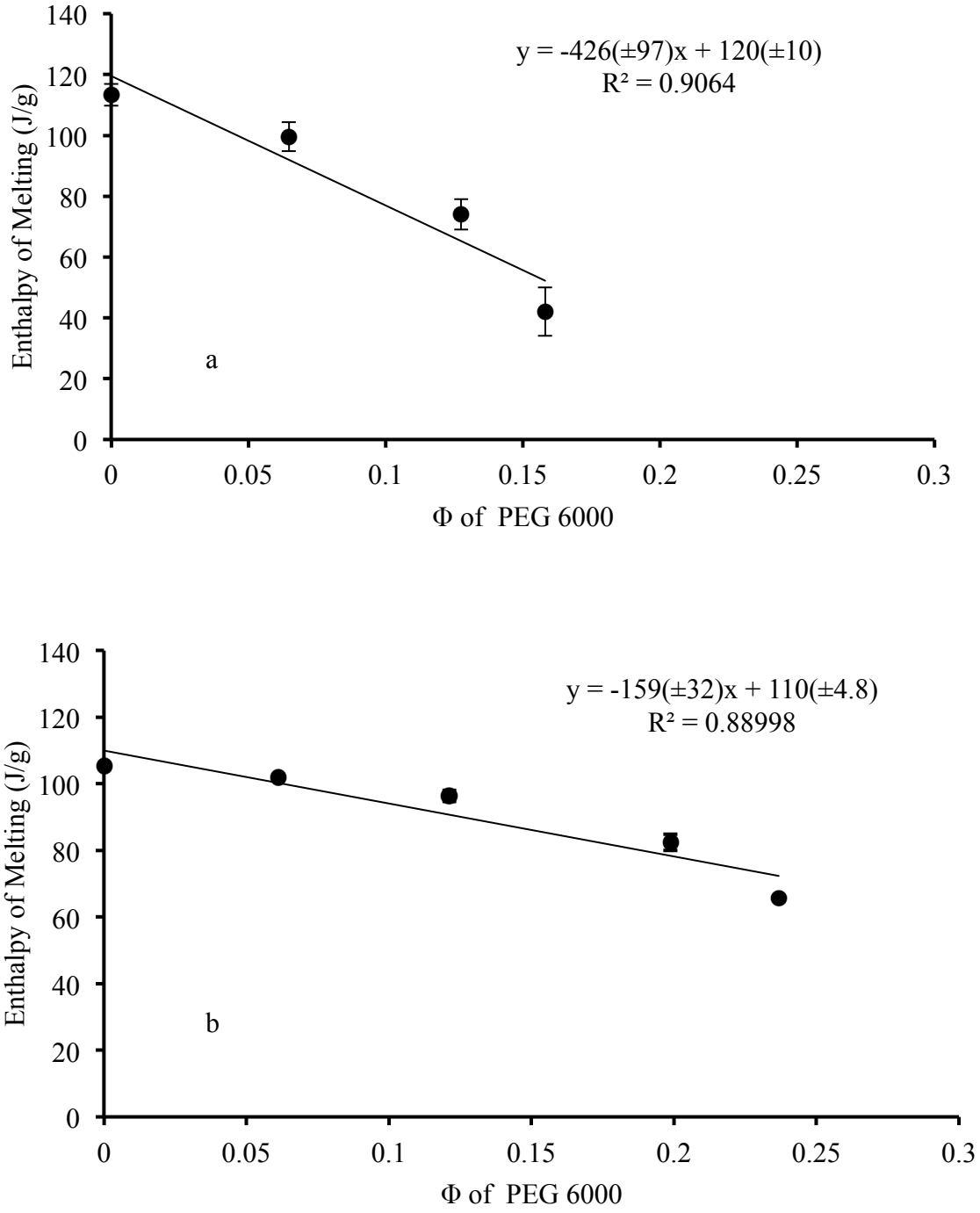

Figure 3.8. DSC results for SMX (a) and NIF (b), showing the enthalpy of melting for each drug at different concentrations of PEG 6000, presented as a function of the volume fraction of PEG 6000. Numbers between the parentheses represent the standard error.

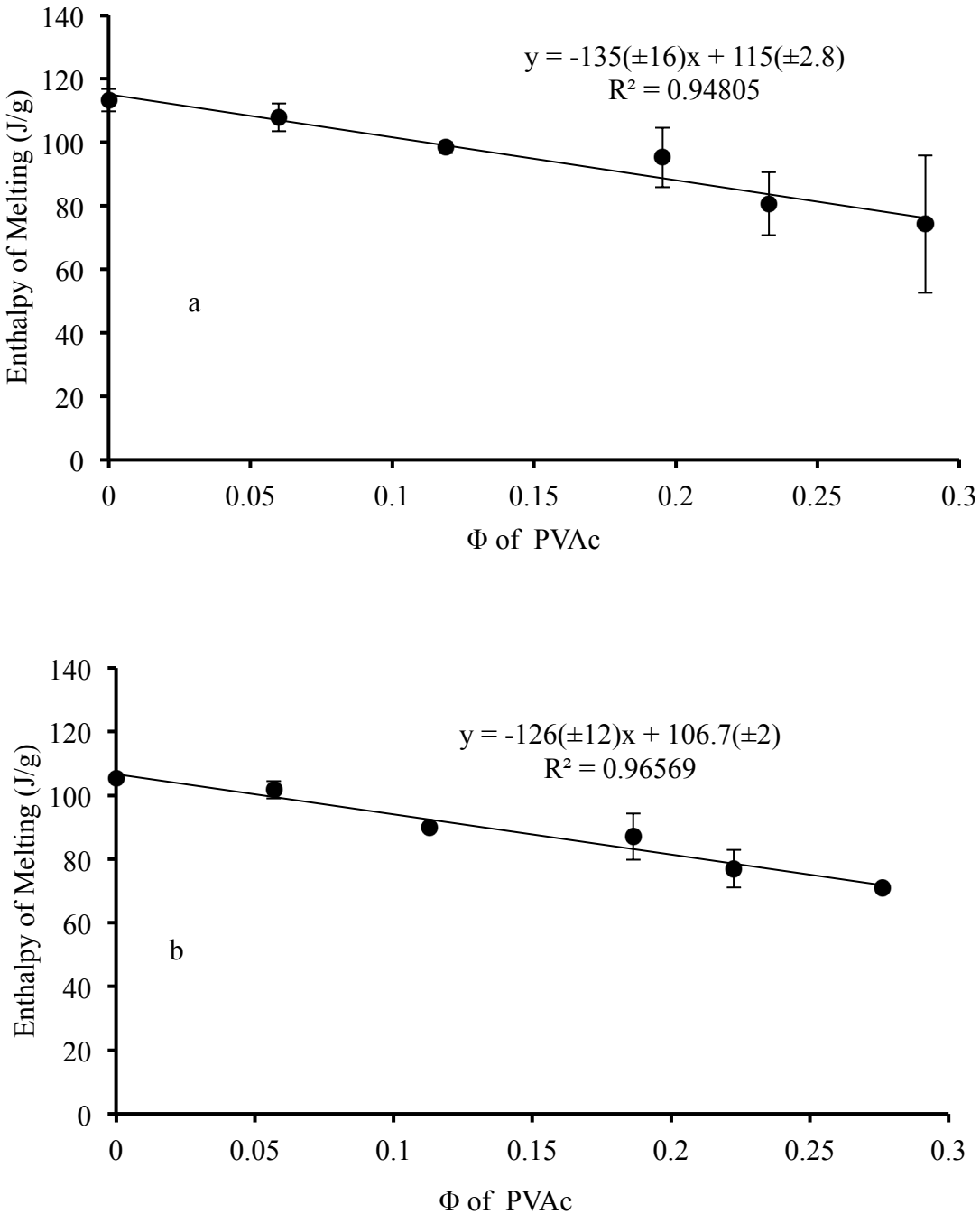

Figure 3.9. DSC results for SMX (a) and NIF (b), showing the enthalpy of melting for each drug at different concentrations of PVAc, presented as a function of the volume fraction of PVAc. Numbers between the parentheses represent the standard error.

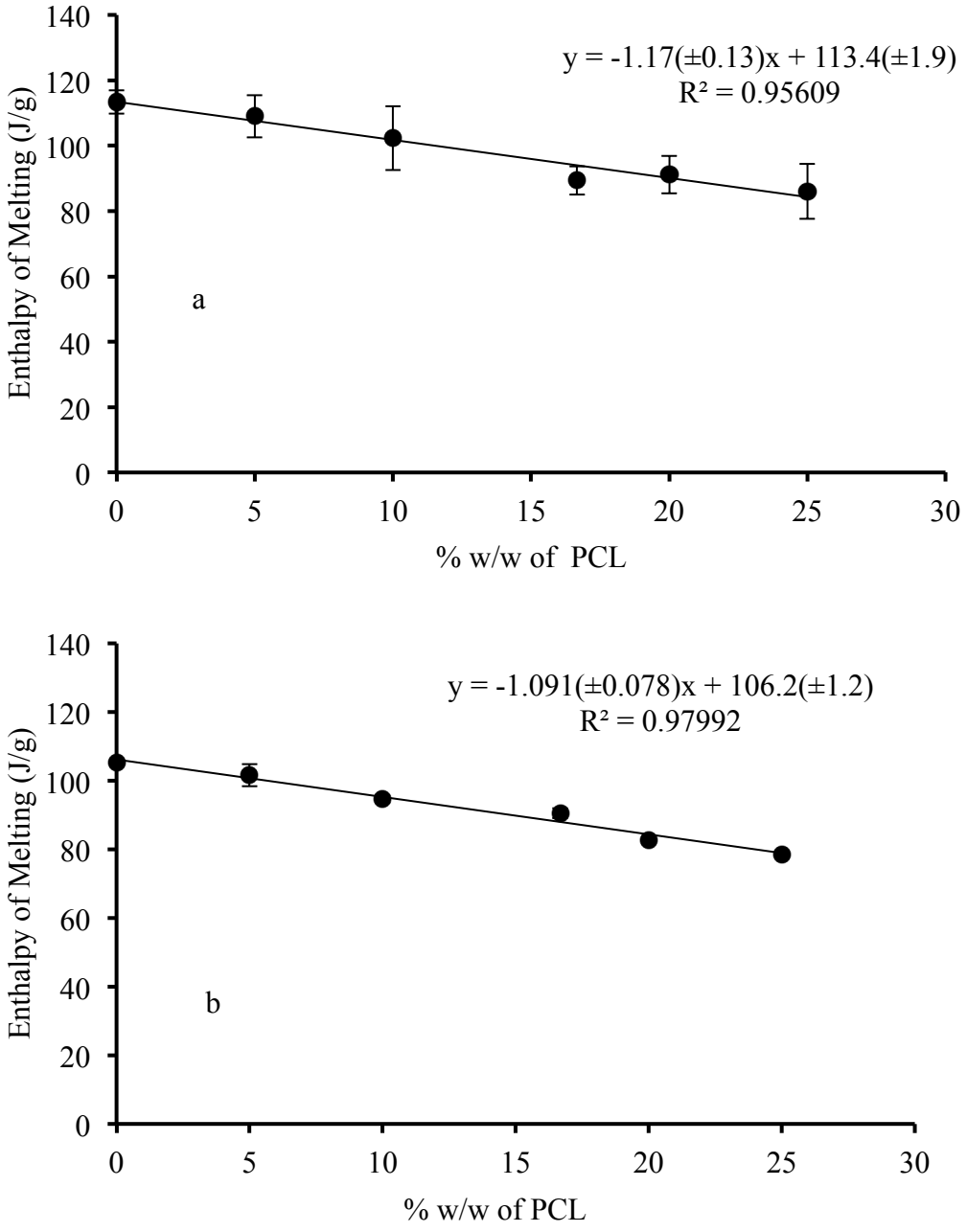

Figure 3.10. DSC results for SMX (a) and NIF (b), showing the enthalpy of melting for each drug at different concentrations of PCL, presented as a function of the volume fraction of PCL. Numbers between the parentheses represent the standard error.

In Figures 3.8. and 3.9., an estimation of the contribution of each polymer to the solubility was obtained by extrapolation of the enthalpy associated with the melting endotherm to 0 J/g. Using the obtained linear data for the reduced melting endotherms reveals the polymer concentration at which no drug melting can be detected, at which, total miscibility between the polymer and the drug is expected. For SMX, the zero enthalpy of melting occurs at 77.90 and 26.41 % w/w in PEG 6000 and PVAc, respectively. For NIF, however, the zero enthalpy occurs at 41.77 and 23.70 % w/w in PEG6000 and PVAc, respectively.

PCL showed a glass transition temperature above the melting endotherm for SMX and NIF. Therefore, the polymer impact on the enthalpy of melting should be minimal. For SMX and NIF the zero enthalpy of melting occurs at around 2 % w/w (Figure 3.10). Such small percentage is ascribed to the experimental error and no polymer effect is expected.

The melting point of crystalline drug in each mixture was measured and introduced into Eq. 3.1 (see Fig. 3.11). The χ value for each mixture is found in Table 2.

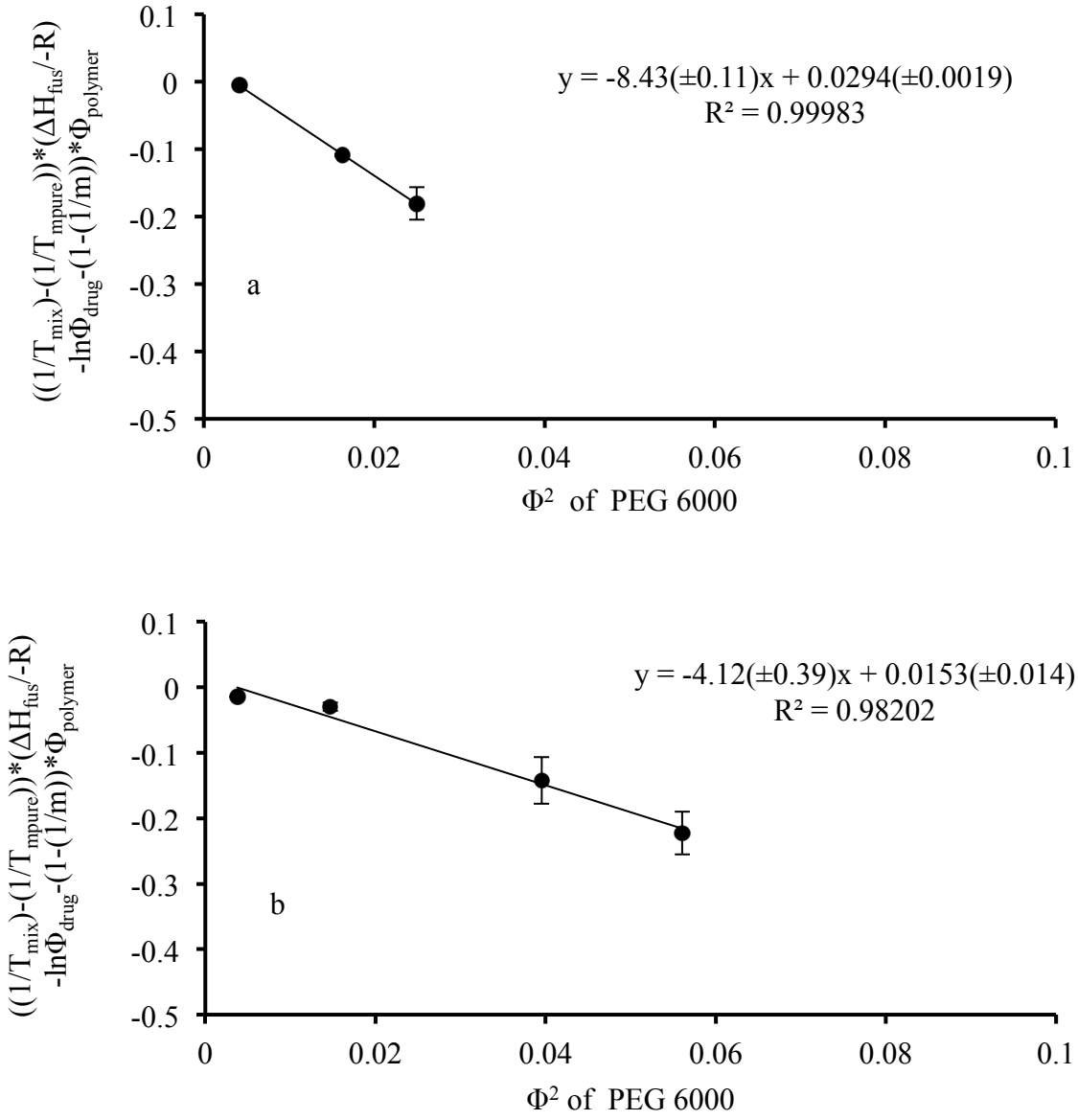

Figure 3.11. Plots to obtain the interaction parameter, χ, for (a) SMX-PEG6000, (b) NIF-PEG6000 binary mixtures. Numbers between the parentheses represent the standard error.

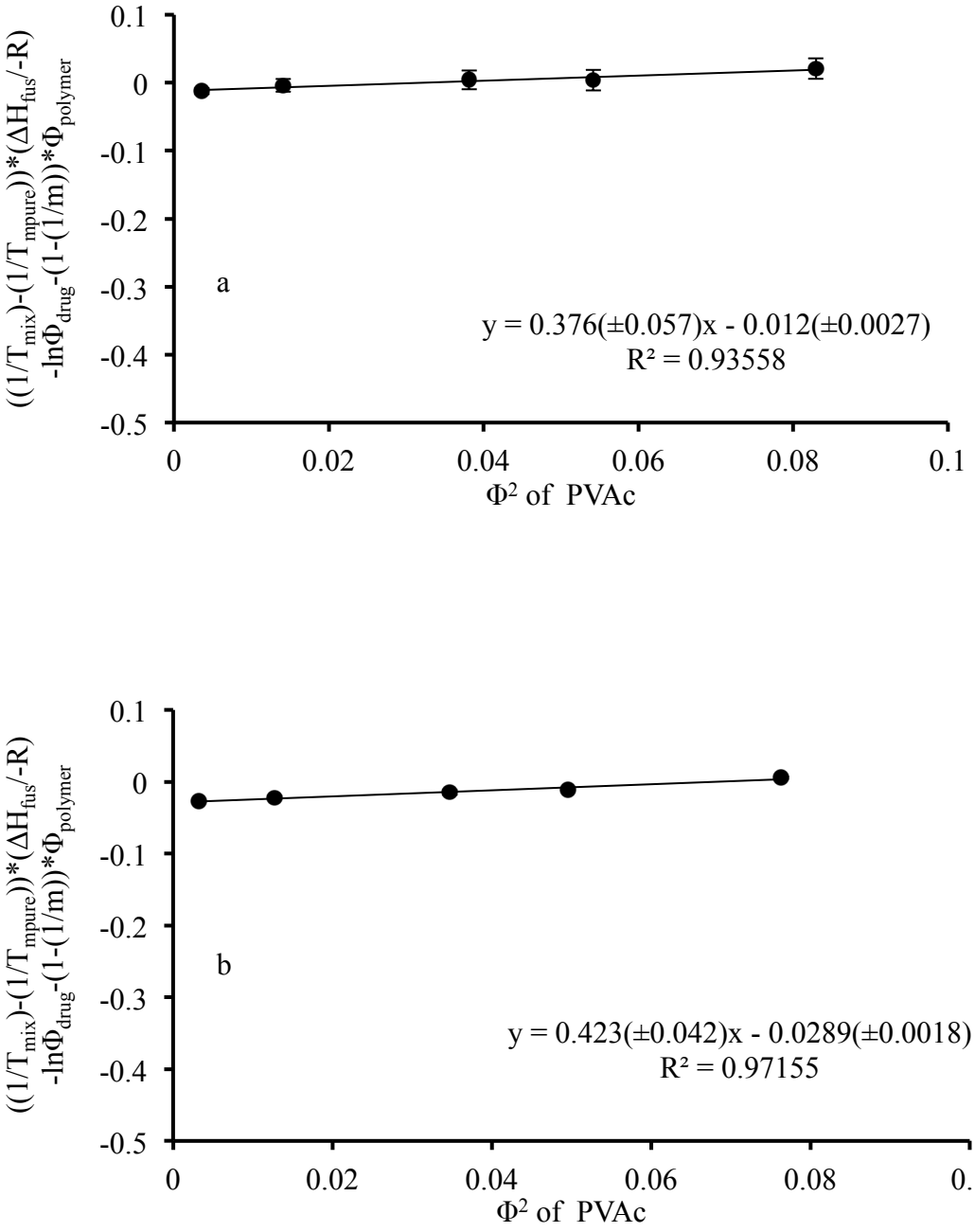

Figure 3.12. Plots to obtain the interaction parameter, χ, for (a) SMX-PVAc, (b) NIF-PVAc binary mixtures. Numbers between the parentheses represent the standard error.

Eq. 3.1 was successfully used to obtain a straight line with R^2 greater than 0.93. For Soluplus® component homopolymers with the two model drugs, the χ values are found in Table 3.2. The negative values for the interaction parameter indicate an exothermic reaction where heat is being released. When adhesive forces between the drug and the polymer are stronger than the cohesive forces within each molecule, an exothermic enthalpy of mixing is expected. Therefore, exothermic reactions of larger magnitude indicate higher affinity between the mixed components. When a positive value is found for the interaction parameter, χ, an endothermic enthalpy of mixing occurred. Heat absorption during mixing describes an endothermic mixing.

Table 3.2. The interaction parameter, χ, for each binary mixture.

	Soluplus®*	Polyethylene glycol 6000	Polyvinyl acetate	Polyvinyl caprolactam
Sulfmethoxazole	-2.87 ± 0.31	-8.43 ± 0.11	0.38 ± 0.06	-
Nifedipine	-1.30 ± 0.10	-4.12 ± 0.39	0.42 ± 0.04	-

* See Chapter Two.

± the standard error.

An amorphous compound is considered to be in a higher energy state than its crystalline counterpart. The glass transition temperature defines the temperature at which the polymer transitions from its glassy to its rubbery state for any amorphous material. The movements of the molecules are restricted in the glassy state and the molecules gain freedom when traversing the glass transition temperature. The viscosity, however, is considered high near the T_g and a reduction in the viscosity of a polymer matrix is expected as the temperature increases. This kinetic factor is important to achieve the equilibrium solubility between the crystalline drug and the amorphous polymer. Flory-Huggins Theory is derived from Regular Solution Theory where a small molecular weight solute and small molecular weight solvent are considered the mixture components. Clearly, the viscosity was never considered when developing that theory, due to the fact that viscosity has little impact on solubility.

The melting point depression approach is limited to a polymer where the T_g is below the melting point of the selected crystalline drug. The viscosity will be different based on the selected polymer and, therefore, equilibrium solubility might not be achieved when using a specific heating rate. PCL, in particular, has a T_g around 185 °C that is higher than the melting temperature of 169.87 and 173.05 °C for SMX and NIF, respectively. That indicates another limitation of the melting point depression method, which required the amorphous polymer to have a T_g below the melting of the crystalline drug. However, to test the sensitivity of this method to access the thermodynamics of mixing, PCL was used at different concentrations with SMX and NIF to identify the melting temperature at each composition (see Fig. 3.7). There was little to no reduction in the melting temperature of the different mixtures. In addition, the melting enthalpy rendered an equation of the line

predicting zero enthalpy as the drug weight fraction approaches zero indicating that no significant impact was found with this polymer (see Fig. 3.10).

A study was devised to find possible miscibility between PCL and the two model drugs. PCL with SMX and NIF went through different heating and cooling cycles in an attempt to obtain an amorphous composition. Essentially the mixture was heated to 210 °C and kept there for 5 min. Then the mixture was cooled to -60 °C at a specific rate of 60 deg/min. The previous cycle was repeated at least two times. The blend is considered compatible if one single T_g is observed. When two glass transition temperatures are detected, the mixture is considered partially miscible to immiscible. The Gordon-Taylor equation is utilized to establish the theoretical T_g curve for PCL with the two model drugs [34-38].

$$T_{g\,mix} = \frac{W_1 * T_{g1} + K * W_2 * T_{g2}}{W_1 + K * W_2} \tag{3.5}$$

$$K = \frac{T_{g1} * \rho_1}{T_{g2} * \rho_2} \tag{3.6}$$

where W_1 and W_2 are the weight fraction of the drug and the polymer. T_{g1} and T_{g2} are the glass transition temperature of the amorphous drug and polymer. K is a constant related to the true density for the drug and the polymer, ρ_1 and ρ_2. The true densities are 1.42 and 1.34 (g/cm^3) for crystalline SMX and NIF, respectively. It is true to estimate the density of the amorphous counterpart of each drug candidates to be 95% of the drug crystalline density resulting in 1.35 and 1.27 (g/cm^3) for amorphous SMX and NIF, respectively [35].

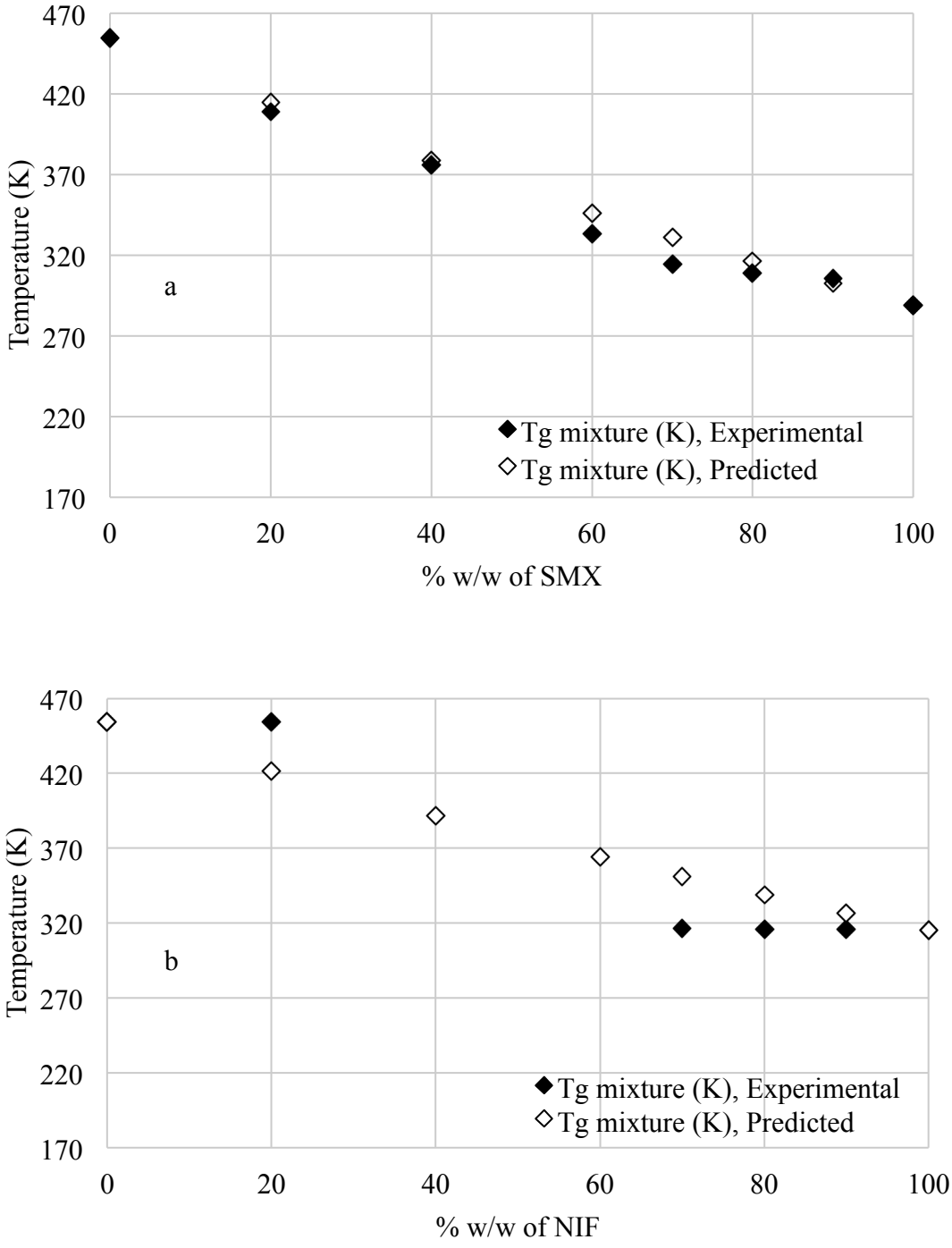

Figure 3.13. T_g temperature-composition profiles for PCL with (a) SMX, and (b) NIF.

Fig. 3.13.a shows the T_g dependence on SMX-PCL composition. The presence of specific chemical interactions between the mixed components renders experimental data that do not match the predicted values. Non-ideal mixing of the mixture yields a similar observation. NIF-PCL, on the other hand, showed a poor dependence of the T_g on the mixed composition. A single glass transition temperature was detected at higher concentrations of each component. This suggests immiscibility between NIF and PCL at wide concentration range.

Clearly these data, at least for SMX-PCL, prove that a miscible blend is obtainable, even though the melting point depression approach was limited to polymers with T_g below the melting of the crystalline drug. However, the thermodynamic driving forces for the mixing and the equilibrium solubility cannot be extracted from the T_g temperature-composition profile.

3.6.2. Gibbs free energy

The mixing spontaneity of the blend is assessed using Eq. 3.2. The entropy term always favors mixing. The interaction parameter term, representing the enthalpy contribution to solubility, largely dominates in this calculation of the free energy of mixing. If the enthalpy was found to be positive, limited mixing is expected.

Due to the profound reduction in the melting endotherm of each of the model drugs with PEG 6000, the interaction parameter showed large negative values. Figs. 3.14. and 3.15., present the temperature normalized Gibbs free energy for χ values found in Table 3.2. Several other values for the interaction parameter were introduced into Eq. 3.2, to predict the Gibbs free energy. A value of 2, for the interaction parameter, indicates endothermic mixing and proves that, for such a value, the temperature normalized Gibbs free energy will be positive over large concentration range.

PVAc renders positive interaction parameter values for SMX and NIF. With this endothermic mixing, the temperature normalized Gibbs free energy presents no positive data at different polymer compositions. It is obvious that the entropy portion contributed to the spontaneity of mixing for each binary mixture. Non-spontaneous mixing is expected when the enthalpy is large enough to overcome the entropy effect.

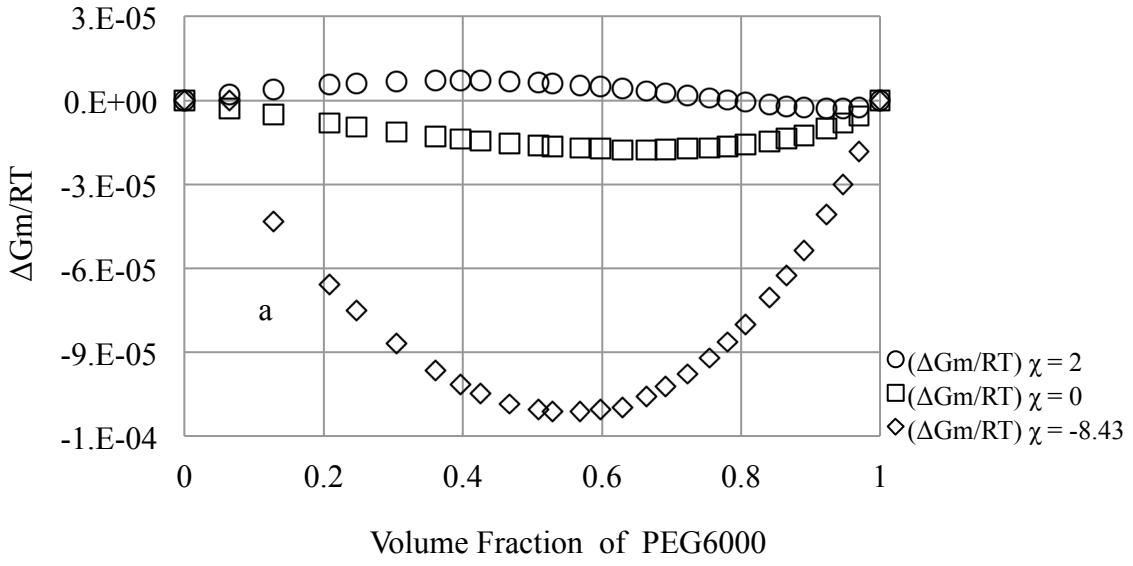

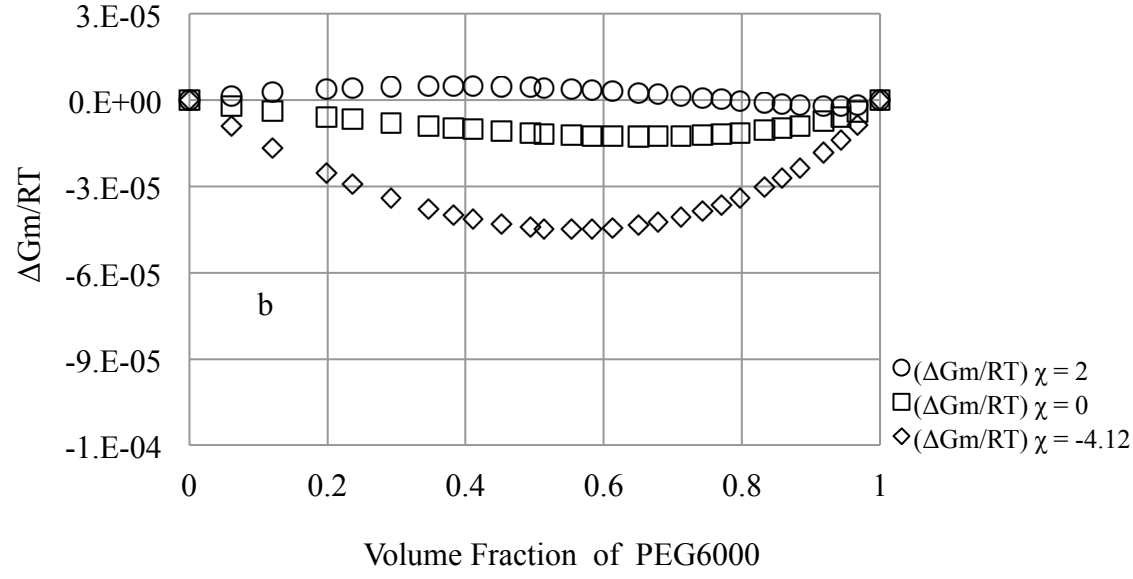

Figure 3.14. Predicted temperature normalized free energy of mixing for (a) SMX and (b) NIF using Eq. 3.2 vs. Φ of PEG 6000 using different values for the interaction parameter.

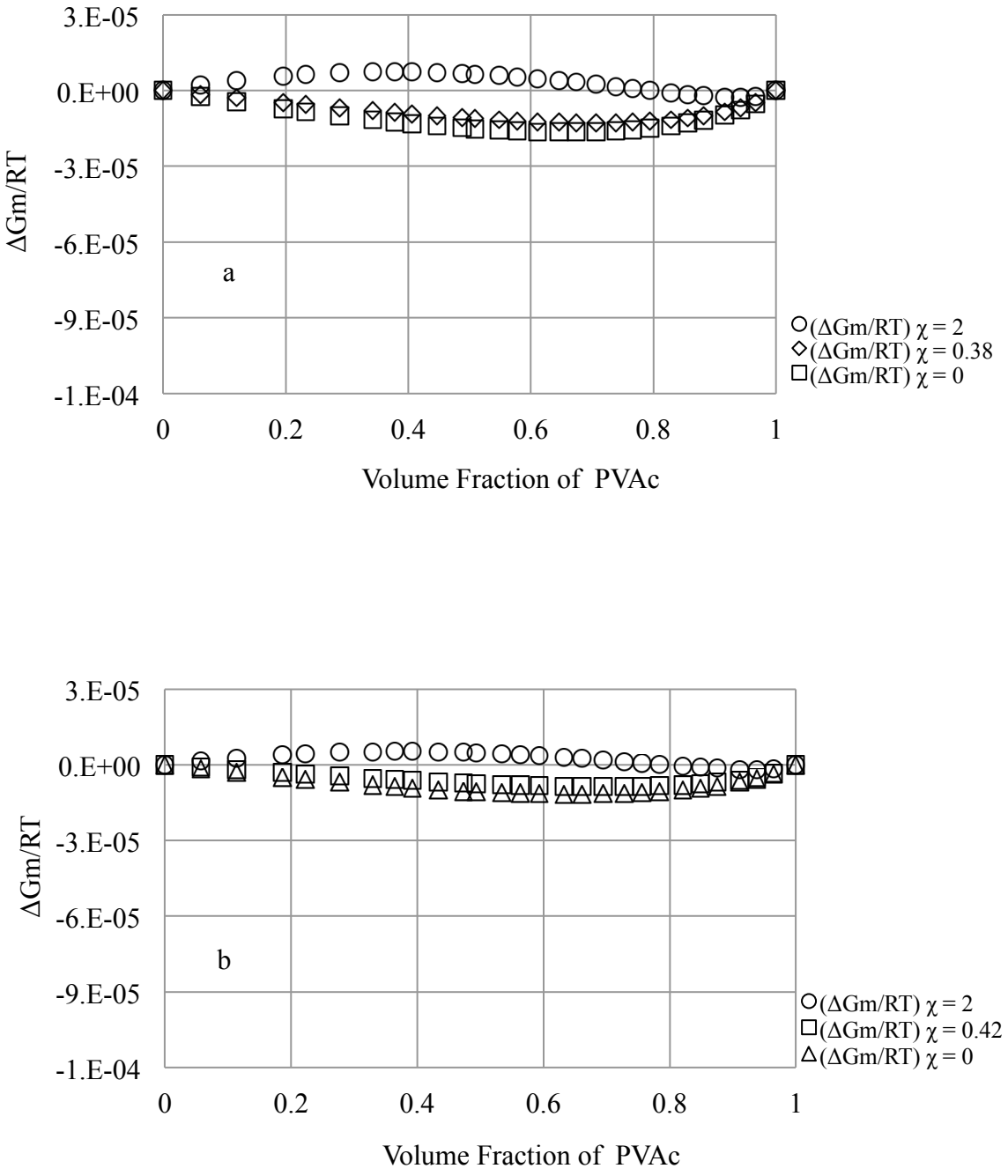

Figure 3.15. Predicted temperature normalized free energy of mixing for (a) SMX and (b) NIF using Eq. 3.2 vs. Φ of PVAc using different values for the interaction parameter.

3.6.3. Predicted solubility

Miscibility is considered evident when drug dissolves in rubbery polymer. A solid dispersion with detectable crystalline drug indicates that the solubility in that particular polymer is exceeded and not necessarily that complete immiscibility exists. If the solubility is assessed and considered when the solid dispersion is manufactured, no crystalline content should be present. Extending the success drawn from the first study of SMX and NIF solubility in Soluplus®, the solubility of small molecular crystalline drug in a small molecular weight solvent is utilized (Eq. 3.3). Assuming that the polymer is the solvent, i.e., considering the monomers of each polymer chain as the small solvent molecules and applying Flory-Huggins Lattice Theory described in Eq. 3.4, the mole fraction solubility, X_{drug}, can be calculated. Eq. 3.4, showed the large impact of the mixing enthalpy, represented by the interaction parameter term, on predicted mole fraction solubility. The mixtures' molecular size disparity had relatively little effect on the predicted values.

The solubility of each model drug in PEG 6000 and PVAc was calculated based on the interaction parameter obtained using the melting point depression approach. Solving Eqs. 3.3 and Eq. 3.4 simultaneously yields the predicted mole fraction solubility (see Table 3.3). This method is validated by constructing the phase diagram (see Chapter Two). PVAc was the only candidates that qualified to be applicable to this method. PVAc has a glass transition temperature well below the melting endotherm of each crystalline drug. In addition, the T_g composition dependence was accessible over the complete binary mixture range. PEG 6000 is mostly crystalline and it is practically difficult to convert to complete amorphous form. Since PCL has a glass transition temperature above

the melting point of the crystalline drugs, this approach to accessing the different thermodynamic parameters is inappropriate.

Table 3.3. The predicted solubility of each drug in Soluplus® and its component homopolymers and the experimental solubility in PEG 400.

Polymer	Predicted solubility	
	SMX (% w/w)	NIF (% w/w)
Soluplus®*	19.3 ± 3.4	5.18 ± 0.54
PEG 6000	49.1 ± 0.61	24.9 ± 3.4
PVAc	1.46 ± 0.081	0.885 ± 0.026
PCL	-	-
Polymer	Experimentally measured solubility	
	SMX (% w/w)	NIF (% w/w)
PEG 400	31.9 ± 4.4	15.3± 0.2

* See Chapter Two.

± Represents the standard error.

From the above table we can perform mathematical calculation to find the percentage error between the total solubility for SMX and NIF in Soluplus® and the combined solubility of each drug in PEG 6000 and PVAc. The total percentage error was found to be around 45 and 14 % for SMX and NIF, respectively. Cleary, both drugs showed a significant error between the predicted solubility in Soluplus® and its component homopolymers. PEG 6000 solubilizes SMX to a large extent resulting in a profound reduction in the melting endotherm. Such reduction renders broader peaks that eventually diminish the accuracy to detect the onset of melting at concentration above 12.5 % w/w. In addition, the contribution of PCL was not accounted for which the error was further propagated.

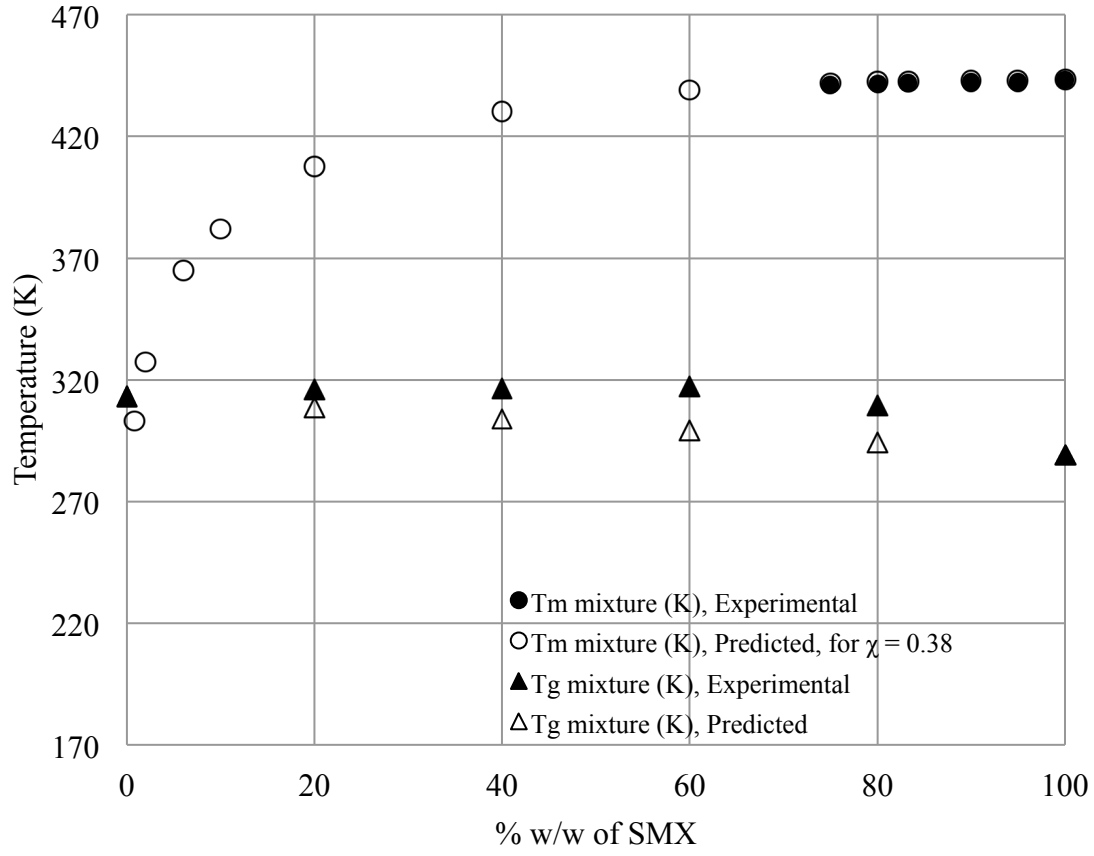

Figure 3.16.a. Phase diagram for SMX with PVAc where the curve predicted using Eq. 3.1 was extrapolated to intersect the $T_{g\,mix}$ curve.

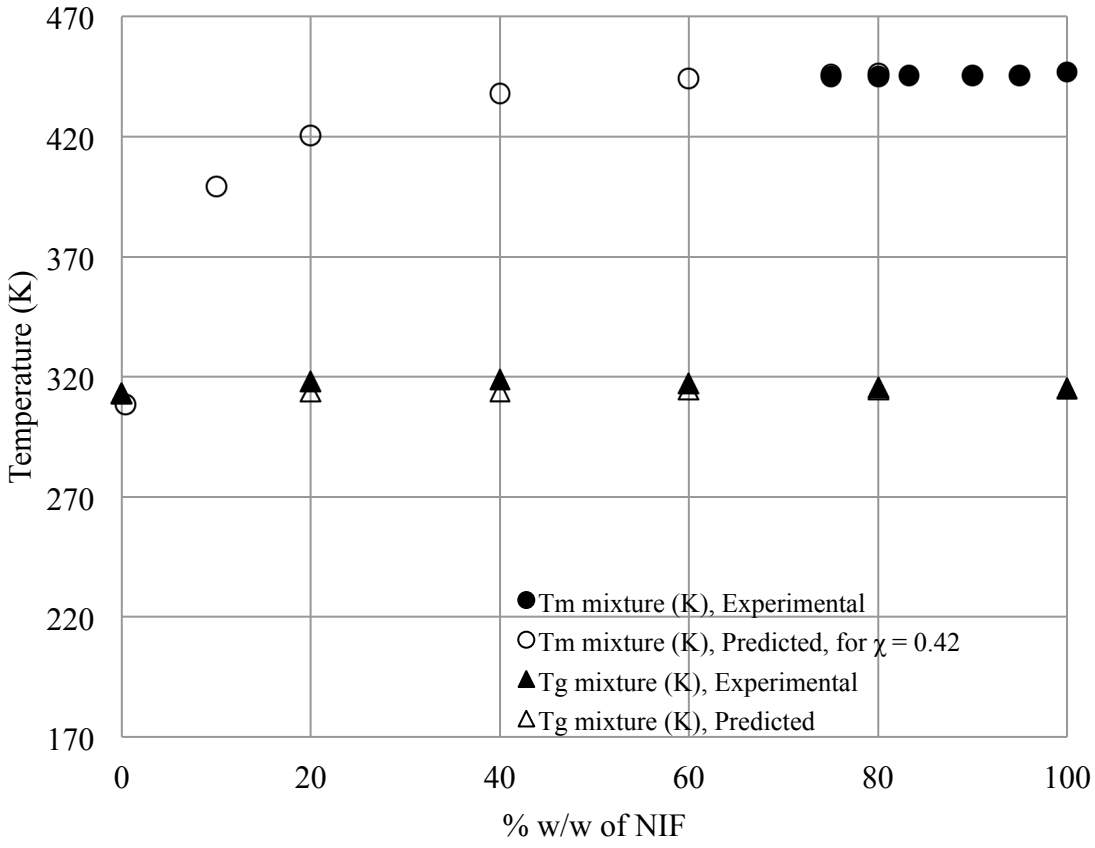

Figure 3.16.b. Phase diagram for NIF with PVAc where the curve predicted using Eq. 3.1 was extrapolated to intersect the $T_{g\,mix}$ curve.

The phase diagram method, described in Chapter Two, was utilized successfully to obtain the solubility of the two model drugs in PVAc (Figs. 3.16.a and 3.16.b). The phase diagram can be divided into four regions. A thermodynamically stable solid solution region is found above the melting point depression curve across the possible compositions. It is important to note that the existence of a certain mixture of a thermodynamically unstable composition does not ensure recrystallization or phase separation. Factors such as the nucleation rate and the viscosity of the mixture play an important role in limiting how fast component separation can take place.

The motion of the mixture molecules is expected to be restricted in the glassy state. As the temperature associated with the onset of the mixture melting endotherm is depressed to the point close to the glass transition temperature, the viscosity of the mixture is expected to rise substantially. The intersection between the melting point depression curve and the mixture glass transition temperature curve is considered the practical solubility limit in the production of solid solutions by methods such as hot melt extrusion. Values of 1.24 and 0.73 % w/w were obtained for SMX and NIF in PVAc, respectively. Good agreement between the solubility data also validates the results found for SMX and NIF in Soluplus® (see Chapter Two).

Polymers that have small molecular weight analogues that are liquid at room temperature prove to be useful to compare experimental and predicted estimations of physical properties. In addition, a difference in molecular weight was shown to have negligible impact on the temperature normalized Gibbs free energy of mixing (see Chapter Two). The experimental solubility value, therefore, should not be profoundly affected since a

difference in PEG molecular weight between 400 and 6000 did not profoundly influence the Gibbs free energy of mixing.

To validate the predicted solubility data in PEG 6000, one can extend the study and use PEG 400 to measure the drug solubility at room temperature. The experimental solubility values, expressed as (% w/w) for SMX and NIF in PEG 400, are found in Table 3.3.

The solubility of SMX and NIF in PEG 400 are experimentally determined to be 32 and 15.3 % w/w, respectively. The predicted solubility, however, are calculated to be 49.1 and 24.9 % w/w, using -8.43, and -4.12 as the interaction parameter for SMX and NIF, respectively. Yang et al., [28] have used PEG 400 to experimentally estimate the acetaminophen solubility in PEO. The experimental value was close to the predicted one for acetaminophen in PEO (PEG with a M_W of 100,000). In the present study, clearly, the predicted and the experimental values are not close, although the solubility of SMX is consistently twice that of NIF in each polymer. We speculate that the crystallinity of PEG 6000, around 98%, was the critical factor as the polymer will be in a complete liquid form after the melting temperature of 65 °C. This means that the crystalline drug is actually dissolving in a liquid (not rubbery) solvent. With the aid of heat that is being infused during the DSC analysis, a profound reduction in the melting endotherms was detected. This renders a negative enthalpy of mixing of high magnitude that eventually led to large predicted solubility. In addition, particularly SMX melting endotherm was detected for polymer concentration only up to 12.5 % w/w, which might be attributed to the overestimation of the predicted solubility.

It can be concluded that PEG 6000 is the main component homopolymer that effectively solubilizes SMX and NIF in Soluplus®. Clearly, measuring the solubility in each individual component homopolymer will give relatively different values than the parent polymer. An important factor that contributes to such differences is the physical state of the parent polymer, being totally or partially amorphous, in comparison to the physical state of the component homopolymers. Also, the parent polymer is a co-polymer where it is practically impossible to identify the specific molecular weight of each component homopolymer. In addition, the inter- and intra-molecular forces within the co-polymer are different from those found in the individual homopolymers.

3.7. Conclusions

Melting point depression as suggested by the Flory-Huggins Theory was utilized successfully with graft copolymer Soluplus® component homopolymers. The contribution of each homopolymer to the solubilization of the two model drugs was assessed and PEG 6000 proved to have the highest influence on the solubility of the drugs in Soluplus®. The interaction parameter for SMX with Soluplus®, PEG 6000, and PVAc was found to be -2.87, -8.43, and 0.38, respectively. The interaction parameter for NIF with Soluplus®, PEG 6000, and PVAc was found to be -1.30, -4.12, and 0.42. From these values it was shown that Soluplus® and PEG 600 have an exothermic mixing with the drugs, whereas PVAc has an endothermic mixing with the drugs. The predicted solubility in PEG 6000 does not closely match the experimental value in PEG 400. The melting point depression method is proved effective when predicting the solubility of each of the two drugs in homopolymer, copolymer, and graft-copolymer. In addition, this method could be extended to reveal the effective component homopolymer that substantially solubilizes the selected drug.

3.8. References

1. Homayouni A, Sadeghi F, Varshosaz J, Afrasiabi Garekani H, Nokhodchi A. Promising dissolution enhancement effect of soluplus on crystallized celecoxib obtained through antisolvent precipitation and high pressure homogenization techniques. Colloids Surf B Biointerfaces. 2014. 122: 591-600

2. Shamma RN, Basha M. Soluplus®: A novel polymeric solubilizer for optimization of Carvedilol solid dispersions: Formulation design and effect of method of preparation. P Tech. 2013. 237: 406-14

3. Özdemir N, Erkin J. Enhancement of dissolution rate and bioavailability of sulfamethoxazole by complexation with β-cyclodextrin. Drug Dev Ind Pharm. 2012. 38(3): 331-40

4. Fouad EA, El-Badry M, Mahrous GM, Alanazi FK, Neau SH, Alsarra IA. The use of spray-drying to enhance celecoxib solubility. Drug Dev Ind Pharm. 2011. 37(12): 1463-72

5. Al-Obaidi H, Buckton G. Evaluation of griseofulvin binary and ternary solid dispersions with HPMCAS. AAPS PharmSciTech. 2009. 10(4): 1172-7

6. Konno H, Handa T, Alonzo DE, Taylor LS. Effect of polymer type on the dissolution profile of amorphous solid dispersions containing felodipine. Eur J Pharm Biopharm. 2008. 70(2): 493-9

7. Ruan L-P, Yu B-Y, Fu G-M, Zhu D-n. Improving the solubility of ampelopsin by solid dispersions and inclusion complexes. J pharm Bio. 2005. 38(3): 457-64

8. Emara LH, Badr RM, Elbary AA. Improving the dissolution and bioavailability of nifedipine using solid dispersions and solubilizers. Drug Dev Ind Pharm. 2002. 28(7): 795-807

9. Van den Mooter G, Augustijns P, Blaton N, Kinget R. Physico-chemical characterization of solid dispersions of temazepam with polyethylene glycol 6000 and PVP K30. Int J pharm. 1998. 164(1): 67-80

10. M. Guyot FF, J. Bildet, F. Bonini, A.-M. Lagueny. Physicochemical characterization and dissolution of norfloxacin/cyclodextrin inclusion compunds and PEG solid dispersions Int J Pharm. 1995. 123: 53-63

11. Save T, Venkitachalam P. Studies on solid dispersions of nifedipine. Drug Dev In Pharm. 1992. 18(15): 1663-79

12. Sathigari SK, Radhakrishnan VK, Davis VA, Parsons DL, Babu RJ. Amorphous-state characterization of efavirenz--polymer hot-melt extrusion systems for dissolution enhancement. J Pharm Sci. 2012. 101(9): 3456-64

13. Huang J, Wigent RJ, Bentzley CM, Schwartz JB. Nifedipine solid dispersion in microparticles of ammonio methacrylate copolymer and ethylcellulose binary blend for controlled drug delivery: Effect of drug loading on release kinetics. Int J Pharm. 2006. 319(1): 44-54

14. Liu X, Lu M, Guo Z, Huang L, Feng X, Wu C. Improving the chemical stability of amorphous solid dispersion with cocrystal technique by hot melt extrusion. Pharm Res. 2012. 29(3): 806-17

15. Huang J, Wigent RJ, Schwartz JB. Nifedipine molecular dispersion in microparticles of ammonio methacrylate copolymer and ethylcellulose binary blends for controlled drug delivery: effect of matrix composition. Drug Dev Ind Pharm. 2006. 32(10): 1185-97

16. Huang J, Wigent RJ, Schwartz JB. Drug-polymer interaction and its significance on the physical stability of nifedipine amorphous dispersion in microparticles of an ammonio methacrylate copolymer and ethylcellulose binary blend. J Pharm Sci. 2008. 97(1): 251-62

17. Vijaya Kumar SG, Mishra DN. Preparation, Characterization and In vitro Dissolution Studies of Solid Dispersion of Meloxicam with PEG 60001). Yakugaku Zasshi. 2006. 126(8): 657-64

18. Ning X, Sun J, Han X, Wu Y, Yan Z, Han J, He Z. Strategies to improve dissolution and oral absorption of glimepiride tablets: solid dispersion versus micronization techniques. Drug Dev In Pharm. 2011. 37(6): 727-36

19. Shamblin SL, Huang EY, Zografi G. The effects of co-lyophilized polymeric additives on the glass transition temperature and crystallization of amorphous sucrose. J Therm Cal. 1996. 47(5): 1567-79

20. Park Y, Veytsman B, Coleman M, Painter P. The miscibility of hydrogen-bonded polymer blends: Two self-associating polymers. Macromolecules. 2005. 38(9): 3703-7

21. Campos A, Gómez CM, García R, Figueruelo JE, Soria V. Extension of the Flory-Huggins theory to study incompatible polymer blends in solution from phase separation data. Polymer. 1996. 37(15): 3361-72

22. Nishil T WT. Melting point depression and kinetic effects of cooling on crystallization in poly(viny1idene fluoride)-poly (methyl methacrylate) mixtures. Macromolecules. 1975. 8: 909-15

23. Marsac PJ, Shamblin SL, Taylor LS. Theoretical and practical approaches for prediction of drug–polymer miscibility and solubility. Pharm Res. 2006. 23(10): 2417-26

24. Tian Y, Booth J, Meehan E, Jones DS, Li S, Andrews GP. Construction of drug–polymer thermodynamic phase diagrams using Flory–Huggins Interaction Theory: Identifying the relevance of temperature and drug weight fraction to phase separation within solid dispersions. Mol Pharm. 2012. 10(1): 236-48

25. Lin D, Huang Y. A thermal analysis method to predict the complete phase diagram of drug–polymer solid dispersions. Int J Pharm. 2010. 399(1–2): 109-15

26. Marsac PJ, Li T, Taylor LS. Estimation of drug-polymer miscibility and solubility in amorphous solid dispersions using experimentally determined interaction parameters. Pharm Res. 2009. 26(1): 139-51

27. Zhao Y, Inbar P, Chokshi HP, Malick AW, Choi DS. Prediction of the thermal phase diagram of amorphous solid dispersions by Flory–Huggins theory. J Pharm Sci. 2011. 100(8): 3196-207

28. Yang M, Wang P, Gogos C. Prediction of acetaminophen's solubility in poly(ethylene oxide) at room temperature using the Flory–Huggins theory. Drug Dev Ind Pharm. 2012. 1-7

29. Zhao Y, Inbar P, Chokshi HP, Malick AW, Choi DS. Prediction of the thermal phase diagram of amorphous solid dispersions by Flory-Huggins theory. J Pharm Sci. 2011. 100(8): 3196-207

30. Hiemenz PC, Lodge TP. Polymer Chemistry, 2nd edition FL: CRC press, Taylor & Francis group; 2007.

31. Baird JA, Van Eerdenbrugh B, Taylor LS. A classification system to assess the crystallization tendency of organic molecules from undercooled melts. J Pharm Sci. 2010. 99(9): 3787-806

32. Kim K, Ingole PG, Yun S, Choi W, Kim J, Lee H. Water vapor removal using CA/PEG blending materials coated hollow fiber membrane. J ChemTech and Bio. 2014.

33. Corrigan DO, Healy AM, Corrigan OI. The effect of spray drying solutions of polyethylene glycol (PEG) and lactose/PEG on their physicochemical properties. Int J pharm. 2002. 235(1): 193-205

34. Baird JA, Taylor LS. Evaluation of amorphous solid dispersion properties using thermal analysis techniques. Adv drug del R. 2012. 64(5): 396-421

35. Weuts I, Van Dycke F, Voorspoels J, De Cort S, Stokbroekx S, Leemans R, Brewster ME, Xu D, Segmuller B, Turner YT, Roberts CJ, Davies MC, Qi S, Craig DQ, Reading M. Physicochemical properties of the amorphous drug, cast films, and spray dried powders to predict formulation probability of success for solid dispersions: Etravirine. J Pharm Sci. 2011. 100(1): 260-74

36. Forster AH, J. Tucker, I. Rades. T. The potential of small-scale fusion experiments and the gordon-taylor equation to predict the suitability of drug/polymer blends for melt extrusion. Drug Dev Ind Pharm. 2001. 27(6): 549-60

37. Plans J, MacKnight WJ, Karasz FE. Equilibrium melting point depression for blends of isotactic polystyrene with poly (2, 6-dimethylphenylene oxide). Macromolecules. 1984. 17(4): 810-4

38. Gordon M, Taylor JS. Ideal copolymers and the second-order transitions of synthetic rubbers. i. non-crystalline copolymers. J Appl Chem. 1952. 2(9): 493-500

4. Investigation of the in vitro characteristics of drug-Soluplus® and drug PEG 6000 dispersions when prepared using spray drying or lyophilization

4.1. Abstract

Purpose: to evaluate the physicochemical and in vitro characteristics of solid dispersions using BCS II model drugs with Soluplus® and one of its component homopolymers, PEG 6000.

Methods: Nifedipine (NIF) and sulfamethoxazole (SMX) of 99.3 and 99.5% purity, respectively, were selected as BCS II model drugs, such that an improved dissolution rate and concentration in the gastrointestinal tract should increase oral bioavailability. Soluplus® (BASF, Tarrytown, NY), with a T_g of about 70 °C, is an amorphous, tri-block, graft co-polymer with polyvinyl caprolactam, polyvinyl acetate, and polyethylene glycol in the ratio 57:30:13. PEG 6000 (BASF) is a waxy material with a T_g of about -22 °C and a melting point of about 60 °C. Solid dispersions were prepared by lyophilization (Virtis AdVantage XL-70) or spray drying (Buchi Mini Spray-Dryer B-290). The dissolution study was conducted in simulated gastric and intestinal fluids without enzymes (SGF and SIF, respectively) at 37 °C. The crystallinity of the drugs in the dispersions was evaluated using a differential scanning calorimeter (TA 2910 DSC).

Results: Although each polymer improved the drug dissolution rate, dissolution from Soluplus® dispersions was slower. Enhanced dissolution rates were observed with NIF solid dispersions, but the dissolution profiles were quite different due to the preparation technique, polymer, and dissolution medium. For SMX, there was similarity across the

dissolution profiles despite the medium, polymer, or preparation technique. Each polymer was able to maintain an elevated drug concentration over the three hour duration of the dissolution profile, i.e., supersaturation was supported by the polymer. DSC thermograms revealed no melting endotherm, suggesting that the drug is amorphous or molecularly dispersed in the solid dispersion.

Conclusion: NIF and SMX solid dispersions were successfully prepared by spray drying and lyophilization using Soluplus® or PEG 6000. Each polymer enhanced the drug dissolution rate; NIF dissolution rate was improved to a greater extent. Dispersions with PEG 6000 had a faster dissolution rate due to its hydrophilic nature. DSC analysis showed that no crystalline material exists in the dispersions.

4.2. Keywords

Spray drying, lyophilization, dissolution, nifedipine, sulfamethoxazole, Soluplus® , PEG 6000, solid dispersion.

4.3. Introduction

Most new chemical entities in the pharmaceutical industry lack a sufficient solubility in water [1-4] and, thus, exhibit a slow dissolution rate and low oral bioavailability. This conundrum drives scientists to develop new strategies to overcome the repercussions of poor solubility. Enhancing the solubility of different chemical substances by forming a solid dispersion with a hydrophilic polymer is one of the most promising methods. Different hydrophilic polymers have been successfully used to enhance oral bioavailability either by enhancing the dissolution rate and/or increasing the drug concentration in the aqueous medium [4-6].

Such solid dispersions also demonstrate an ability to maintain the amorphous state of a given drug during processing and storage. The amorphous form of a drug has a 10-1000 fold higher solubility than the crystalline form [7]. Keeping this amorphous state, in part, is a function of drug concentration in the dispersion, indicating that some of the drug will recrystallize after exceeding a particular drug-polymer ratio [8].

Polymers can possess different chemical and physical characteristics, such as functional groups, molecular weight, melting temperature T_m, and glass transition temperature T_g. Therefore, each polymer has a different ability to maintain dispersed drug at a particular drug-carrier ratio without recrystallization [9].

An approach to understand drug-carrier relationship in a solid dispersion took advantage of the thermodynamics described by the Flory-Huggins Theory [10, 11]. From this theory, a prediction of the polymer saturation is calculated and proved to show promising results.

Sulfamethoxazole and nifedipine are the selected drug candidates for this study. The two drugs have a limited dissolution rate due to lower solubility. However, forming a complex or dispersing the drug in a hydrophilic carrier can often improve the dissolution rate [4, 12]

In Chapters 2 and 3, the saturation limits of these drugs in Soluplus® and its component homopolymers were investigated. PEG 6000 was found to exhibit a profound impact on the reduction of the SMX and NIF melting endotherm. PVAc and PCL showed essentially no reduction in the melting endotherm. Both polymers, also, proved to be practically difficult to process due to their hydrophobic nature. Therefore, PVAc and PCL were excluded from this study.

In this chapter, Soluplus® as a parent polymer and one of its component homopolymers, PEG 6000, are assessed for their ability to form a solid dispersion by two different manufacturing techniques, spray drying and lyophilization, as they are the methods often used to produce solid dispersions. Stability, morphology, in vitro release profile, and the release kinetics of the dispersed materials are investigated.

4.4. Materials

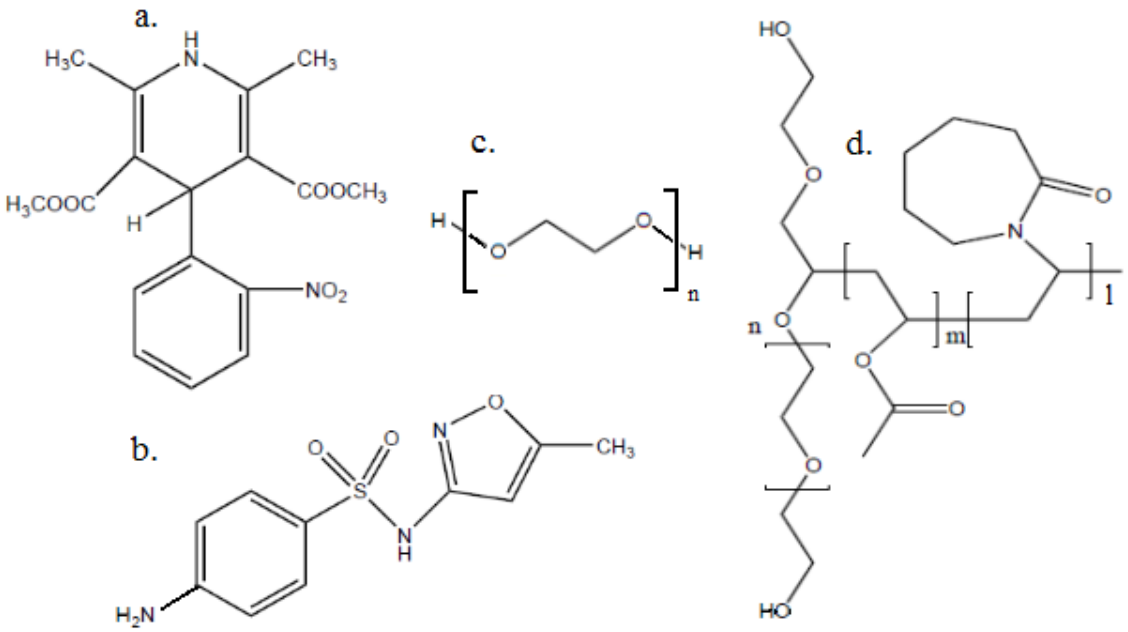

Figure 4.1. Chemical structures of a. nifedipine, b. sulfamethoxazole, and c. polyethylene glycol, and d. Soluplus®.

Crystalline sulfamethoxazole (SMX, M_w = 253.28 g/mol, density = 1.42 g/cm^3) was purchased from (Flavine International Inc., Closter, NJ). Crystalline nifedipine (NIF, M_w = 346.34 g/mol, density = 1.34 g/cm^3) was purchased from C.F.M. Co. Farmaceutica Milanese S.P.A. (Milano, Italia). Soluplus® (M_w = 118000 g/mol, density = 1.08 g/cm^3) and PEG 6000 (M_w = 6000 g/mol, density = 1.08 g/cm^3) were generous gifts from BASF (Tarrytown, NY). Other properties of these materials are presented in table 4.1.

Table 4.1. Material properties

	M_W (g/mol)	*Densiy (g/cm^3)	Molar volume (cm^3/mol)	ΔH_{fus} (kJ/mo)	T_m (K)	T_g (K)
Sulfamethoxazole	253	1.42	172.30	28.70	443	289**
Nifedipine	346	1.34	288.62	36.5	447	316
Soluplus®	118000	1.08	109000	-	-	347
PEG	6000	1.08	5556	1072	333	251

* True density, measured using helium pycnometry.

** Ref. [13, 14]

4.5. Methods

4.5.1. Preparation of a solid dispersion

4.5.1.a. Spray drying

Sulfamethoxazole and nifedipine with each polymer were prepared in drug:polymer mass ratios of 1:1, 1:5, and 1:9. Each drug with Soluplus® or PEG 6000, at the selected mass ratio, was dissolved in 250 ml of water/acetonitrile (1:5). A magnetic bar was used to stir the mixture until a clear solution was observed. The solution was spray-dried using a Mini Spray-Dryer B-290 (Büchi Labortechnik AG, Flawil, Switzerland). The air flow was set to be 40 m^3/h. For Soluplus® mixtures, the solution was sprayed with an inlet air temperature of 90 °C and a flow rate of 25%. For PEG 6000 mixtures, the inlet temperature was 60 °C with a flow rate of 20%.

4.5.1.b. Lyophilization

Sulfamethoxazole and nifedipine with each polymer were prepared in drug:polymer mass ratios of 1:1, 1:5, and 1:9. Each drug with Soluplus® or PEG 6000, at the selected mass ratio, were dissolved in 250 ml of water/acetonitrile (1:5). A magnetic bar was used to stir the mixture until a clear solution was observed. The solution was placed in a -80 ^oC freezer for 24 h. The frozen solutions were then placed in an AdVantage XL-70 freeze dryer (Virtis, Gardiner, NY) at a condenser temperature of -60 °C and reduced pressure of 20 mbar for at least 24 h. The shelf temperature was -40 °C in the first day for primary drying. The lyophilized mixtures were taken from the lyophilizer and placed in a desiccator at 25 °C the following day for secondary drying.

4.5.2. Differential scanning calorimetry

Thermal analysis was conducted using a TA 2910 DSC (TA Instruments, New Castle, DE, USA) at a scan rate of 10 °C/min. Samples of 3-7 mg were weighed and placed in an aluminum pan and an aluminum lid was crimped to form a hermetic seal. The DSC was calibrated for temperature and enthalpy with indium (100% pure, melting point 156.60 °C, heat of fusion 6.80 cal/g). The sample and reference cells were purged with nitrogen at 50 ml/min. The results were analyzed using Thermal Advantage 1.1 A software.

4.5.3. Scanning electron microscopy

The morphology of the solid dispersions was examined using an SSx-500 scanning electron microscope (Shimadzu, Kyoto, Japan). Samples were placed on a carbon specimen peg and dried under air. Samples were then coated with gold under vacuum using a Desk V sputter coater (Denton Vacuum, Moorestown, NJ). The accelerated voltage was 20 kV [15, 16].

4.5.4. Fourier transform infrared spectroscopy

The infrared spectrum of the drugs, the polymers, and their spray-dried and lyophilized mixtures were obtained using a Nicolet iS10 Fourier transform infrared (FTIR) spectrometer (Thermo Fisher Scientific, Madison, WI, USA). The materials were prepared as KBr pellets and spectra were collected across 4000 to 600 cm^{-1} wavenumber using 64 scans and 2 cm^{-1} resolution [5, 17].

4.5.5. Drug dissolution studies

4.5.5.1. Dissolution tests

In vitro dissolution tests of SMX, NIF, and solid dispersions were conducted in 900 ml of SGF or SIF at 37.0 ± 0.2 °C using a Distek model 2100C (Distek, North Brunswick, NJ) with paddle rotation of 100 rpm. At designated time points, samples were drawn and filtered through a 0.45μm in-line filter using a Distek model 2230A autosampler, and then analyzed using UV spectrophotometry at 260 and 240 nm for SMX and NIF, respectively. Each experiment was conducted at least in triplicate [18].

4.5.5.2. Data analysis of release data

4.5.5.2.a. Mathematical models of release kinetics

Drug-polymer mixture release kinetics were evaluated using zero-order, first-order, Hixson-Crowell, Higuchi, and Ritger-Peppas model equations [19-21].

Zero-order kinetic model

If a plot of the cumulative amount of drug released as a function of release time presents linear data, zero-order kinetics is suggested and the release rate is independent of the drug concentration.

$$\frac{M_t}{M_\infty} = M_o + k_o t \tag{4.1}$$

Where M_o, M_t, and M_∞ are the amount of drug released at the beginning, at time t in the release period, and the total mass of drug released at infinite time (typically taken to be

the mass of drug available in the sample), respectively. The coefficient k_o is the zero order rate constant.

First-order kinetic model

If a plot of the negative of the log (base e) of 1 minus the cumulative fraction of drug released versus time is linear, drug is said to undergo first-order release. Eq. 4.2 shows the dependence of the release rate on the drug concentration.

$$-\ln(1-\frac{M_t}{M_\infty}) = k_1 t \tag{4.2}$$

Higuchi kinetic model

Plotting the cumulative amount of the released drug as a function of the square root of the release time renders linearized data if the drug is released by kinetics described by the Higuchi model. The model was developed to describe drug release from a matrix that remains intact during drug release:

$$\frac{M_t}{M_\infty} = M_o + k_H\sqrt{t} \tag{4.3}$$

where k_H is the Higuchi rate constant.

Hixson-Crowell kinetic model

The Hixson-Crowell kinetic model applies if a plot of the difference between the cube root of the mass of drug initially in a matrix, i.e., M_∞, and the cube root of the mass of drug remaining in that matrix at time t, M_∞ - M_t, as a function of release time presents

linearized data. The model describes drug release from a spherical matrix that erodes or dissolves proportionally across its surface area over time to release the drug.

$$(M_\infty)^{1/3} - (M_\infty - M_t)^{1/3} = k_{HC}t \quad (4.4)$$

k_{HC} is the Hixson-Crowell rate constant.

Ritger-Peppas kinetic model

The plot for this kinetic model presents the fraction of drug released from the solid dosage form as a function of release time.

$$\frac{M_t}{M_\infty} = k_{RP}t^n \quad (4.5)$$

where k_{RP} is the Ritger- Peppas rate constant. The exponent, n, can provide some insight into the release mechanism, with dissolved drug diffusion from an essentially intact matrix at its low value (typically about 0.5) and polymer relaxation (hydration, swelling, and possibly gelling of the polymer) at the high extreme (typically about 1.0). At values between these extremes, the release mechanism is described as anomalous, indicating that drug release is achieved by a combination of mechanisms or by an undefined mechanism.

4.5.5.2.b. Analysis of the drug release data

Sigma Plot 2002 for Windows, version 12.0 (SPSS, Inc., Chicago, IL) was used to analyze and fit equations to the release data. The variables were predicted and $p<0.05$ was considered significant [23].

4.5.5.2.c. Comparison of release profiles

To evaluate the similarity of in vitro release profiles before and after the stability study, the similarity factor, f_2, will be calculated. The similarity factor, as defined in Eq. 4.6 is based on the difference in drug percent dissolved between the test and the reference product at specific time points:

$$f_2 = 50 * \log\left\{\left(1 + \left(\frac{1}{n}\right)\sum_{i=1}^{n}\left|R_i - T_i\right|^2\right)^{-0.5} * 100\right\} \quad (4.6)$$

where n is the number of time points, R_i is the percentage of drug released from the reference product, and T_i is the percentage released from the comparison product at different time points. The f_2 value is 50-100 for similarity and less than 50 for dissimilarity in the dissolution profiles [3, 21, 22] .

4.5.6. Drug stability studies

4.5.6.1. Storage conditions for stability studies

Pure drug, pure polymer, and solid dispersions will be stored under 50 °C/ 0% RH and 25 °C/ 0% RH conditions. Thermal analysis was conducted after six months by DSC to evaluate the degree of crystallinity of the drug following each storage condition [5].

4.6. Results and Discussions

4.6.1. Differential scanning calorimetry

The melting endotherm of each drug and polymer is found in Fig. 4.2. Sulfamethoxazole has a melting point of 169.87 °C, nifedipine has a melting point of 173.05 °C, Soluplus® has a T_g around 70 °C, and PEG 6000 is semi crystalline with T_g around -22 °C (not shown in the figure) and a melting point of 60 °C.

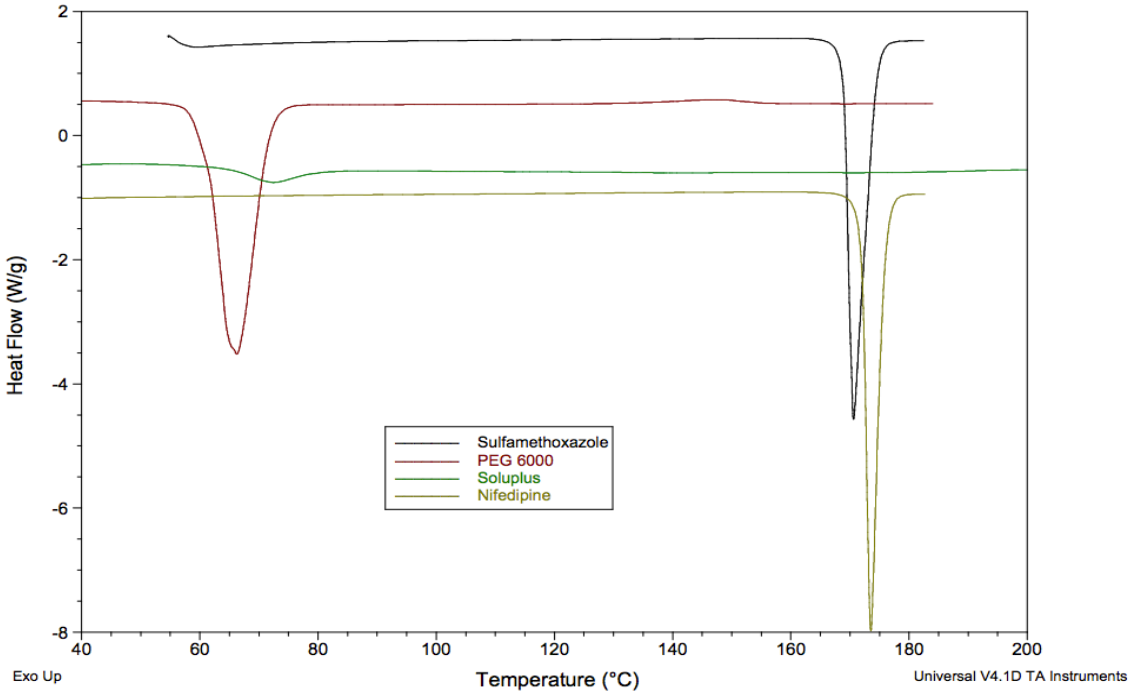

Figure 4.2. DSC thermograms for (top to bottom) sulfamethoxazole, PEG 6000, Soluplus®, and nifedipine.

4.6.1.a. Spray dried solid dispersion

The DSC analysis for SMX-Soluplus® at different ratios is found in Fig. 4.3.a., The melting endotherm for SMX is 169.9 °C, however, no melting endotherm was evident at any drug-polymer ratio in this experiment. This analysis proves that Soluplus®, even at a 1:1 mass ratio, successfully dispersed SMX with no trace of crystallinity when the spray drying method was used. The T_g for the dispersed mixtures is shifting toward the original glass transition temperature of neat Soluplus® as the polymer content increases. This shift reveals an effective interaction between the drug and the polymer. Such a change in T_g indicates that the drug works as a plasticizer [24]. Gordon-Taylor (G-T) and Fox equations have been developed to predict the glass transition temperature of blends. However, the experimental T_g deviates from the T_g predicted by these equations. Such deviation is attributed to non-ideal mixing due to an unexpected change in volume [8, 17, 25, 26]. Andronis et al., showed that an increase in moisture content substantially reduced the glass transition temperature of indomethacin [27]. The moisture uptake was larger for the amorphous form of the drug. A significant reduction in the crystallization temperature as the moisture content increased is reported [28]. In this work, focus is on the appearance of the melting endotherm at different polymer ratios. Each of the preparation methods renders dispersed materials with different moisture content. However, it has been reported that the freeze drying method might induce drug crystallization. Such induction happens during the freezing step. In that step the solution will not freeze instantaneously allowing the water to form crystals. Finally the sample freezes as a material that is amorphous, crystalline, or a combination of the two. The percentage of

the solvent that does not freeze is considered bound solvent [29]. In the literature, however, both methods, demonstrated a moisture content of up to 5% [30].

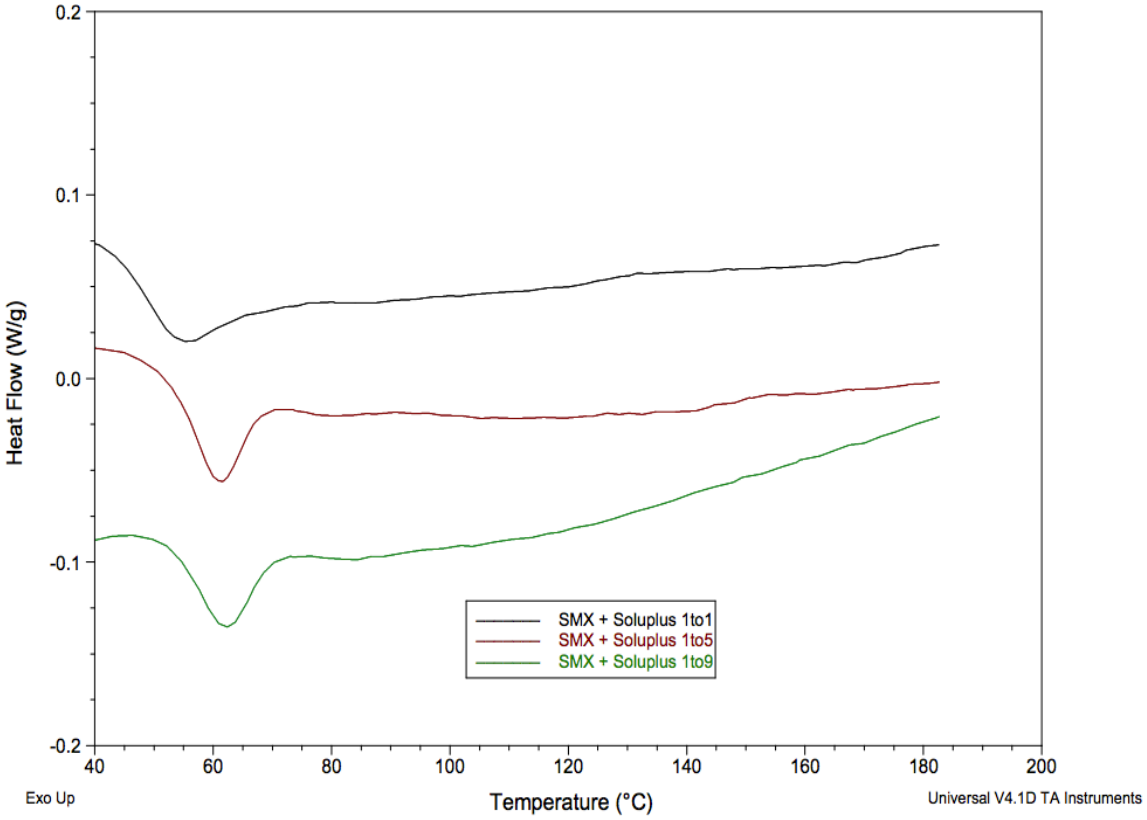

Figure 4.3.a. DSC thermograms of sulfamethoxazole:Soluplus® spray dried mixtures at a mass ratio of 1:1, 1:5, and 1:9.

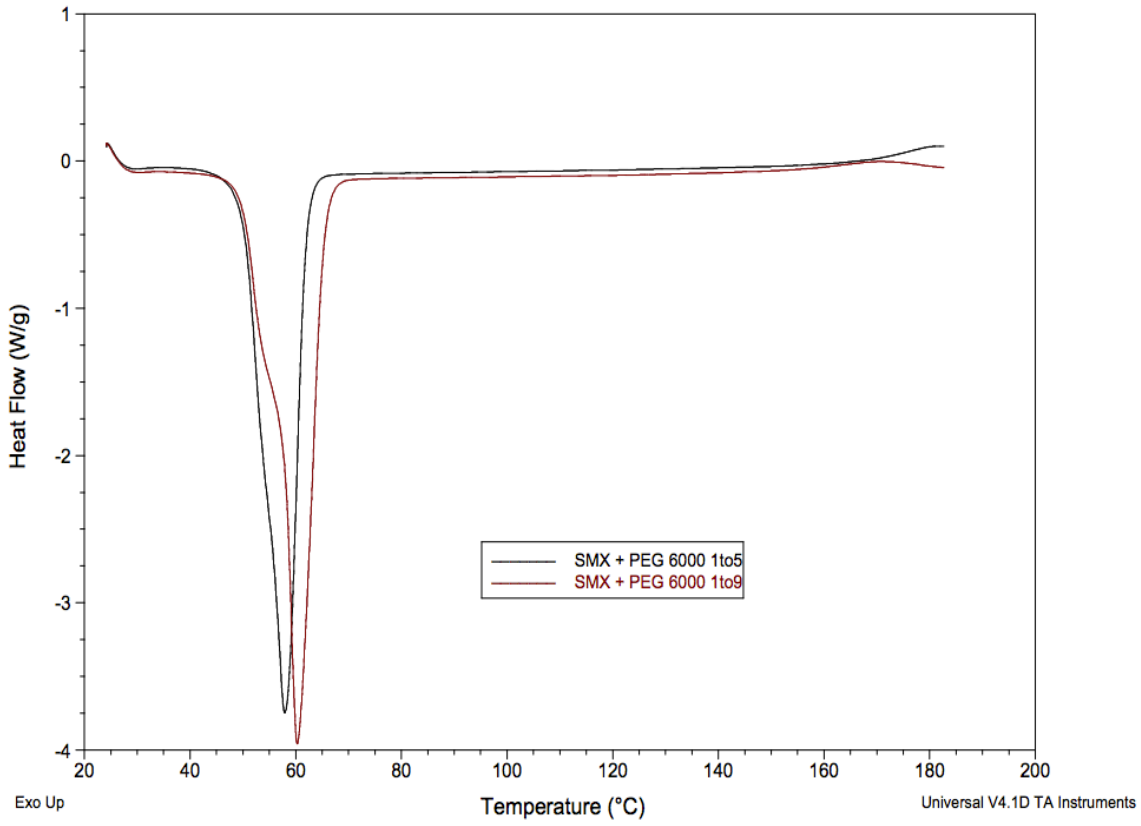

Figure 4.3.b. DSC thermograms of sulfamethoxazole:PEG 6000 spray dried mixtures at mass ratios of 1:5 and 1:9.

DSC analysis for the SMX-PEG 6000 dispersions prepared using spray drying is found in Fig. 4.3.b., The melting endotherm of PEG 6000 was around 57 °C, whereas, no melting endotherm was found for SMX. It is obvious that the large melting endotherm of PEG 6000 in the mixture enlarges the y-axis and, thus, obscures any melting endotherm for SMX at higher temperatures. However, there was no melting endotherm for SMX at temperature ranging from 75 to 160 °C, see Appendix D, Figure 1.

When the drug dissolves in the polymer and forms a solid solution, or when drug is dispersed in the polymer carrier as amorphous material, no drug melting endotherm can be detected. The slight change in PEG 6000 melting might be attributed to the dispersed drug or residual moisture effect. In addition, PEG 6000 exists in an extended or folded form. The latter will render a shoulder that precedes the melting of the extended form of the polymer [31]. This shoulder is attributed to the polymer chains that have folded during drying. Observed broad peaks at temperatures above 160 °C have been reported elsewhere [1, 32]. The collected materials for 1:1 ratio were excluded due to some technical difficulty.

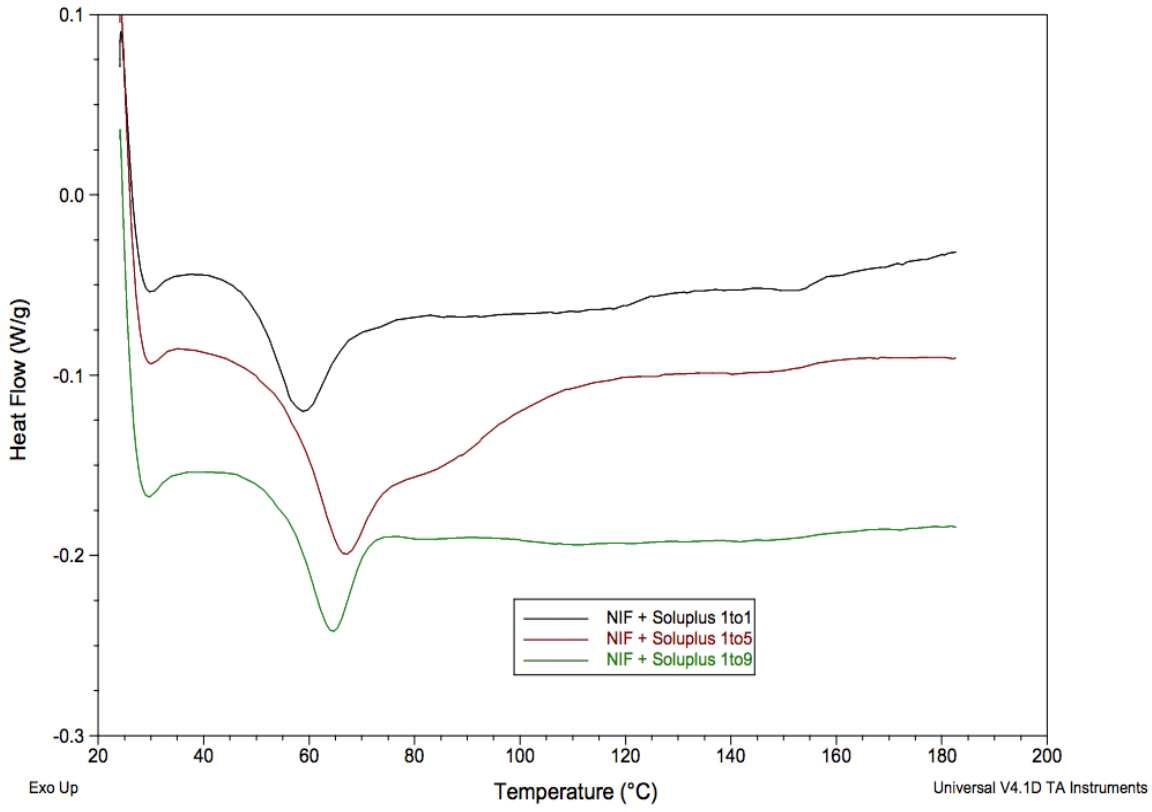

Figure 4.4.a. DSC thermograms of nifedipine:Soluplus® spray dried mixtures at mass ratios of 1:1, 1:5, and 1:9.

Thermal analyses of spray dried NIF-Soluplus® samples are found in Figure 4.4.a. A sharp melting endotherm was not found at any mass ratio. Negligible endothermic events were found in the thermograms for the mixtures at 1:1 and 1:5 mass ratios that might be due to traces of crystalline NIF that did not dissolve in the polymer. An increase in the glass transition temperature with higher polymer ratios was observed, with a similar trend found for SMX-Soluplus® mixtures. SMX and NIF have melting endotherms around 170 °C, however, the thermodynamic driving force for solubility in Soluplus® is larger for SMX than for NIF (see chapter 1 and 2). Therefore, it was expected that Soluplus would dissolves SMX to a greater extent than NIF when making a solid dispersion.

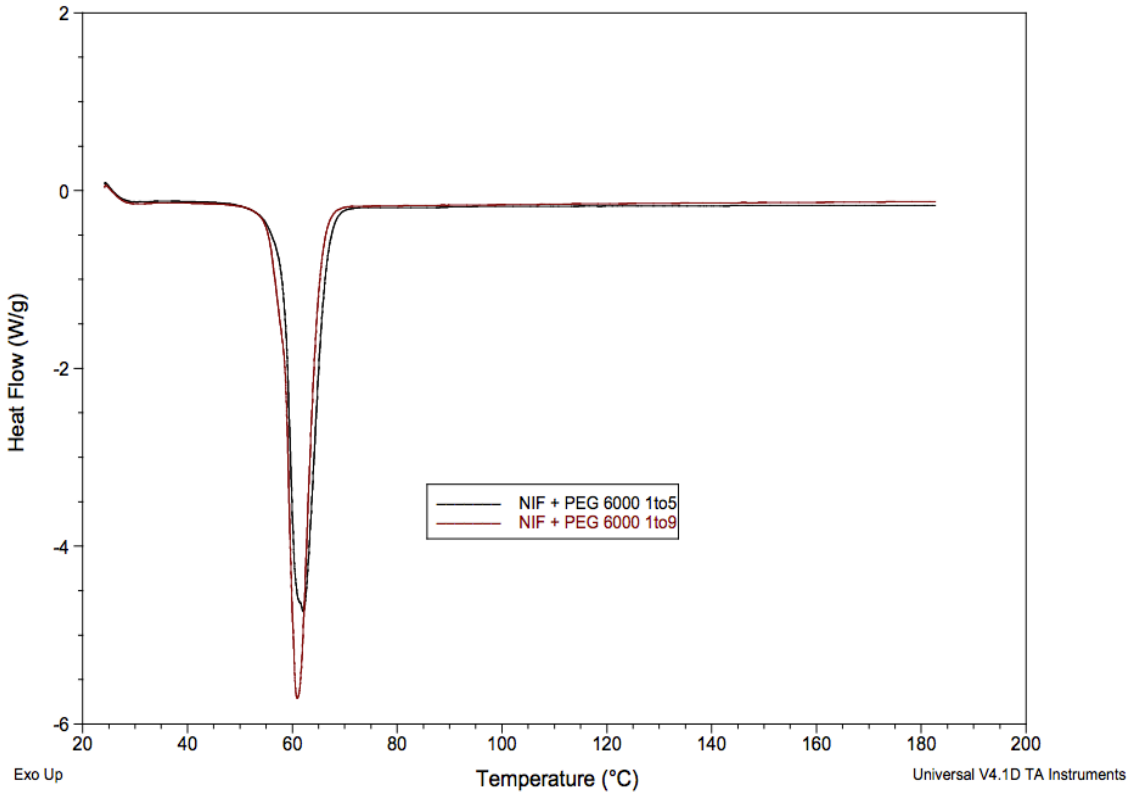

Figure 4.4.b. DSC thermograms for nifedipine:PEG 6000 spray dried mixtures at mass ratios of 1:5, and 1:9.

Thermograms for the spray dried mixtures of NIF-PEG 6000 at 1:5 and 1:9 mass ratios reveal the absence of the NIF melting endotherm, indicating a complete conversion of crystalline NIF to its amorphous form or complete molecular level dispersion of the drug in the polymer matrix, see Fig. 4.4.b.

4.6.1.b. Lyophilized solid dispersions

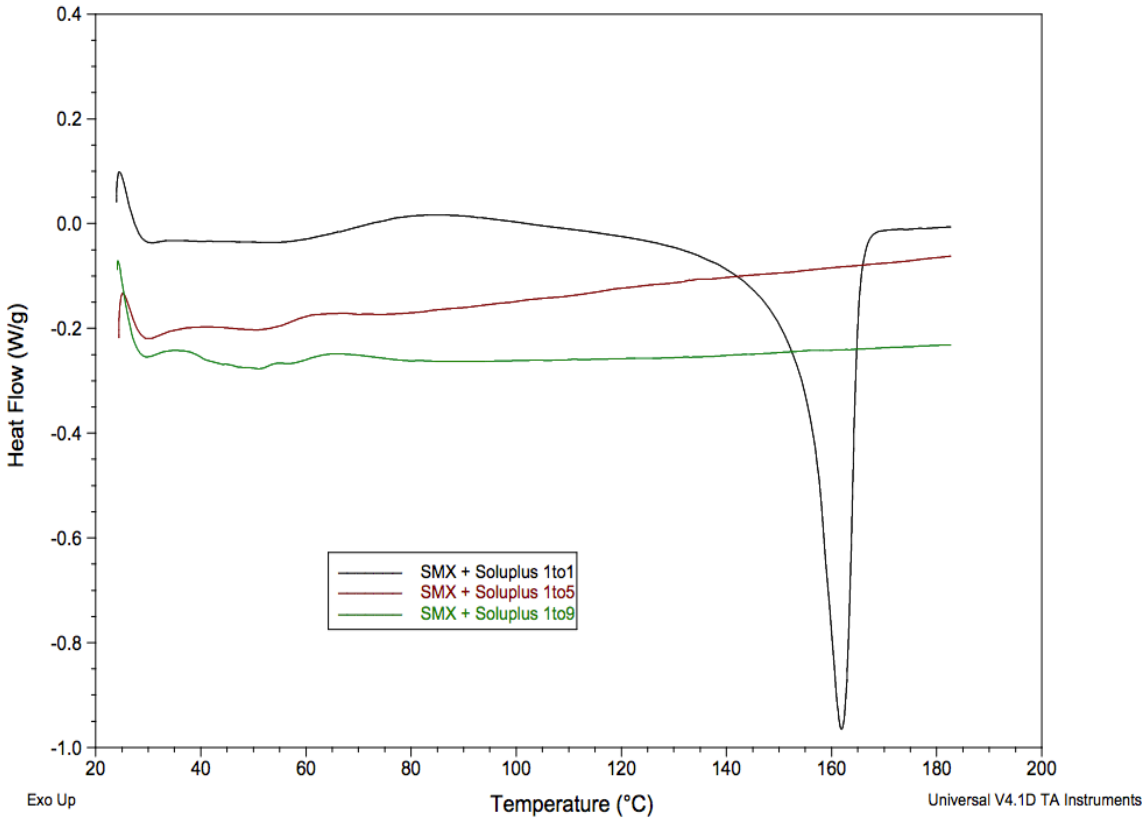

Figure 4.5.a. DSC thermograms for sulfamethoxazole:Soluplus® lyophilized mixtures at mass ratios of 1:1, 1:5, and 1:9.

Thermograms for the lyophilized SMX-Soluplus® and SMX-PEG 6000 mixtures are found in Figure 4.5.a. and 4.5.b., respectively. The melting endotherm was obvious in the thermogram for each dispersion with the 1:1 mass ratio, indicating the presence of crystalline drug. The melting endotherm is not evident in the thermograms for mixtures with higher polymer levels.

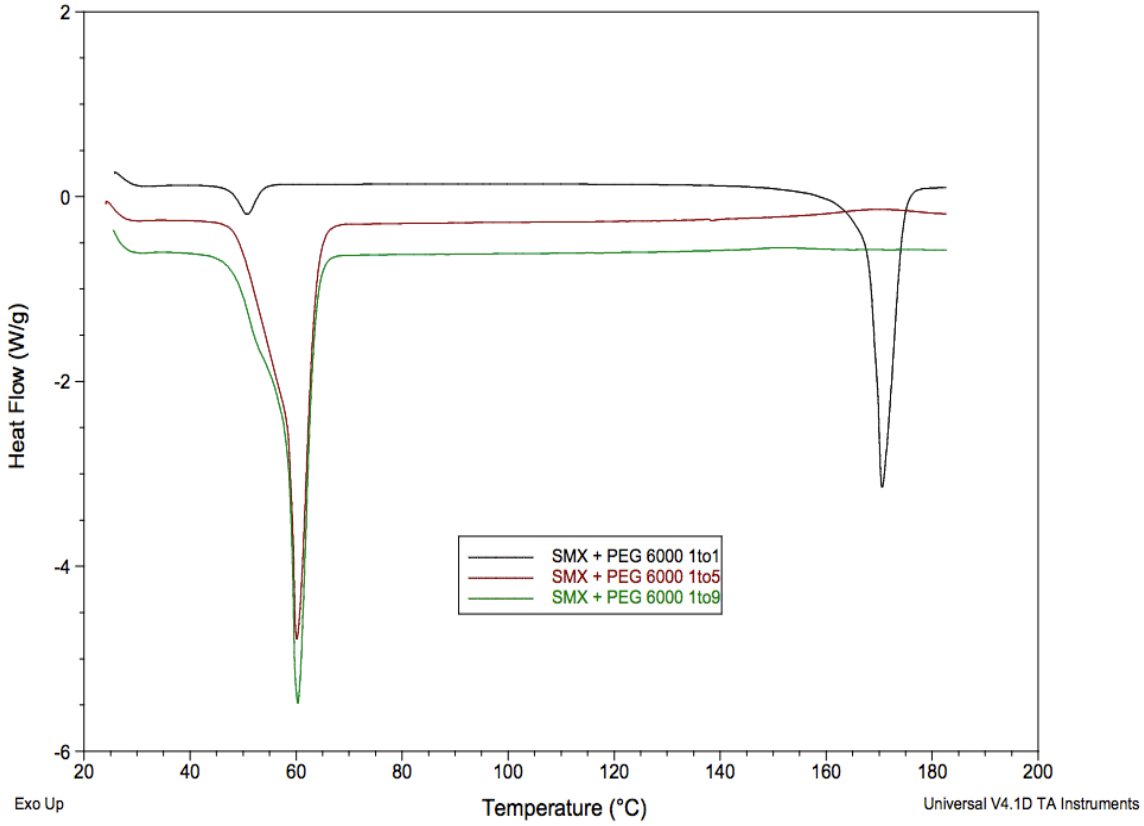

Figure 4.5.b. DSC thermograms for the sulfamethoxazole:PEG 6000 lyophilized mixtures at mass ratios of 1:1, 1:5, and 1:9.

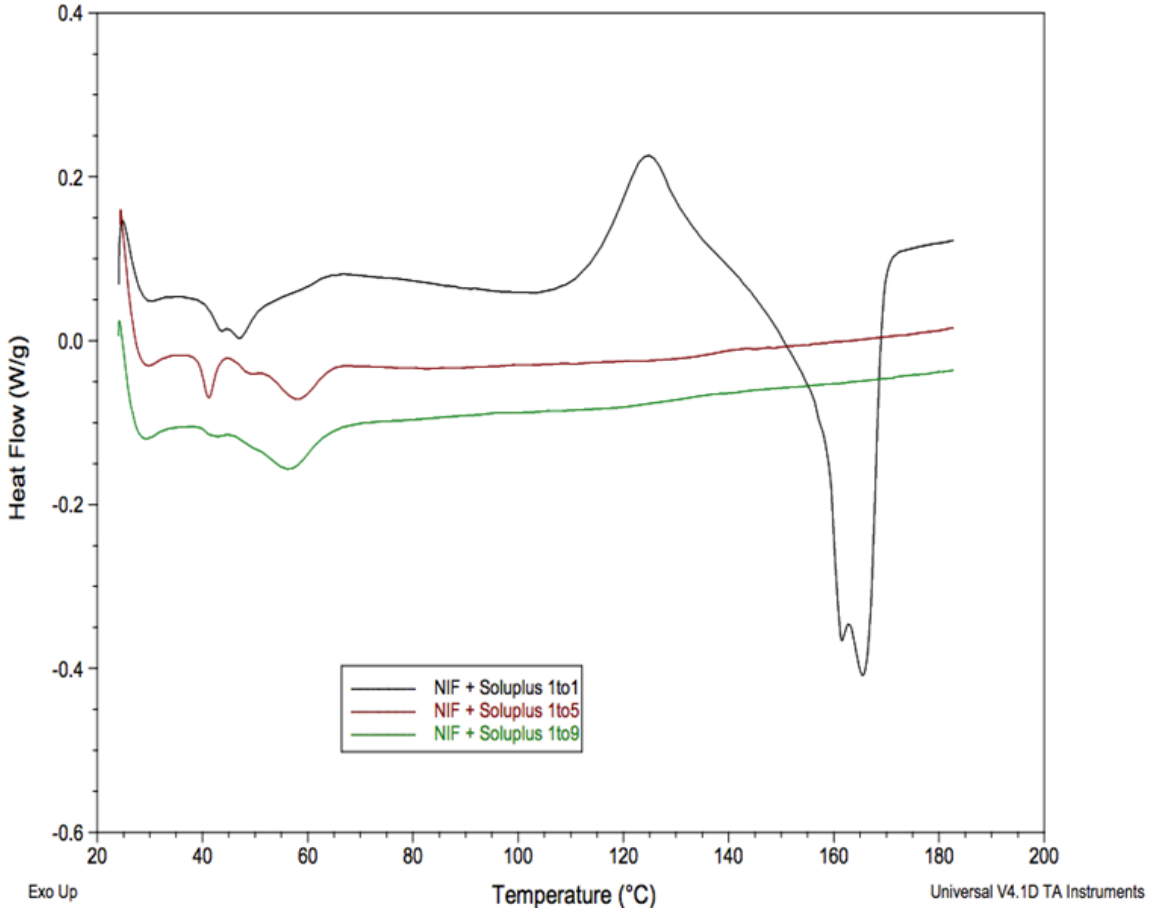

Figure 4.6.a. DSC thermograms for the nifedipine:Soluplus® lyophilized mixtures at mass ratios of 1:1, 1:5, and 1:9.

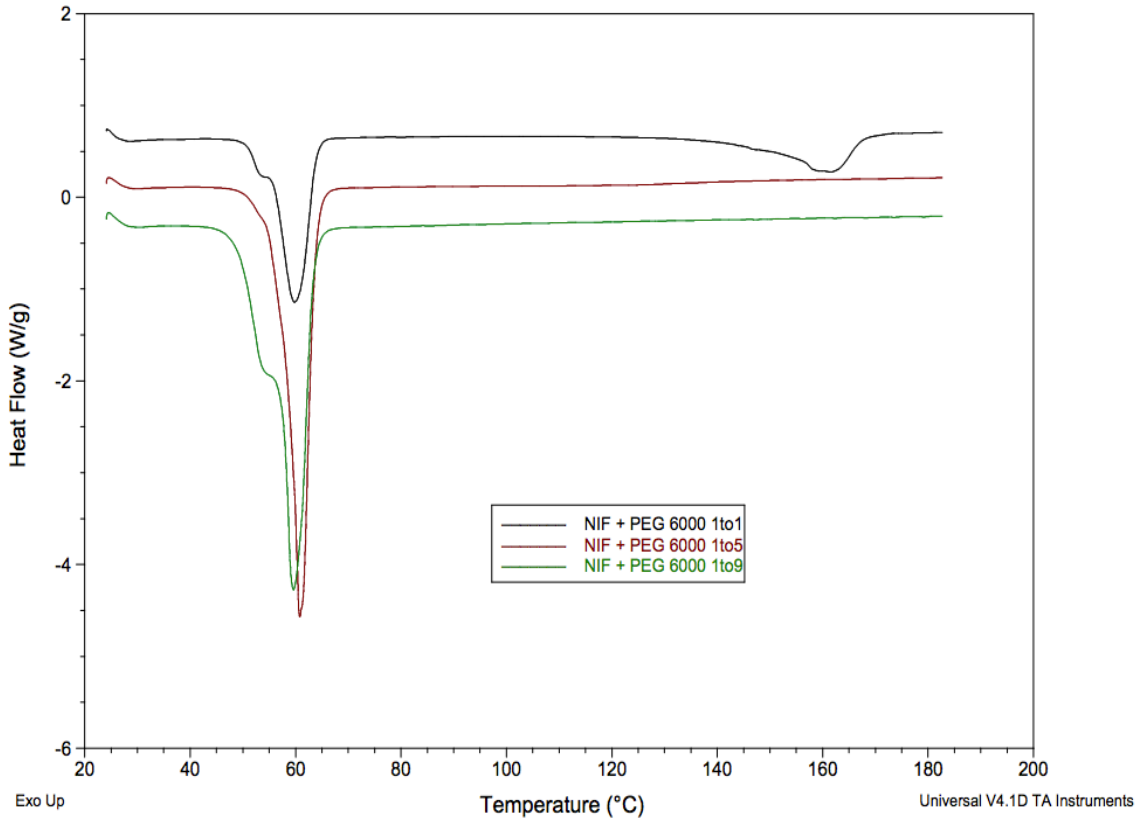

Figure 4.6.b. DSC thermograms for nifedipine:PEG 6000 lyophilized mixtures at mass ratios of 1:1, 1:5, and 1:9.

In Figures 4.6.a. and 4.6.b., the melting endotherm was absent except for 1:1 ratio. In particular, Figure 4.6.a., a recrystallization peak was found before the melting of nifedipine.

The preparation methods for the solid dispersion mixtures are of crucial importance. The detectable sharp melting endotherm for the lyophilized 1:1 mixture of NIF or SMX with PEG 6000 proves the superiority of spray drying to form solid dispersions. The freezing step in lyophilization fixes the solution components in space because the viscosity of the liquid would rise quickly, whereas spray drying should allow a greater time frame over which rearrangement of solute molecules can take place as the solvent evaporates from

each sprayed drop. In the freezing step, bound water does not freeze. This bound water will not sublime in the reduced pressure environment [29], but is more likely to be removed during secondary drying in a lyophilizer or with sufficient extended time in the desiccator at room temperature. In spray drying, bound water should evaporate due to the higher temperature providing sufficient energy to break the bonds of water with the polymer hydrophilic functional group(s) that lead to bound water.

Water in the lyophilized mixture is more likely found in the amorphous part of the drug but its presence can induce crystallization. Such induction occurs due the greater mobility that the water gives to the amorphous form of the drug [27, 28]. For every SMX:Soluplus® ratio, single detectable T_g was missing in lyophilized mixtures, which also indicates less efficient mixing of the two in the lyophilized mixtures.

When SMX- or NIF- PEG 6000 samples were lyophilized, the solid dispersion successfully maintained the amorphous form of the drug at higher polymer levels in the samples, with mass ratios of 1:5, and 1:9 (Figures 4.5.b and 4.6.b., respectively). At the 1:1 mass ratio, the melting endotherms for each drug were detected, exhibiting a trend similar to that observed with Soluplus®.

4.6.2. Drug stability studies

The drug and the 1:9 mass ratio drug:polymer mixtures, prepared using either spray drying or lyophilization techniques, are subjected to a 6 month study under different temperature conditions. No recrystallization was found with either of the dispersed drugs (see Figures 4.7.a., 4.7.b, 4.7.c., and 4.7.d.).

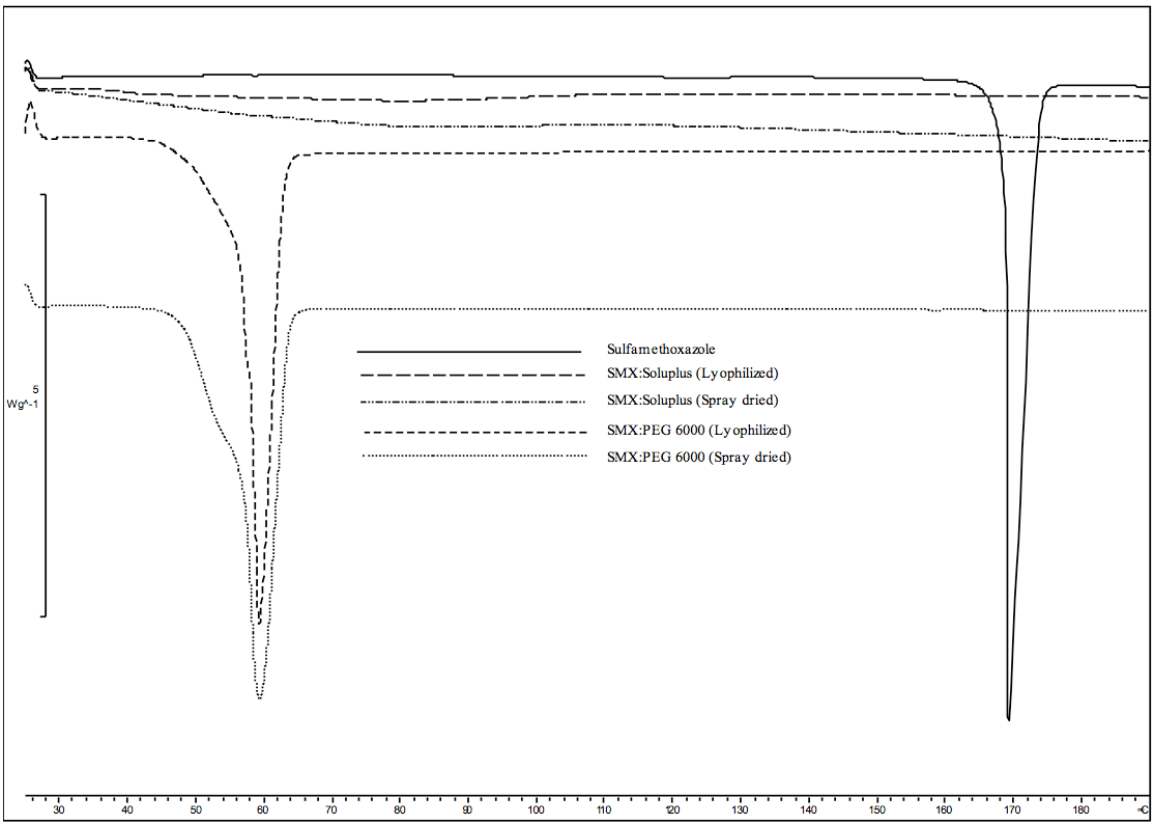

Figure 4.7.a. DSC thermograms for SMX mixtures with Soluplus® and with PEG 6000 at a mass ratio of 1:9 stored for six months at 0% RH and 25 °C.

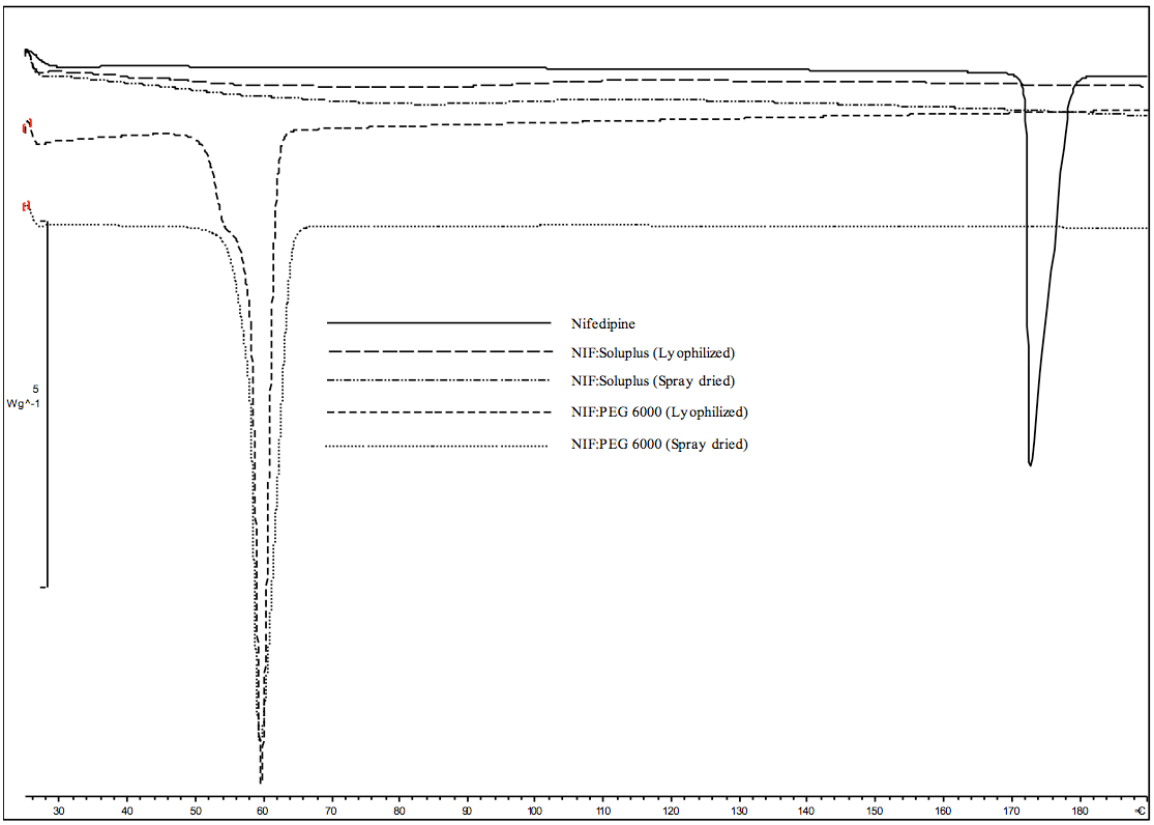

Figure 4.7.b. DSC thermograms for NIF mixtures with Soluplus® and with PEG 6000 at a mass ratio of 1:9 stored for six months at 0% RH and 25 °C.

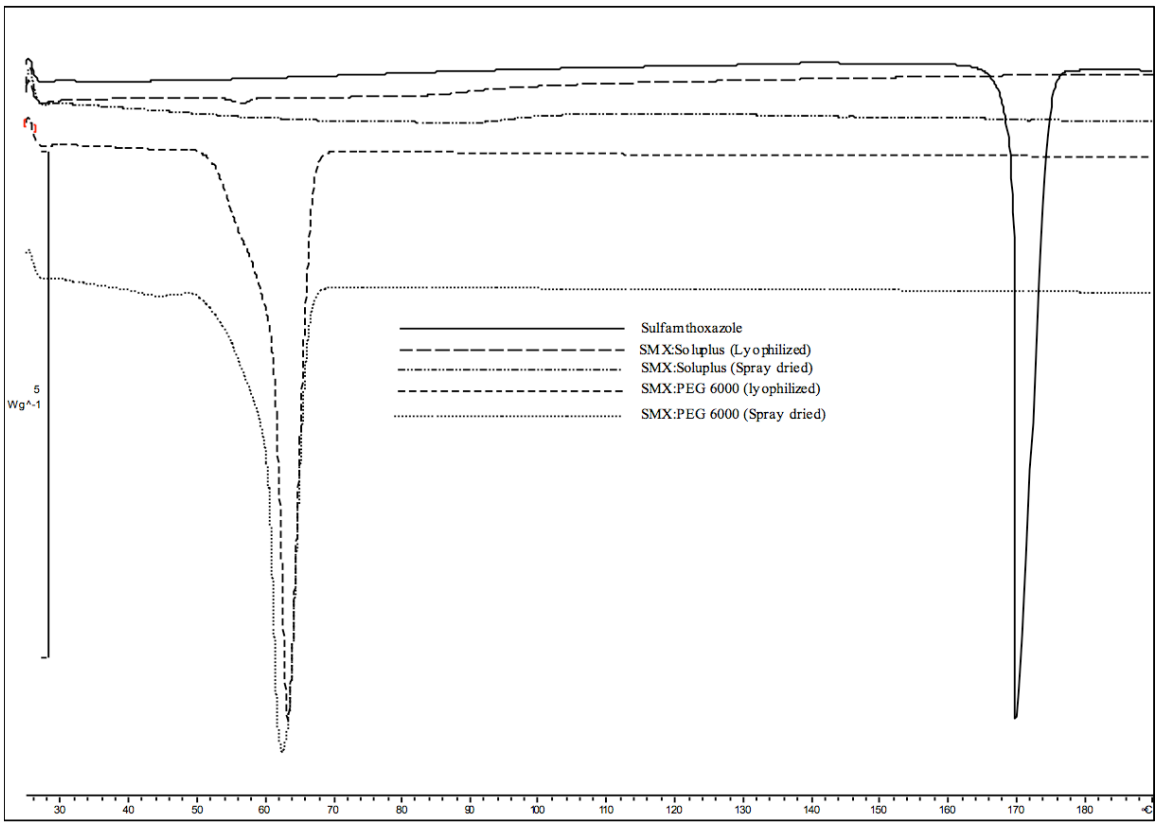

Figure 4.7.c. DSC thermograms for SMX mixtures with Soluplus® and with PEG 6000 at a mass ratio of 1:9 stored for six months at 0% R.H. and 50 °C.

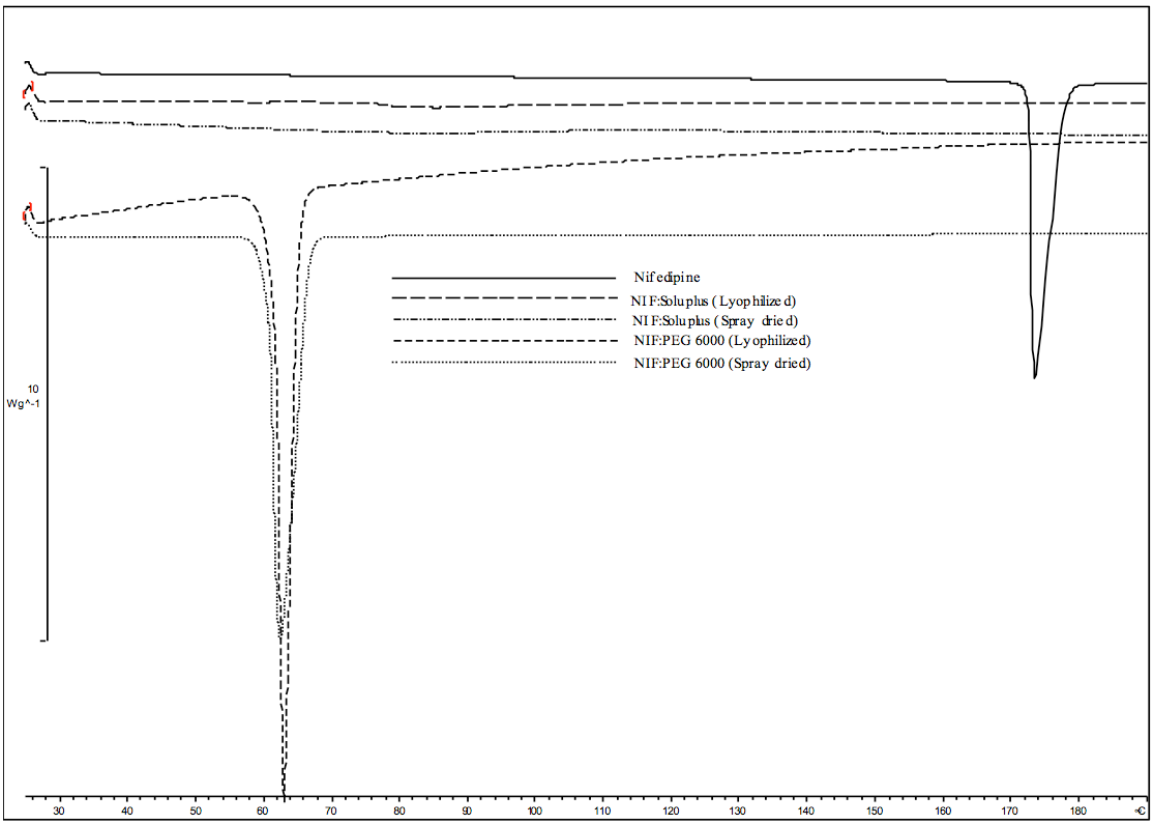

Figure 4.7.d. DSC thermograms for NIF mixtures with Soluplus® and with PEG 6000 at a mass ratio of 1:9 stored for six months at 0% RH and 50 °C.

4.6.3. Scanning electron microscopy

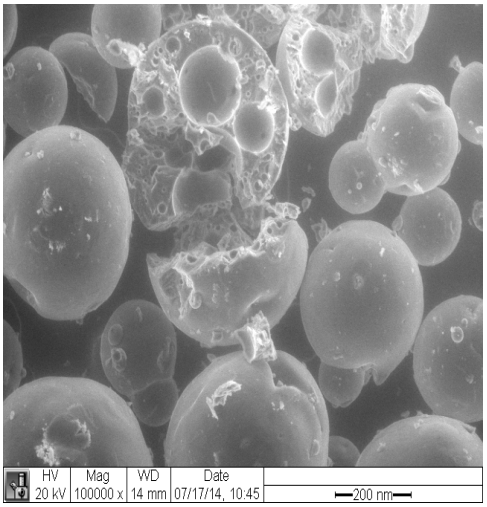

a. PEG 6000

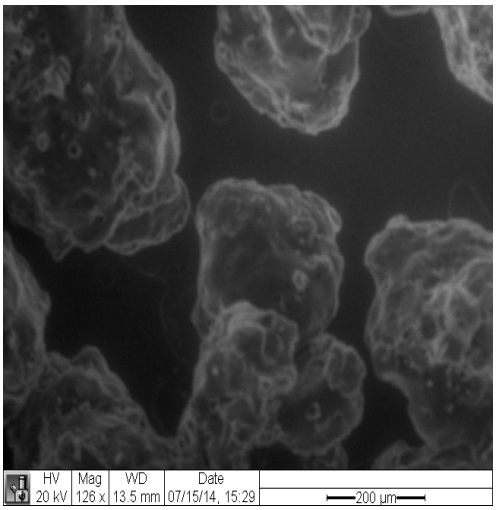

b. Soluplus

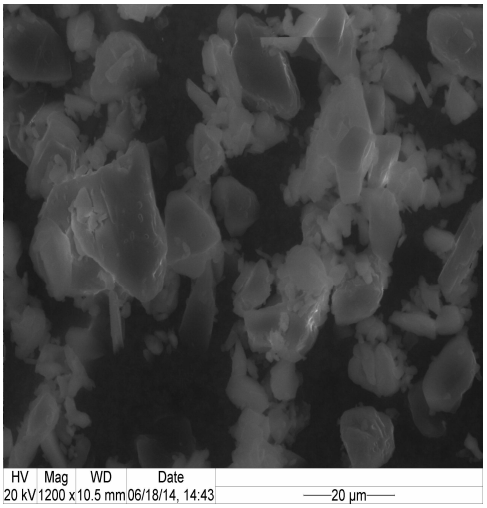

c. Sulfamethoxazole

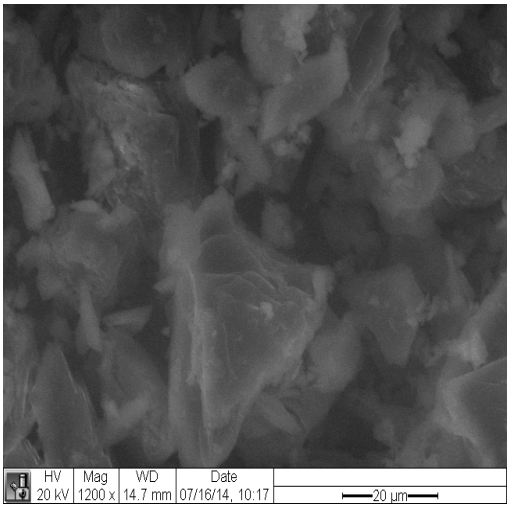

d. Nifedipine

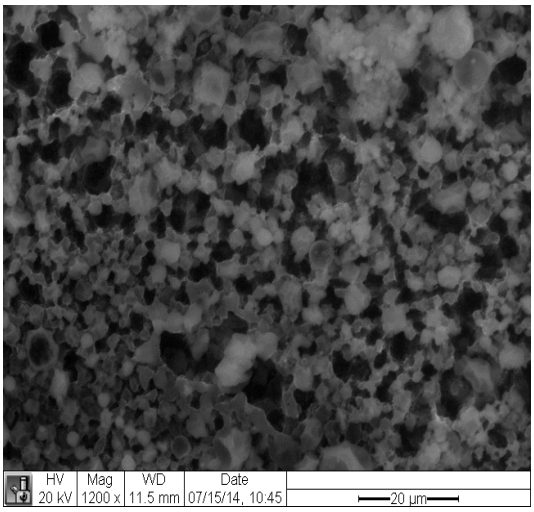

e. SMX+ Soluplus (spray dried)

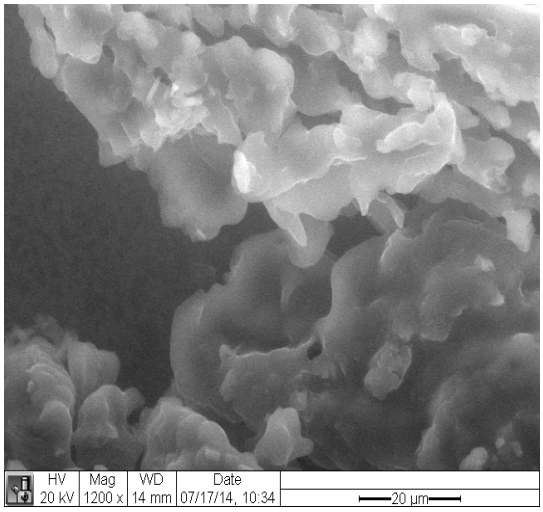

f. SMX+ PEG 6000 (spray dried)

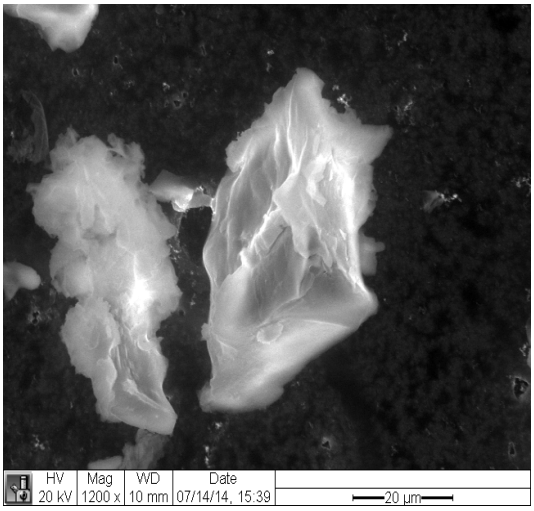

g. SMX+ Soluplus (Lyophilized)

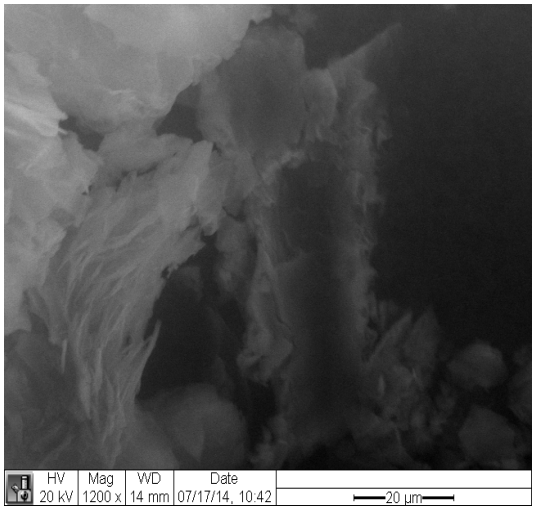

h. SMX+ PEG 6000 (Lyophilized)

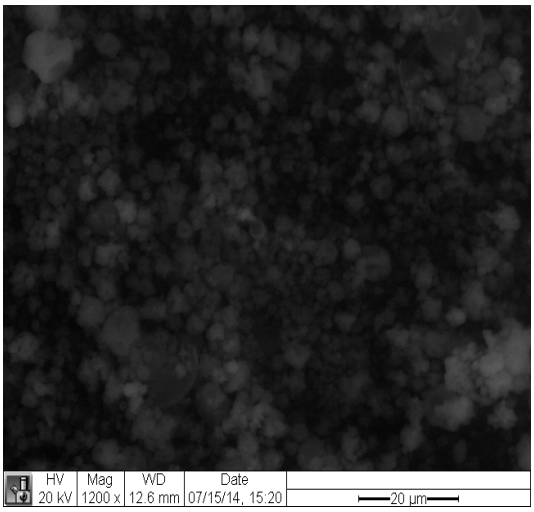

i. NIF + Soluplus (spray dried)

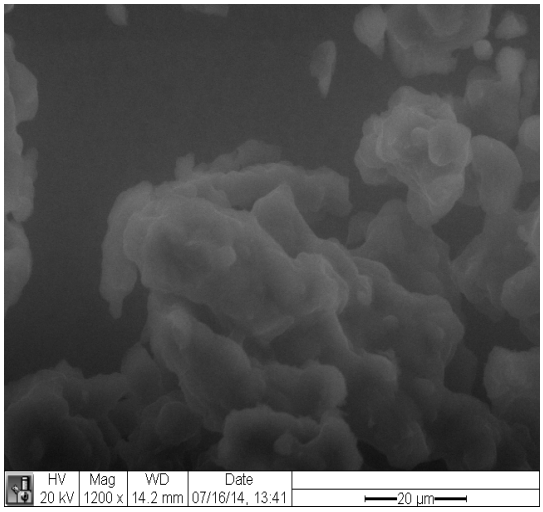

j. NIF + PEG 6000 (spray dried)

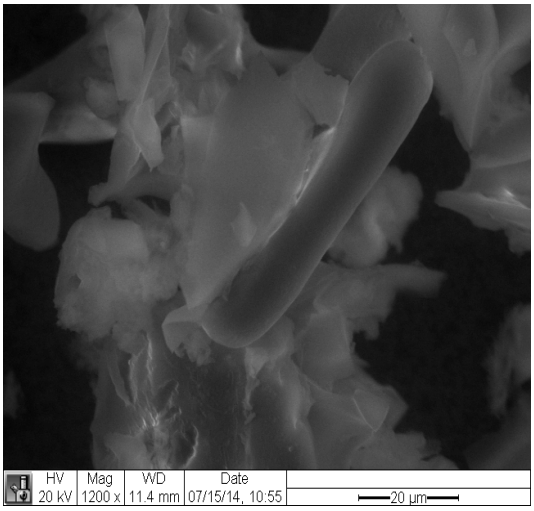

k. NIF + Soluplus (Lyophilized)

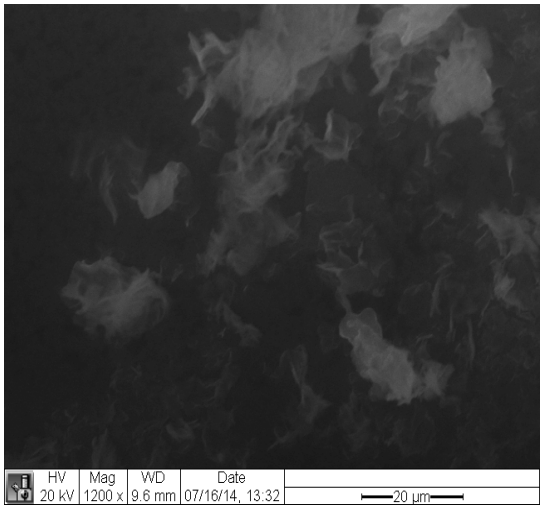

l. NIF + PEG 6000 (Lyophilized)

Figure 4.8. Scanning electron microscopy images showing the morphology of the neat drugs and polymers, and their respective dispersed mixtures.

The morphology of PEG 6000 and Soluplus® are found in Figures 4.8.a. and 4.8.b. The morphology of SMX and NIF indicate sharp edges, thus, indicates crystallinity (Figures 4.8.c. and 4.8.d. Smooth spheres were successfully obtained with spray dried Soluplus® mixtures (Figures 4.8.e and 4.8.i.). It is expected that spray drying renders spherical particles as the evaporation of the solvent leads to droplets that form a spherical shape upon drying. Also, it has been reported that the drug dispersed in PEG 6000 did not form a smooth sphere upon spray drying Figure 4.8.f. and 4.8.j. [1]. No spherical particles were found with the lyophilized mixtures. PEG 6000 mixtures formed hairy materials with sharp needles Figure 4.8.g., 4.8.h, 4.8.k., and 4.8.l. This vast difference in shapes will prove to profoundly impact the dissolution profile of these dispersed mixtures.

4.6.4. Fourier transform infrared spectroscopy

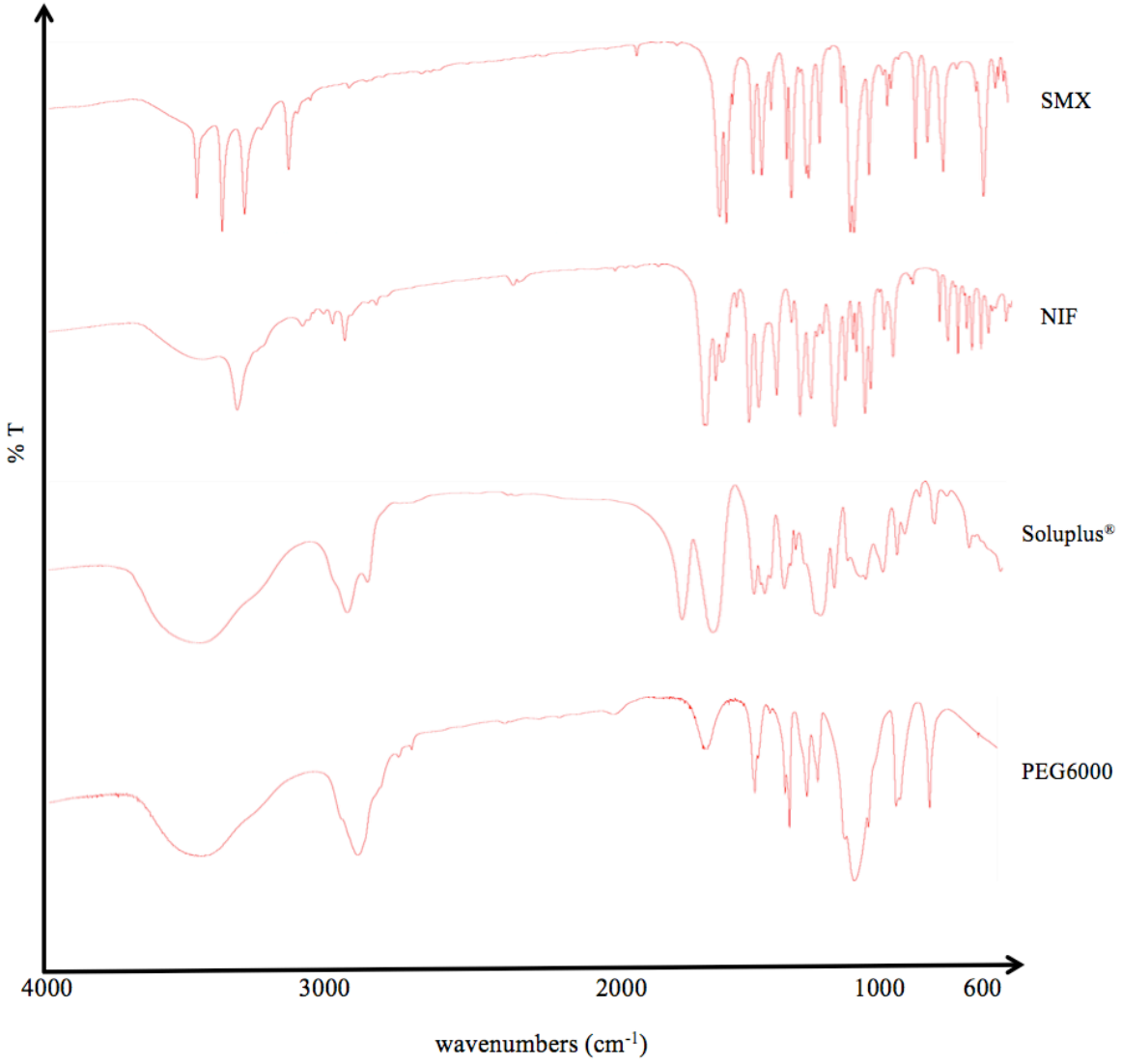

Figure 4.9.a. FTIR analysis for the used materials.

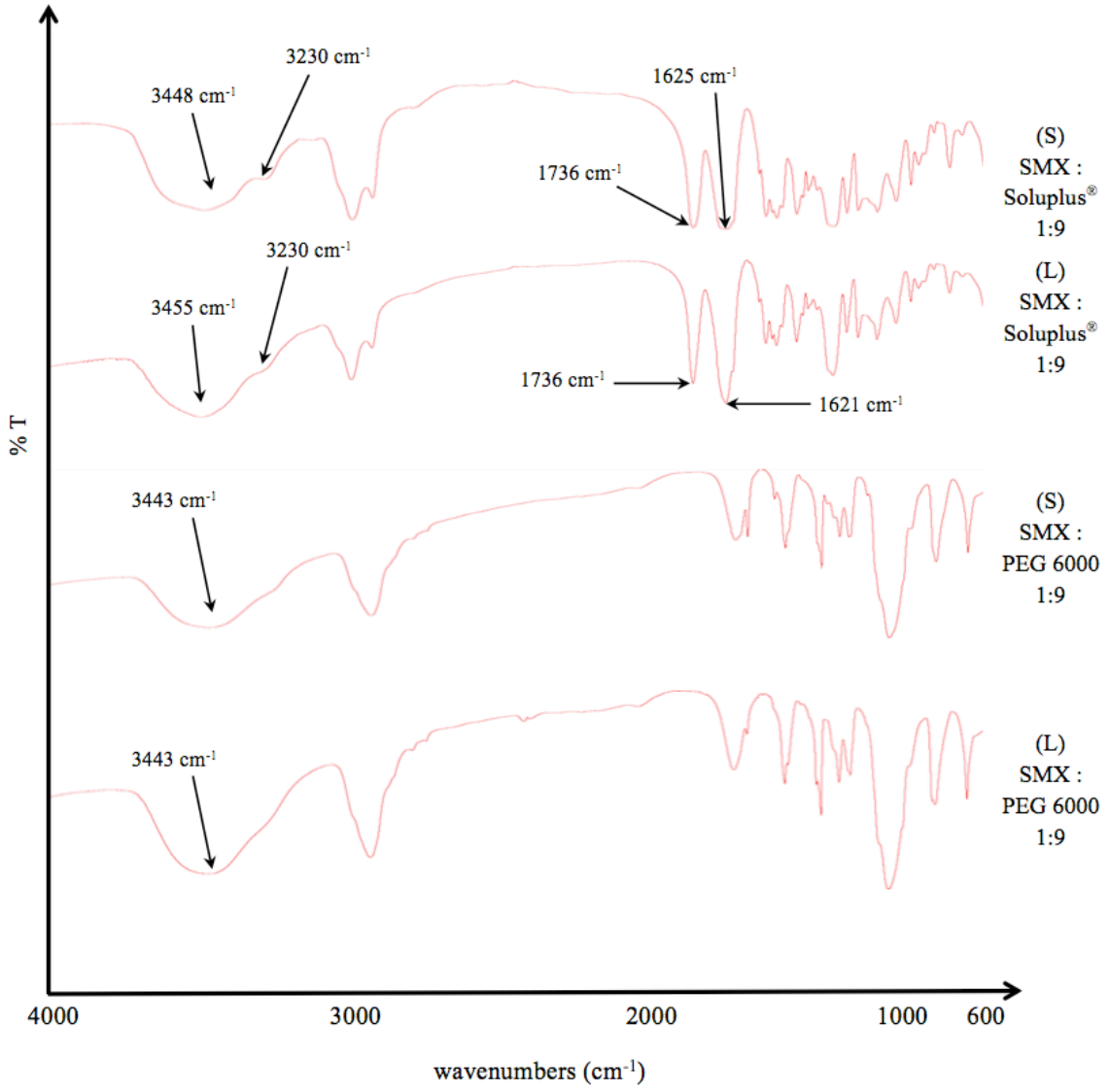

Figure 4.9.b. FTIR analysis for SMX-polymer mixtures (S denotes spray dried, and L denotes lyophilized).

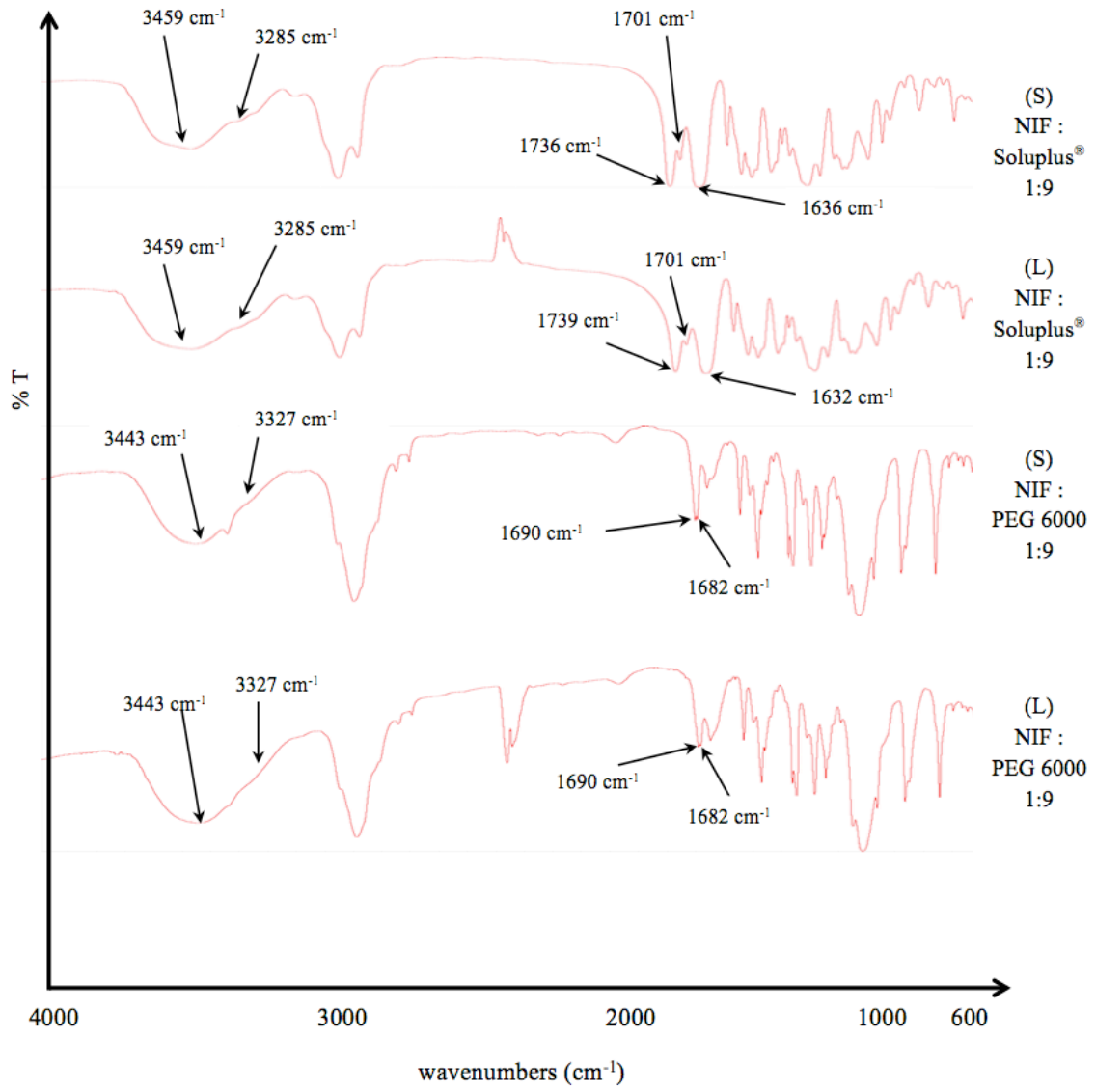

Figure 4.9.c. FTIR analysis for NIF-polymer mixtures (S denotes spray dried, and L denotes lyophilized).

The energy in the infrared IR region is not sufficient to excite electrons of a molecule. Upon absorption, however, the energy is enough to stretch or bend the bonds of a particular molecule. Therefore, the vibrational frequencies of certain chemical bonds involving specific atoms are detected using IR spectroscopy [33]. The IR spectrum provides the fingerprint of different chemical substances and specifically can detect the newly formed hydrogen bonds when molecules are dispersed in polymers [34].

The IR spectrum for crystalline SMX is found in Figure 4.9.a. For SMX, the first three distinctive peaks starting from the higher wavenumbers is attributed to N−H vibrations. NH_2 stretching shows sharp peaks at 3468 and 3378 cm^{-1} for asymmetric and symmetric stretching, respectively. The detected peak at 3299 cm^{-1} is attributed to N−H stretching in the amide functional group. C−H stretching shows a clear peak at 3144 cm^{-1} [35]. C−C and C−N vibrational stretching is assigned to the peaks at 1597 and 1502 $cm^{-1,}$ respectively. The peaks at 1267, 1092, and 1043 cm^{-1} are attributed to the SO_2 stretching vibrations [36].

The crystalline NIF IR spectrum is found Figure 4.9.a. The distinctive vibrational bands at 3332, and 1682-1690 cm^{-1} are attributed to N−H and C=O, respectively [34]. The peak at 2954 cm^{-1} is assigned to C−H aliphatic stretching. NO_2 symmetric stretching is found at 1350 cm^{-1} [37].

Soluplus® showed a broad peak centered at 3463 cm^{-1} that is attributed to O−H vibrational stretching. C−H stretching is found to be the peak at 2933 cm^{-1}. Peaks at 1739, and 1635 cm^{-1} are attributed to C=O in the ester and tertiary amide, respectively [38]. The ether C−O−C has a distinctive peak at 1483 cm^{-1} [39].

PEG 6000 showed peaks at 3439, 2887, and 1113 cm^{-1} that are attributed to O−H, C−H and C−O−C vibrational stretching [40-43]. The observed peak wavenumbers in the IR spectra of each functional group are summarized in table 4.2., along with the wavenumber found in the literature.

There are different functional groups in SMX and NIF that are capable of donating or accepting protons to form hydrogen bonds. The primary amine and the nitrogen in the sulfonamide group in SMX can donate protons to higher electronegativity atoms. In fact, SMX is expected to form hydrogen bonding with itself when the two oxygen atoms associated with the sulfur atom (SO_2) accept the protons. Also, The nitrogen atom in the isoxazole ring can also act as a proton acceptor.

The proton donor site in NIF is the nitrogen in the dihydropyridine ring. The oxygens in the carbonyl functional groups are proton acceptors. The NO_2 functional group is expected to have no hydrogen bonding capability [34]. Soluplus® has carbonyl, hydroxyl, and ether functional groups capable of hydrogen bonding. PEG 6000 likewise can donate or accept a proton through the hydroxyl groups and the oxygen in each of the ether groups.

Figure 4.9.b., shows the IR spectrum of spray dried (S) and lyophilized (L) SMX with either Soluplus® and PEG 6000. For the SMX-Soluplus® solid dispersion, the four distinctive peaks between 3000-3500 cm^{-1} for crystalline SMX have disappeared. This disappearance is ascribed to the disruption of hydrogen bonding between the SMX molecules and forming new bonds with the polymer. The shift in the broad peak from 3463 cm^{-1} for neat Soluplus® to 3448 and 3455 cm^{-1} for the spray dried and lyophilized

SMX-Soluplus® mixtures is postulated to be the O-H stretching vibrations which strongly indicate hydrogen bond formation with either the primary amine or one of the oxygen atoms found on the sulfur. There is a small but detectable shoulder at 3230 cm^{-1}, which might indicate a stretch of the amide N-H in SMX. The two carbonyl peaks at 1739, and 1635 cm^{-1} have shifted to lower wavenumbers in the mixture. The new peaks are evident at 1736, 1625, and 1621 cm^{-1}**,** suggesting a new hydrogen bond stretching with the primary amine and amide N-H.

The broad peak at 3439 cm^{-1} for neat PEG 6000 has shifted to 3443 $cm^{-1}$for spray dried and lyophilized dispersed mixtures. Such a shift is postulated to be stretching in the hydrogen bond of the hydroxyl groups of the polymer. The ether group shifted to 1112 cm^{-1} for the dispersed mixtures. This slight difference might not be compelling for hydrogen bond formation, however, the difficulty to demonstrate the hydrogen bond formation with PEG 6000 has been reported elsewhere [43].

Figure 4.9.c., shows the IR spectrum of spray dried (S) and lyophilized (L) NIF with either Soluplus® or PEG 6000. For NIF-Soluplus® solid dispersion, the broad peak for Soluplus® has shifted to 3459 cm^{-1}. The shift in this peak is attributed to hydrogen bond formation between the carbonyl group found in NIF with the hydroxyl group found in Soluplus®. The small shoulder at 3285 is postulated to be N−H stretching of NIF due to hydrogen bond formation with Soluplus® carbonyl or ether groups. The carbonyl groups of NIF exhibits sharp peaks at 1682-1690 cm^{-1}, whereas Soluplus® exhibits distinctive carbonyl peaks at 1739 and 1635 cm^{-1}. For the dispersions, however, the peak moved higher to 1701 cm^{-1} which is attributed to the stretch in the C=O when engaged in hydrogen bond formation with the polymer. Huang et al., suggested that the peak at 1701

cm^{-1} indicates formation of amorphous NIF, and the carbonyl stretch for NIF at 1702-1728 cm^{-1} should indicate hydrogen bond formation [34]. However, forming an amorphous drug is expected and it was previously confirmed using DSC analysis. In addition, having carbonyl groups in both the polymer and the drug might obscure the shift of the stretch in the NIF carbonyl groups. Soluplus® carbonyl group peaks have shifted to 1736, 1636 and 1739, 1632 for spray dried and lyophilized mixtures, respectively.

The change in the wavenumber of the PEG 6000 broad peak from 3439 to 3443 cm^{-1} in NIF-PEG 6000 dispersions is similar to the one found for SMX-PEG 6000 dispersions, which is due to stretching in the hydroxyl groups of the polymer. The small shoulder at 3327 cm^{-1} is expected to be the vibrational stretch of N−H upon hydrogen bond formation with the polymer. The carbonyl group exhibits distinctive peaks at 1682-1690 cm^{-1}. The absence of any stretching indicates that there was no hydrogen bond between the carbonyl group and the polymer.

The FTIR studies exhibit compelling evidences of change in the vibrational stretching within the different dispersions. The missing distinctive peaks, for instance, between pure SMX and SMX in dispersions are attributed to the inclusion of the drug in the polymer cavity [32]. Using the drug in smaller mass ratios with the polymer might prevent the instrument from acknowledging the vibrational stretching.

Between spray drying and lyophilization there were no significant differences in the IR spectra. The lack of any differences indicates that the preparation methods used to form solid dispersion have comparable efficiency.

Assignments	Literature SMX wavenumbers cm^{-1}	Experimental SMX wavenumbers cm^{-1}	Literature NIF wavenumbers cm^{-1}	Experimental NIF wavenumbers cm^{-1}	Literature Soluplus® wavenumbers cm^{-1}	Experimental Soluplus® wavenumbers cm^{-1}	Literature PEG 6000 wavenumbers cm^{-1}	Experimental PEG 6000 wavenumbers cm^{-1}
as,1(N−H) s,1(N−H) 2(N−H)	3470[a], 3467[b] 3381[a], 3378[b] 3301[b]	3468 3378 3299	- - 3332[c], 3330[d]	- - 3332	- - -	- - -	- - -	- - -
O−H	-			-	3449[e]	3463	3445[g], 3446[h], 3510[k]	3439
C−H	3145[a], 3143[b]	3144	2953[d]	2954	2928[e]	2933	2887[g], 2889[h], 2880[k]	2887
C−C	1619[b], 1597[b]	1621, 1597	-	-	-	-	-	-
C=O	-	-	(1679, 1689)[c] (1679, 1682)[d]	(1682, 1690)	(1739, 1643)[e] (1736, 1635)[f]	(1739, 1635)	-	-
C−O−C	-	-	-	-	1477[e]	1483	1110[g, l]	1113
N=O	-	-	1530[d]	1530	-	-	-	-
S=O	1266[b], 1091[b]	1267, 1092	-	-	-	-	-	-

Table 4.2. The characteristic vibrational stretching wavenumbers for functional groups found in the materials and their corresponding values from the literature.

(a, as) are asymmetric and symmetric vibrational stretching
(1, 2) are primary and secondary amines.
[a, b] are references 30, 31, respectively.
[c, d] are references 29, 32, respectively.
[e, f, g, h, k, l] are references 33, 34, 35, 36, 37, 38 respectively

4.6.5. Drug dissolution studies

It is crucial to test the dissolution characteristics of the drug and the drug-polymer mixtures prepared using different methods. As described in the method section, the preparation parameters were kept exactly the same, except when final products were made. Therefore, we expect any differences to be due to the preparation methods only. Two different enzyme-free media were selected, namely simulated intestinal fluid SIF (pH = 6.8 ± 0.1) and simulated gastric fluid SGF (pH = 1.2 ± 0.1) at 37 ± 0.2 °C. The model drugs, only, were tested in water for comparison. Each drug is ionized at a particular pH range or ranges. Sulfamethoxazole has two pKa values, namely 1.7 and 5.7. At pH above 5.7 SMX becomes anionic losing the proton on $-SO_2-NH-$ group. In very acidic conditions, with pH less than 1.7, the cationic form of SMX is found by protonating the aromatic NH_2 group. For pH between 1.7 and 5.7 SMX is expected to be uncharged [44, 45]. For NIF, however, the pKa was reported to be around 1 [46, 47]. Therefore, except in very acidic condition of pH ≤ 1.0, NIF is expected to be predominantly uncharged.

A three hour dissolution study (Figures 4.10.a and 4.10.b.) proved to be sufficient to identify the highest drug concentration [6]. Reduction in the drug concentration due to recrystallization can, therefore, be identified [5].

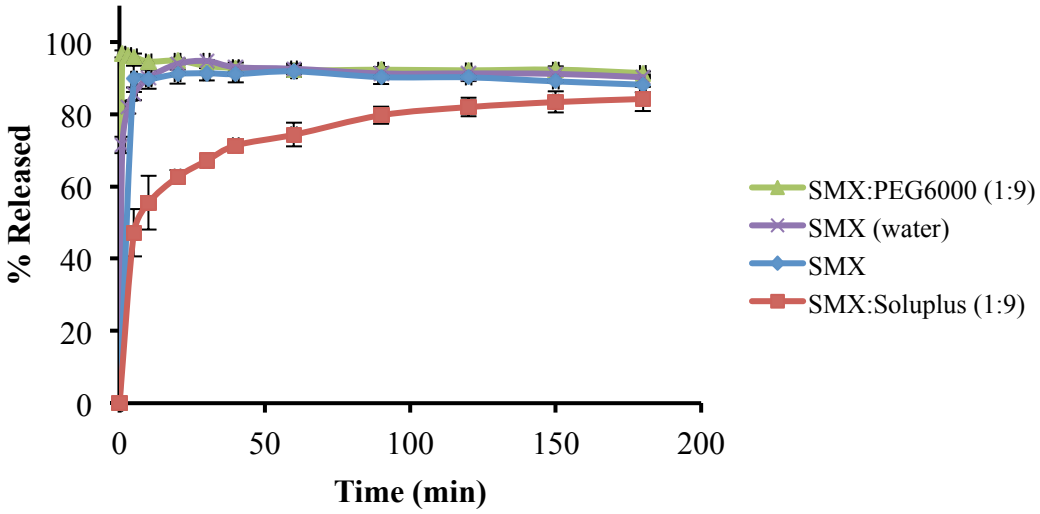

Figure 4.10.a. Sulfamethoxazole and spray dried SMX with Soluplus® or PEG 6000 in SIF (n=3). SMX alone in deionized water was added for comparison. Error bars represent standard deviation.

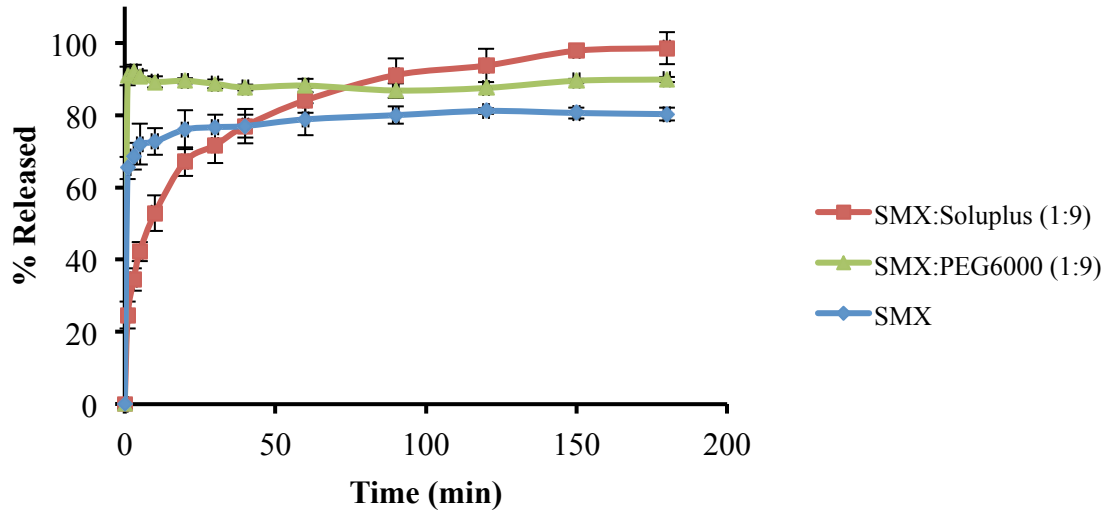

Figure 4.10.b. Sulfamethoxazole and spray dried SMX with Soluplus® or PEG 6000 in SGF (n=3). Error bars represent standard deviation.

In Figure 4.10.a., pure SMX exhibited a high dissolution rate in water and SIF. Spray dried SMX with PEG 6000 revealed the higher dissolution rate with nearly complete drug dissolution in the first 15 min of the dissolution profile. The concentration was maintained at 91% at 180 min, which suggests a slight precipitation of SMX under these conditions. SMX-Soluplus® spray dried mixture exhibits a slower release rate than does the pure SMX. Soluplus® is an amphiphlic polymer that might contribute to the dissolution with a slower rate due to its own slower dissolution rate. The drug release profile for Soluplus®, however, provided 85% release at 180 min. It is important to note that SMX-Soluplus® spray dried mixture showed a potential of continual increase in SMX concentration after 3 h period.

In Figure 4.10.b., the dissolution rate and the percentage released of pure SMX in SGF is lower than the one found in SIF. It suggests that the cationic form of SMX has a lower dissolution rate and overall solubility than the anionic form. A separate study was conducted to find the solubility of SMX in SIF and SGF proved this finding (see appendix A, Figure 3.). PEG 6000 was effective in enhancing the drug release rate and in maintaining the drug concentration over the experimental time period. SMX-Soluplus® spray dried mixture provided a complete dissolution of the drug after 150 min in SGF.

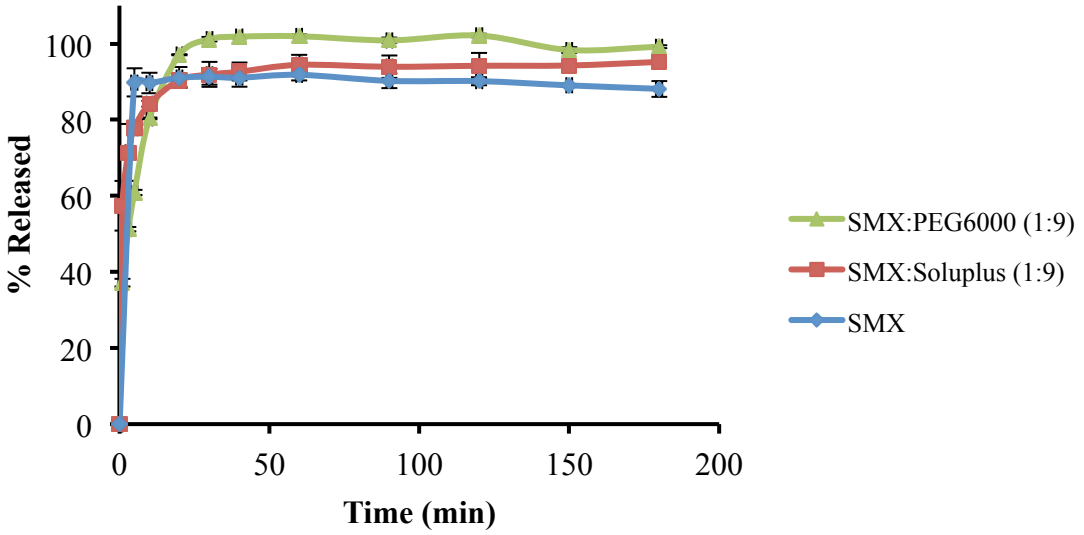

Figure 4.10.c. Sulfamethoxazole and lyophilized SMX with Soluplus® or PEG 6000 in SIF (n=3). Error bars represent standard deviation.

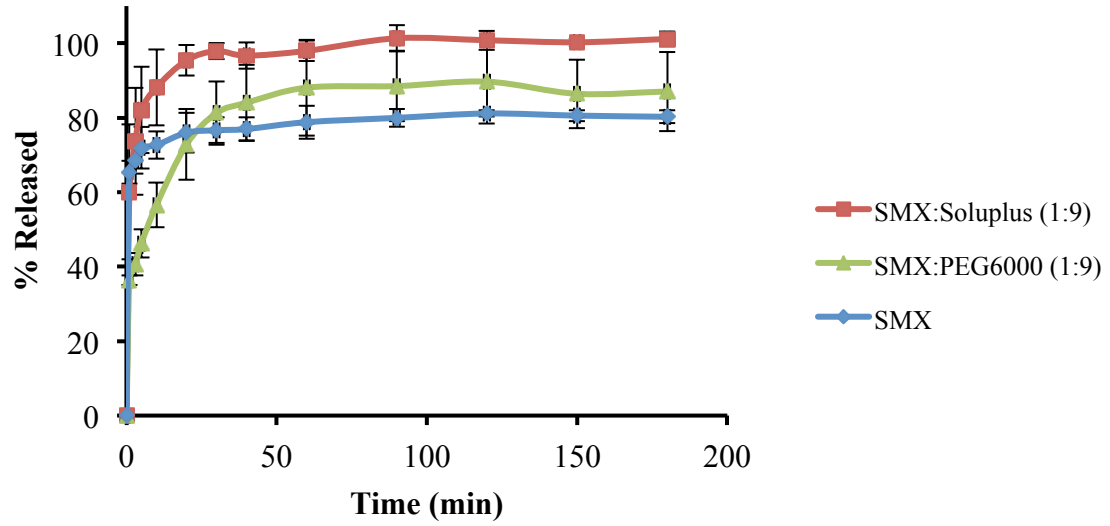

Figure 4.10.d. Sulfamethoxazole and lyophilized SMX with Soluplus® or PEG 6000 in SGF (n=3). Error bars represent standard deviation.

In Figure 4.10.c., SMX and the lyophilized mixtures exhibited high, but similar, dissolution rates. The lyophilized product showed an enhanced dissolution rate for SMX-Soluplus® mixture with similar tendency for greater improvement in the drug concentration with time. A similar trend was observed for SMX-PEG 6000 with a slight reduction in drug concentration after 120 min, which might be attributed to precipitation.

In Figure 4.10.d., The dissolution rate for lyophilized SMX-PEG 6000 in SGF is slower than in SIF, whereas, the SMX-Soluplus® mixture maintained a complete dissolution level for the last 90 min. The two polymers maintain higher drug concentrations than the pure drug can achieve.

The spray dried mixtures are more sensitive to the ionization form of SMX. It has been reported that at high Soluplus® concentrations the drug should exhibit slower dissolution rate due to the increase in the medium viscosity [38]. Furthermore, Soluplus® forms micelles [48] and it was suggested that polymers that form micelles with higher loading and lower polymer concentration in the medium should induce less interaction between the drug and the polymer and, thus, impose greater pressure on the micelle wall. Therefore, they enhance the dissolution rate [48, 49], but might exceed the capacity of the micelles to contain the poorly soluble drug. In contrast, when the PEG 6000 ratio increased, a large increase in drug dissolution rate and overall drug concentration was found. However, an optimal PEG 6000:drug ratio is likely to exist [32, 41, 50] above which PEG can no longer improve on this function . We hypothesis that the enhanced dissolution performance by the lyophilized mixtures is attributed to the higher porosity that led to improve wettability of the materials. Such improvement, also, obscured the ionization effect of the drug. PEG 6000 and Soluplus® maintained higher drug

concentration indicating a potential to maintain a supersaturated state of drug in the medium. No significant reduction in the drug concentration was observed over the experimental time-frame. SMX inherently has a fast dissolution rate at these media pH which might negate the advantages to solid dispersions using these polymers.

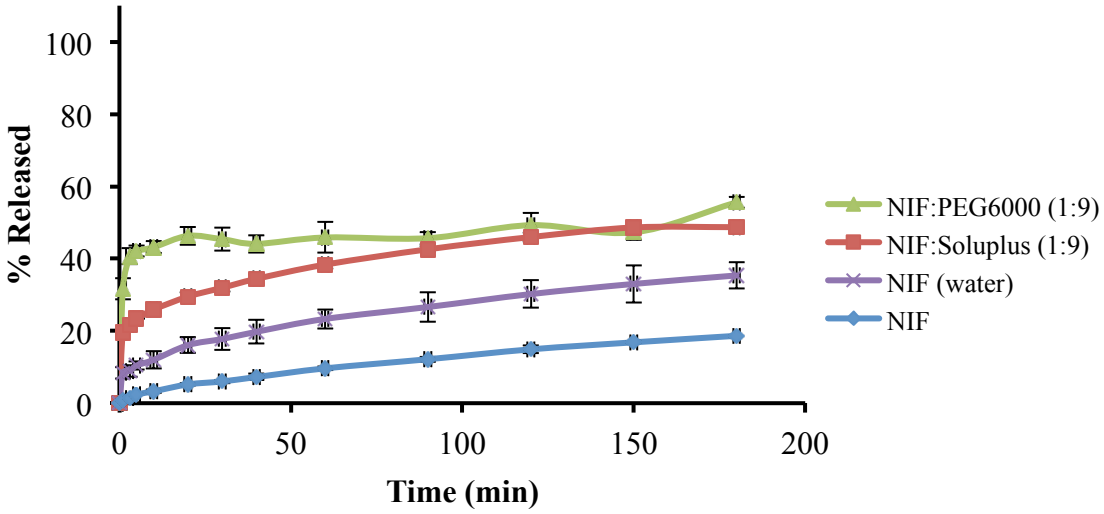

Figure 4.11.a. Nifedipine and spray dried NIF with Soluplus® or PEG 6000 in SIF (n=3). NIF alone in deionized water was added for comparison. Error bars represent standard deviation.

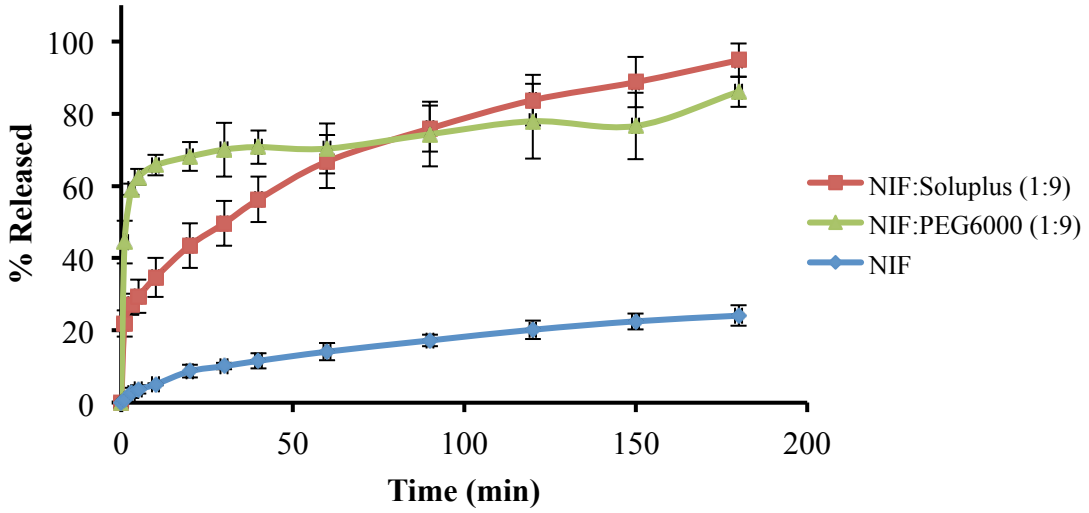

Figure 4.11.b. Nifedipine and spray dried NIF with Soluplus® or PEG 6000 in SGF (n=3). Error bars represent standard deviation.

In Figure 4.11.a., pure NIF exhibited a low dissolution rate in SIF showing only 19% drug dissolved after three hours. In water, however, NIF has an improved dissolution rate and exhibited 35% drug dissolved at 180 min. A separate solubility study was conducted for NIF in SIF, SGF, and water, that proved that water allows the highest solubility (see appendix A, Figure 4.). Spray dried NIF with PEG 6000 provided a higher dissolution rate with incomplete drug dissolution at 3 h. Such incomplete dissolution has been reported elsewhere [51]. The sample allowed more than 40% to be released rapidly in the first few minutes and then slowly achieved 56% released at 180 min. Soluplus® again contributed to a slower dissolution rate. The drug release profile for Soluplus®, however, provided 49% drug release at 180 min, but showed a burst release of 20% drug released in a few minutes.

NIF has a pKa of about 1 and is expected to be mostly ionized at a pH of 1.2. In Figure 4.11.b., the dissolution rate and the percentage dissolved at any time for pure NIF in SGF is higher than found in SIF. This simply confirms that the ionized form of NIF has a higher solubility than its unionized form. Spray dried NIF with PEG 6000 provided a higher dissolution rate with incomplete drug dissolution at 3 h in each medium. The concentration rapidly achieved greater than 60% in the first few minutes and slowly increased to reach 86% at 180 min. The drug release profile for NIF dispersion in Soluplus®, however, provided 95% release at 180 min in SGF, but showed a lower level of drug release in the first few minutes than provided by PEG 6000. It is important to note that the performance of the spray dried mixtures in the different media displayed the potential for continued release of NIF after 180 min.

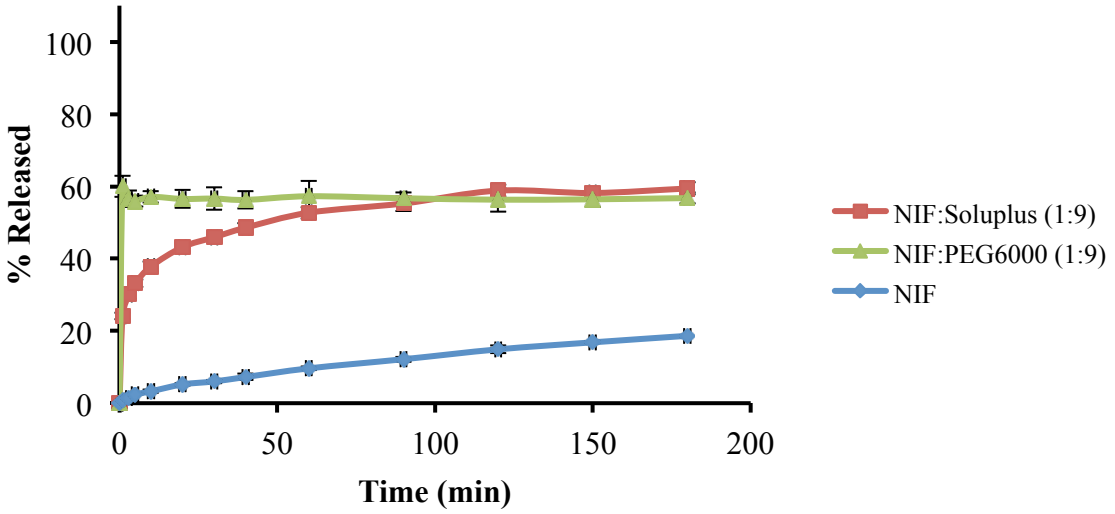

Figure 4.11.c. Nifedipine and lyophilized NIF with Soluplus® or PEG 6000 in SIF (n=3). Error bars represent standard deviation.

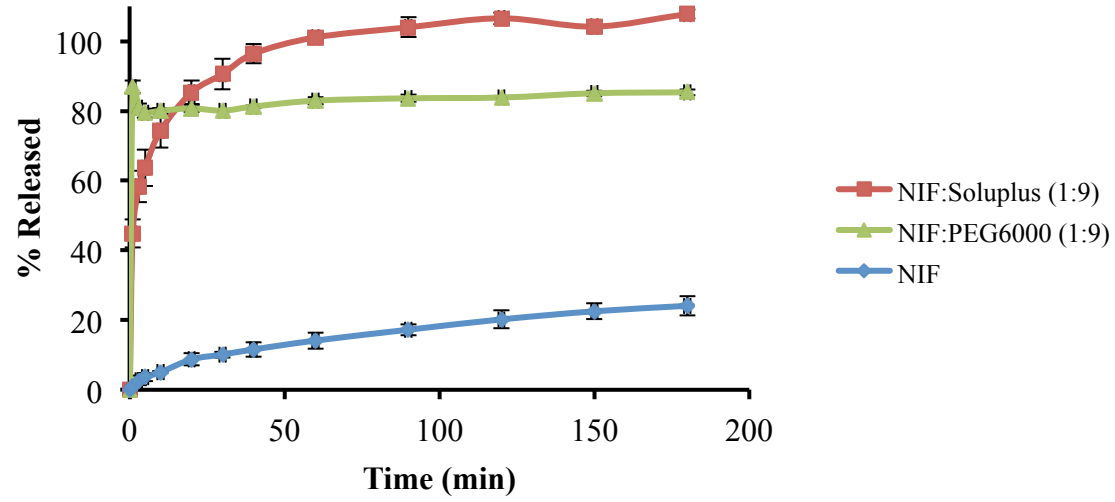

Figure 4.11.d. Nifedipine and lyophilized NIF with Soluplus® or PEG 6000 in SGF (n=3). Error bars represent standard deviation.

In Figure 4.11.c., a rapid dissolution rate was found for the lyophilized NIF dispersion in PEG 6000. However, a slight reduction in NIF concentration after the first reading might indicate precipitation of a portion of the released drug. The lyophilized product showed an enhanced dissolution rate and extent of drug released in comparison to the performance of the spray dried mixtures. A similar trend was observed for NIF dispersions in Soluplus with a slower release rate followed by an improved drug release at 180 min.

In Figure 4.11.d., the dissolution rate and the extent of drug released for lyophilized NIF-PEG 6000 in SGF is higher than found in SIF. An enhanced dissolution rate and complete dissolution for NIF-Soluplus® was observed.

Soluplus® and PEG 6000 demonstrated tremendous potential for enhancing the dissolution rate and maintaining the supersaturated state for the model drugs. That can be attributed to different reasons. The first reason is the ability of the polymers to inhibit the crystallization tendency of the amorphous materials in supersaturated states [5]. Secondly, polymer behavior in the medium can enhance the equilibrium concentration of the drug [6, 52], PEG by acting as a cosolvent and Soluplus® by micelle formation. Furthermore, others suggested that dispersed mixtures enhanced dissolution rates by improved wetting of drug due to the inherent higher dissolution rate of hydrophilic polymers [1, 19].

Both Soluplus® and PEG 6000 showed an initial burst release of drug, which is expected from highly soluble polymers [19, 24, 53]. However, PEG 6000-drug mixtures exhibited a slight reduction in concentration which might be attributed to precipitation. As an amphiphilic polymer, Soluplus® provided a slower dissolution rate for SMX and NIF dispersions at this particular mass ratio, yet this was followed by a higher extent of drug released than observed with PEG 6000 dispersions. The ionization state of the drug will also enhance or reduce the dissolution rate and limit the equilibrium drug concentration based on its inherent characteristics. This phenomenon is demonstrated well when using NIF as a model drug. The lyophilized mixtures showed higher dissolution rates and extents of drug release than each spray dried counterpart.

4.6.6. Mathematical models for the release profiles

The kinetic models for the release profiles for different mixtures are found in tables 4.3. and 4.4. Release profiles for spray dried SMX dispersions with Soluplus® in simulated intestinal and gastric fluids are best described by the Ritger-Peppas equation. This equation utilizes n as the exponent to describe the release mechanism. The diffusion coefficient n indicates a Fickian diffusion at a value of 0.45 and case II transport at a value $\geq$ 0.89. An anomalous release mechanism is expected when $0.45 < n < 0.89$ [19, 20]. However, n with values less than 0.45 have been reported [19, 20]. The n values were found to be 0.1929 in SIF and 0.3399 in SGF, which suggests a combination of diffusion, relaxation and erosion mechanisms.

For lyophilized SMX-PEG 6000 dispersions, the n values for drug release in SIF and SGF were found to be 0.3083 and 0.2887, respectively. A complex release mechanisms is also expected based on these n values. Also, such close n values might indicate that the medium does not substantially impact the release rate. Spray dried NIF-Soluplus® mixtures were described, rather well, using the Higuchi diffusion model. On the contrary, NIF-PEG 6000 dispersed mixtures were poorly described by all the employed release models indicating a complicated release mechanism. When release data for lyophilized NIF-Soluplus® dispersions are considered, the Higuchi and Ritger-Peppas models showed the best fit. However, the n value below 0.45 indicates mixed release mechanisms. The fit of the kinetic models to the release data indicates not only dissolution, but also diffusion, erosion, and swelling during drug release. These potential mixed mechanisms exerted a considerable impact on drug release profiles.

	Zero Order		First Order		Higuchi		Hixson-Crowell		Ritger-Peppas		
Materials	R^2	K_0 (min^{-1})	R^2	K_1 (min^{-1})	R^2	K_H ($min^{-1/2}$)	R^2	K_{HC} ($min^{-1/3}$)	R^2	n	K_{RP}(min^{-n})
Spray Dried Materials											
SMX:PEG 6000 (1:9) (SIF)	-	-	-	-	-	-	-	-	-	-	-
SMX (Water)	-	-	-	-	-	-	-	-	-	-	-
SMX (SIF)	-	-	-	-	-	-	-	-	-	-	-
SMX:Soluplus® (1:9) (SIF)	0.937	0.0065 ± 0.001	0.9725	0.0167 ± 0.0016	0.9829	0.0573 ± 0.0044	0.9146	0.0110 ± 0.0013	0.9996	0.1929 ± 0.0059	0.3502 ± 0.0064
SMX:PEG 6000 (1:9) (SGF)	-	-	-	-	-	-	-	-	-	-	-
SMX (SGF)	0.8185	0.0049 ± 0.0013	0.8577	0.0171 ± 0.004	0.9224	0.0291 ± 0.0049	0.8451	0.0101 ± 0.0025	0.9712	0.0497 ± 0.005	0.654 ± 0.0064
SMX:Soluplus® (1:9) (SGF)	0.9389	0.021 ± 0.0031	0.9843	0.0422 ± 0.0031	0.9958	0.122 ± 0.0046	0.9725	0.0301 ± 0.0029	0.9992	0.3399 ± 0.006	0.2421 ± 0.0034
Lyophilized Materials											
SMX:PEG 6000 (1:9) (SIF)	0.9877	0.0594 ± 0.0066	0.9981	0.1187 ± 0.0052	0.9999	0.1924 ± 0.0009	0.9956	0.0851 ± 0.0057	0.9988	0.308 ± 0.012	0.3689 ± 0.0056
SMX:Soluplus® (1:9) (SIF)	-	-	-	-	-	-	-	-	-	-	-
SMX:PEG 6000 (1:9) (SGF)	0.9913	0.0191 ± 0.001	0.9992	0.0452 ± 0.0007	0.9875	0.1079 ± 0.007	0.9995	0.0305 ± 0.0004	0.9527	0.262 ± 0.035	0.320 ± 0.026
SMX:Soluplus® (1:9) (SGF)	-	-	-	-	-	-	-	-	-	-	-

Table 4.3. The kinetic models for dissolution of SMX or release of SMX from Soluplus® or PEG 6000 dispersions prepared using spray drying or lyophilization techniques. ± standard errors ($p < 0.05$).

	Zero Order		First Order		Higuchi		Hixson-Crowell		Ritger-Peppas		
Materials	R^2	$K_{0(min^{-1})}$	R^2	$K_{1(min^{-1})}$	R^2	$K_{H(min^{-1/2})}$	R^2	$K_{HC\ (min^{-1/3})}$	R^2	n	$K_{RP\ (min^{-n})}$
Spray Dried Materials											
NIF:PEG 6000 (1:9) (SIF)	0.6102	0.0007 ± 0.0002	0.6510	0.0013 ± 0.0003	0.6890	0.0110 ± 0.0023	0.6385	0.0009 ± 0.0002	0.7716	0.0677 ± 0.0122	0.358 ± 0.017
NIF (Water)	0.9437	0.0015 ± 0.0001	0.9632	0.0019 ± 0.001	0.9984	0.0224 ± 0.0003	0.9571	0.0015 ± 0.0001	0.9891	0.344 ± 0.014	0.0579 ± 0.0037
NIF (SIF)	0.9720	0.0010 ± 0.0001	0.9798	0.0011 ± 0.0001	0.9948	0.0145 ± 0.0003	0.9773	0.0009 ± 0.0000	0.9990	0.6084 ± 0.0091	.0080 ± 0.0003
NIF:Soluplus® (1:9) (SIF)	0.9018	0.0016 ± 0.0002	0.9318	0.0026 ± 0.0002	0.9903	0.0248 ± 0.0008	0.9225	0.0018 ± 0.0002	0.9833	0.2075 ± 0.0097	0.1663 ± 0.0068
NIF:PEG 6000 (1:9) (SGF)	0.5809	0.0063 ± 0.0027	0.6661	0.0160 ± 0.0057	0.7372	0.0468 ± 0.0140	0.6375	0.0096 ± 0.0036*	0.9679	0.213 ± 0.041	0.452 ± 0.023
NIF (SGF)	0.9316	0.0012 ± 0.0001	0.9485	0.0014 ± 0.0001	0.9978	0.0187 ± 0.0003	0.9431	0.0011 ± 0.0001	0.9970	0.511 ± 0.013	0.0173 ± 0.0010
NIF:Soluplus® (1:9) (SGF)	0.9721	0.0074 ± 0.0005	0.9962	0.0139 ± 0.0004	0.9971	0.0654 ± 0.0014	0.9914	0.0092 ± 0.0003	0.9811	0.2761 ± 0.0019	0.195 ± 0.011
Lyophilized Materials											
NIF:PEG 6000 (1:9) (SIF)	-	-	-	-	-	-	-	-	-	-	-
NIF:Soluplus® (1:9) (SIF)	0.7526	0.0017 ± 0.0003	0.8138	0.0032 ± 0.0005	0.9158	0.0271 ± 0.0026	0.7943	0.0021 ± 0.0003	0.9901	0.1695 ± 0.0060	0.2553 ± 0.0064
NIF:PEG 6000 (1:9) (SGF)	-	-	-	-	-	-	-	-	-	-	-
NIF:Soluplus® (1:9) (SGF)	0.9163	0.0304 ± 0.0065	0.9719	0.0812 ± 0.0098	0.9818	0.134 ± 0.028	0.9567	0.0479 ± 0.0072	0.9944	0.218 ± 0.017*	0.4521 ± 0.0097

Table 4.4. The kinetic models for dissolution of SMX or release of SMX from Soluplus® or PEG 6000 dispersions prepared using spray drying or lyophilization techniques. ± standard errors ($p < 0.05$). * For ($p > 0.05$).

	Spray dried materials							
Reference material	SMX(SIF)		SMX(SGF)		SMX:Soluplus® (1:9) (SIF)	SMX:PEG6000 (1:9) (SIF)	SMX:PEG6000 (1:9) (SIF)	SMX:Soluplus® (1:9) (SIF)
	SMX:PEG6000 (1:9) (SIF)	SMX:Soluplus® (1:9) (SIF)	SMX:PEG6000 (1:9) (SGF)	SMX:Soluplus® (1:9) (SGF)	SMX:PEG6000 (1:9) (SGF)	SMX:Soluplus® (1:9) (SGF)	SMX:PEG6000 (1:9) (SGF)	SMX:Soluplus® (1:9) (SGF)
f_2	72.87	31.85	24.55	34.18	32.84	22.37	66.10	51.21
	Lyophilized Materials							
	SMX(SIF)		SMX(SGF)		SMX:Soluplus® (1:9) (SIF)	SMX:PEG6000 (1:9) (SIF)	SMX:PEG6000 (1:9) (SIF)	SMX:Soluplus® (1:9) (SIF)
	SMX:PEG6000 (1:9) (SIF)	SMX:Soluplus® (1:9) (SIF)	SMX:PEG6000 (1:9) (SGF)	SMX:Soluplus® (1:9) (SGF)	SMX:PEG6000 (1:9) (SGF)	SMX:Soluplus® (1:9) (SGF)	SMX:PEG6000 (1:9) (SGF)	SMX:Soluplus® (1:9) (SGF)
f_2	43.93	63.07	37.88	40.22	37.26	46.76	40.05	64.38

Table 4.5. The release profile comparisons for SMX-polymer mixtures.

	Spray dried materials							
Reference material	NIF(SIF)		NIF(SGF)		NIF:Soluplus® (1:9) (SIF)	NIF:PEG6000 (1:9) (SIF)	NIF:PEG6000 (1:9) (SIF)	NIF:Soluplus® (1:9) (SIF)
	NIF:PEG6000 (1:9) (SIF)	NIF:Soluplus® (1:9) (SIF)	NIF:PEG6000 (1:9) (SGF)	NIF:Soluplus® (1:9) (SGF)	NIF:PEG6000 (1:9) (SGF)	NIF:Soluplus® (1:9) (SGF)	NIF:PEG6000 (1:9) (SGF)	NIF:Soluplus® (1:9) (SGF)
f_2	21.76	28.93	12.11	16.21	22.85	31.68	30.47	29.12
	Lyophilized Materials							
	NIF(SIF)		NIF(SGF)		NIF:Soluplus® (1:9) (SIF)	NIF:PEG6000 (1:9) (SIF)	NIF:PEG6000 (1:9) (SIF)	NIF:Soluplus® (1:9) (SIF)
	NIF:PEG6000 (1:9) (SIF)	NIF:Soluplus® (1:9) (SIF)	NIF:PEG6000 (1:9) (SGF)	NIF:Soluplus® (1:9) (SGF)	NIF:PEG6000 (1:9) (SGF)	NIF:Soluplus® (1:9) (SGF)	NIF:PEG6000 (1:9) (SGF)	NIF:Soluplus® (1:9) (SGF)
f_2	15.46	21.05	7.41	5.97	20.70	22.03	29.47	18.91

Table 4.6. The release profile comparisons for NIF-polymer mixtures.

4.6.7. Comparison of release profiles

Comparison between release profiles can be executed using analysis of variance (ANOVA) between two or multiple data points (MANOVA). However, the f_2, similarity test, is usually preferable when comparing the entire dissolution release profile. Furthermore, the similarity test has been adapted by the FDA for just this sort of in vitro dissolution release profile comparison [21, 54]. One of the disadvantages of this method is the dependency on the dissolution profile length. It might show similarity at certain time points and dissimilarity at different time points between the same two dissolution profiles. However, the values will be hovering around 50 [55], the cut-off for similarity of the two profiles.

To elucidate the impact of the selected polymer, preparation techniques, and the chosen medium the dissolution profiles were compared using this test.

The spray dried SMX dispersion with Soluplus® or PEG 6000 exhibited a similarity in their dissolution profiles when placed in either SIF or SGF, f_2 = 66.10 and 51.21, respectively. However, only the lyophilized SMX-Soluplus® dispersion showed similarity (f_2 = 64.38) in the two release media. On the other hand, NIF dispersions did not show any similarity across the media or techniques. This suggests that the similarity that was found for SMX mixture is due to the close resemblance of SMX behavior to that of its dispersions. This is not surprising in light of the solubility of SMX under the release conditions.

4.7. Conclusions

NIF and SMX solid dispersions were successfully prepared by spray drying and lyophilization using Soluplus® and PEG 6000. Thermal analyses showed no melting endotherm indicating the absent of crystallinity at higher polymer concentrations. Drugs dispersed in Soluplus® demonstrated a spherical shape when spray dried.

The drugs dissolution rates were significantly enhanced. However, NIF dissolution rate was improved to a greater extent due to its inherent low solubility in the two release media. Dispersions with PEG 6000 had a faster dissolution rate due to its hydrophilic nature. However, Soluplus® exhibited a tendency to maintain higher drug concentrations over time. The dissolution profiles of the different mixtures proved to be dissimilar across the preparation techniques and/or media.

4.8. References

1. Fouad EA, El-Badry M, Mahrous GM, Alanazi FK, Neau SH, Alsarra IA. The use of spray-drying to enhance celecoxib solubility. Drug Dev Ind Pharm. 2011. 37(12): 1463-72

2. Al-Obaidi H, Buckton G. Evaluation of griseofulvin binary and ternary solid dispersions with HPMCAS. AAPS PharmSciTech. 2009. 10(4): 1172-7

3. Ning X, Sun J, Han X, Wu Y, Yan Z, Han J, He Z. Strategies to improve dissolution and oral absorption of glimepiride tablets: solid dispersion versus micronization techniques. Drug Dev In Pharm. 2011. 37(6): 727-36

4. Emara LH, Badr RM, Elbary AA. Improving the dissolution and bioavailability of nifedipine using solid dispersions and solubilizers. Drug Dev Ind Pharm. 2002. 28(7): 795-807

5. Tanno F, Nishiyama Y, Kokubo H, Obara S. Evaluation of Hypromellose Acetate Succinate (HPMCAS) as a Carrier in Solid Dispersions. Drug Development and Industrial Pharmacy. 2004. 30(1): 9-17

6. Konno H, Handa T, Alonzo DE, Taylor LS. Effect of polymer type on the dissolution profile of amorphous solid dispersions containing felodipine. Eur J Pharm Biopharm. 2008. 70(2): 493-9

7. Lakshman JP, Cao Y, Kowalski J, Serajuddin AT. Application of melt extrusion in the development of a physically and chemically stable high-energy amorphous solid dispersion of a poorly water-soluble drug. Mol Pharm. 2008. 5(6): 994-1002

8. Weuts I, Van Dycke F, Voorspoels J, De Cort S, Stokbroekx S, Leemans R, Brewster ME, Xu D, Segmuller B, Turner YT, Roberts CJ, Davies MC, Qi S, Craig DQ, Reading M. Physicochemical properties of the amorphous drug, cast films, and spray dried powders to predict formulation probability of success for solid dispersions: Etravirine. J Pharm Sci. 2011. 100(1): 260-74

9. Mahieu A, Willart J-F, Dudognon E, Danède F, Descamps M. A new protocol to determine the solubility of drugs into polymer matrixes. Mol Pharm. 2012. 10(2): 560-6

10. Marsac PJ, Shamblin SL, Taylor LS. Theoretical and practical approaches for prediction of drug–polymer miscibility and solubility. Pharm Res. 2006. 23(10): 2417-26

11. Marsac PJ, Li T, Taylor LS. Estimation of drug-polymer miscibility and solubility in amorphous solid dispersions using experimentally determined interaction parameters. Pharm Res. 2009. 26(1): 139-51

12. Özdemir N, Erkin J. Enhancement of dissolution rate and bioavailability of sulfamethoxazole by complexation with β-cyclodextrin. Drug Dev Ind Pharm. 2012. 38(3): 331-40

13. Baird JA, Van Eerdenbrugh B, Taylor LS. A classification system to assess the crystallization tendency of organic molecules from undercooled melts. J Pharm Sci. 2010. 99(9): 3787-806

14. Mahlin D, Bergström CA. Early drug development predictions of glass-forming ability and physical stability of drugs. E J Pharm Sci. 2013. 49(2): 323-32

15. Xu M, Zhang C, Luo Y, Xu L, Tao X, Wang Y, He H, Tang X. Application and functional characterization of POVACOAT, a hydrophilic co-polymer poly(vinyl alcohol/acrylic acid/methyl methacrylate) as a hot-melt extrusion carrier. Drug Dev Ind Pharm. 2014. 40((1)): 126-35

16. Zidan AS, Rahman Z, Sayeed V, Raw A, Yu L, Khan MA. Crystallinity evaluation of tacrolimus solid dispersions by chemometric analysis. Int J Pharm. 2012. 423(2): 341-50

17. Sathigari SK, Radhakrishnan VK, Davis VA, Parsons DL, Babu RJ. Amorphous-state characterization of efavirenz--polymer hot-melt extrusion systems for dissolution enhancement. J Pharm Sci. 2012. 101(9): 3456-64

18. Tao T, Zhao Y, Wu J, Zhou B. Preparation and evaluation of itraconazole dihydrochloride for the solubility and dissolution rate enhancement. Int J Pharm. 2009. 367(1-2): 109-14

19. Khan S, Batchelor H, Hanson P, Saleem IY, Perrie Y, Mohammed AR. Dissolution rate enhancement, in vitro evaluation and investigation of drug release kinetics of chloramphenicol and sulphamethoxazole solid dispersions. Drug Dev Ind Pharm. 2012.

20. Shoaib MH, Tazeen J, Merchant HA, Yousuf RI. Evaluation of drug release kinetics from ibuprofen matrix tablets using HPMC. Pak J Pharm Sci. 2006. 19(2): 119-24

21. Costa P, Sousa Lobo JM. Modeling and comparison of dissolution profiles. European Journal of Pharmaceutical Sciences. 2001. 13(2): 123-33

22. Flanner JMaH. Mathematical comparison of curves with an emphasis on in-vitro dissolution profiles. Pharm Tech. 1996. 20(6): 64-74

23. Huang J, Wigent RJ, Bentzley CM, Schwartz JB. Nifedipine solid dispersion in microparticles of ammonio methacrylate copolymer and ethylcellulose binary blend for controlled drug delivery: Effect of drug loading on release kinetics. Int J Pharm. 2006. 319(1): 44-54

24. Nagy ZK, Balogh A, Vajna B, Farkas A, Patyi G, Kramarics A, Marosi G. Comparison of electrospun and extruded Soluplus(R)-based solid dosage forms of improved dissolution. J Pharm Sci. 2012. 101(1): 322-32

25. Brostow, W., Chiu, R., Kalogeras, I. M., & Vassilikou-Dova, A. (2008). Prediction of glass transition temperatures: binary blends and copolymers. Materials Letters, 62(17), 3152-3155.

26. Forster AH, J. Tucker, I. Rades. T. The potential of small-scale fusion experiments and the gordon-taylor equation to predict the suitability of drug/polymer blends for melt extrusion. Drug Dev Ind Pharm. 2001. 27(6): 549-60

27. Vlassios Andronis MY, ans George Zografi. Effect of sorbed water on the crystalliztion of indomethacin from the amorphous state. J Pharm Sci. 1996. 86(3): 346-51

28. Grisedale LC, Belton PS, Jamieson MJ, Barker SA, Craig DQ. An investigation into water interactions with amorphous and milled salbutamol sulphate: the development of predictive models for uptake and recrystallization. Int J Pharm. 2012. 422(1-2): 220-8

29. Abdelwahed W, Degobert G, Stainmesse S, Fessi H. Freeze-drying of nanoparticles: formulation, process and storage considerations. Adv Drug Deliv Rev. 2006. 58(15): 1688-713

30. Maa YF, Nguyen PA, Andya JD, Dasovich N, Sweeney TD, Shire SJ, Hsu CC. Effect of spray drying and subsequent processing conditions on residual moisture content and physical/biochemical stability of protein inhalation powders. Pharm Res. 1998. 15(5): 768-75

31. Corrigan DO, Healy AM, Corrigan OI. The effect of spray drying solutions of polyethylene glycol (PEG) and lactose/PEG on their physicochemical properties. Int J pharm. 2002. 235(1): 193-205

32. Guyot, M., Fawaz, F., Bildet, J., Bonini, F., & Lagueny, A. M. (1995). Physicochemical characterization and dissolution of norfloxacin/cyclodextrin inclusion compounds and PEG solid dispersions.Int J Pharm., 123(1), 53-63.

33. Watson DG. Pharmaceutical Analysis. Philadelphia, PA, USA: Elsevier's Health Sciences; 2005.

34. Huang J, Wigent RJ, Schwartz JB. Drug-polymer interaction and its significance on the physical stability of nifedipine amorphous dispersion in microparticles of an ammonio methacrylate copolymer and ethylcellulose binary blend. J Pharm Sci. 2008. 97(1): 251-62

35. Takasuka M, Nakai H. IR and Raman spectral and X-ray structural studies of polymorphic forms of sulfamethoxazole. Vibrational Spectroscopy. 2001. 25(2): 197-204

36. Vijaya Chamundeeswari SP, James Jebaseelan Samuel E, Sundaraganesan N. Molecular structure, vibrational spectra, NMR and UV spectral analysis of sulfamethoxazole. Spectrochim Acta A Mol Biomol Spectrosc. 2014. 118: 1-10

37. Chan KLA, Fleming OS, Kazarian SG, Vassou D, Chryssikos GD, Gionis V. Polymorphism and devitrification of nifedipine under controlled humidity: a combined FT-Raman, IR and Raman microscopic investigation. Journal of Raman Spectroscopy. 2004. 35(5): 353-9

38. Homayouni A, Sadeghi F, Varshosaz J, Afrasiabi Garekani H, Nokhodchi A. Promising dissolution enhancement effect of soluplus on crystallized celecoxib obtained through antisolvent precipitation and high pressure homogenization techniques. Colloids Surf B Biointerfaces. 2014. 122: 591-600

39. Shamma RN, Basha M. Soluplus®: A novel polymeric solubilizer for optimization of Carvedilol solid dispersions: Formulation design and effect of method of preparation. P Tech. 2013. 237: 406-14

40. Vijaya Kumar SG, Mishra DN. Preparation, Characterization and In vitro Dissolution Studies of Solid Dispersion of Meloxicam with PEG 60001). Yakugaku Zasshi. 2006. 126(8): 657-64

41. Ruan L-P, Yu B-Y, Fu G-M, Zhu D-n. Improving the solubility of ampelopsin by solid dispersions and inclusion complexes. J pharm Bio. 2005. 38(3): 457-64

42. Sawhney AS, Pathak CP, Hubbell JA. Bioerodible hydrogels based on photopolymerized poly (ethylene glycol)-co-poly (. alpha.-hydroxy acid) diacrylate macromers. Macromolecules. 1993. 26(4): 581-7

43. Van den Mooter G, Augustijns P, Blaton N, Kinget R. Physico-chemical characterization of solid dispersions of temazepam with polyethylene glycol 6000 and PVP K30. Int J pharm. 1998. 164(1): 67-80

44. Gokturk S, Caliskan E, Talman RY, Var U. A study on solubilization of poorly soluble drugs by cyclodextrins and micelles: complexation and binding characteristics of sulfamethoxazole and trimethoprim. Scientific World J. 2012. 2012: 718791

45. Lucida H, Parkin J, Sunderland V. Kinetic study of the reaction of sulfamethoxazole and glucose under acidic conditions: I. Effect of pH and temperature. International journal of pharmaceutics. 2000. 202(1): 47-62

46. Zhang X, Anderson JW, Fedida D. Characterization of nifedipine block of the human heart delayed rectifier, hKv1. 5. Journal of Pharmacology and Experimental Therapeutics. 1997. 281(3): 1247-56

47. Zendelovska D, Simeska S, Sibinovska O, Kostova E, Miloševska K, Jakovski K, Jovanovska E, Kikerkov I, Trojačanec J, Zafirov D. Development of an HPLC method for the determination of nifedipine in human plasma by solid-phase extraction. Journal of Chromatography B. 2006. 839(1–2): 85-8

48. Yu H, Xia D, Zhu Q, Zhu C, Chen D, Gan Y. Supersaturated polymeric micelles for oral cyclosporine A delivery. European Journal of Pharmaceutics and Biopharmaceutics. 2013. 85(3, Part B): 1325-36

49. Huh KM, Lee SC, Cho YW, Lee J, Jeong JH, Park K. Hydrotropic polymer micelle system for delivery of paclitaxel. Journal of Controlled Release. 2005. 101(1): 59-68

50. Save T, Venkitachalam P. Studies on solid dispersions of nifedipine. Drug Dev In Pharm. 1992. 18(15): 1663-79

51. Hecq J, Deleers M, Fanara D, Vranckx H, Amighi K. Preparation and characterization of nanocrystals for solubility and dissolution rate enhancement of nifedipine. Int J Pharm. 2005. 299(1-2): 167-77

52. Loftsson T, Fri∂riksdóttir H, Gu∂mundsdóttir TK. The effect of water-soluble polymers on aqueous solubility of drugs. International Journal of Pharmaceutics. 1996. 127(2): 293-6

53. Karavas E, Georgarakis E, Sigalas MP, Avgoustakis K, Bikiaris D. Investigation of the release mechanism of a sparingly water-soluble drug from solid dispersions in hydrophilic carriers based on physical state of drug, particle size distribution and drug-polymer interactions. Eur J Pharm Biopharm. 2007. 66(3): 334-47

54. Polli JE, Rekhi GS, Augsburger LL, Shah VP. Methods to compare dissolution profiles and a rationale for wide dissolution specifications for metoprolol tartrate tablets. Journal of pharmaceutical sciences. 1997. 86(6): 690-700

55. Pillay V, Fassihi R. Evaluation and comparison of dissolution data derived from different modified release dosage forms: an alternative method. Journal of Controlled Release. 1998. 55(1): 45-55

5. Appendix A

Chapter One: Supplemental information

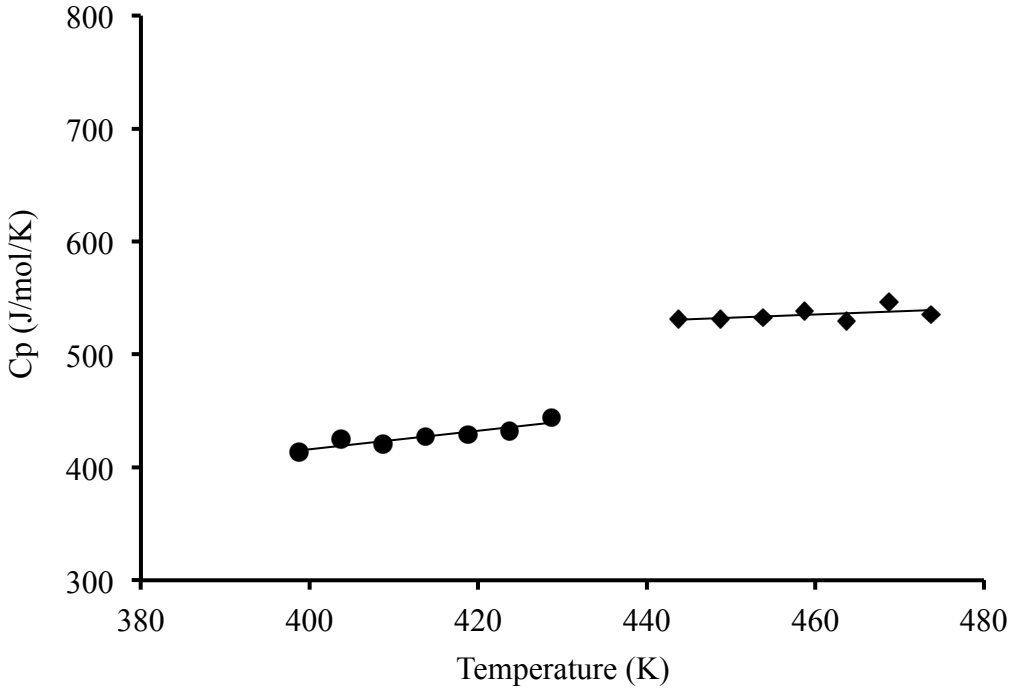

Figure 5.1. Heat capacity for SMX as a function of temperature. The area of discontinuity represents sulfamethoxazole melting temperature.

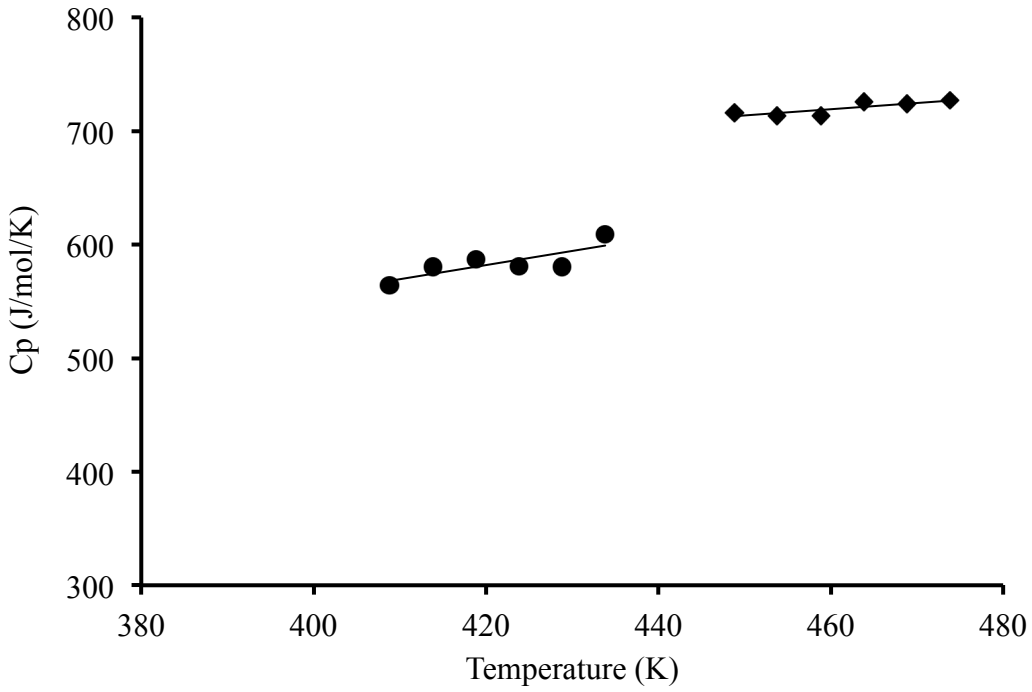

Figure 5.2. Heat capacity for NIF as a function of temperature. The area of discontinuity represents nifedipine melting temperature.

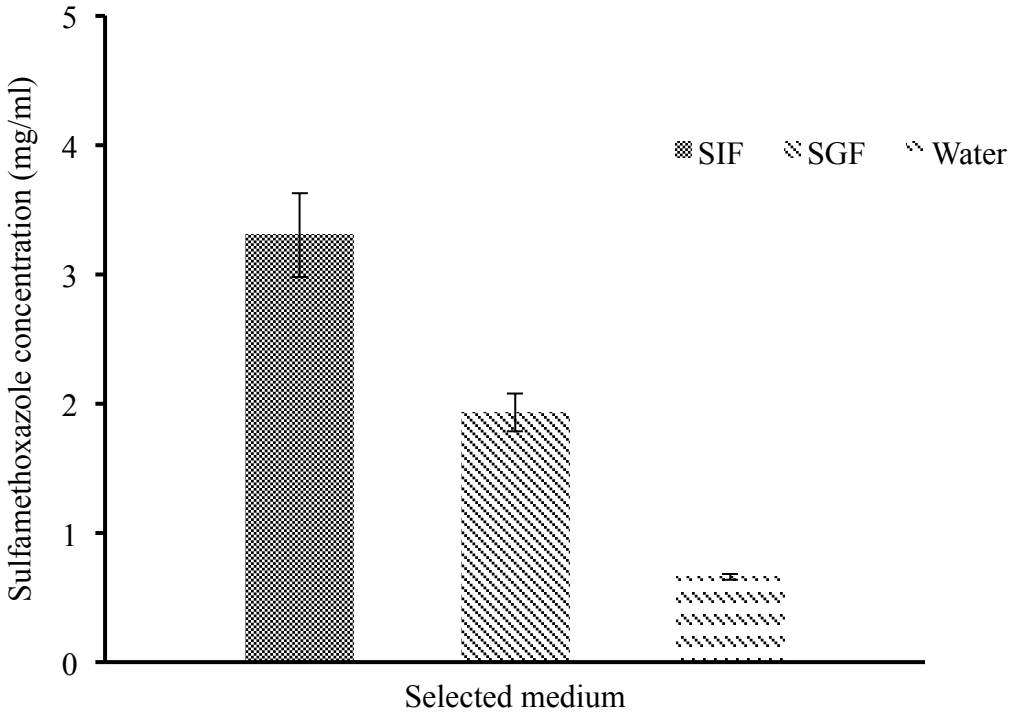

Figure 5.3. Experimental 37 ^{o}C equilibrium solubility of sulfamethoxazole in simulated gastric fluid, intestinal fluid, and water.

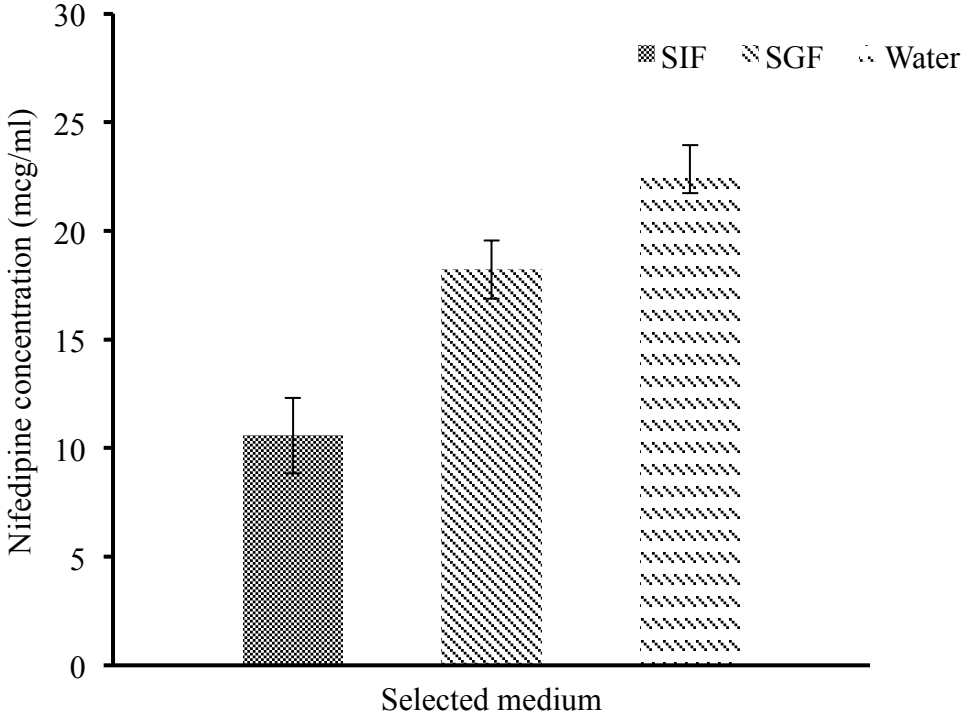

Figure 5.4. Experimental 37 ^{o}C equilibrium solubility of nifedipine in simulated gastric fluid, intestinal fluid, and water.

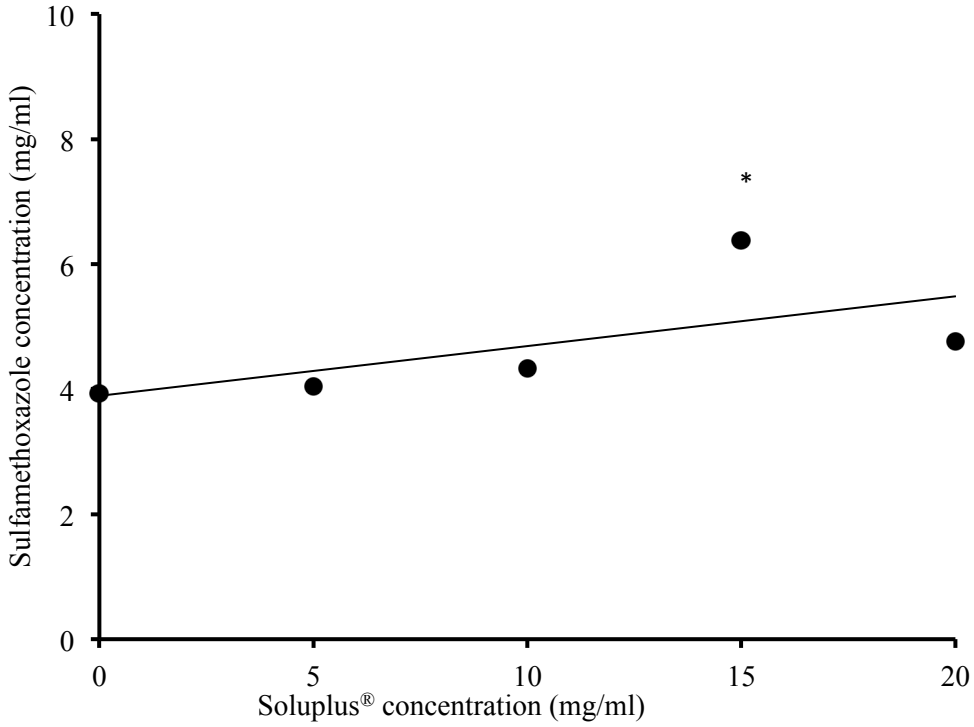

Figure 5.5. Experimental 37 ^{o}C concentration of sulfamethoxazole in simulated intestinal fluids in the presence of different Soluplus® concentrations.

*This data point was not used in the estimation of the association constant.

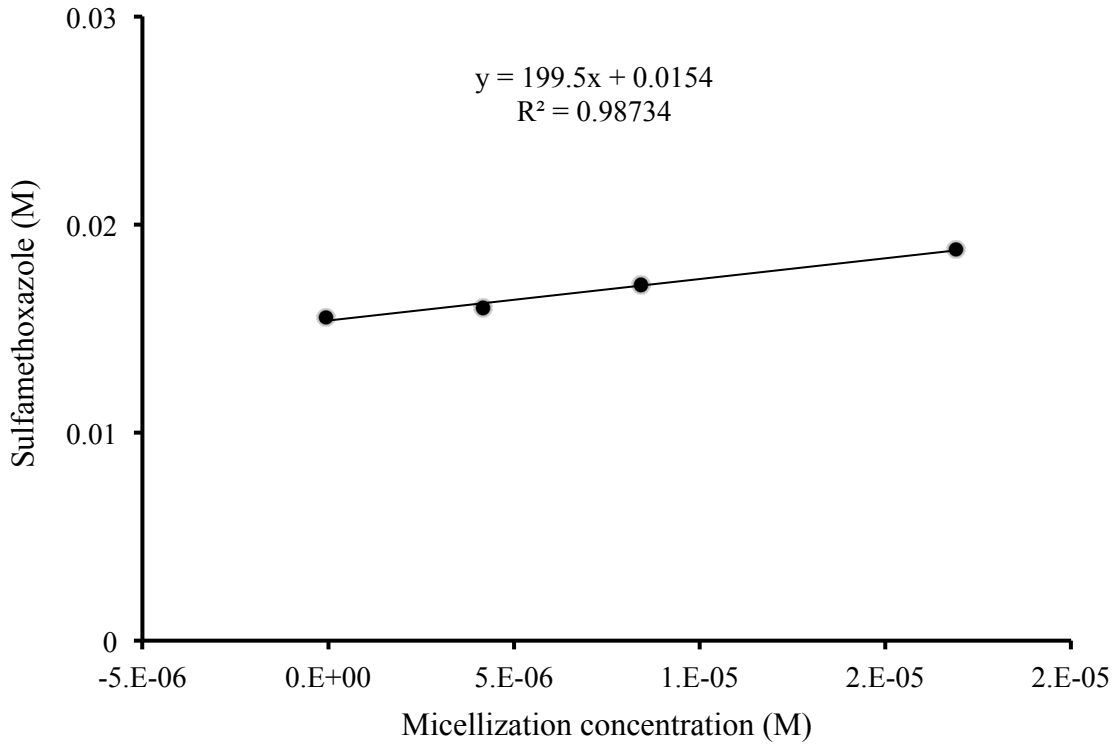

Figure 5.6. Molar solubilization capacity of Soluplus® with sulfamethoxazole in simulated intestinal fluids.

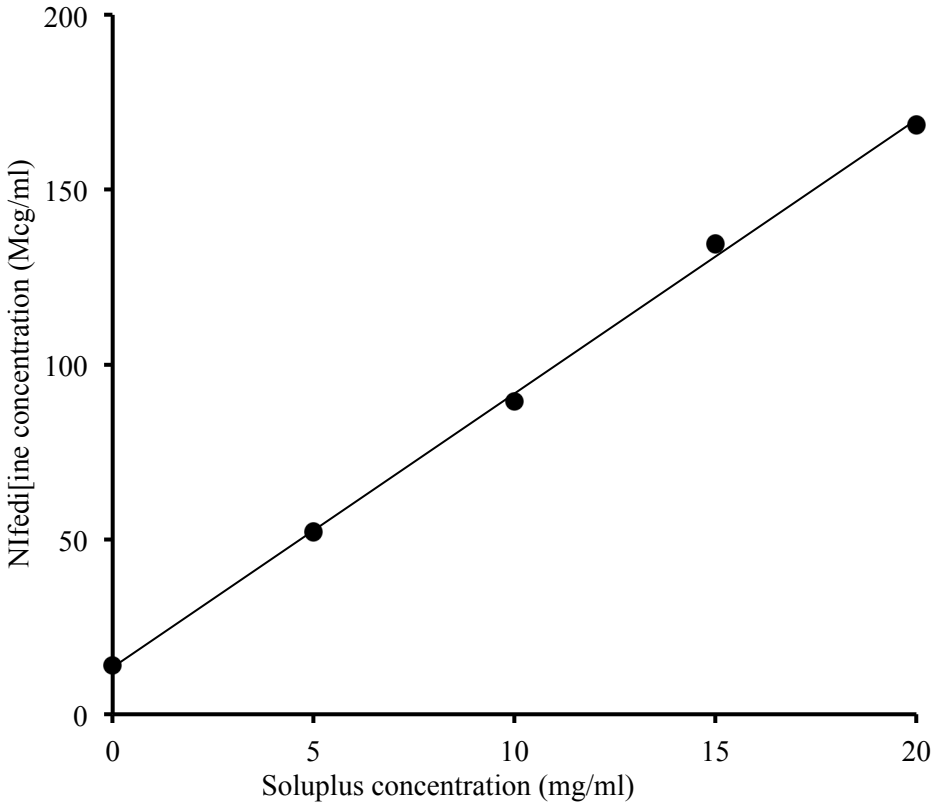

Figure 5.7. Experimental 37 ^{o}C concentration of nifedipine in simulated intestinal fluids in the presence of different Soluplus® concentrations.

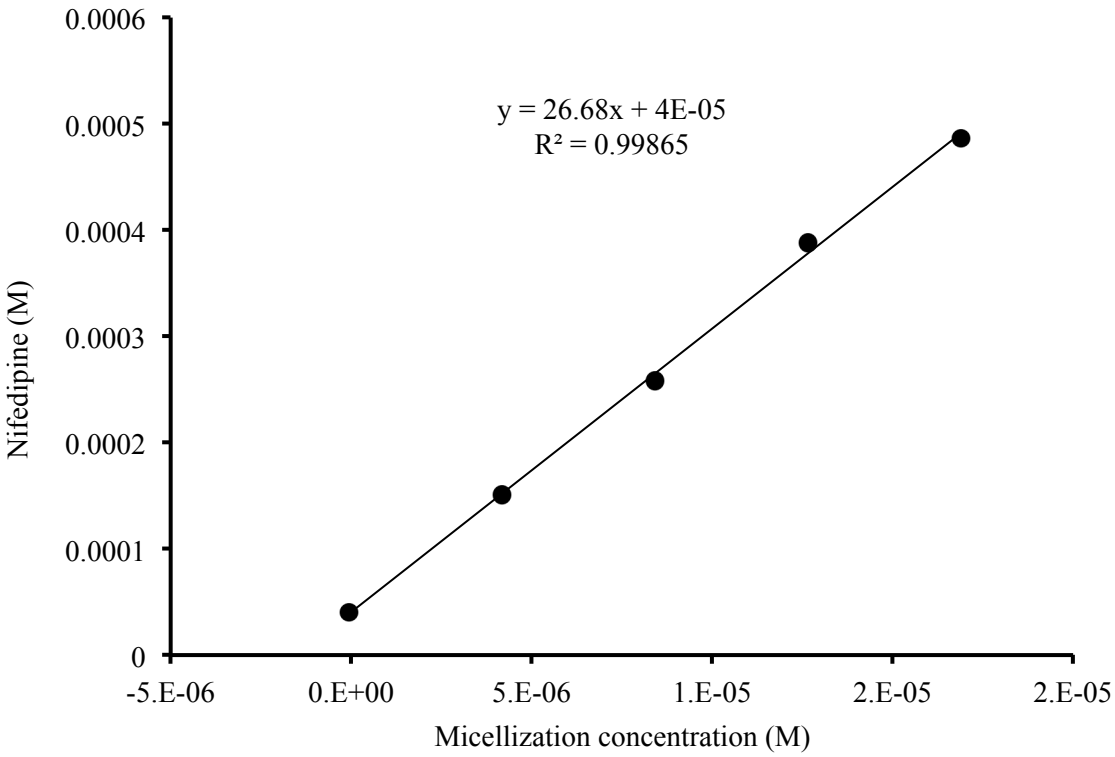

Figure 5.8. Molar solubilization capacity of Soluplus® with nifedipine in simulated intestinal fluids.

6. Appendix B

Chapter Two: Supplemental information

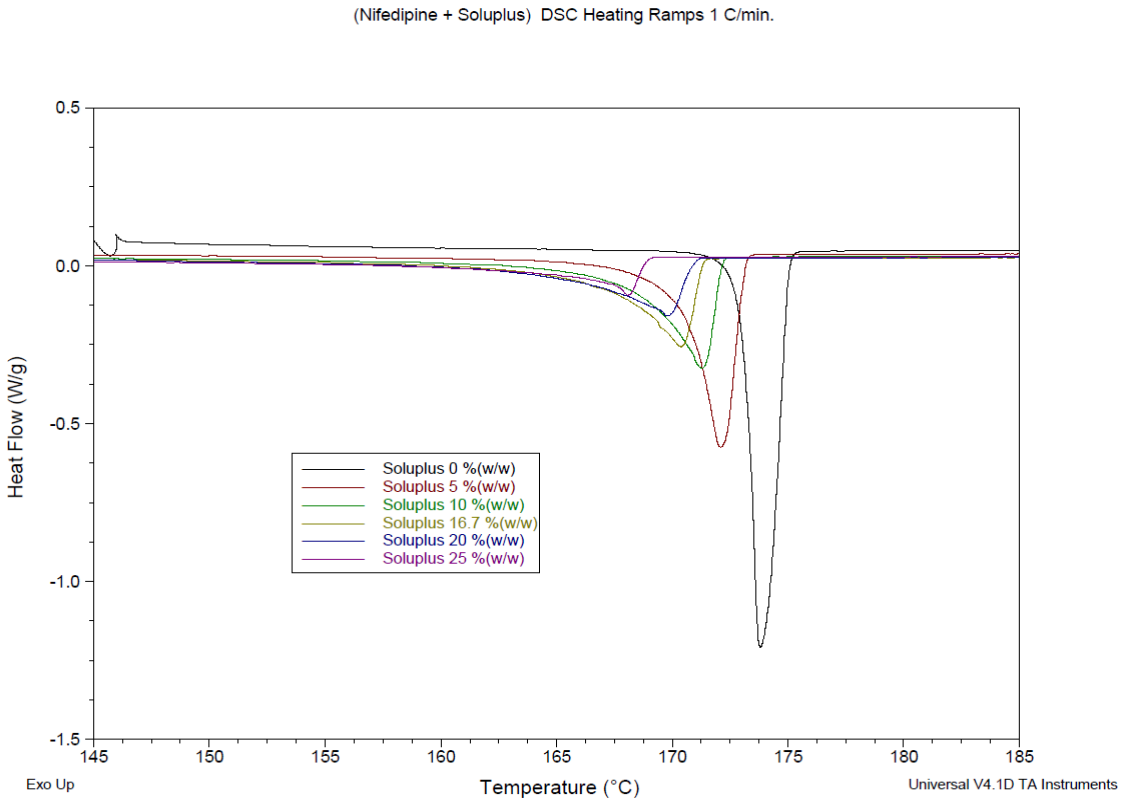

Figure 6.1. DSC thermograms of the melting endotherm for nifedipine mixtures with 0, 5, 10, 16.7, 20, and 25 % w/w Soluplus®.

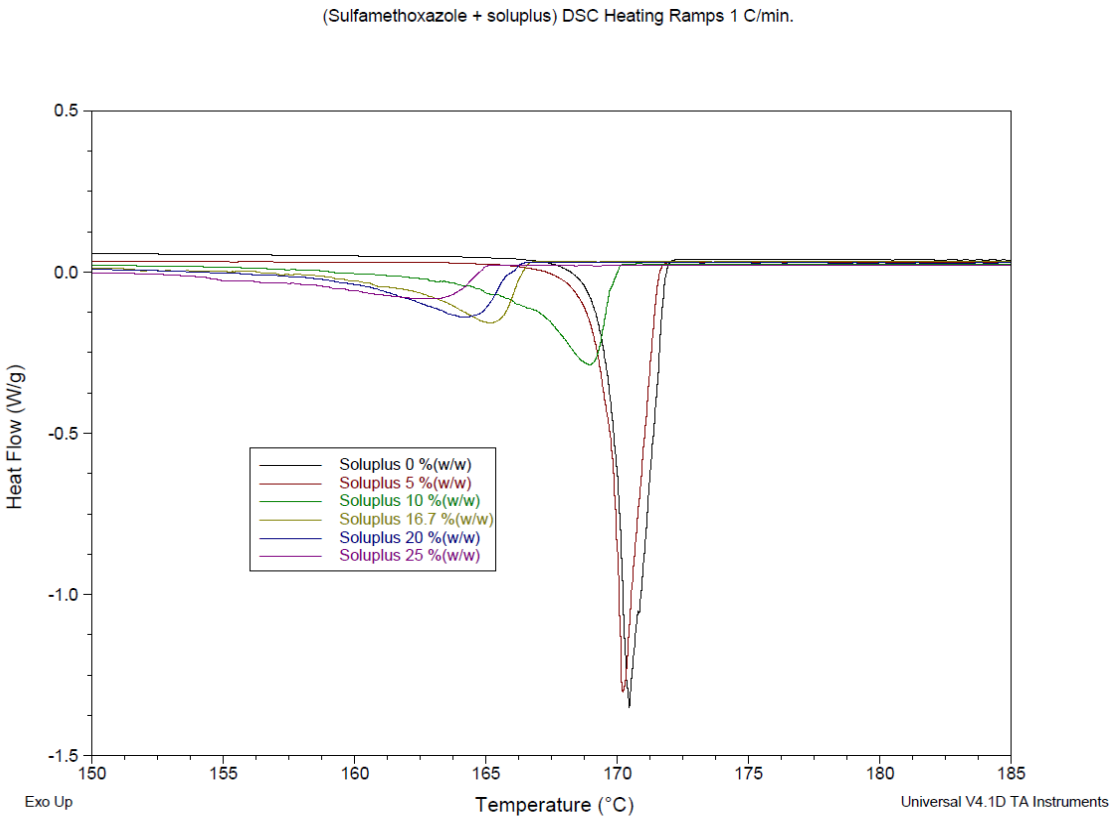

Figure 6.2. DSC thermograms of the melting endotherm for sulfamehtoxazole mixtures with 0, 5, 10, 16.7, 20, and 25 % w/w Soluplus®.

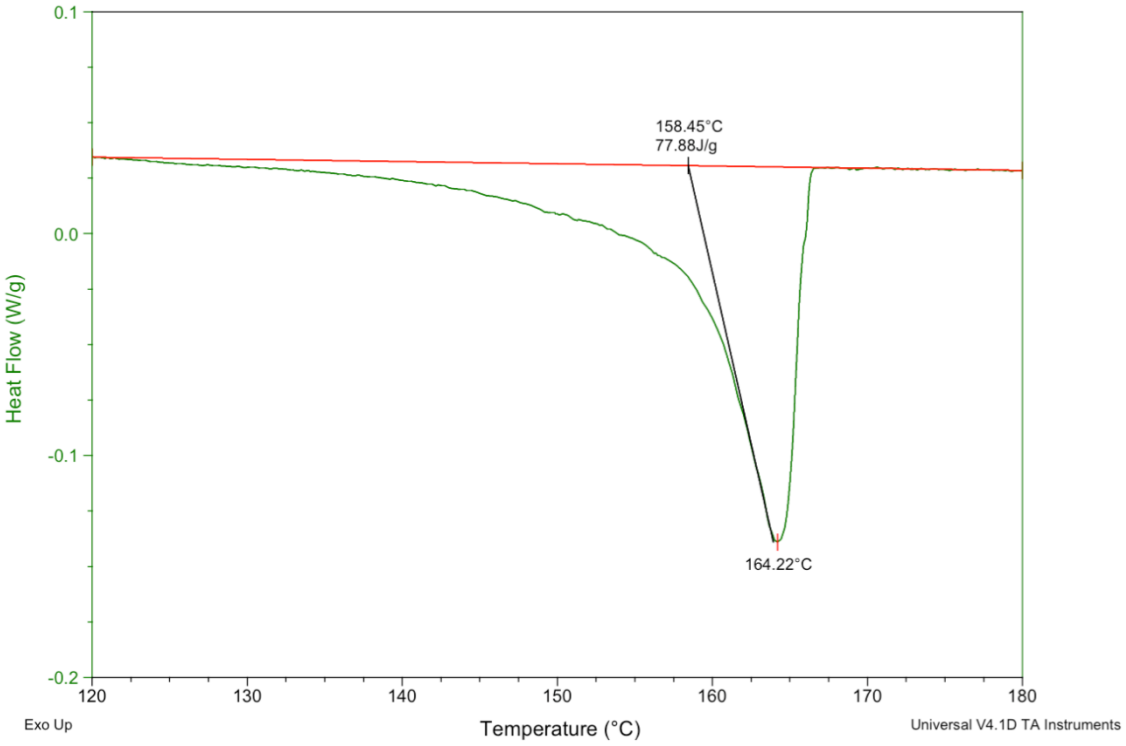

Figure 6.3. DSC thermogram representing the onset of melting at 20% w/w for SMX-Soluplus® mixture.

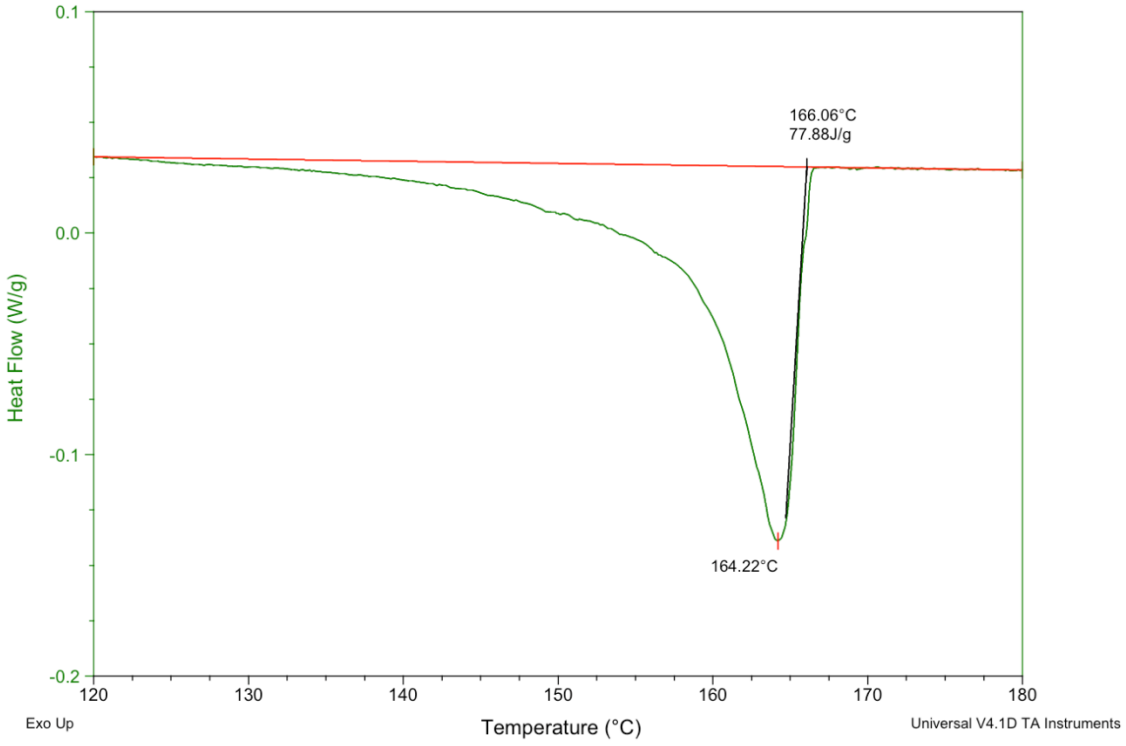

Figure 6.4. DSC thermogram representing the T_{end} of melting at 20% w/w for SMX-Soluplus® mixture.

Sulfamethoxazole + Soluplus Experiment									
Temperature readings (°C)									
Actual Amounts	% W/W	1st Run	2nd Run	3rd Run	4th Run	5th Run	Average (°C)	Average (K)	Standard deviation
SMX 5mg	0%	170.22	169.78	170.29			170.1	443.2	0.2764
SMX 38 mg+2 mg Soluplus®	5.0%	167.16	169.69	167.94			168.3	441.4	1.295
SMX 45 mg+5 mg Soluplus®	10.0%	167.1	165.94	167.04			166.7	439.8	0.6531
SMX 50 mg+10 mg Soluplus®	16.7%	162.4	165.68	168.63	160.65	157.48	163.0	436.1	4.337
SMX 40 mg+10 mg Soluplus®	20.0%	156.35	155.24	158.65			156.7	429.9	1.739
SMX 30 mg+10 mg Soluplus®	25.0%	142.26	160.08	153.57			152.0	425.1	9.017

Table 6.1. DSC onset of melting endotherm for SMX-Soluplus® mixtures.

Nifedipine + Soluplus Experiments										
Temperature readings (°C)										
Actual Amounts	% W/W	1st Run	2nd Run	3rd Run	4th Run	5th Run	6th Run	Average (°C)	Average (K)	Standard Deviation
NIF 5mg	0%	173.68	173.6	173.93				173.7	446.9	0.1721
NIF 38 mg+2 mg Soluplus®	5.0%	170.29	170.46	172.45	171.92	171.32		171.3	444.4	0.9263
NIF 45 mg+5 mg Soluplus®	10.0%	168.64	169.66	170.09	170.94	172.59	170.76	170.4	443.6	1.337
NIF 50 mg+10 mg Soluplus®	16.7%	169.41	171.57	170.37	166.53	166.92	166.29	168.5	441.7	2.236
NIF 40 mg+10 mg Soluplus®	20.0%	168.08	168.01	165.71				167.3	440.4	1.348
NIF 30 mg+10 mg Soluplus®	25.0%	166.04	162.28	164.16				164.2	437.3	1.880

Table 6.2. DSC onset of melting endotherm for NIF-Soluplus® mixtures.

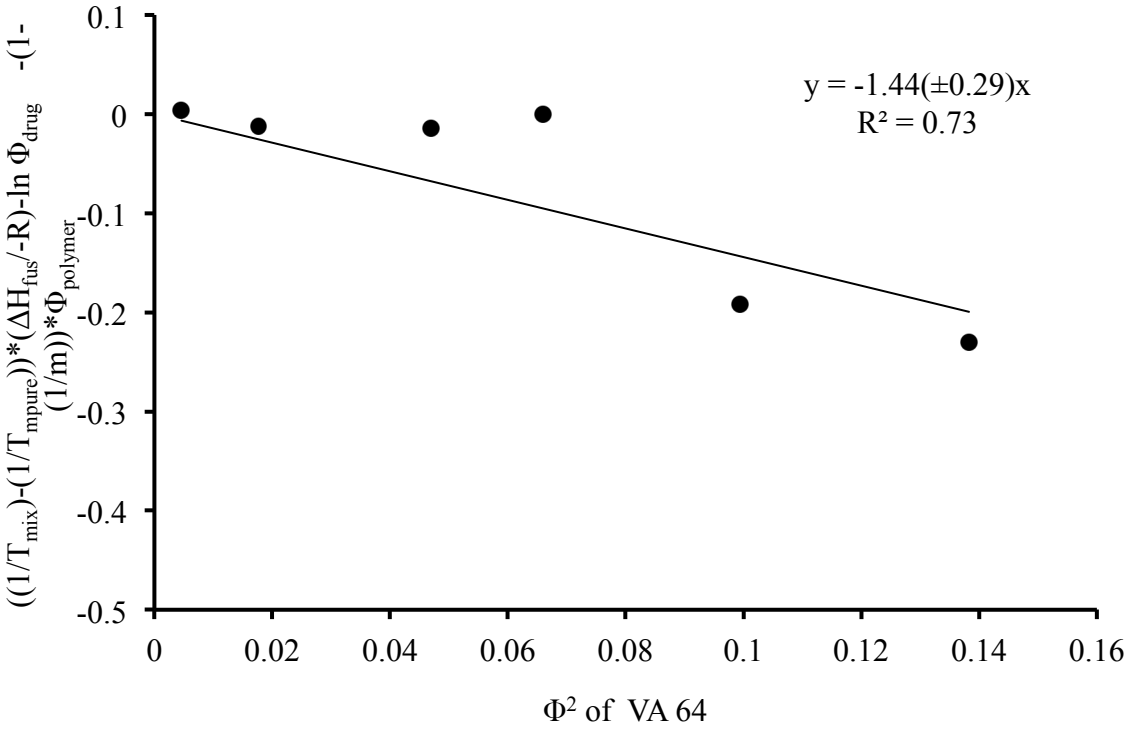

Figure 6.5. The interaction parameter, χ, calculated using the T_{onset} for NIF with VA64. Number between the parenthesis represents the standard error.

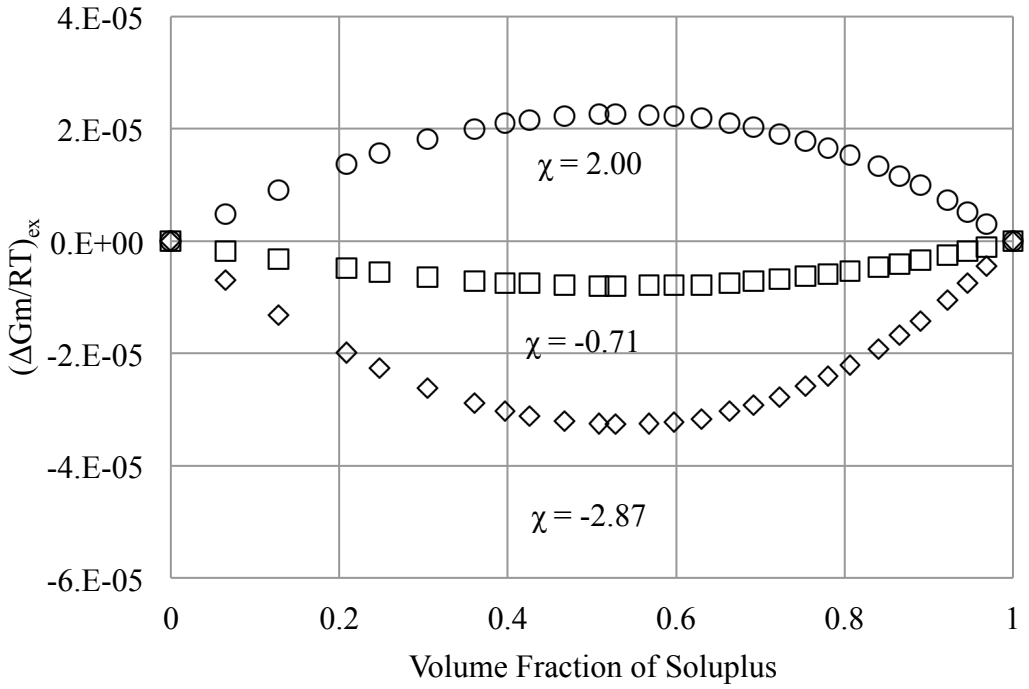

Figure 6.6. The excess, non-ideal, Gibbs free energy of mixing for SMX in Soluplus®. This plot shows the impact of the enthalpy after subtracting the entropy from equation 2.4.

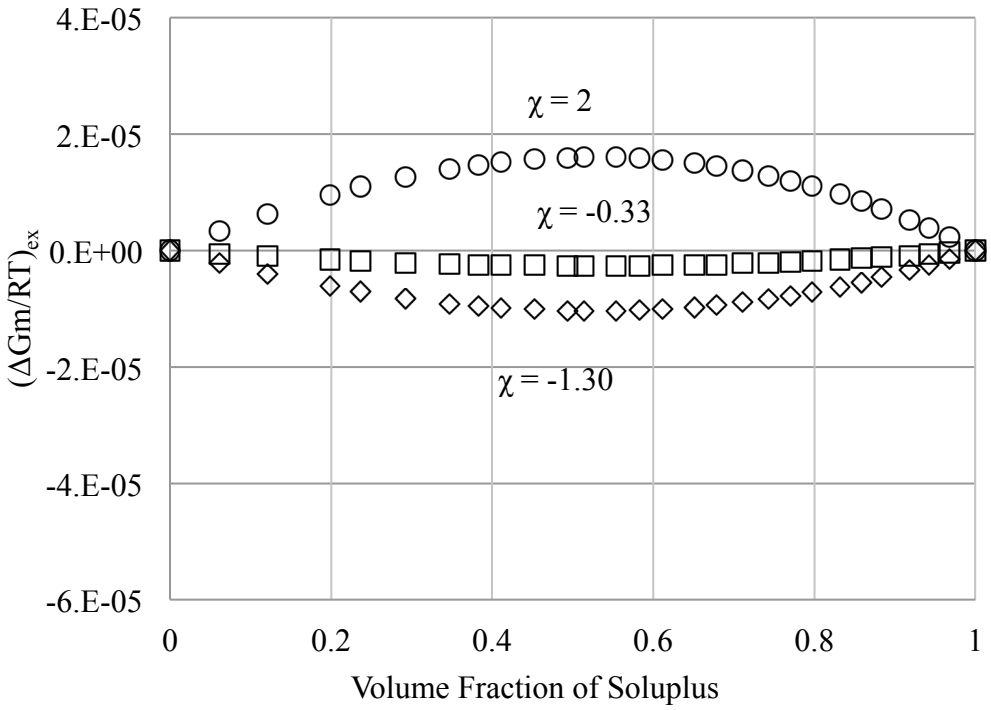

Figure 6.7. The excess, non-ideal, Gibbs free energy of mixing for NIF in Soluplus®. This plot shows the impact of the enthalpy after subtracting the entropy from equation 2.4.

7. Appendix C

Chapter Three: Supplemental information

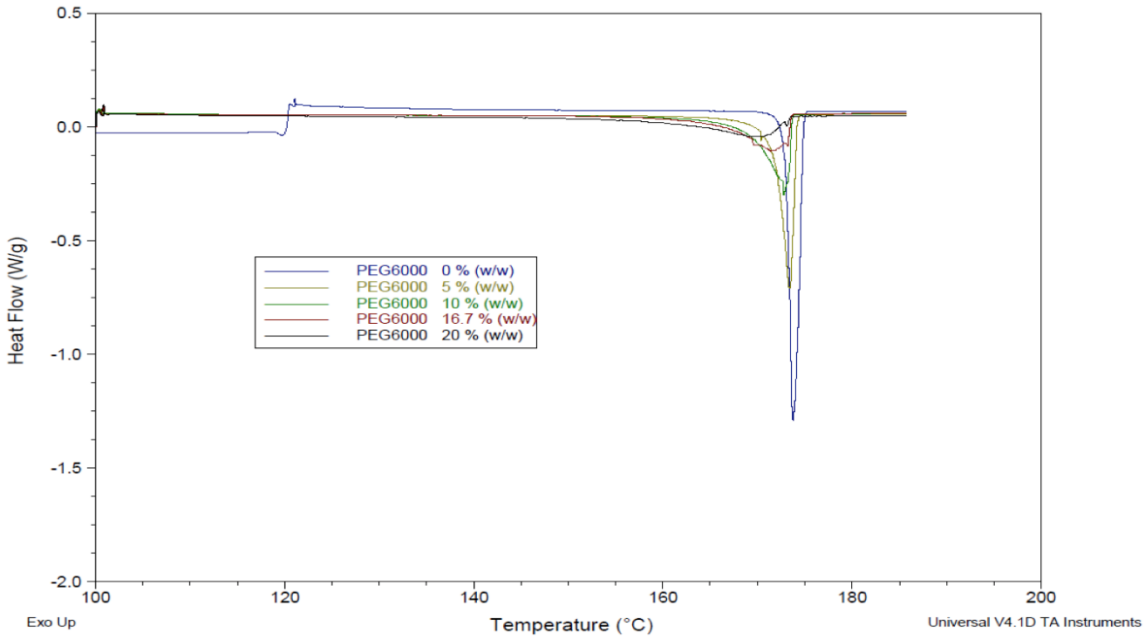

Figure 7.1. DSC thermograms of the melting endotherm for nifedipine mixtures with 0, 5, 10, 16.7, and 20 % w/w PEG 6000.

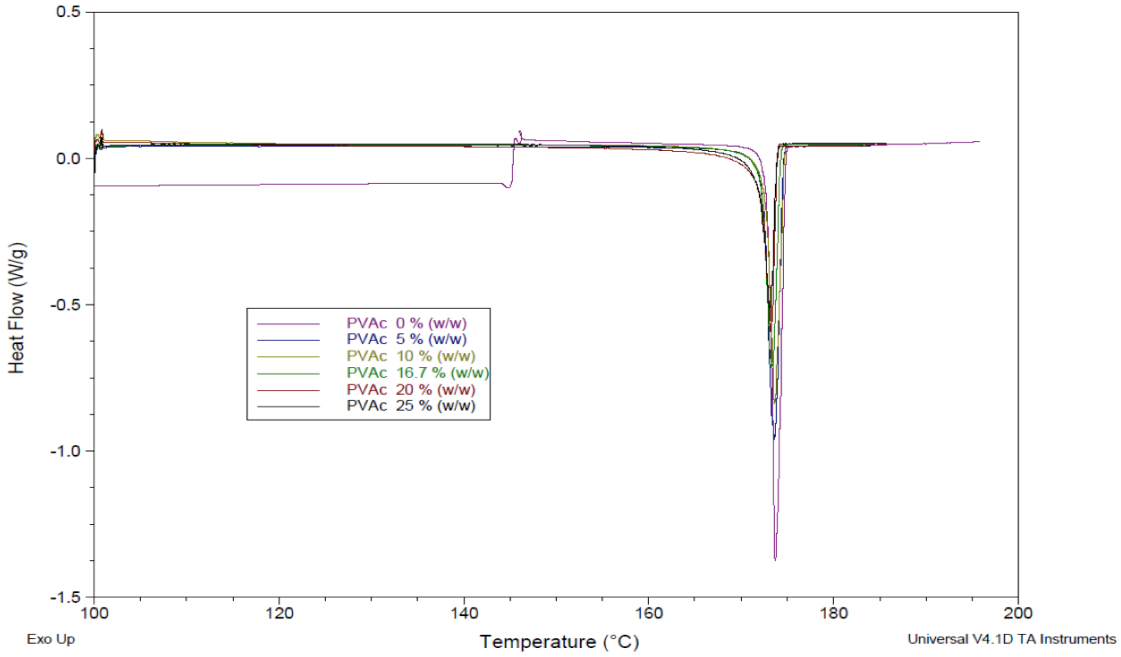

Figure 7.2. DSC thermograms of the melting endotherm for nifedipine mixtures with 0, 5, 10, 16.7, 20, and 25 % w/w PVAc.

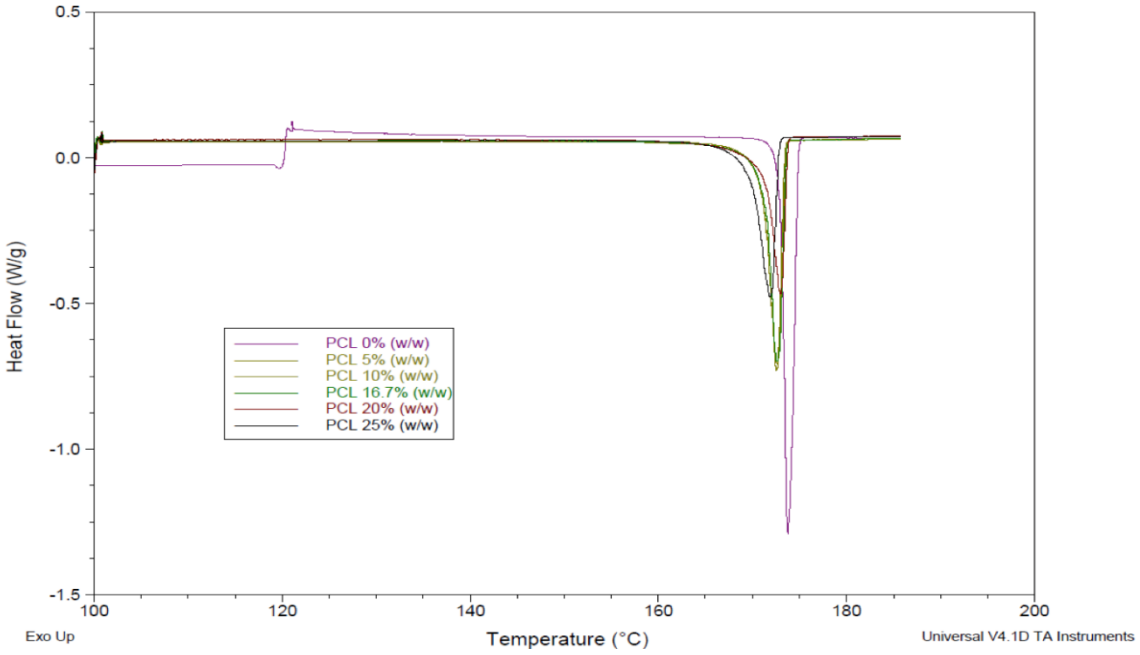

Figure 7.3. DSC thermograms of the melting endotherm for nifedipine mixtures with 0, 5, 10, 16.7, 20, and 25 % w/w PCL.

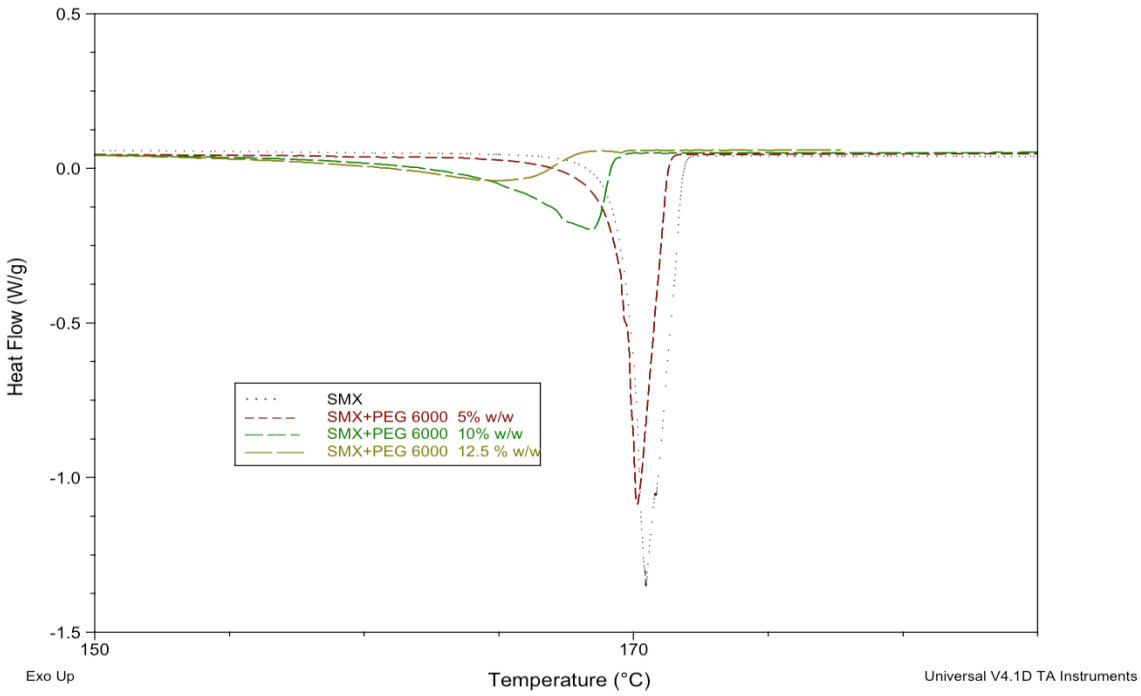

Figure 7.4. DSC thermograms of the melting endotherm for sulfamethoxazole mixtures with 0, 5, 10, and 12.5 % w/w PEG 6000.

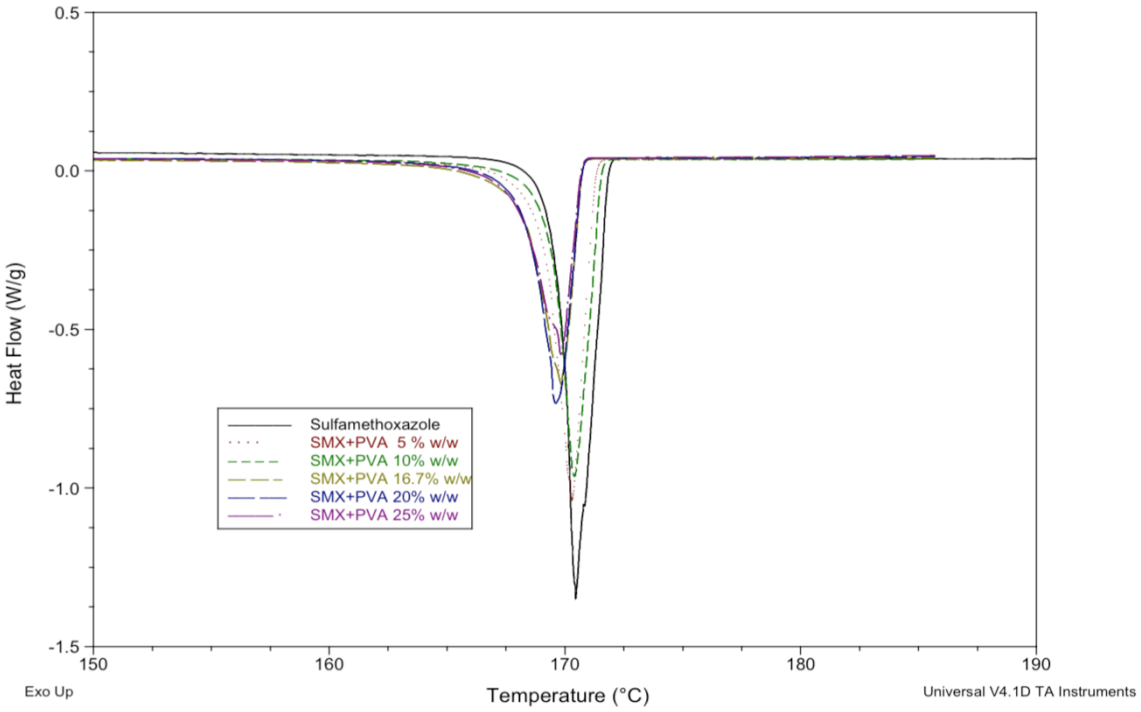

Figure 7.5. DSC thermograms of the melting endotherm for sulfathoxazole mixtures with 0, 5, 10, 16.7, 20, and 25 % w/w Soluplus®.

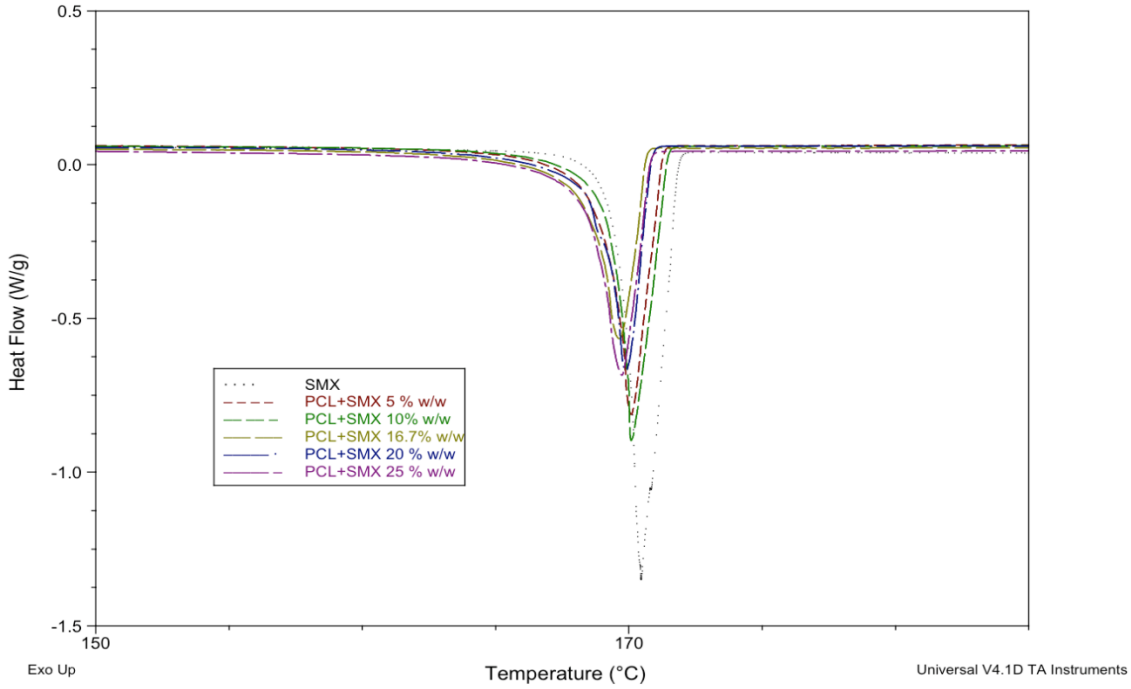

Figure 7.6. DSC thermograms of the melting endotherm for sulfamethoxazole mixtures with 0, 5, 10, 16.7, 20, and 25 % w/w PCL.

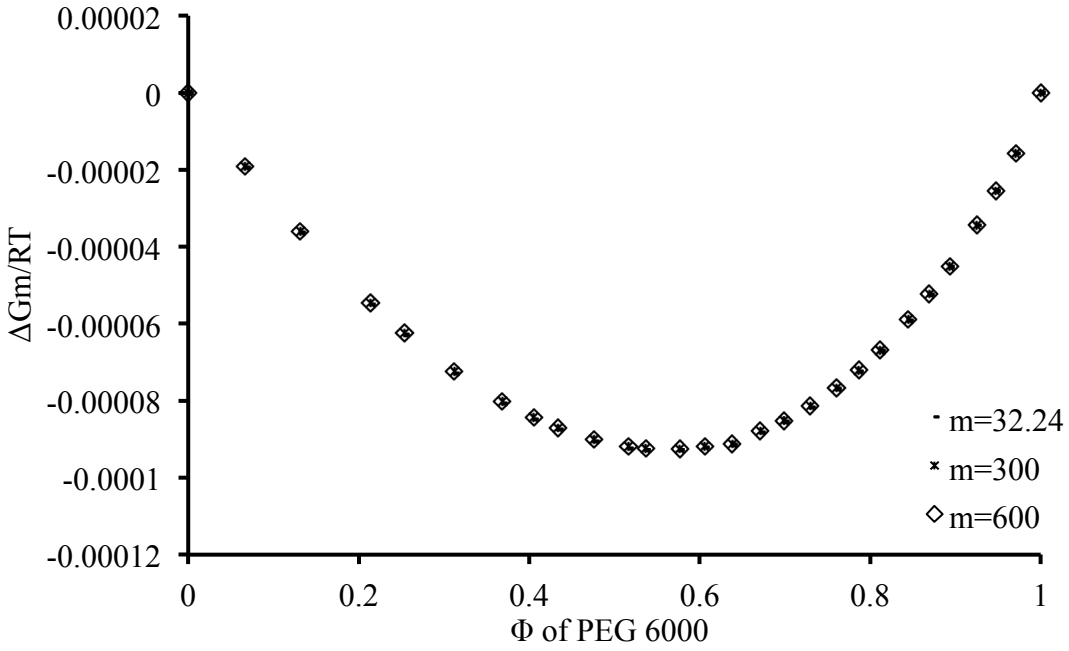

Figure 7.7. The predicted temperature normalized Gibbs free energy of mixing for PEG 6000 and SMX, with inclusion of different M_W of PEG.

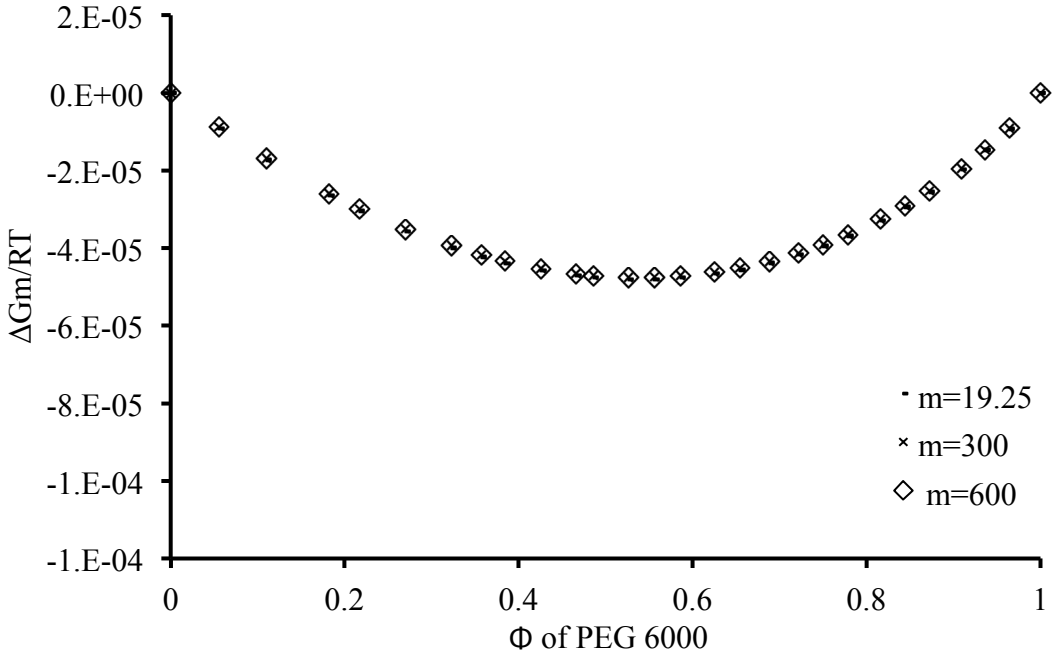

Figure 7.8. The predicted temperature normalized Gibbs free energy of mixing for PEG 6000 and NIF, with inclusion of different M_W of PEG.

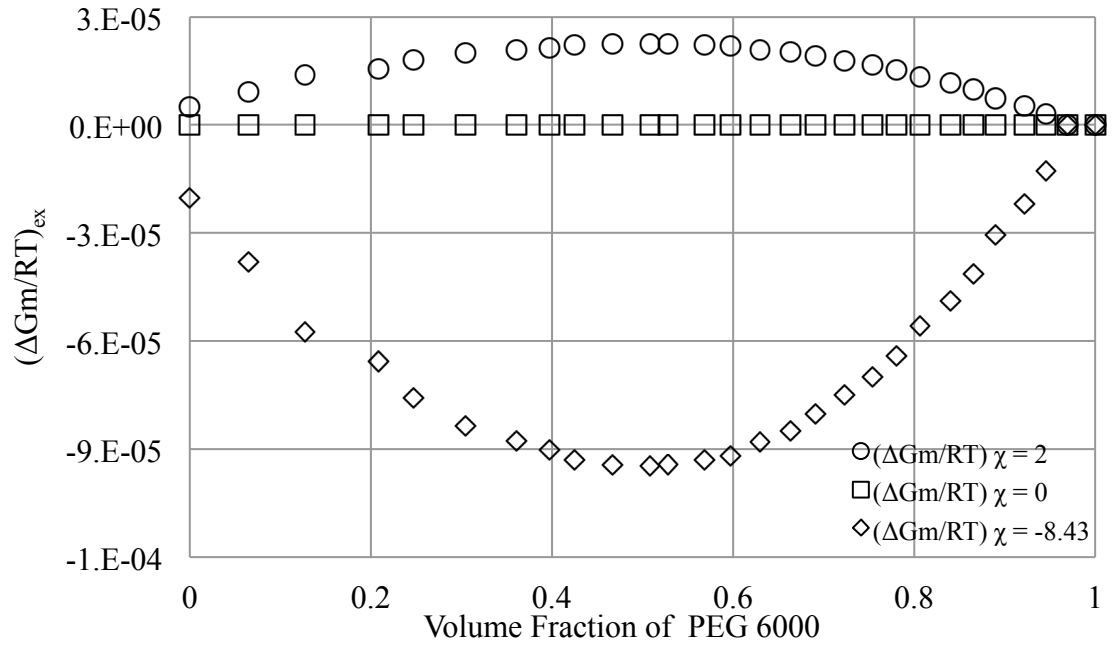

Figure 7.9. The excess, non-ideal, Gibbs free energy of mixing for SMX in PEG 6000. This plot shows the impact of the enthalpy after subtracting the entropy from equation 3.2.

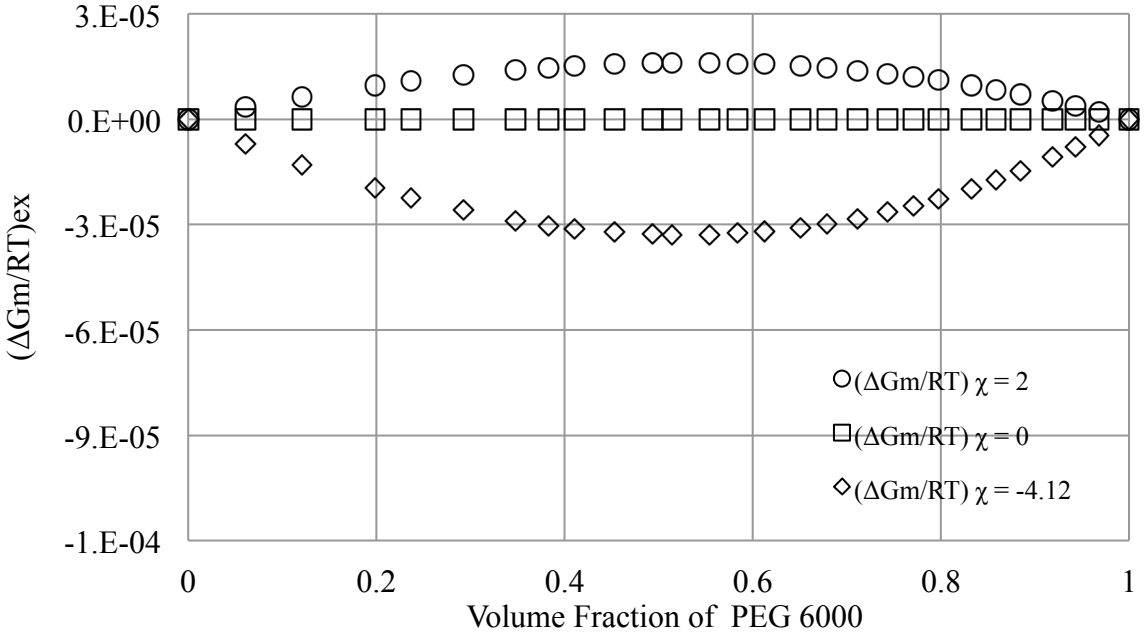

Figure 7.10. The excess, non-ideal, Gibbs free energy of mixing for NIF in PEG 6000. This plot shows the impact of the enthalpy after subtracting the entropy from equation 3.2.

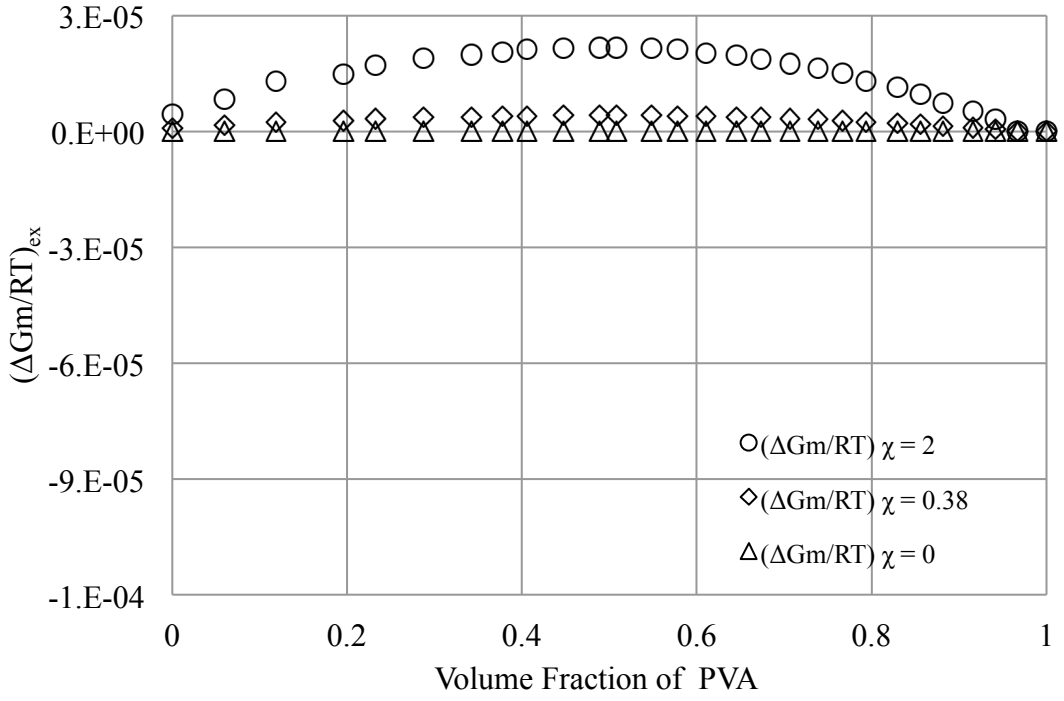

Figure 7.11. The excess, non-ideal, Gibbs free energy of mixing for SMX in PVAc. This plot shows the impact of the enthalpy after subtracting the entropy from equation 3.2.

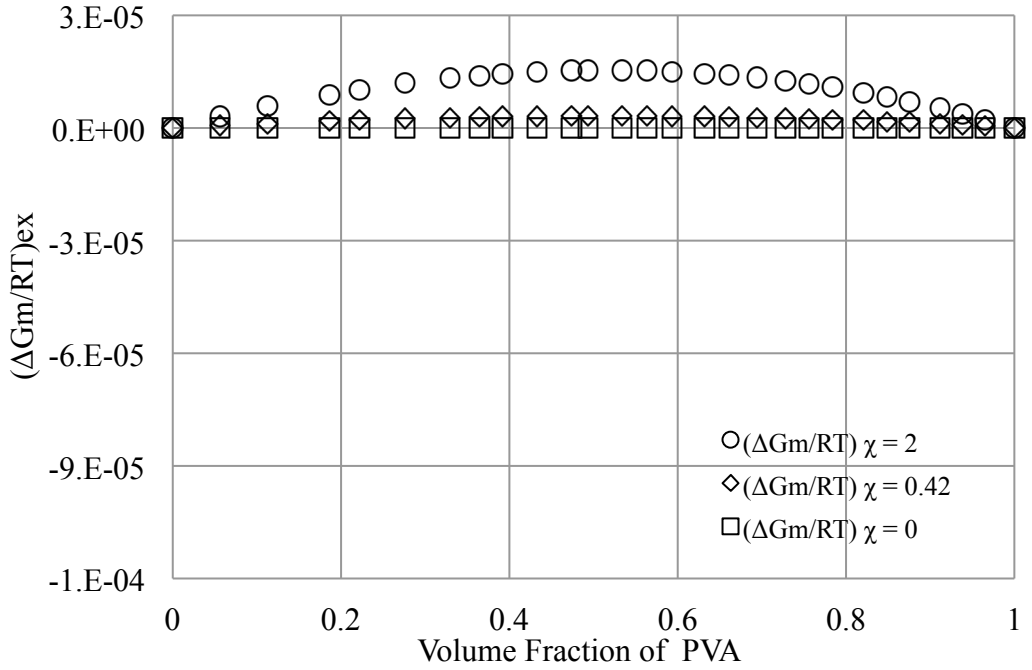

Figure 7.12. The excess, non-ideal, Gibbs free energy of mixing for NIF in PVAc. This plot shows the impact of the enthalpy after subtracting the entropy from equation 3.2.

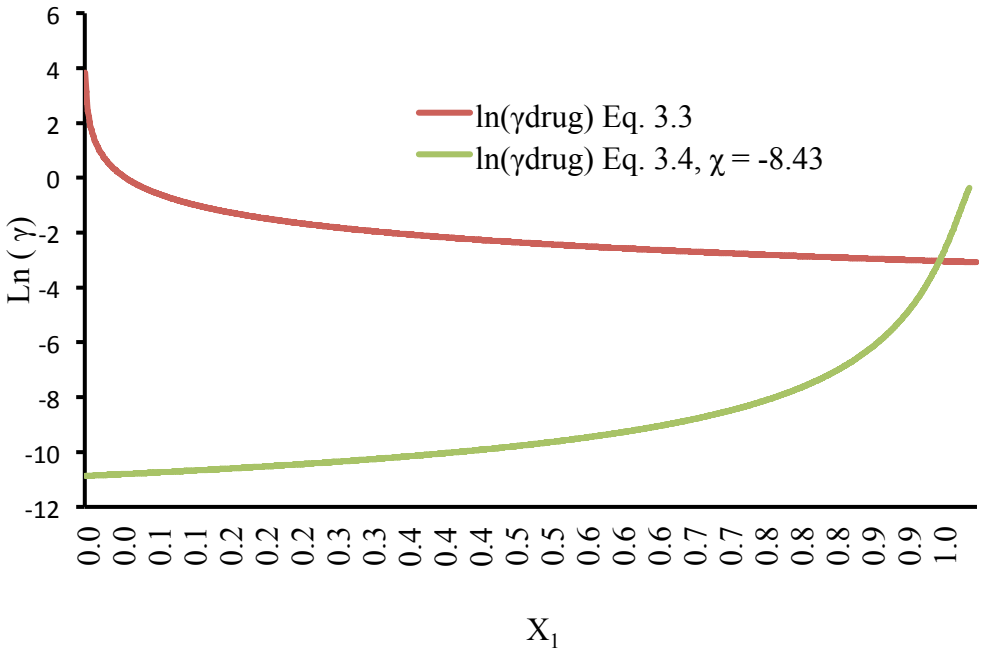

Figure 7.13. Determination of mole fraction solubility for SMX in PEG 6000 at 298 K.

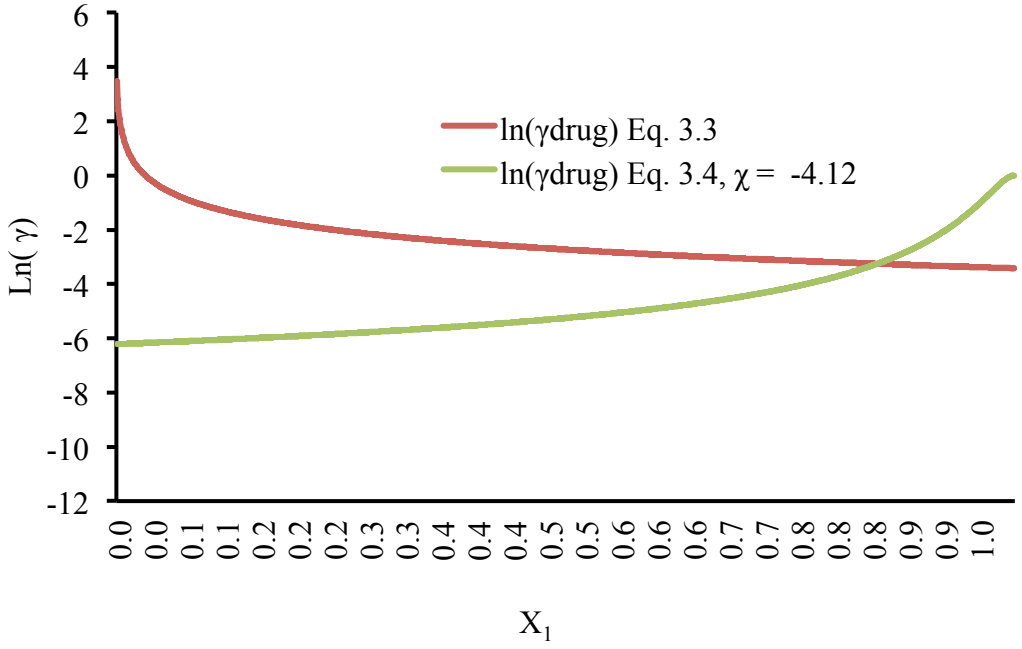

Figure 7.14. Determination of mole fraction solubility for NIF in PEG 6000 at 298 K.

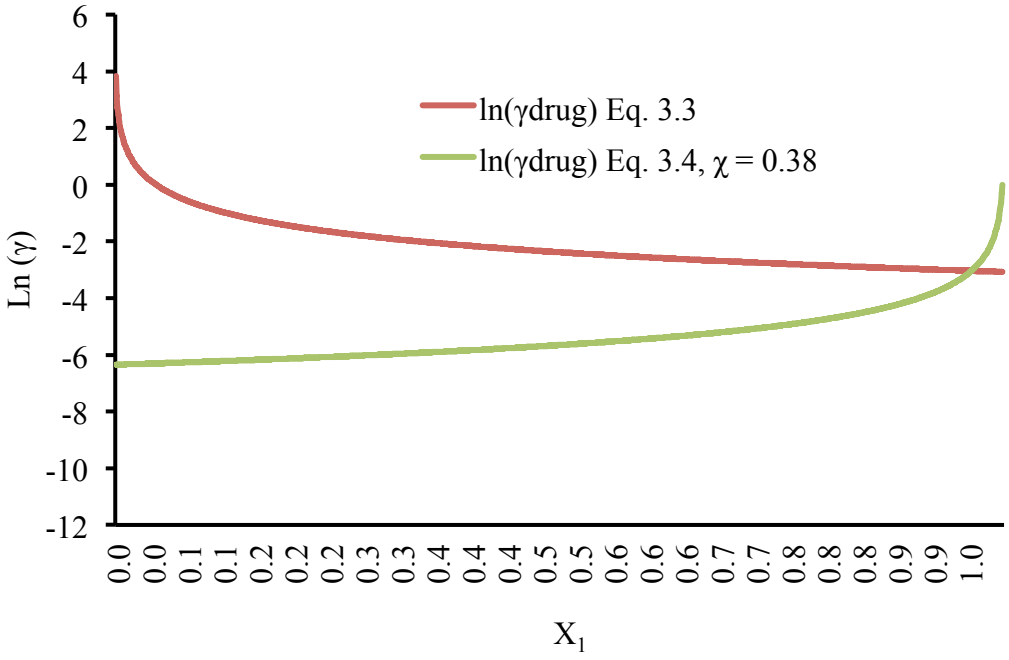

Figure 7.15. Determination of mole fraction solubility for SMX in PVAc at 298 K.

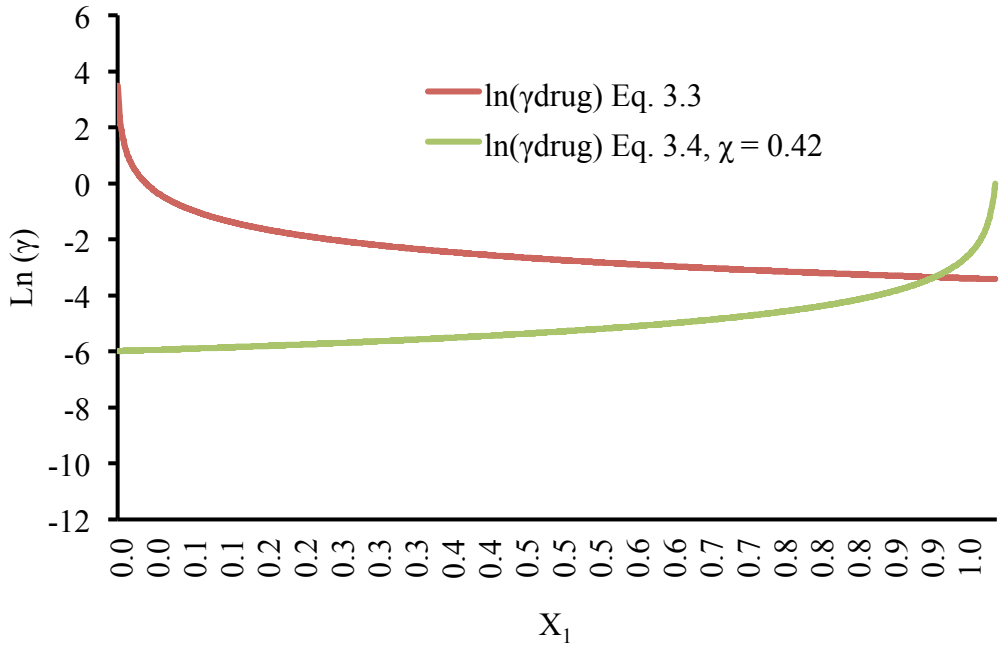

Figure 7.16. Determination of mole fraction solubility for NIF in PVAc at 298 K.

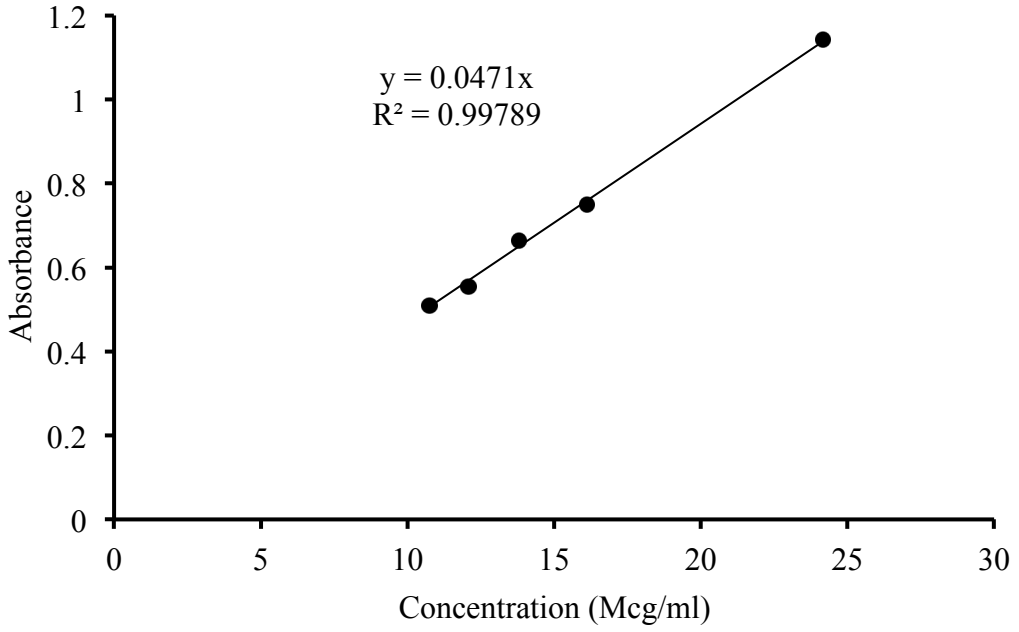

Figure 7.17. Standard curve representing the absorbance of different concentrations of SMX in PEG 400 at 260 nm.

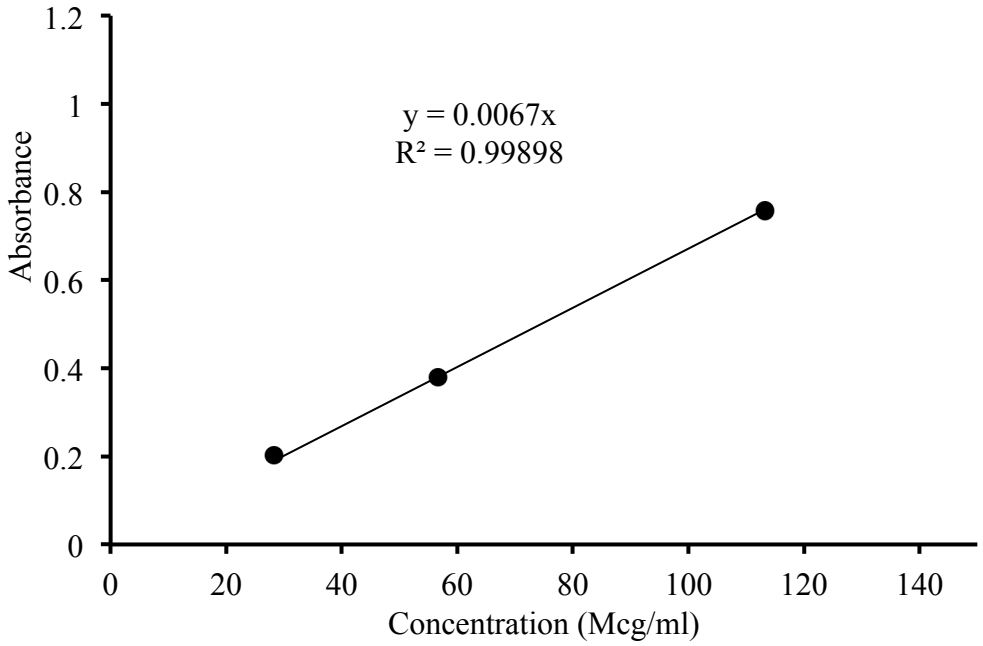

Figure 7.18. Standard curve representing the absorbance of different concentrations of NIF in PEG 400 at 350 nm.

8. Appendix D

Chapter Four: Supplemental information

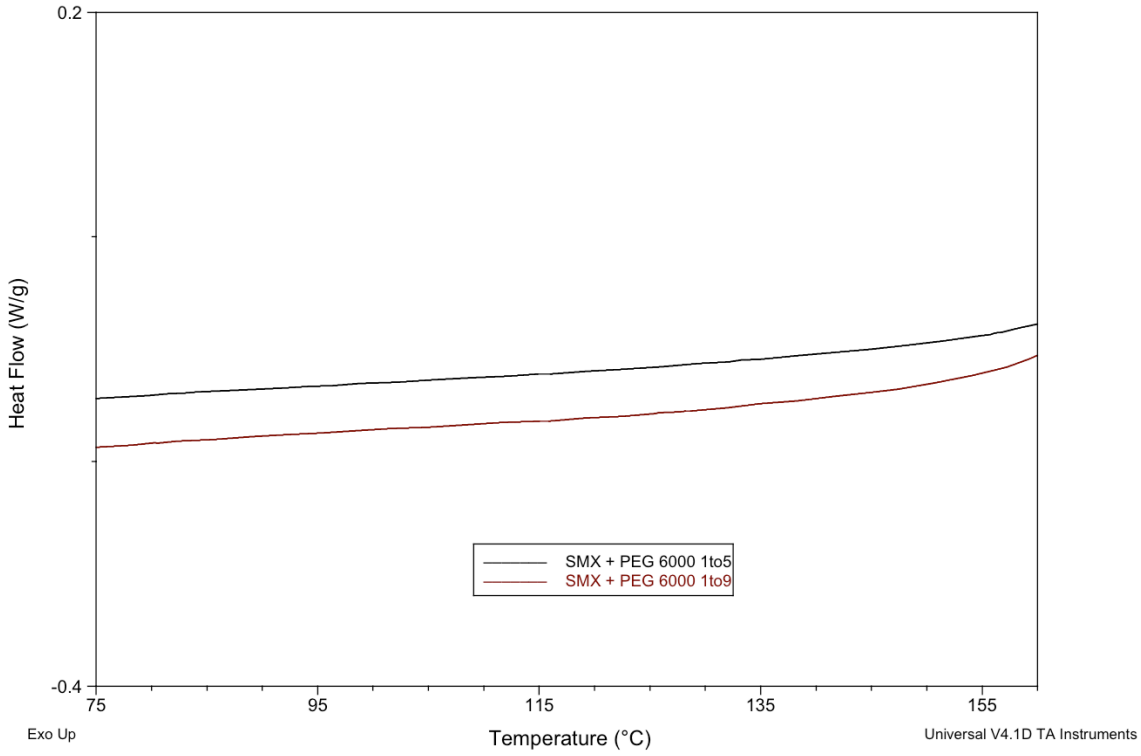

Figure 8.1. DSC thermograms of sulfamethoxazole:PEG 6000 spray dried mixtures at mass ratios of 1:5 and 1:9.

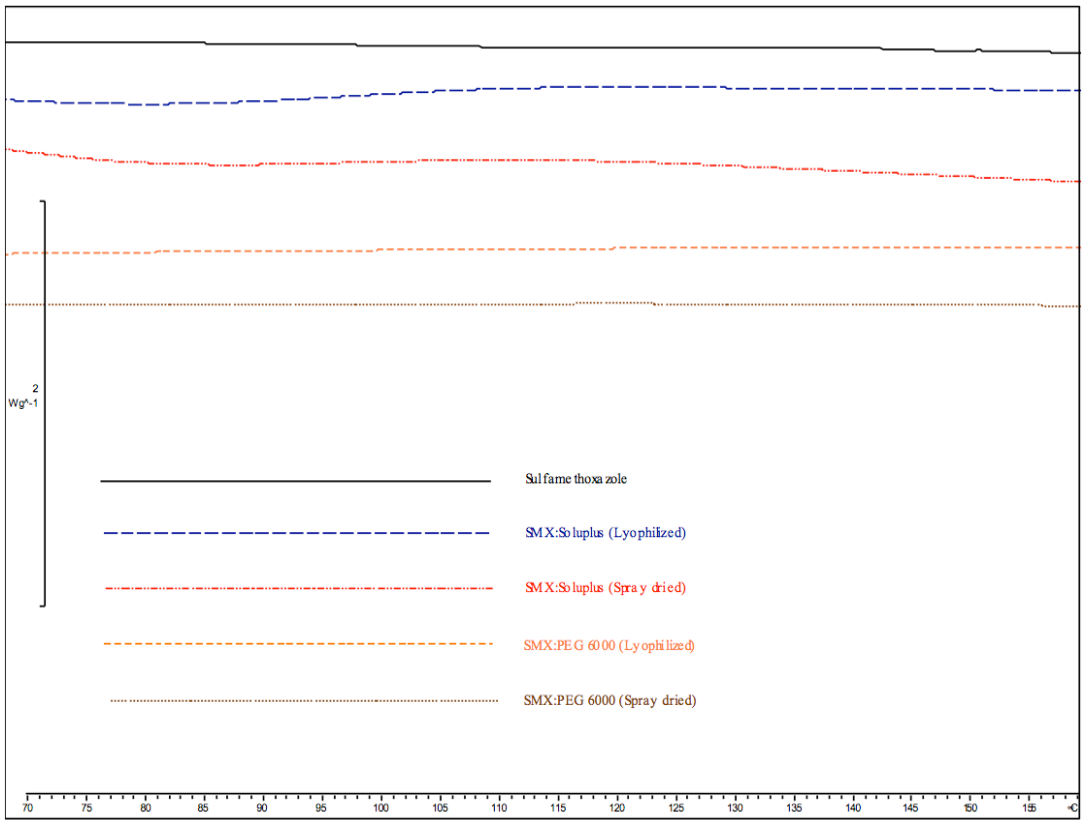

Figure 8.2. DSC thermograms for SMX mixtures with Soluplus® and with PEG 6000 at a mass ratio of 1:9 stored for six months at 0% RH and 25 °C.

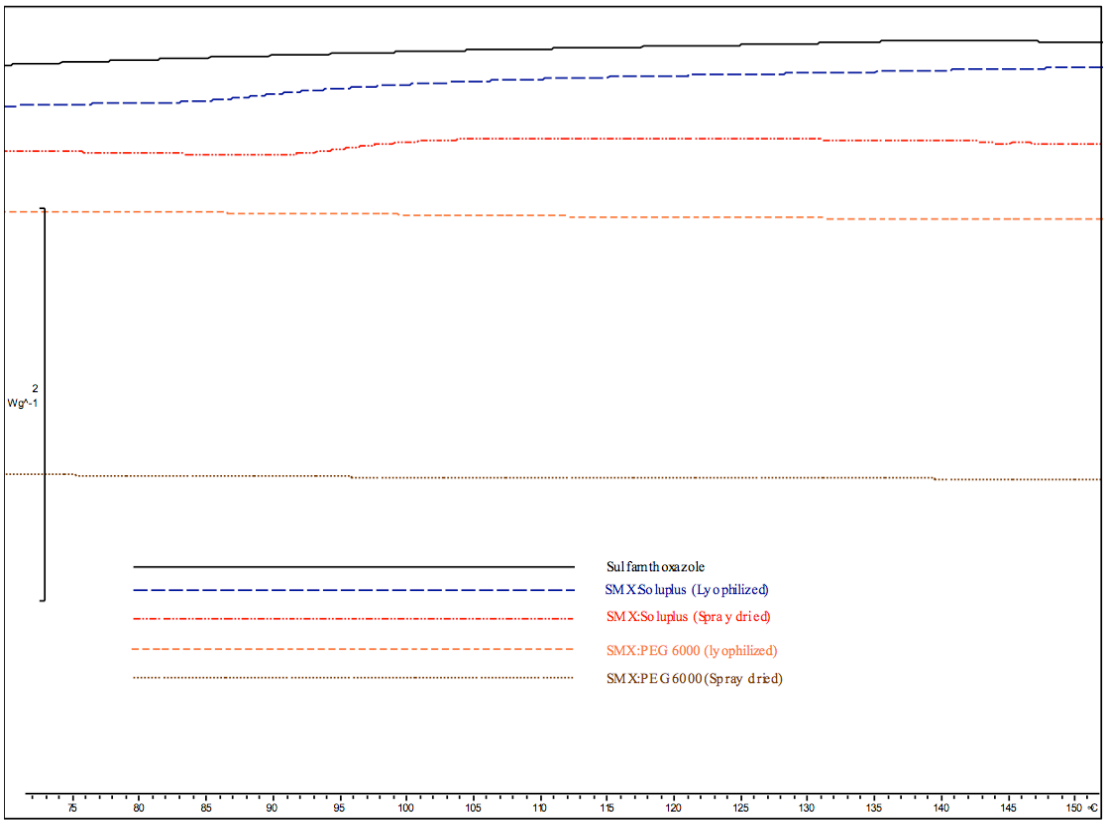

Figure 8.3. DSC thermograms for SMX mixtures with Soluplus® and with PEG 6000 at a mass ratio of 1:9 stored for six months at 0% R.H. and 50 °C.

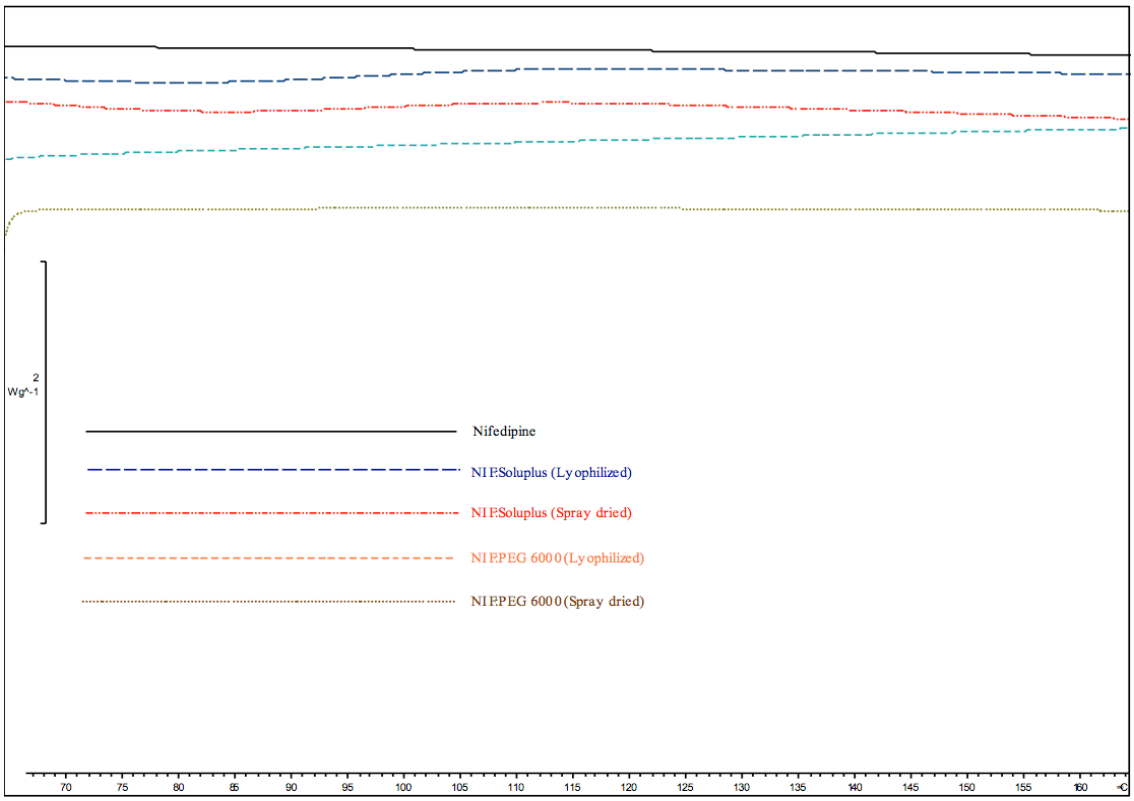

Figure 8.4. DSC thermograms for NIF mixtures with Soluplus® and with PEG 6000 at a mass ratio of 1:9 stored for six months at 0% RH and 25 °C.

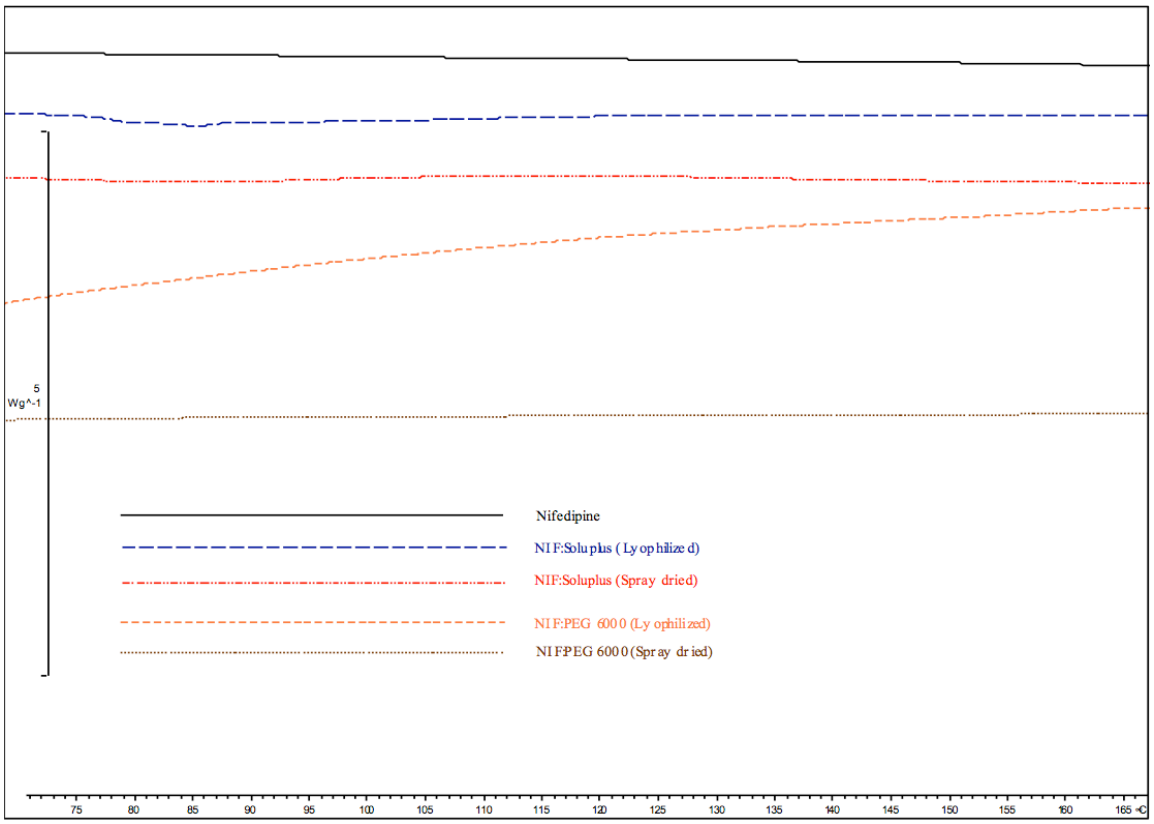

Figure 8.5. DSC thermograms of sulfamethoxazole:PEG 6000 spray dried mixtures at mass ratios of 1:5 and 1:9.

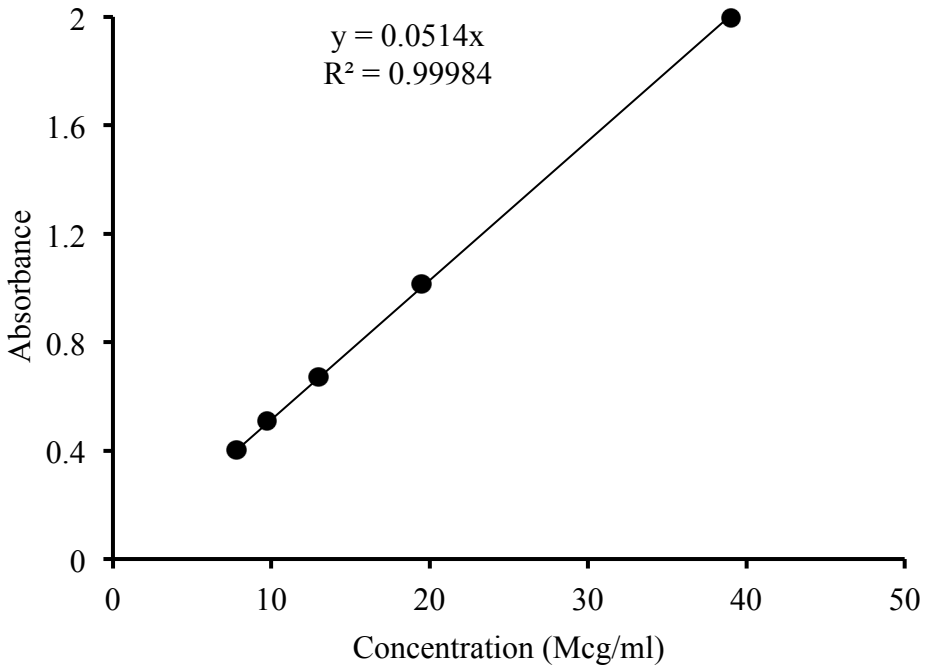

Figure 8.6. Standard curve representing the absorbance of different concentrations of SMX in SIF at 260 nm.

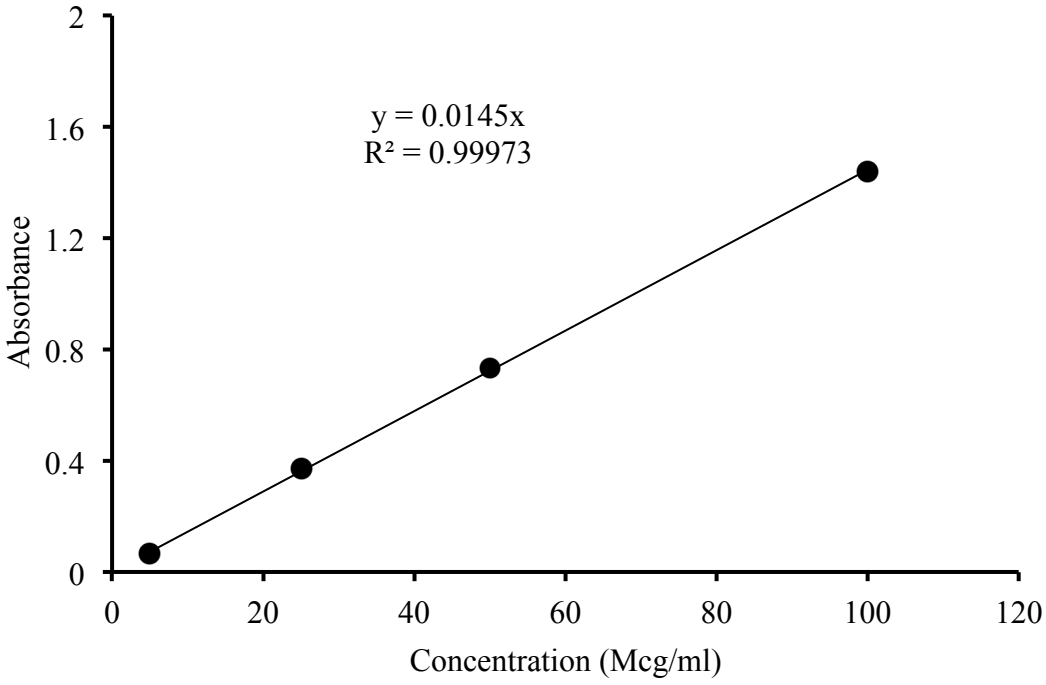

Figure 8.7. Standard curve representing the absorbance of different concentrations of SMX in SGF at 260 nm.

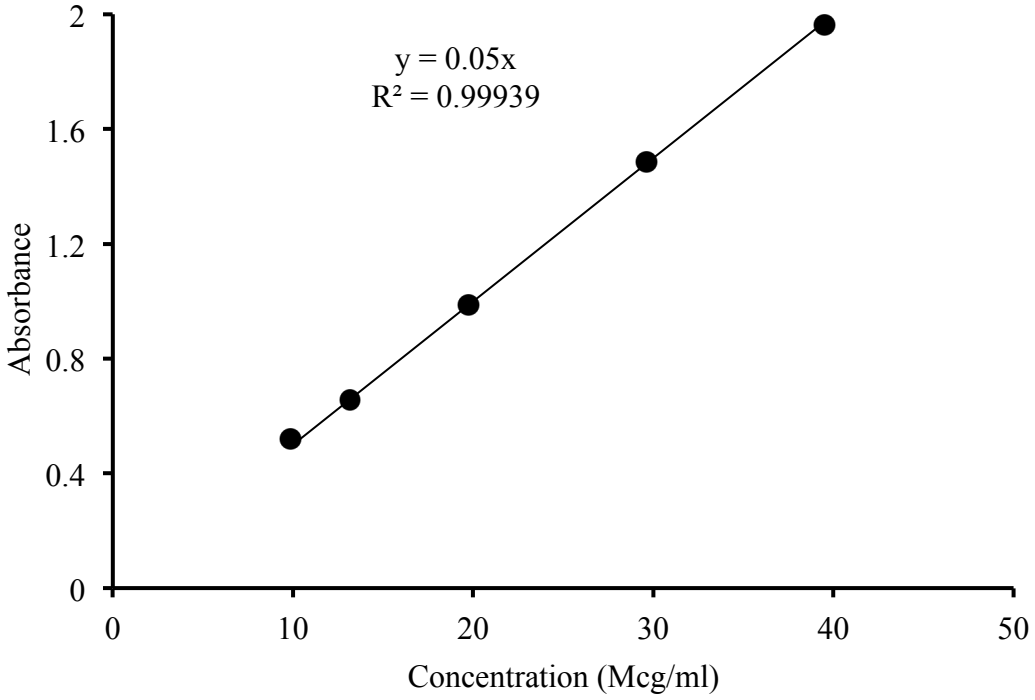

Figure 8.8. Standard curve representing the absorbance of different concentrations of SMX in water at 260 nm.

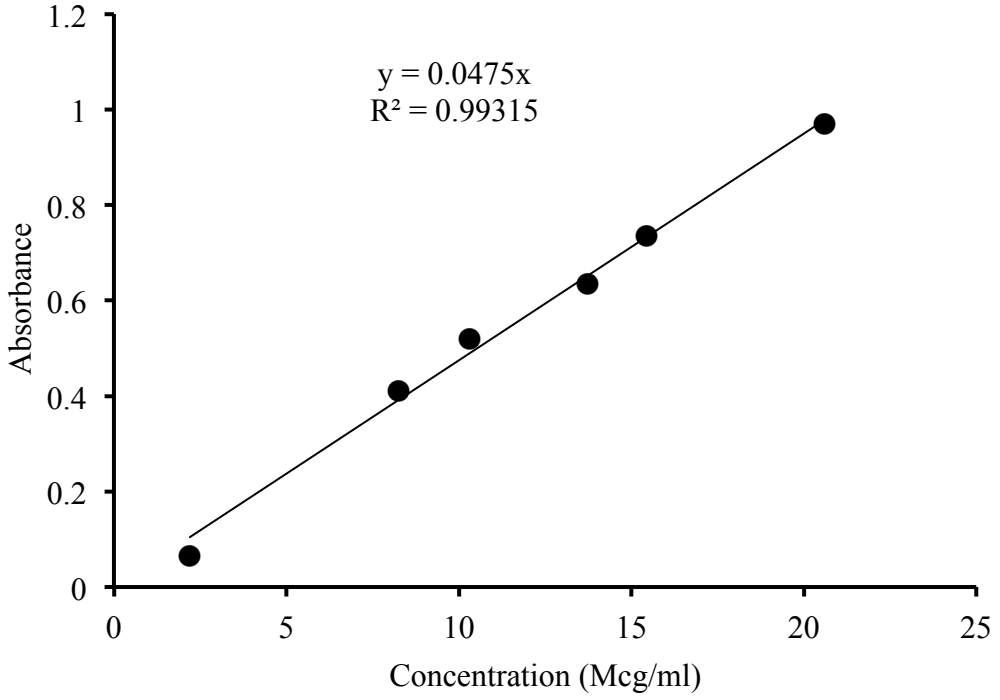

Figure 8.9. Standard curve representing the absorbance of different concentrations of NIF in SIF at 240 nm.

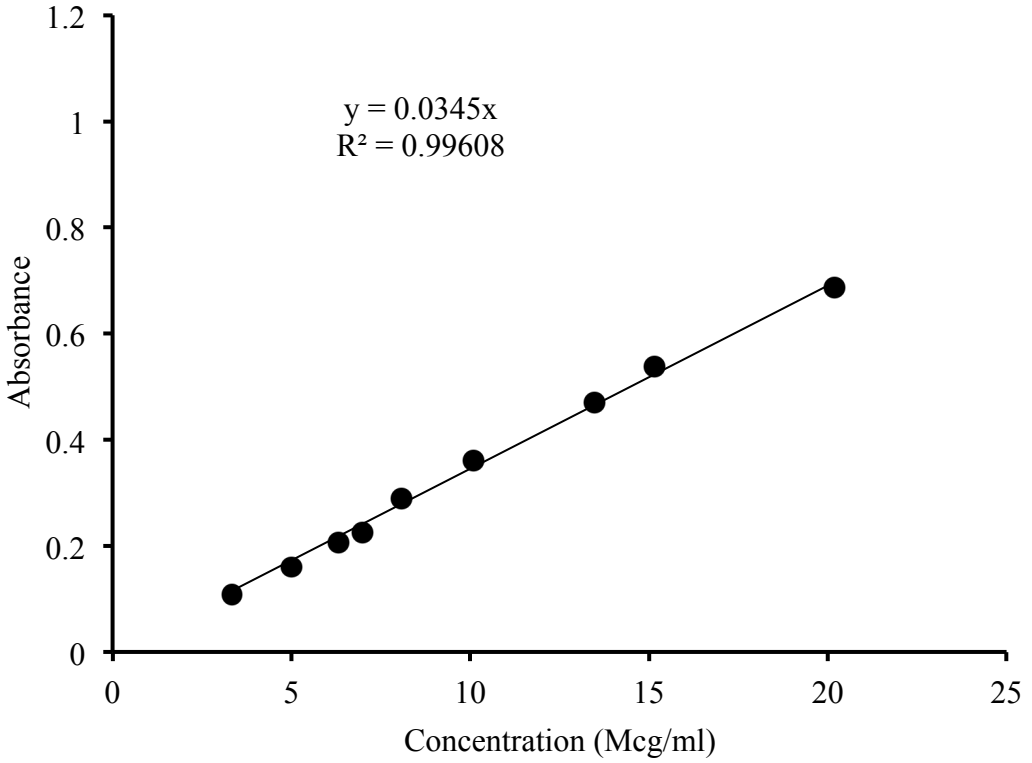

Figure 8.10. Standard curve representing the absorbance of different concentrations of NIF in SGF at 240 nm.

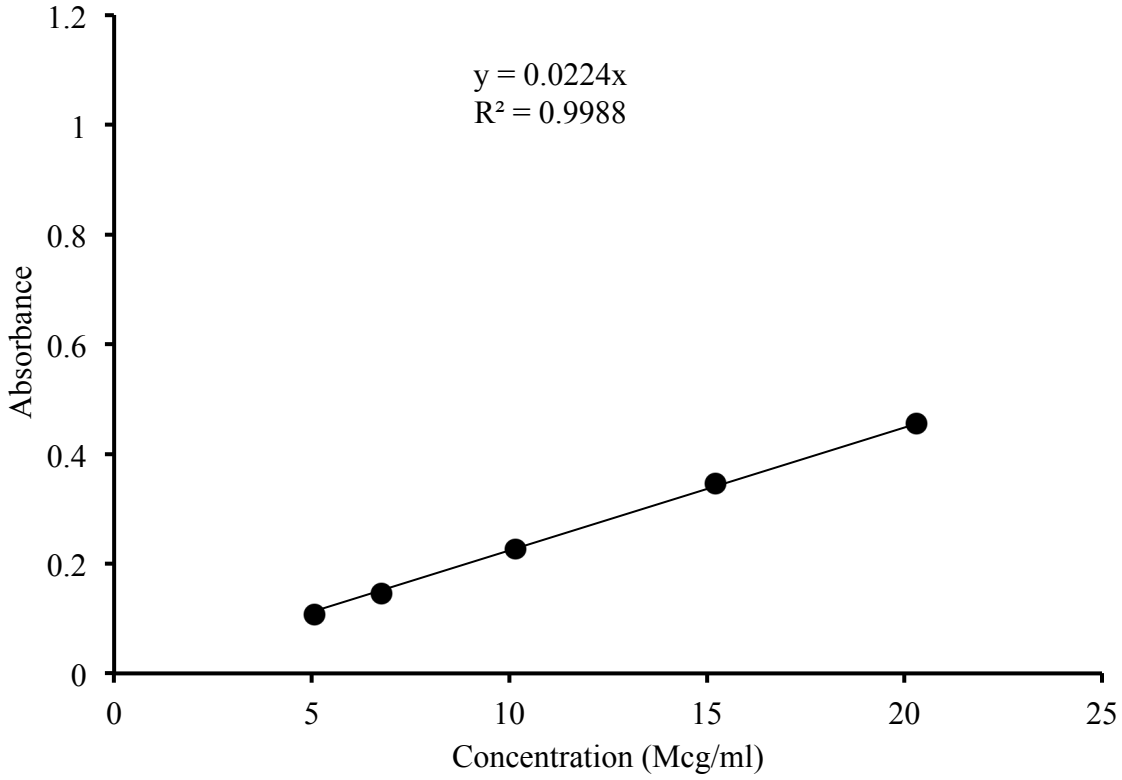

Figure 8.11. Standard curve representing the absorbance of different concentrations of NIF in water at 240 nm.